

Differential Tetraspanin Expression in Monocyte Subsets May Regulate the Formation of Multinucleated Giant Cells



The
University
Of
Sheffield.



SiGN

A Thesis Submitted for the Degree of Doctor of Philosophy

Thomas Stephen Christian CHAMPION

Dr Pete Monk*, Dr Lynda Partridge & Dr Siew Cheng Wong

Academic Unit of Infection, Immunity and Cardiovascular Disease

Section of Infection, Inflammation and Immunity

Department of Medicine

University of Sheffield

October 2016

DECLARATION

The work presented in this thesis is the work of the candidate, with the following exceptions:

- Luminex™ ELISAs were performed by Esther Mok at Immunos, SIGN, Singapore.
- SEM was performed by Benoit Malleret, Tan Suat Hoon and Lu Thong Beng at Immunos, SIGN, Singapore.
- The adherence assay macro and acquisition set-up were generated by Dr Robert Wallin.
- The original nuclei counting macro was written by John Lim and later adapted with permission.

This research was funded by the Biomedical Research Council of the Agency for Science (BMRC-A*STAR).

ACKNOWLEDGEMENTS

I could not give enough gratitude to my three supervisors; **Dr Pete Monk, Dr Lynda Partridge and Dr Siew Cheng Wong** for their unending support, patience and guidance.

To Pete; your intellectual insights were only ever matched by your sarcasm. Thank you for all the 10k and half-marathon races we ran against one another, you kept me checking my heels and even left me in the dust on a few occasions!

To Lynda; your vast understanding of the immune system was only surpassed by the encouragement and support you gave at times when things seemed more apoptotic than proliferative.

To Siew Cheng (lǎobǎn); your determination and drive were only exceeded by your seemingly infinite patience and hospitality to a young Ang Moh so far away from home.

To my two *viva voce* examiners:

Prof Siamon Gordon; thank you for all your interesting insights and advice on my research and the discussions we held during my exam. Though I was terrified to be facing you as one of my examiners, in hindsight, I would refuse to have it any other way.

Dr Heather Wilson; thank you for your comments, insights and all the time you dedicated to reviewing and correcting my thesis. You have my utmost gratitude.

From University of Sheffield, UK Lab:

Dr Marzieh Fanaei - I must give particular thanks to Dr Fanaei who taught me all the fundamentals of PBMC isolation, MGC culturing and that sometimes, with lab work you need to call it a day and walk away.

Dr Andrew O'Leary – Thank you 'Gandy' for all your help with the early flow work, your guidance with lab techniques, political debates and cherished friendship.

Dr John Palmer – Thank John for always reminding me that some people have it worse. Your determination and sense of humour in the face of unending set-backs has inspired me over the years to never give up. P.S. Thank you for effectively getting me this PhD.

I give my gratitude to **Dr Dan Cozens, Dr Atiga Elgawidi, Rachel Bell, Ahmed Alobaidy, Dr Fawwaz Ali, Ibrahim Yaseen, Shaymaa Abbas, Muslim Aledami, Katherine Marsay and Lewis Burton** who have all given me support and friendship every day in the lab.

Dr Jenny Ventress – Last but not least I thank Jen for her unending support, guidance with my thesis writing and unfathomable patience while I was working away in Singapore for 2 years. Over these past 4 years you have been my biggest source of both comfort and stress; I wouldn't have it any other way.

From A*STAR, Singapore Lab:

Dr Siew Min Ong – Thank you for all your help and discussions about data and protocols. Your insights into this project during our meetings were invaluable!

Dr Robert Wallin – Thank you for all the time and patience you dedicated to me in

the microscope suite teaching me acquisition and analysis techniques.

Dr Eva Hadadi – Thank you for teaching me how to process blood cones and perform MACs and FACs. I have never met a harder working person in all PhD and you remain a constant inspiration to me.

June Tai – Thank you for teaching me how to use the flow cytometry machines and compensate antibody panels.

Wei Hseun Yeap – Thank you for your help in setting up the ELISA and for the times you helped me get the blood cones I needed! Thank you for all the time you spent maintaining stocks and antibodies for everyday use in the lab, you kept our ship afloat!

Lisa Mauracher – To list all the aspects of my project you helped me with would double the length of this thesis. In particular, thank you for teaching me how to set up acquisition protocols on the microscopes, for teaching me your adherence assay protocols and for all the insights you gave.

I am truly thankful for the support and friendship given to me by **Dr Hwei Xian Leong, Biyan Zhang, Charleen Wong and Jelin Lovelle Sieow**. I fail to recall a single memory of you all where you were not smiling and making my day a better one.

Dr Kia Joo Puan – Thank you for all your help in teaching me about the principles of flow cytometry, panel design, ordering antibodies, compensation etc.

Akhila Balachander – Thank you for taking the time to have all those lengthy discussions about microscopy techniques and for giving me stains to trail. Also, thank you for all your kindness and friendship during my stay in Singapore.

John Lim – You have my utmost gratitude for teaching me all about writing macros for ImageJ analysis.

Esther Mok – Thank you for your help setting up and performing the Luminex™ ELISAs and showing me how to handle the data.

Funding & Resources

FACS Operators: A big thank you to **Ivy Low, Nurhidaya Binte Shadan, Seri Munirah Mustafah and Thye Seng Leck** who performed all the FACS sorts of cells.

SEM Operators: Thank you and credit to **Benoit Malleret, Tan Suat Hoon and Lu Thong Beng** who performed the SEM imaging of my giant cell samples.

Blood: Thank you to all the in-house and anonymous blood donors; without you this research would not be possible. Thank you to the Blood Services Group (BSG) of the Health Sciences Authority in Singapore for all the cones they sent me which was essential for all the monocyte subset work.

Funding: My utmost gratitude to the Biomedical Research Council of the Agency for Science (BMRC-A*STAR) for funding this research and for covering my travel grants to conferences.

Facilities: My thanks to the Department of Microbiology and Biotechnology and Medical School of Sheffield University for use of their laboratories and to A*STAR in Singapore for granting access to their technologies and expertise at Biopolis.

Friends & Honourable Mentions

The following people are mentioned here in recognition of all their support and friendship. I have learnt so much through you all and for that I give my thanks to:

Jessica Ebo, Kira Shaw, Mark Hayhurst, Alasdair McComb, Jonathan Cox, Josie Gibson, Adam Pyrah, Dawn Thean and Tim Luxton – Tropical rain or shine

you were always there to give me support and a good drink. You were all terrible distractions from my work and for that I thank you from the bottom of my heart.

Lisa Mauracher – No one in my lab supported me more as a friend than you. Thank you for all your guidance, support, laughter and German lessons. Vielen herzlichen Dank, Frau Mauracher.

Flora Teoh, Ian Prise, Catherine Diamond, Brian Abel, Muhammad Irfan Khalis, Dan McGuire, Günsu Yeşilyaprak, Olya Fromkief, Julia Bolme, Derya Bercin, Peter Brauer, Shikin Yusof, Hanif Javanmard, Anand Kumar Andiappan, Young Cheng and Tuang Yeow Poh – You all deserve a paragraph each but I hope you can all accept this show of gratitude for all the kindness and friendship you gave me every day in the labs and office.

Tobias Dierkes, Tyson Cross, David Mateo, Stephanie Lorraine, Lora Senrob, Anupriya Khemka, Palak Jain, Thomas Braud, Gianni Monaco, Galvin Chung and Wenny Cai – To my flatmates in Singapore; thank you for making my time in Singapore such a joyous one. I have learnt so much from all of you about the world and of different cultures.

Isabella Watson and Banico Nicholas – Thank you for taking the time to travel half the world to see me and bringing me a little bit of home.

Andrew Lockie – Thank you for all your hospitality when I first moved to Singapore. You gave me more wine and welcome than I deserved.

Kevin & Michelle Ventress – Thank you for homing me for the final 6 weeks of write-up! I can't thank you enough for all the loving support, coffee and snacks!

To the comedic geniuses at **Rooster Teeth** – I could not thank you enough for all the hours of entertainment you brought me during the long hours of image analysis and MGC identification. Your podcasts kept me laughing during all those late nights working in the office alone in Singapore.

To my intellectual hero **Stephen Fry** – Thank you for wishing me well at the start of my PhD! You have always inspired me to have an equal love of learning as we do for laughter.

"Wine can be a better teacher than ink, and banter is often better than books" – Stephen Fry

I thank all my family for their love and support. Their patience with faulty skype connections and dealing with 8 hour time differences was infinite. My sincerest gratitude to my grandad **Charles "Nobby" Champion** who wished me well when I left but unfortunately could not welcome me back. To my father **Charles "Charlie" Champion**; thank you for teaching me to never be afraid to dive in and make friends with anyone as life is so often about who you know than what you know.

To my big brother **Charles "Chas" Champion**; thank you for all the times at the weekends when you woke up super early just to play xbox games and talk with me.

To my mother **Theresa Champion**, no amount of words would be sufficient to thank you for all the support you have given me over the years so I hope in this case to show sincerity in simplicity. Thank you for your unending support and understanding, you taught me that persistence and hard work can achieve anything. How right you were.

CONTENTS

Front Cover	1
Declaration	2
Acknowledgements	3
List of Figures	10
List of Tables	12
Abstract	13
Abbreviations.....	14
1 Chapter 1: Introduction.....	17
1.1 The Human Immune System	17
1.1.1 The Monocyte Lineage	18
1.1.1.1 Tissue Resident Macrophages – A Story of Origins.....	23
1.1.1.2 Of Mice and Men – A Tale of Two Models.....	24
1.1.1.3 Monocyte Subsets.....	25
1.1.1.4 Monocyte Subset Signalling	27
1.2 Monocyte Mononuclear Descendants: Macrophages and Dendritic Cells.....	30
1.3 Multinucleated Giant Cells	34
1.3.1 Osteoclasts: An MGC for Bone Homeostasis	34
1.3.2 Foreign Body Giant Cells: An Inflammatory MGC for Foreign Body Destruction.....	35
1.3.3 Langhans Giant Cell: An Inflammatory MGC for Bacterial Encasement.	37
1.3.3.1 Mtb and HIV Coinfection	37
1.3.3.2 Mechanisms of Mtb Drug Resistance	38
1.3.3.3 The Molecular Basis of Mtb Entry.....	40
1.4 Mechanisms of Monocyte Fusion.....	42
1.4.1 Monocyte Fusion: Competence & Communication	42
1.4.2 Monocyte Fusion: Contact and Contraction.....	46
1.4.3 Monocyte Fusion: Commitment and Completion	47
1.4.4 Fusion Mechanisms in Alternative Systems	49
1.5 Tetraspanins	54
1.6 Tetraspanin Structural Features	54
1.6.1 EC1 & EC2	54

1.6.2	The Four Transmembrane Helices.....	57
1.6.3	Palmitoylated Cysteines.....	58
1.7	Tetraspanin Enriched Microdomains and the "Tetraspanin Web"	58
1.8	Tetraspanins and Fusion	60
1.9	Expression of Tetraspanins in monocyte subsets.....	64
1.10	Hypotheses, Aims and Objectives	65
1.10.1	Hypotheses	65
1.10.2	Aims & Objectives.....	65
2	Chapter 2: Materials and Methods.....	66
2.1	Materials	66
2.1.1	Cell Samples.....	68
2.1.2	Media, Buffers & Solutions	68
2.1.3	Antibodies & Markers	71
2.2	Methods.....	76
2.2.1	Primary Cell Preparation.....	76
2.2.1.1	Purification of Monocytes by Adherence	76
	77
2.2.1.2	Isolation of Monocytes by Magnetic-Activated Cell Sorting Using Negative-Selection	78
2.2.1.3	Sorting Monocyte Subsets Using Fluorescence-Activated Cell Sorting	78
2.2.2	Flow Cytometric Analysis of Tetraspanins	82
2.2.2.1	Staining Freshly Isolated Peripheral Blood Monocytes for Flow Cytometry	84
2.2.2.2	Fluorescence Compensation	85
2.2.2.3	Monocytes Cultured for 4 hrs in IMDM vs IMDM+ConA	85
2.2.3	Fusion Assays.....	88
2.2.4	Staining Cells for Fluorescence Microscopy	88
2.2.4.1	Staining Lab-Tek II slides:.....	88
2.2.4.2	Optimised Staining of 96-Well Plates:.....	89
2.2.5	Fluorescence Imaging	89
2.2.6	Image Optimisation	90
2.2.7	Image Analysis	90
2.2.7.1	Macros for Analysing Images.....	94
2.2.8	Fusion Assay Mathematics & Equations	95

2.2.9	Adhesion Assay	98
2.2.10	Tandem Fluorescence-Scanning Electron Microscopy (Flu-SEM) of MGCs 100	
2.2.11	Luminex® ELISA of Fusion Assay Supernatants.....	101
3	Chapter 3: Total Monocyte Fusion.....	103
3.1	Results.....	103
3.1.1	Optimisation of the Fusion Assay	103
3.1.2	Fusion Kinetics of Total Monocytes	109
3.1.3	Adherence of Total Monocytes Cultured In Anti-Tetraspanin Antibodies 113	
3.1.4	Comparison of Fusion from Adherence and MACS Purified Total Monocytes.....	113
3.1.5	Fusion of Adherence Purified Total Monocytes Cultured With Dual Anti- Tetraspanin Antibodies.....	121
3.2	Discussion.....	129
4	Chapter 4: Monocyte Subset Fusion	138
4.1	Introduction	138
4.2	Fusogenic Properties of Monocyte Subsets	138
4.3	Subset Contributions to Fusion	140
4.4	Fluorescence-Scanning Electron Microscopy of Monocyte Subsets	144
4.5	Fusion Kinetics of Monocyte Subsets.....	148
4.6	Analysis of Cytokine Production by Monocyte Subsets Undergoing Fusion	153
4.7	Monocyte Subsets Cultured with Anti-Tetraspanin Antibodies	158
4.8	Discussion:.....	168
5	Chapter 5: Tetraspanin Expression in Monocyte Subsets	177
5.1	Introduction	177
5.2	Results.....	178
5.2.1	Surface Expression of Tetraspanins on Human Monocyte Subsets.....	178
5.2.2	Comparison of CD9 ^{Low} and CD9 ^{High} Classical Monocytes.....	182
5.2.3	Surface Expression of Tetraspanins on FACS Sorted Monocyte Subsets After 4hrs Culture in +/-ConA Media.	188
5.3	Discussion.....	195
6	Chapter 6: Final Discussion.....	200
6.1	Introduction	200
6.2	Thesis Summary	201

6.3	Differential Expression of Tetraspanins in Monocyte Subsets	203
6.4	Different Fusion Potentials of Monocyte Subsets	204
6.5	Assessing The Role of Tetraspanins with Anti-tetraspanin Antibodies	206
6.6	Conclusion and Future Directions.....	208
7	Bibliography	210

LIST OF FIGURES

Figure 1.1: Differentiation of Human Monocyte Subsets from Haematopoietic Stem Cells.....	20
Figure 1.2: Classification of the three monocyte subsets based on relative CD14 and CD16 expression.	22
Figure 1.3: Simplified Mechanism of TNF α and IL-1 Activation of the NF- κ B.....	29
Figure 1.4: Polarised vs Spectral Activation Model for Monocyte Differentiation.....	31
Figure 1.5: The Monocyte Family Tree.....	32
Figure 1.6: Structure of a TB Induced Granuloma	41
Figure 1.7: Mechanisms of Macrophage Polarisation.....	44
Figure 1.8: Theoretical Model of MFR-CD47 Tethering of Fusing Membranes	48
Figure 1.9: Tetraspanin Primary Structure Distance Tree	55
Figure 1.10: 3D Crystal Structure of CD81 with Predicted Transmembrane Regions.	56
Figure 1.11: Theoretical Model for Formation of a Tetraspanin Enriched Microdomain or “Tetraspanin Web”	59
Figure 1.12: Interactions of Tetraspanins, Adherence Proteins and Fusion Receptors.	62
Figure 2.1: Components of PBMCs Isolated from Human Blood.....	77
Figure 2.2: Components of MACs Isolated Cells from Human Blood.....	79
Figure 2.3: FACS Gating Strategy of Monocyte Subsets from MACs Isolated Cells...	81
Figure 2.4: FACS Gating Strategy of CD9 ^{Low} CD36 ^{Low} and CD9 ^{High} CD36 ^{High} Classical Monocytes	83
Figure 2.5: Gating of Subset Derived MGCs for Flow Cytometric Analysis.....	87
Figure 2.6: Effect of Background Reduction on Image Channel Noise	91
Figure 2.7: Morphologies of The Three MGC Types Observed During Fusion Assays.	92
Figure 3.1: Optimisation of Fusion Assay	104
Figure 3.2: Fusion Kinetics of Total Monocytes.....	110
Figure 3.3: MGC Types Generated from Fusion Kinetics Analysis of MACS Purified Total Monocytes.	112
Figure 3.4: Total Monocyte Adherence after 2hr Incubation with Anti-Tetraspanin Antibodies.	114
Figure 3.5a: Sample 10x Images from Fusion Assays (Part 1/2).....	115
Figure 3.6a: Comparison of Fusion Results from Adherence and MACs Purified Monocytes (Part 1/2)	117
Figure 3.7: MGC Types Generated from Adherence or MACs Purified Total Monocytes.	119
Figure 3.8a: Median Nuclei per MGC of Adherence Purified Monocytes Cultured with Dual Anti-Tetraspanin Antibodies.	122

Figure 3.9: MGC Types Generated from Adherence Purified Monocytes Cultured with Dual Anti-Tetraspanin Antibodies.	127
Figure 4.1: Monocyte Subset Contributions During Fusion.	139
Figure 4.2: Fluorescence Microscopy of Monocyte Subset Derived MGCs.	141
Figure 4.3: Fusion Parameters for Monocyte Subset Fusion.	142
Figure 4.4: MGC Types Generated from FACS Purified Monocyte Subsets.	143
Figure 4.5: SEM Monocyte Subset Derived MGCs.	145
Figure 4.6: Flu-SEM Images of Nuclear Arrangement Within MGCs.	149
Figure 4.7: Fusion Kinetics of Monocyte Subsets.	150
Figure 4.8: Subset Fusion Kinetics - Nuclear State Analysis.	151
Figure 4.9: Subset Fusion Kinetics – MGC Type Analysis.	152
Figure 4.10: Fusion Cytokines	154
Figure 4.11: Fluorescence Microscopy of Monocyte Subset Derived MGCs Cultured with Anti-Tetraspanin Antibodies.	159
Figure 4.12: Fusion Parameters for Monocyte Subsets Cultured with Anti-Tetraspanin Antibodies.	164
Figure 4.13: Monocyte Subsets Cultured with Anti-Tetraspanin Antibodies - Nuclear State Analysis.	165
Figure 4.14: Monocyte Subsets Cultured with Anti-Tetraspanin Antibodies – MGC Type.	167
Figure 5.1: Surface Expression of Tetraspanins on Human Monocyte Subsets.	179
Figure 5.2: Histograms for Surface Expression of Tetraspanins on Human Monocyte Subsets.	180
Figure 5.3: Tetraspanin Co-Expression on Human Monocyte Subsets.	181
Figure 5.4: Surface Expression of Tetraspanins on CD9 ^{Low} vs CD9 ^{High} Classical Monocytes	183
Figure 5.5: Histograms for Surface Expression of Tetraspanins on CD9 ^{Low} and CD9 ^{High} Classical Monocytes.	184
Figure 5.6: Comparison of Fusion Results from Total, CD9 ^{Low} & CD9 ^{High} Classical Monocytes from Different FACS Isolation Methods.	185
Figure 5.7: MGC Types Formed from CD9 ^{Low} vs CD9 ^{High} Classical Monocytes from Different FACS Isolation Methods.	186
Figure 5.8: Surface Expression of Tetraspanins on FACS Sorted Monocyte Subsets After 4hrs Culture in +/-ConA Media.	189
Figure 5.9: Comparison of Surface Tetraspanin Expression on FACS Sorted Monocyte Subsets After 4hrs Culturing in ConA Media.	190
Figure 5.10: Histograms for Surface Expression of Tetraspanins on Monocyte Subsets in +/-ConA Media.	191
Figure 5.11: Quantification of Bimodal Populations in Fusion Initiated Monocyte Subsets.	194
Figure 5.12: Theoretical Explanation for the Increased Fusion in Indirectly labelled CD9 ^{High} Classical Monocytes.	199

LIST OF TABLES

Table 1: Lab Consumables.....	66
Table 2: Monocyte Negative-Selection: Magnetic Bead-Antibodies.....	71
Table 3: FACS: Monocyte Sorting Antibodies.....	72
Table 4: Flow Cytometry: Anti-Tetraspanin Positive Reporter Antibodies.....	72
Table 5: Flow Cytometry: Anti-Tetraspanin Isotype Control Antibodies	73
Table 6: Fluorescence Microscopy	73
Table 7: Other Marker Reagents	73
Table 8: Fusion Assay: Anti-Tetraspanin Phenotyping Antibodies	74
Table 9: Software	75
Table 10: MGC Types	93

ABSTRACT

Monocytes are able to undergo homotypic fusion to produce different types of multinucleated giant cells in response to infection (Langhans giant cells in tuberculosis) or rejection of foreign bodies (foreign body giant cells on medical implants). Monocytes exist as a heterogeneous population consisting of three subsets: ~85% classical, ~5% intermediate and ~10% nonclassical at steady state. However, during tuberculosis, the circulating populations of intermediate and nonclassical monocytes increase, suggesting they may play a role in the disease outcome. Monocyte fusion is a highly coordinated and complex process requiring the upregulation and expression of multiple proteins to carry out fusion. Tetraspanins are a family of membrane proteins that associate with partner proteins and other tetraspanins to form a tetraspanin enriched microdomain. Tetraspanins have been shown to associate with fusion proteins and it has been suggested that they play a role in coordinating homotypic monocyte fusion.

In this study, peripheral human monocytes were purified by FACS into classical (CD14⁺⁺CD16⁻), intermediate (CD14⁺⁺CD16⁺) and non-classical (CD14⁺CD16⁺⁺) monocytes. Monocyte subsets were induced to fuse using concanavalin A (ConA) and we showed the intermediate monocytes were able to fuse faster and form significantly larger giant cell types. Furthermore, when antibodies targeting CD9, CD53, CD63 and CD151 were added, only the intermediate monocytes showed any inhibition of fusion. A flow cytometry panel was used to report on the expression of 7 tetraspanins (CD9, CD37, CD53, CD63, CD81, CD82 & CD151) on the surface of monocytes before and after addition of ConA. We found that freshly isolated intermediate monocytes are particularly tetraspanin abundant. After 4hrs of culture in ConA, the subsets all show a significantly decreased expression of CD37, CD53 and CD82. We also identified a small population of CD9^{High} CI that also expressed higher levels of CD63, CD81 and CD151 compared to CD9^{Low}. However, the CD9^{High} CI did not show any greater potential to fuse and its role in immunity remains unknown.

ABBREVIATIONS

µm/µg	Micrometre/microgram
Å	Ångström
Akt	Protein kinase B (or PKB)
APC	Antigen presenting cell
β-hCG	β-human chorionic gonadotropin
B-S	Biotin-Streptavidin
BSA	Bovine Serum Albumin
CCL2	Chemokine receptor type 2 ligand (or MCP-1)
CCR#	Chemokine receptor type #
cDC	Classical dendritic cells
cIMDM	Complete Iscove's Modified Dulbecco's Medium
CI	Classical monocyte
CLP	Common lymphoid progenitor
cMOP	Common monocyte progenitor
CMP	Common myeloid progenitor
ConA	Concanavalin A
CX3CR1	CX3C chemokine receptor 1
Da	Daltons
DAMP	Damage-associated molecular pattern
DAP12	DNAX activating protein of 12kD
DC-STAMP	Dendritic cell-specific transmembrane protein
EC	Extracellular
EDTA	Ethylenediaminetetraacetic acid
ERM	Ezrin-radixin-moesin
EWI-2	Glu-Trp-Ile motif protein 2 (or immunoglobulin superfamily member 8 or IGSF8 or CD316)
FACS	Fluorescence-Activated Cell Sorting
FBGC	Foreign Body Giant Cell
FCS	Foetal calf serum
FcεRI	Fragment crystallisable epsilon receptor 1 (IgE receptor)
FI	Fusion Index
Flu-SEM	Tandem fluorescence-scanning electron microscopy
GAS	Gamma activated sequence
GM-CSF	Granulocyte-macrophage colony-stimulating factor
GMP	Granulocyte-macrophage progenitor
hASCT1/2	Human sodium-dependent neutral amino acid transporter type 1/2
HEPES	4-(2-hydroxyethyl)-1-piperazineethanesulfonic acid
HLA-DR	Human leukocyte antigen – antigen D related
hPL	Human placental lactogen
HS	Human Serum
HSC	Hematopoietic stem cell

HTLV-1	Human T-cell leukaemia virus type 1
IC	Intracellular
ICAM-1	Intercellular adhesion molecule 1 (or CD54)
IFNγ	Interferon gamma
IgG	Immunoglobulin G
IKK	I κ B kinase
IL-#	Interleukin-#
IL-1RA	IL-1 receptor antagonist
IMCB	Institute of Molecular and Cell Biology
Int	Intermediate monocyte
ITAM	Immunoreceptor tyrosine-based activation motif
Jak	Janus kinase
LFA-1	Lymphocyte function-associated antigen 1 (or α L β 2 or CD11a:CD18)
LGC	Langhans Giant Cell
LPS	Lipopolysaccharide
Ly6C+	Lymphocyte antigen 6 complex
M1/M2	Pro-inflammatory/Alternative Macrophage
MACS	Magnetic-Activated Cell Sorting
M-CSF	Macrophage colony-stimulating factor
MDP	Macrophage-dendritic precursor
MDR-TB	Multiple drug resistant <i>Mycobacterium tuberculosis</i>
MFR	Macrophage fusion receptor
MGC	Multinucleated giant cell
MHC-II	Major histocompatibility complex 2
MMP-9	Matrix metalloprotease-9
moDC	Monocyte derived inflammatory dendritic cells
Mtb	<i>Mycobacterium tuberculosis</i>
MyD88	Myeloid differentiation primary response gene 88
Mϕ	Macrophage (unpolarised)
n/a	Not applicable
NADPH	Nicotinamide adenine dinucleotide phosphate
NCI	Nonclassical monocyte
NFATc1	Nuclear factor of activated T-cells, cytoplasmic 1
NF-κB	Nuclear factor kappa-light-chain-enhancer of activated B cells
NK-cell	Natural killer cell
p/s	Penicillin + streptomycin
P2X7	P2X purinoceptor 7
PAMP	Pathogen-associated molecular pattern
PBMC	Peripheral blood mononuclear cell
PBS(w/o)	Phosphate Buffered Saline (without Ca ²⁺ or Mg ²⁺)
PBSE	Phosphate Buffered Saline + EDTA
pDC	Plasmacytoid dendritic cells
PFA	Paraformaldehyde
pH	Potential Hydrogen
PI3K	Phosphatidylinositol 3-kinase

PRR	Pattern recognition receptor
psi	Pounds per square inch
Rab#	Ras-related protein #
RANKL	Receptor activator of NF- κ B ligand
RANTES	Regulated on activation, normal T cell expressed and secreted (or CCL5)
RBC	Red blood cell
RGB	Red green blue
RNA	Ribonucleic acid
ROI	Region Of Interest
SEM	Scanning electron microscopy
SGC	Syncytial Giant Cell
SIgN	Singapore Immunology Network
STAT	Signal transducer and activator of transcription
STED	Stimulated emission depletion
TB	Tuberculosis
TEM	Tetraspanin enriched microdomain
TGF-β1	Transforming growth factor- β 1
Th1/Th2	T-cell helper cells type 1/type 2
TLR	Toll-like receptor
TNFα	Tumour necrosis factor alpha
TRADD	Tumour necrosis factor receptor type 1-associated DEATH domain protein
TRAP	Tartrate-resistant acid phosphatase
TREM-2	Triggering receptor expressed by myeloid cells 2
Tspan	Tetraspanin
Tyk#	Tyrosine kinase #
v/v or w/v	Volume/volume or weight/volume
WD	Working distance
WHO	World Health Organisation
XDR-TB	extensively drug-resistant <i>Mycobacterium tuberculosis</i>

CHAPTER 1: INTRODUCTION

1.1 THE HUMAN IMMUNE SYSTEM

The human immune system is a dynamic multicellular network that has evolved to respond to a seemingly limitless array of threats. The cells of the immune system, leukocytes, are able to sense and eliminate foreign threats with a variety of different methods. All leukocytes originate from a single multipotent hematopoietic stem cell (HSC) progenitor in the bone marrow. Leukocytes are formed as a result of multiple differentiations co-ordinated by an ensemble of different signals. Leukocytes are divided into two major types based on their initial differentiation from HSC; myeloid or lymphoid.

The myeloid cells consist of the monocytes, granulocytes and mast cells of the innate immune system. These cells are typically short lived and are able to sense and respond to a broad range pathogens. Myeloid progenitors are also able to differentiate into platelet-producing megakaryocytes and erythrocyte precursors that develop into oxygen-carrying red blood cells. The lymphoid cells consist of the T-cells and B-cells of the adaptive immune system and the natural killer cells (NK-cells) of the innate immune system. T-cells are able to interact, detect and kill virally infected host cells. B-cells confer humoral responses by secreting antibodies to pathogenic antigens that can agglutinate bacteria and enhance phagocytosis. NK-cells are able to sense and attack virally infected host cells (like T-cells) and even identify and eliminate tumour cells. Though NK-cells are derived from lymphoid cell progenitors they have long been classified in the innate immune system, however, recent studies (Arase *et al.*, 2002; Daniels *et al.*, 2001; Peng *et al.*, 2013; Sun *et al.*, 2009) have identified NK-cells with memory features just like T-cells and B-cells.

Leukocytes are not limited to this brief list of processes but are in fact versatile and able to alter their functions further depending on the location and severity of a threat. Throughout the course of human existence there have been viruses and pathogens that test our immune systems each in their own unique way. Human immune systems have evolved in a way to combat a wide-range of both new and old threats. The

attempt to unravel the intricacy of the human immune system has led to the discoveries of various subsets, elaborate cytokine networks and novel mechanisms of host defence. This introduction will focus on the complexities associated with just one cell type, the monocyte.

1.1.1 THE MONOCYTE LINEAGE

Before describing the biological origins of the monocyte it is important to explore and respect the historical origins of the phagocytic system. The age of leukocytes began in 1843, when, rather miraculously, the French pathologist Gabriel Andral (1797-1876) and British physician William Addison (1802-1881) both reported independently the first ever descriptions of leukocytes. These findings opened up new avenues for future research into the role of these odd new white-blood cells in human pathology. In 1873, Julius Cohnheim (1839-1884) observed and demonstrated the migration and extravasation of leukocytes to a site of inflammation in frog's tongues that he pinned to a corkboard. Cohnheim's simple model demonstrated that leukocytes could actively target injured tissues and laid the groundwork for future studies in chemotaxis.

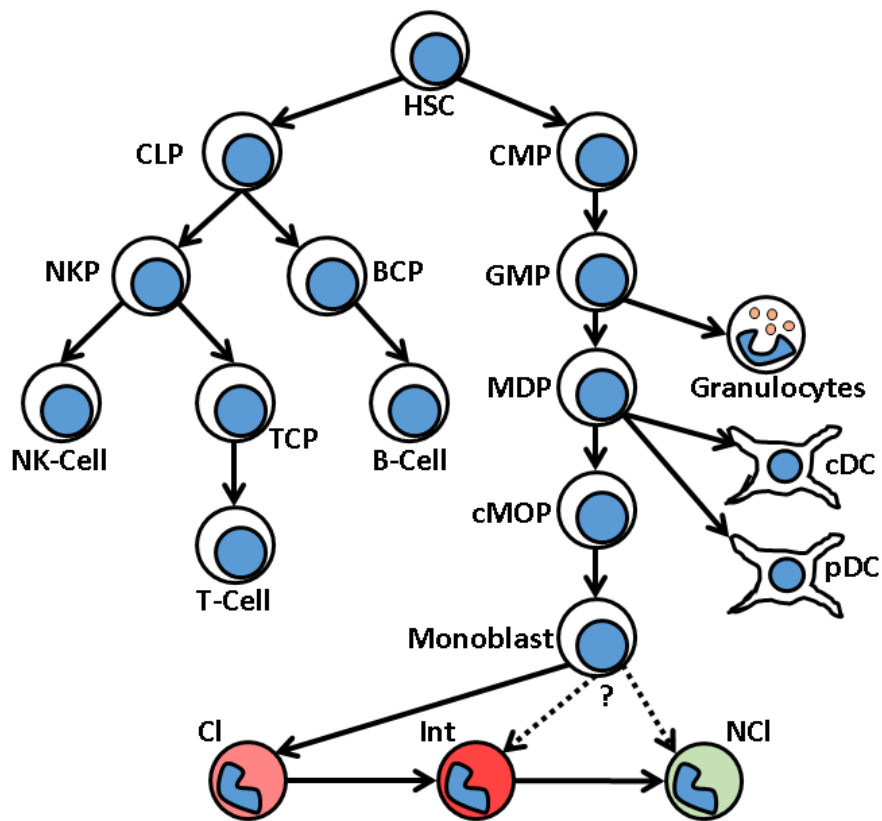
The first description and identification of phagocytes from leukocytes came from a Russian zoologist named Elie Metchnikoff (1845-1916). In 1882 Metchnikoff observed for the first time phagocytes surrounding and digesting foreign bodies in transparent starfish larvae. He also injected bacilli into the subcutaneous tissues of frogs and observed host leukocyte chemoattraction to the site of infection. Metchnikoff has since been credited as the discoverer of cell mediated immunity and in 1908 shared a Nobel Prize in physiology and medicine with Paul Ehrlich who is equally credited as the discoverer of humoral immunity. Controversially, Metchnikoff believed that phagocytosis occurred in both steady-state tissues to clear away host debris as well as in inflamed tissues to target pathogens.

The discovery of phagocytes by Metchnikoff set into motion a tide of further research in the field of immunology. In 1901 Rudolf von Limbeck (1862-1900) demonstrated that phagocytes were recruited from the blood and targeted sites of inflammation through chemoattraction. Von Limbeck did this by injecting *Staphylococcus aureus*

into the joints of dogs and observed that the number of circulating leukocytes increased before accumulating in the infected tissues. This phenomenon would later be attributed to the differentiation of circulating monocytes into tissue-bound macrophages. Less than a decade later, in 1909, the advances in cinematography allowed Jean Comandon (1877-1970) and colleagues to record and distribute moving images of *Trypanosomes* being phagocytosed for the first time. The monocyte/macrophage family grew by another member in 1973 when Zanvil Cohn (1926-1993) and Ralph Steinman (1943-2011) published their findings on the isolation and identification of dendritic cells from mouse spleen. The discovery of dendritic cells as antigen presenting cells was a pinnacle finding in linking the innate and adaptive immune systems. Over the last few decades, with the use of immunolabeling and flow cytometry, the complexity and diversity of the innate immune system has exploded. It is unlikely that 134 years ago when Metchnikoff was observing phagocytes surrounding splinters within transparent larvae that he grasped the complexity of the system he had discovered. The more recent discoveries in monocyte differentiation and origins from the bone marrow will now be explored in detail.

Monocytes, unlike most other leukocytes, are able to differentiate into distinct cell types that possess their own morphological features and immunological processes. Like other myeloid cells, monocytes originate within the bone marrow. HSCs differentiate into a common lymphoid progenitor (CLP) or a common myeloid progenitor (CMP) that subsequently differentiates into granulocyte-macrophage progenitors (GMP) (Figure 1.1). Further differentiation in the bone marrow transforms GMP into monoblasts – the committed monocyte precursor. Once these mature into monocytes, they enter the bloodstream where they circulate continuously and act as a reservoir ready to migrate and enter into steady-state or inflamed tissues and further differentiate into macrophages (M ϕ) or dendritic cells (moDC).

Current research in mice has shown that between the GMP to monocyte stage, the GMP cells differentiate into a macrophage-dendritic precursor (MDP) that after transplantation could no longer form granulocytic cells but could generate new monocytes, macrophages and DC (Fogg *et al.*, 2006).



Classical	Intermediate	NonClassical
Subset Markers: CD14 ⁺⁺ CD16 ⁻ HLA-DR: Low	Subset Markers: CD14 ⁺⁺ CD16 ⁺ HLA-DR: High	Subset Markers: CD14 ⁺ CD16 ⁺⁺ HLA-DR: Med
Adhesion: CD11b: High CD54: Med CD62L: High	Adhesion: CD11b: High CD54: High CD62L: Low	Adhesion: CD11b: Low CD54: Med CD62L: Low
Migration: CCR2: High CX3CR1: Low	Migration: CCR2: Low CX3CR1: Med	Migration: CCR2: Low CX3CR1: High
Differentiation: CSF1R: Low CSF3R: High	Differentiation: CSF1R: Med CSF3R: Med	Differentiation: CSF1R: High CSF3R: Low

Figure 1.1: Differentiation of Human Monocyte Subsets from Haematopoietic Stem Cells

In the bone marrow HSCs are able to differentiate to produce any of the leukocytes of both the lymphatic and myeloid lineages. Various myeloid precursors have been isolated and ordered based on their potential to differentiate into decedent cells. HSC: Haematopoietic stem cell, CLP: Common lymphocyte progenitor, NKP: Natural killer progenitor, TCP: T-cell progenitor, BCP: B-cell progenitor, CMP: Common myeloid progenitor, GMP: Granulocyte-macrophage progenitor, MDP: Macrophage-dendritic precursor, cDC: Classical Dendritic Cell, pDC: plasmacytoid Dendritic Cell, cMOP: Common monocyte progenitor CI: Classical, Int: Intermediate, NCI: Nonclassical monocyte.

In 2013, Hettinger *et al.* identified a common monocyte progenitor (cMOP) in mice that could no longer differentiate into classical dendritic cells (cDC) or plasmacytoid dendritic cells (pDC) but could still form monocytes, M ϕ and monocyte-derived dendritic cells. Human equivalents of MDP and cMOP have also been recently reported (Lee *et al.*, 2015).

Human blood monocytes do not exist as one single population. In 1989, Passlick and colleagues used flow cytometric analysis to identify a small monocyte subset that expressed both CD14 and CD16; later termed 'nonclassical' monocytes to distinguish them from the CD14^{High}CD16⁻ 'classical' monocytes. CD14 is a co-receptor for toll-like receptor 4 (TLR4), together they detect extracellular bacterial lipopolysaccharide (LPS). CD16 is a low-affinity Fc γ RIII receptor that binds the Fc domain of IgG and has been suggest to aid monocytes in the phagocytosis of antibody opsonised pathogens (Clarkson and Ory, 1988). The complexity of monocyte subsets grew when in 2001 a paper by Grage-Griebenow *et al.* reported the existence of more than one population of CD16⁺ monocytes. Like classical monocytes these cells expressed high levels of CD14 but had low CD16 expression, existed as a very small percentage of the blood monocyte population (<10%) and served separate functions. These monocytes were therefore thought to be an "intermediate" state between the classical and the nonclassical monocytes and were largely overlooked as a unique subset (Figure 1.2).

In 2010 the Nomenclature Committee of the International Union of Immunological Societies accepted the classification of human monocytes into classical (Cl), intermediate (Int) and nonclassical (NCl) monocytes (Ziegler-Heitbrock *et al.*, 2010). The very next year two vast gene profiling reports were published detailing many of the unique attributes of each subset and solidifying their individual nature (Wong *et al.*, 2011; Zawada *et al.*, 2011). The origin of the Int and NCl monocytes is largely unknown. Multiple studies have observed an increase in the NCl monocyte population coupled with a decrease in Cl monocytes but with no overall change to total monocyte number (Mukherjee *et al.*, 2015; Semnani *et al.*, 2014; Sunderkotter *et al.*, 2004; Ziegler-Heitbrock *et al.*, 2010). It is therefore widely regarded that Int and NCl monocytes are at least in some part derived from Cl monocytes (Zawada *et al.*, 2012).

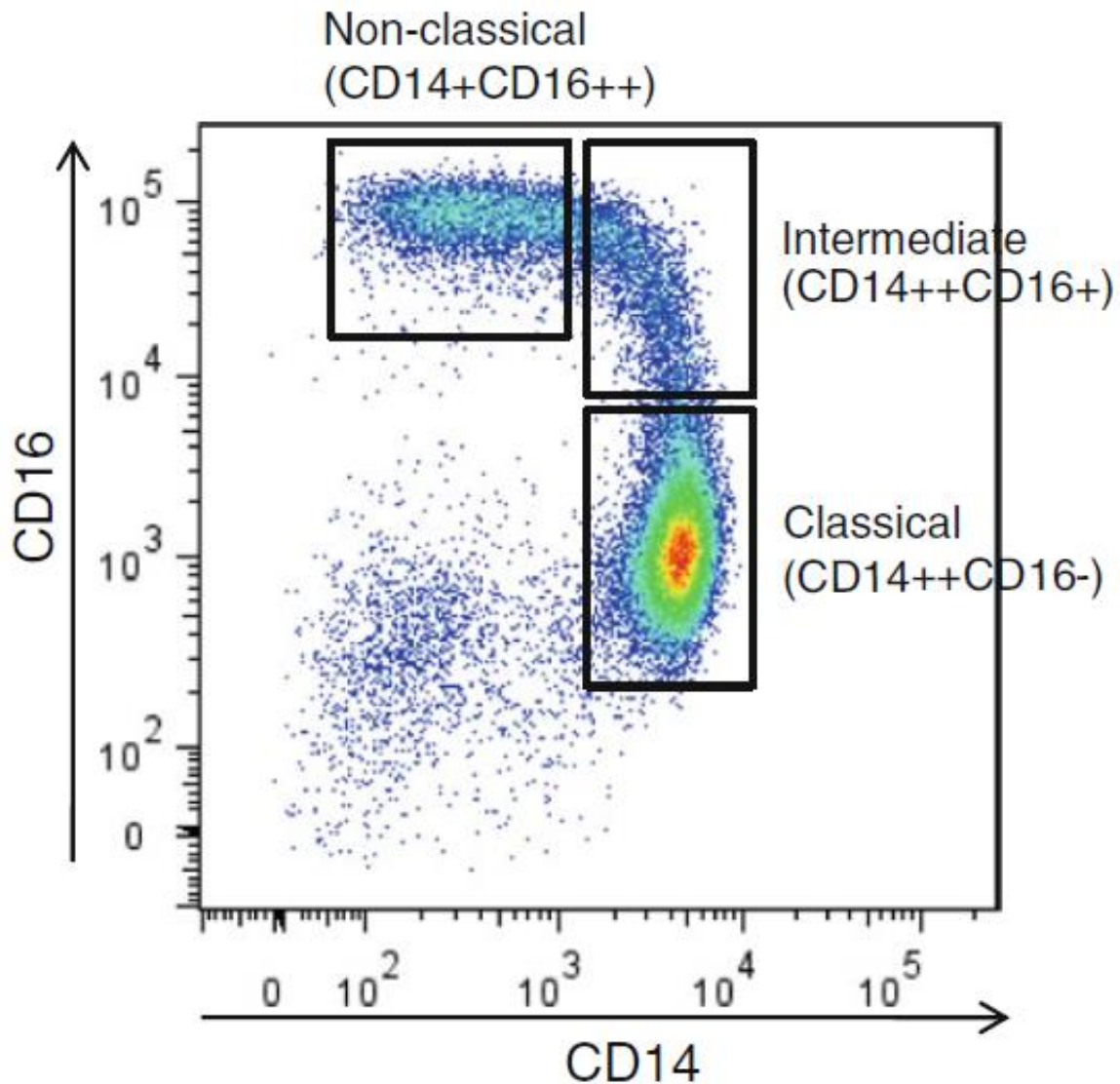


Figure 1.2: Classification of the three monocyte subsets based on relative CD14 and CD16 expression.

Human monocyte subsets in blood can be separated into three functionally distinct subsets. Classical monocytes are characterised by high expression of CD14 and lack of CD16 expression, intermediate monocytes are positive for both CD14 and CD16 and nonclassical monocytes express less CD14 and have a relatively high CD16 expression. Subset population sizes are donor dependent and many diseases cause shifts of one subset to another. At steady state the ratio of Classical: Intermediate: Nonclassical $\sim 85:5:10\%$.

From (Wong et al., 2012) with permissions.

1.1.1.1 TISSUE RESIDENT MACROPHAGES – A STORY OF ORIGINS

It was originally thought that M ϕ found in the tissues all originated from circulating monocytes in the blood. This concept of a mononuclear phagocytic system from bone marrow to blood to tissue was coined by van Furth and colleagues in 1972 (van Furth et al., 1972). However, the simple inflammatory M ϕ concept evolved as tissue specific M ϕ were identified and were found to possess proliferative abilities (Gordon and Taylor, 2005; Lichanska and Hume, 2000; Ovchinnikov, 2008). In 2004, Kanitakis and colleagues reported their observations made on a double hand transplant patient who possessed Langerhans macrophages from the donor, but were still self-proliferating four years after amputation. In 2013 two independent studies used fate mapping and murine models to show that tissue resident alveolar macrophages were self-proliferative cells that were not seeded from circulating monocytes (Hashimoto et al., 2013; Yona et al., 2013).

It is now known that tissue resident macrophages exist in a number of different tissues and organs such as brain microglia (Ajami et al., 2007), cardiac macrophages (Epelman et al., 2014), adipose tissue (Amano et al., 2014) and more. Some tissue macrophages such as those found in the intestine (Bain et al., 2014) and dermis (Zigmond and Jung, 2013) are in least some part replenished from monocyte precursors. Studies in murine models has led to the current paradigm that tissue resident macrophages originate during early yolk sac to embryo development and are seeded from erythromyeloid progenitor cells (Lavin et al., 2015; Yona et al., 2013). As the foetus develops organs and defined tissues these tissue resident macrophages are incorporated into the tissues and self-proliferate throughout life.

Compared to the monocyte-derived inflammatory macrophages, tissue resident macrophages tend to play a more M2-like role and maintain the resident tissue by scavenging dead cells, promoting wound healing and carrying out tissue specific functions (Davies et al., 2013; Kierdorf et al., 2015). Such examples of tissue specific maintenance include synaptic pruning of neurones by microglia (Paolicelli et al., 2012),

regulation of insulin sensitivity by adipose M ϕ (Odegaard et al., 2007), clearance of debris in the lung by alveolar M ϕ (Maus et al., 2002) and ruptured erythrocyte clearance by Kupffer cells in the liver (Ganz, 2012).

1.1.1.2 OF MICE AND MEN – A TALE OF TWO MODELS

Before exploring further into the literature on monocyte subsets and their possible pathways of differentiation in the tissues it is important to address the differences between human and mouse models. Much, if not most, of the experimental studies conducted on monocyte subsets, mapping their differentiation pathways and formation of multinucleated giant cells (MGC) has been conducted in mice. An increasing number of studies are revealing biologically significant differences between the two species which raises doubts about the applicability of the mouse model to human immunity. Human monocyte subsets are usually described as CI (CD14⁺⁺CD16⁻), Int (CD14⁺⁺CD16⁺) and NCI (CD14⁺CD16⁺⁺) monocytes (Ziegler-Heitbrock *et al.*, 2010). At steady state, the distribution of the subsets is 85% CI, 5% Int and 10% NCI in the bloodstream (or 17:1:2) (Wong *et al.*, 2012). Multiple studies have shown an expansion of the Int and NCI subsets during fusion-related inflammatory diseases such as tuberculosis (Castaño *et al.*, 2011), Crohn's disease (Grip *et al.*, 2007), hepatitis B (Zhang *et al.*, 2011a) and rheumatoid arthritis (Rossol *et al.*, 2012).

Murine monocyte subsets have been categorised in multiple ways over the past decade due to the ever growing list of their markers. A team in 2014 sought to simplify the nomenclature based on cell ontogeny and proposed that mouse subsets can be regarded as classical (Ly6C^{High}) or nonclassical (Ly6C^{Low}) (Guilliams *et al.*, 2014). Though many other labelling systems exist for mouse subsets the predominating feature is the absence of the intermediate subset. Some studies have tried to classify mouse monocyte subsets phenotypically into 3 subsets in harmony with the human subsets (Ziegler-Heitbrock *et al.*, 2010), however, most studies persist in a classical and nonclassical nomenclature. Unlike humans, murine models possess an equal 1:1 ratio of classical (Ly6C^{High}): nonclassical (Ly6C^{Low}) monocytes (Geissmann *et al.*, 2003; Sunderkotter *et al.*, 2004).

The greatest discrepancies between human and mouse models was revealed in 2010 by Ingersoll *et al.* who utilised microarrays to screen hundreds of expressed genes in both human and mouse subsets. They also used flow cytometry to compare the expression levels of 24 proteins of interest. In relation to this study in monocyte fusion, they found that three monocyte fusion markers CD9, CD81 and CD36 (their roles in fusion are discussed below) were all differently expressed between human and mouse monocytes (Ingersoll *et al.*, 2010). Specifically, CD9 expression was higher in human CD16⁻ monocytes than CD16⁺, however, in mice this was reversed as Ly6C^{High} classical monocytes possessed the higher expression of CD9. CD81 was detected by flow cytometry in both human subsets but only detected at very low levels in all mouse monocytes. CD36 was higher in human CD16⁻ than CD16⁺ monocytes but in mice the Ly6C^{High} was lower than Ly6C^{Low} monocytes for CD36. CD9 and CD81 have been reported to play a vital role in monocyte fusion (Parthasarathy *et al.*, 2009; Takeda *et al.*, 2003) and CD36 is a scavenger receptor that has been shown to participate in the formation of multinucleated giant cells (Helming *et al.*, 2009). Because of these differences, any murine-derived fusion studies should be viewed with caution and for the purposes of this investigation only human monocytes will be used.

1.1.1.3 MONOCYTE SUBSETS

As previously mentioned there are currently three accepted subsets of human monocytes; CI, Int and NCI monocytes (Ziegler-Heitbrock *et al.*, 2010). Much research in the past decade has attempted to reveal the specific roles of each of the different subsets and their contribution to disease. It should be noted however, that there remain many mysteries of the pathways of differentiation and there appear to be many overlaps in functions shared between the subsets. On a transcriptomic level, the Int and NCI monocytes share more similarities with one another, differing in only 249 genes. Understandably, the Int monocytes were found to be the most transcriptomically similar of the CD16⁺ monocytes to the CI subset – differing by the expression of 942 genes (Wong *et al.*, 2011). Interestingly the Int and NCI subsets showed a greater susceptibility to apoptosis compared to the classical monocytes when exposed to reactive oxygen species (Zhao *et al.*, 2010) and TB (Castaño *et al.*,

2011). These findings were later confirmed on a genetic level by Wong *et al.* (2011) and attributed to the concept that Int and NCI are late-stage monocytes.

CI have been labelled as the primary phagocytosing cells (Cros *et al.*, 2010) and have been shown to be able to detect pathogen-associated molecular patterns (PAMP) via pattern recognition receptors (PRR) such as toll-like receptors and respond by internalising bacterial antigens by phagocytosis (Antonelli *et al.*, 2014; Cros *et al.*, 2010; Yang *et al.*, 2014a). CI have also been shown to be the most responsive of the three subsets to multicellular nematode antigens (Semnani *et al.*, 2014). However, two different studies have reported that the Int were the most effective at phagocytosing *Plasmodium vivax* infected red blood cells (Antonelli *et al.*, 2014; Zhou *et al.*, 2015). Wong and colleagues also found that steady state CI transcribed genes for angiogenesis at far higher levels than the Int or NCI, whose transcription patterns favoured MHC class II production and cell migration proteins respectively (Wong *et al.*, 2011). This is in accordance with the Int subset being labelled the “inflammatory” subset and NCI the “patrolling” subset (Antonelli *et al.*, 2014; Yang *et al.*, 2014a). It seems that the subsets exist in such a way that each one can specialise to specific pathogens and responses.

Though monocytes exist in high numbers in the bloodstream, their major role is to enter the tissues, patrol, respond to steady-state or inflammatory signals and differentiate into effector cells. The Int and NCI have been shown in functional studies to be the most effective at migration and endothelial transmigration (Randolph *et al.*, 2002; Semnani *et al.*, 2014). These properties are conferred by their mutually high expression of migration proteins (Wong *et al.*, 2011) and the Int’s high transcription of cytoskeletal rearrangement genes (Semnani *et al.*, 2014) granting them the ability to rapidly reorganise their morphology during transmigration. NCI also possess the ability to inhibit tumour proliferation, in Ly6C⁻ (NCI-equivalent) deficient mice; introduction of Ly6C⁻ monocytes resulted in NCI migration to the tumour site, activation of NK-cells and prevention of tumour invasion in the lung (Hanna *et al.*, 2015).

1.1.1.4 MONOCYTE SUBSET SIGNALLING

The monocyte subsets differentially express two different chemokine receptors that coordinate their migration; C-C chemokine receptor type 2 (CCR2) and CX3C chemokine receptor 1 (CX3CR1). The CCR2 ligand (CCL2 or MCP-1) is associated with an inflammatory state and is a powerful chemoattractant for monocytes. In functional studies the subsets showed a Cl>Int>NCl order of secretion of CCL2 when infected with *P. vivax* (Antonelli *et al.*, 2014) or exposed to LPS (Cros *et al.*, 2010). On the other hand, the CX3CR1 ligand (CX3CL1) is constitutively expressed in the tissues and confers an anti-inflammatory and homeostatic setting (Griffith *et al.*, 2014). In accordance with their previously mentioned roles the Cl are (CCR2^{High}CX3CR1^{Low}), Int (CCR2^{Low}CX3CR1^{Med}) and NCl (CCR2^{Low}CX3CR1^{High}) (Wong *et al.*, 2011). Compared to the other two subsets, Int expresses much higher levels of the MHC class II complex (or HLA-DR) which presents peptides from phagocytosed pathogens to T-cells and bridges the innate and adaptive immune systems (Abeles *et al.*, 2012; Wong *et al.*, 2011).

The Cl and Int subsets secrete a repertoire of pro-inflammatory cytokines in response to PAMP to generate a local inflammatory state. Upon stimulation with LPS, the Int closely followed by the Cl subset were found to secrete the highest levels of IL-1 α , IL-1 β , IL-6 and TNF α (Cros *et al.*, 2010; Semnani *et al.*, 2014). In both studies there was no pro-inflammatory cytokine production by the NCl when cultured in LPS. Furthermore, Cros *et al.* (2010) found that after 18hrs of culturing in steady state conditions, the NCl produced significantly higher levels of IL-1 receptor antagonist (IL-1RA) compared to Cl and Int. IL-1RA binds the IL-1 receptor and acts as a competitive inhibitor dampening signalling from the pro-inflammatory IL-1 (Weber *et al.*, 2010). Walter *et al.* (2013) demonstrated that CD14^{High} (Cl and Int) monocytes when cultured in pro-inflammatory cytokines associated with rheumatoid arthritis were able to augment Treg cells into a pro-inflammatory state and secrete more pro-inflammatory cytokines.

The IL-1 family of pro-inflammatory cytokines and TNF α are all able to activate the canonical pathway of NF- κ B (Figure 1.3) (Tedgui and Mallat, 2006; Wajant *et al.*,

2003). IL-1, PAMPS and/or TNF α bind their respective receptors on the membrane (IL-1R, TLR4 and TNFR1 respectively). Once bound the IL-1R or TLR4 recruit a MyD88 adaptor (Weber *et al.*, 2010) and the TNFR1 utilises a TRADD adaptor (Wajant *et al.*, 2003) to facilitate the activation of the I κ B kinase (IKK) complex. The IKK complex is made of two kinases (α -unit and β -unit) and one regulatory protein (γ -unit), once activated the IKK complex facilitates the phosphorylation of I κ B (Pelzer and Thome, 2011; Tedgui and Mallat, 2006). In steady-state I κ B is bound to NF- κ B to inactivate it but once I κ B is phosphorylated by the IKK complex it becomes further ubiquitylated and is degraded by the proteasome. Free NF- κ B is able to enter the nucleus and enhance the expression of a whole host of pro-inflammatory cytokines; IL-1 α (Mori and Prager, 1996), IL-1 β (Hiscott *et al.*, 1993), IL-6 (Libermann and Baltimore, 1990), IL-17A (Shen *et al.*, 2006), TNF α (Shakhov *et al.*, 1990) and chemoattractants CCL2 (Ueda *et al.*, 1994), CCL3 (Widmer *et al.*, 1993) and RANTES (Moriuchi *et al.*, 1997) to attract more leukocytes to the site of inflammation.

The NF- κ B pathway also enhances the secretion of anti-inflammatory cytokines, this has been suggested to act as a dampening reaction to avoid over-inflammation (Williams *et al.*, 2004). NF- κ B is able to produce anti-inflammatory IL-10 (Cao *et al.*, 2006) and IL-13 (Hinz *et al.*, 2002). As with the pro-inflammatory cytokines, when cultured in LPS the CI and Int subsets secreted significantly more IL-10 but the NCI subset secreted significantly less (Cros *et al.*, 2010; Semnani *et al.*, 2014). IL-10 inhibition has been shown to inhibit the NF- κ B pathway by blocking the function of the IKK complex (Schottelius *et al.*, 1999) and by blocking the RNA polymerase II loading-site on the promotor (Zhou *et al.*, 2004). Another NF- κ B anti-inflammatory cytokine; IL-13, has been observed to be significantly increased in the serum of chronic systolic heart failure patients. Amir *et al.* (2012) used intracellular flow cytometry to show that NCI were able to produce high levels of IL-13 but the CI and Int did not produce any detectable IL-13.

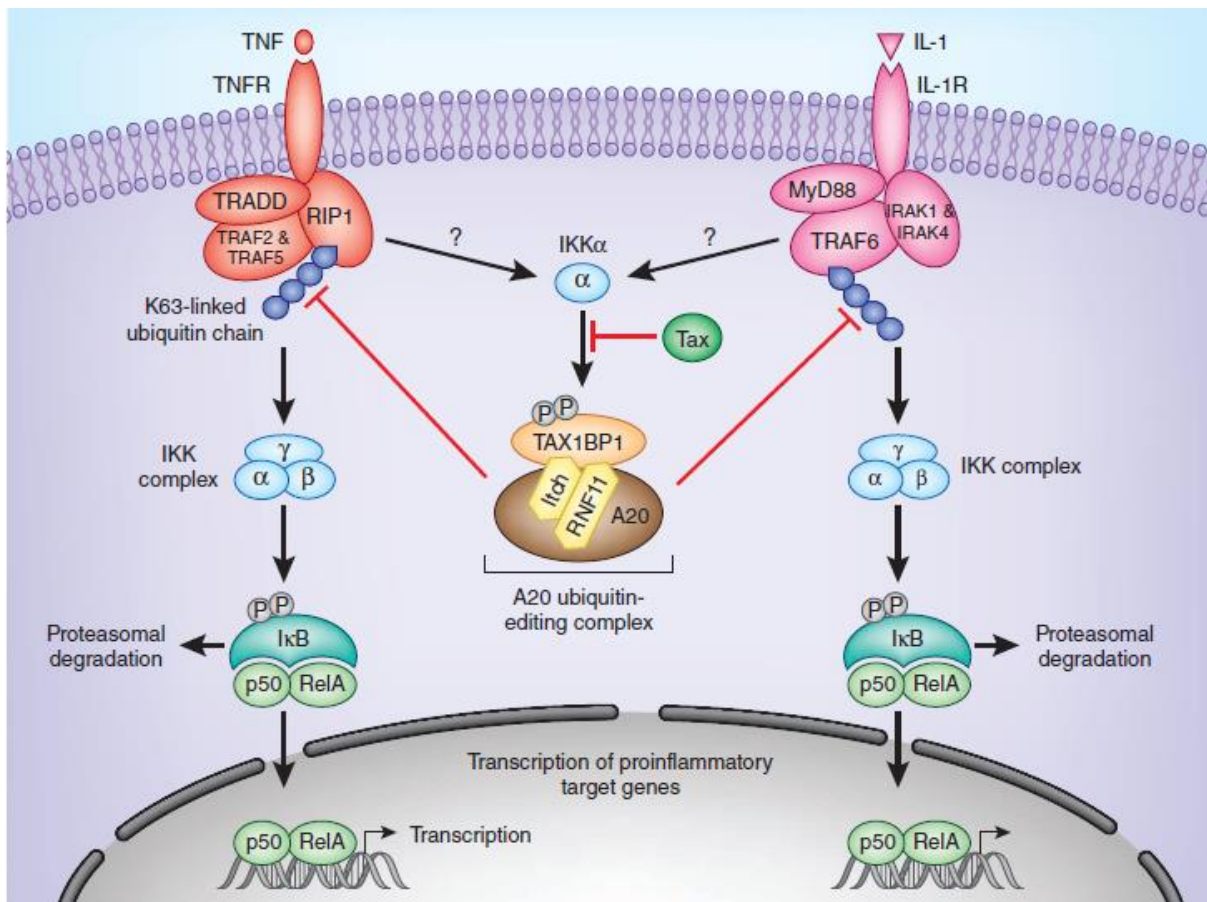


Figure 1.3: Simplified Mechanism of TNF α and IL-1 Activation of the NF- κ B

Proinflammatory cytokines TNF α and IL-1 bind their respective receptors. Binding of ligand induces TRADD or MyD88 recruitment to the respective receptors. Through a series of steps these adapter proteins lead to the activation of the I κ B kinase (IKK) complex. NF- κ B is constitutively expressed in the cytoplasm however it exists in an inactive form bound to I κ B. The now active IKK complex phosphorylates I κ B leading to its ubiquitinylation, detachment from NF- κ B and designation for degradation. Free NF- κ B enters the nucleus and promotes the transcription of gamma activated sequences (GAS).

From (Pelzer and Thome, 2011) with permissions.

1.2 MONOCYTE MONONUCLEAR DESCENDANTS: MACROPHAGES AND DENDRITIC CELLS

As mentioned previously monocytes are not terminally differentiated but can in fact sense local cytokines and react accordingly by forming effector cells that are more specialised to deal with the signal. In steady-state, NCI monocytes will enter the tissues from the bloodstream and patrol the tissues while the classical and intermediate monocytes are recruited from the bloodstream into the tissues by inflammatory signals such as CCL2. Depending on the cytokine signals and tissue location, monocytes are able to differentiate into pro-inflammatory (M1) or anti-inflammatory (M2) macrophages, inflammatory dendritic cells (moDC) or MGC.

There have been multiple studies with conflicting results on the differentiation of monocytes and what cytokines drive which destiny. Initially, macrophages were subcategorised as either "inflammatory" M1 or "repair/alternative" M2 to match their differentiation destinies with T-helper 1 and 2 cells (Th1 & Th2). Th1 cells produce IFN γ as their primary response to activation whereas Th2 cells secrete IL-4 and IL-13. IFN γ induces monocytes to form M1 (Nathan *et al.*, 1983) whereas IL-4 and IL-13 induces them to form M2 (Mills *et al.*, 2000). M1 were found to be highly pro-inflammatory, able to rapidly engulf microbes and secrete IL-1, TNF α and IL-6. M2 respond by augmenting the local environment into a wound-healing state by secreting IL-10 and IL-1RA to inhibit inflammatory cytokine production (Mantovani *et al.*, 2004).

However, the view that monocyte to M ϕ differentiation is either inflammatory M1 or repair M2 is primitive and simplified (Figure 1.4). The emerging consensus is that monocytes differentiate into a spectrum of different effector M ϕ and moDC, capable of producing different levels of pro-inflammatory and anti-inflammatory responses. Early this year Ohradanova-Repic *et al.* (2016) isolated CD14+ human monocytes, exposed them to an array of differentiation factors and used a panel of 70 antibodies to culture and classify the resultant M ϕ and moDC (Figure 1.5). They characterised seven different M ϕ ranging in function from highly M1-like (GM-CSF culture, LPS+IFN γ primed) to the highly M2-like (M-CSF culture, IL-10 primed). Granulocyte macrophage colony-stimulating factor (GM-CSF) induces the upregulation of M1 genes and is

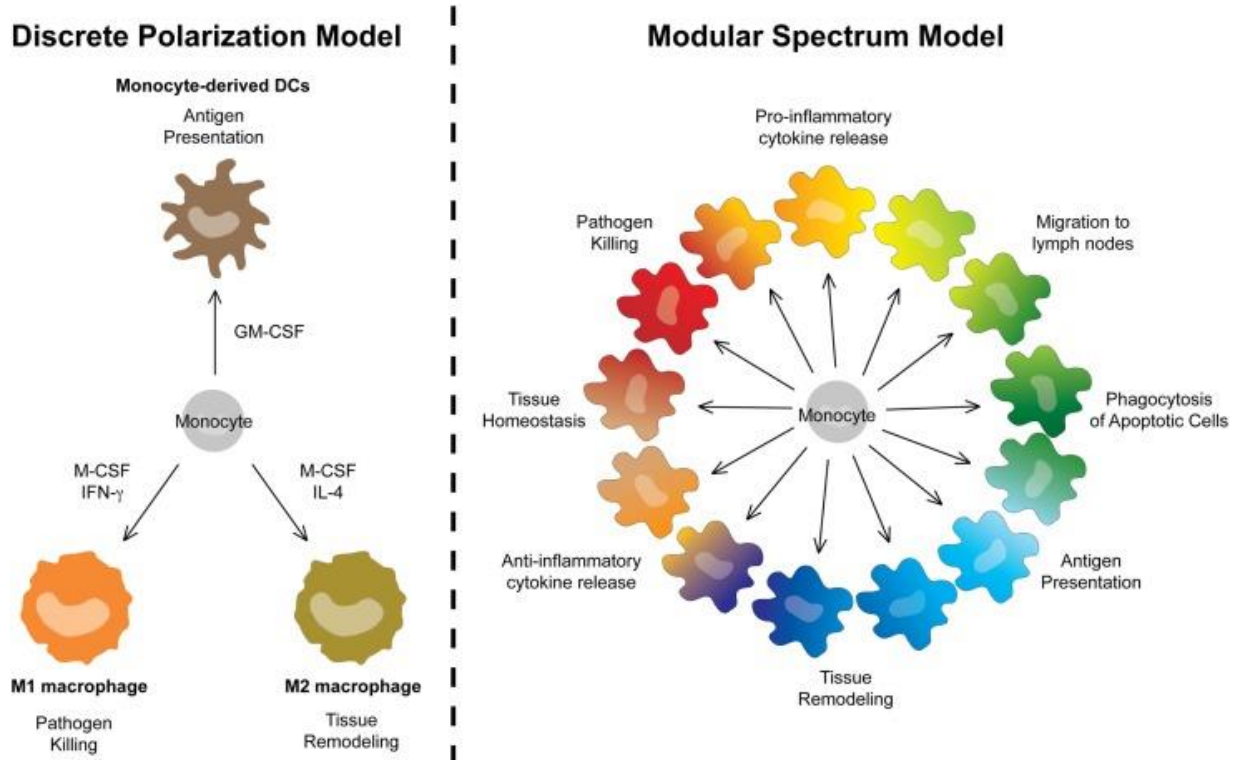


Figure 1.4: Polarised vs Spectral Activation Model for Monocyte Differentiation.

Previously it was thought that monocytes differentiate into either M1 or M2 macrophages or monocyte derived dendritic cells. However the increasing number of differentiation pathways and identification of new monocyte derived species has demonstrated the incredible plasticity of monocytes and their descendants.

From (Guilliams and van de Laar, 2015) with permissions.

associated with pro-inflammatory microenvironments while macrophage colony-stimulating factor (M-CSF) induces the expression of M2-like homeostasis and wound repair genes and is constitutively expressed in many tissues (Van Overmeire *et al.*, 2016). However, the generation of both pro-inflammatory and alternative macrophages from both GM-CSF and M-CSF as demonstrated by Ohradanova-Repic *et al.* (2016) agrees with the findings of earlier studies (Jaguin *et al.*, 2013) and demonstrates that macrophage polarity is a variable process. Ohradanova-Repic *et al.* (2016) also categorised two moDC subsets (immature and mature) from human CD14⁺ monocytes, these could be generated by culture in GM-CSF+IL-4 and the mature moDC were primed with LPS.

Little is known about the individual contribution of the monocyte subsets to the formation of different types of M ϕ and moDC and most of the work thus far has compared CD16⁻ (CI) and CD16⁺ (Int and NCI) monocytes. However, CD16⁻ monocytes have been shown in microarray analyses to express higher levels of the GM-CSF receptor while CD16⁺ monocytes express higher M-CSF receptor (Martinez *et al.*, 2006). This suggests that as the monocyte subsets mature from CI to NCI they increase in their tissue patrolling and homeostatic functions.

moDC play an important role as antigen presenting cells (APC) as they are able to phagocytose and digest pathogens and present their peptides on the MHC class II complex. The moDC can then migrate to the lymph nodes and present the peptide to B-cells to elicit a humoral response and T-cells to couple with the T-cell receptor and potentially form an immune synapse for the transfer of mRNAs, endosomes and proteins (Alarcón *et al.*, 2011; Angus and Griffiths, 2013; Martín-Cófreces *et al.*, 2014). moDC therefore represent an important bridge between the innate and adaptive immune systems. Sánchez-Torres *et al.* (2001) found that CD16⁻ derived moDC that had been cultured in LPS; secreted more IL-12. IL-12 activates NK-cells into a pro-inflammatory state and to secrete TNF α and IFN γ (Zhang *et al.*, 2011b). The CD16⁺ derived moDC responded differently; by transcribing more transforming growth factor- β 1 (TGF- β 1; dampens pro-inflammatory reactions in monocytes and M ϕ) and were able to stimulate IL-4 secretion in T-cells more than CD16⁻ moDC.

A later study confirmed that CD16⁺ monocytes form moDC that can transmigrate and reverse-transmigrate the endothelium and stimulate T-cells to a greater extent than CD16⁻ monocytes (Randolph *et al.*, 2002). Conversely, monocyte to moDC differentiation may not be necessary for effective antigen presentation. Jakubzick *et al.* (2013) showed that mouse classical (Ly6C⁺) monocytes could patrol tissues and acquire antigen before migrating to the lymph nodes without differentiating into M ϕ or moDC.

1.3 MULTINUCLEATED GIANT CELLS

Monocytes are able to undergo homotypic fusion in certain microenvironments to form a variety of different types of MGC (or polykaryons). For example, in bone tissues, monocytes are able to fuse in steady state to form multinucleated osteoclasts which digest bone material as part of bone homeostasis. However, osteoclast production and activity has been shown to be upregulated in chronic inflammatory disorders such as rheumatoid arthritis (Aeberli *et al.*, 2016), Crohn's disease (Park *et al.*, 2013) and calcified atherosclerotic plaques (Qiao *et al.*, 2015). At sites of placement of surgical implants, foreign body giant cells (FBGC) are reported to be found proximal to osteoclasts (Barbeck *et al.*, 2016; Chappuis *et al.*, 2015; Lorenz *et al.*, 2015; Morishita *et al.*, 2016). As their name suggests, FBGC form in response to foreign matter that pro-inflammatory M ϕ cannot phagocytose. When bacterial pathogens such as *Mycobacterium tuberculosis* are phagocytosed by M ϕ they are able to avoid destruction by inhibiting lysosome-phagosome fusion and arrest apoptotic pathways (Behar *et al.*, 2010; Bocchino *et al.*, 2005; Lee *et al.*, 2009) to allow the bacterium to proliferate intracellularly. Newly recruited M ϕ react to these infected M ϕ by fusing with one another to form Langhans giant cells (LGC) to engulf and encapsulate the infected cells and form a granuloma (Guirado and Schlesinger, 2013).

1.3.1 OSTEOCLASTS: AN MGC FOR BONE HOMEOSTASIS

Osteoclasts are generated *in vitro* by culturing monocytes in M-CSF and receptor activator of NF- κ B ligand (RANKL) (Cody *et al.*, 2011; Long and Humphrey, 2012). RANKL is a member of the TNF superfamily and can activate NF- κ B and its

transcription pathway to initiate the transcription of fusion promoting genes (Yu *et al.*, 2011). Komano *et al.* (2006) showed that in the presence of M-CSF and RANKL, CD16⁺ monocytes differentiated and fused to make osteoclasts more favourably than CD16⁺ monocytes. Yu *et al.* (2011) demonstrated that IL-4 and RANKL induced both inflammatory MGC and homeostatic osteoclast formation through the activation of the NF- κ B pathway. They then went on to show that in the presence of both cytokines IL-4 directed MGC formation predominated over RANKL mediated fusion. More recently, Rivollier *et al.* (2013) demonstrated that human monocytes could be differentiated into immature moDC with GM-CSF and IL-4 and were still able to form osteoclasts when cultured in M-CSF and RANKL. It seems the formation of osteoclasts is fairly flexible in regard to the source of the fusing cells but is dependent on the presence of RANKL.

Until recently, osteoclasts were distinguished from FBGC in immunohistological samples by their high production of cathepsin K (Costa *et al.*, 2011) and tartrate-resistant acid phosphatase (TRAP) (Hayman, 2008). However, Park *et al.* (2013) recently demonstrated that inflammatory MGC in granuloma biopsies produce high levels of TRAP and cathepsin K and argued that the latter was a better marker for inflammatory MGC. As osteoclasts are steady-state MGC and their generation from fusion is initiated through different factors (Yu *et al.*, 2011) the focus henceforth will be on MGC formed in inflammatory microenvironments.

1.3.2 FOREIGN BODY GIANT CELLS: AN INFLAMMATORY MGC FOR FOREIGN BODY DESTRUCTION

FBGC form *in vivo* from the fusion of monocytes attempting to engulf and degrade foreign material extracellularly in the tissues. FBGC are larger than LGC, contain disorganised clusters of nuclei and are regularly observed on the surface of medical implants and stents (Chappuis *et al.*, 2015; Khandwekar *et al.*, 2010). Like osteoclasts, FBGC are able to bind tightly to the synthetic surface and form a suction-plug space between the surface and the cell (called a podosome) where digestive molecules are secreted (DeFife *et al.*, 1999; Zhao *et al.*, 1991).

A degradative environment is established within the podosome by secreting reactive oxygen species from NADPH oxidase (Quinn and Schepetkin, 2009), exocytosis of lysozymes (Harkel *et al.*, 2015), matrix metalloprotease-9 (MMP-9) (Zhu *et al.*, 2007) and cathepsin K (Park *et al.*, 2013). FBGC have also been shown to have very high phagocytic potential. Milde *et al.*, (2015) compared the ability of IL-4 derived FBGC and M2 macrophages to phagocytose antibody and complement-opsonised beads of different sizes. They found that of the bead sizes that both could engulf (10-20 μ m); FBGC were able to phagocytose significantly more beads than M2. Furthermore, FBGC were confirmed by confocal microscopy to phagocytose 45 μ m beads which the M2 could not.

FBGC can be generated *in vitro* by a range of cytokine treatments:, such as IL-4 alone, GM-CSF+IL-4, IL-3+IL-4 (McNally and Anderson, 1995), IL-13 alone (DeFife *et al.*, 1997), M-CSF+IL-4 and M-CSF+IL-13 (Ikeda *et al.*, 1998). Thus, IL-4 appears to be a key cytokine inducing the multinucleation of macrophages into a FBGC destiny. Interestingly, IL-4, IL-13 (Ikeda *et al.*, 1998), GM-CSF and IL-3 (Miyamoto *et al.*, 2001) have been shown to inhibit osteoclast formation if added in the early stages of differentiation.

In vivo FBGC can be generated by surgical implants when new materials are being tested for use as medical implants. Different materials generate different levels of FBGC growth though Brodbeck and colleagues demonstrated in 2002 that IL-4 derived MGC developed less favourably on materials that were pre-treated to be hydrophilic compared to hydrophobic, cationic and anionic surfaces. Many inorganic materials used in medical implants induce a greater FBGC response than xenogeneic equivalents (Lorenz *et al.*, 2015), however, these animal alternatives come with ethical issues and are not appropriate for joint replacements. Between 2005-2030 it is estimated in the USA alone that hip and knee arthroplasties are to grow from 328,000 to 572,000 (174%) and 517,000 to 3.48 million (673%) cases respectfully (Kurtz *et al.*, 2007).

1.3.3 LANGHANS GIANT CELL: AN INFLAMMATORY MGC FOR BACTERIAL ENCASEMENT

In 1886 Theodor Langhans first published his sketches and notes on *M. tuberculosis* infected lung in "*Archiv fur Pathologische Anatomie und Physiologie und fur Klinische Medicin*" (Langhans, 1868). He drew detailed sketches of large cellular bodies residing in the granuloma that possessed multiple nuclei (3-20 nuclei) arranged in a ring or horse-shoe pattern (Byrd, 1998). LGC are commonly found in granulomas of patients suffering from tuberculosis infections (Lever and Sheer, 2010) or sarcoidosis (Van Maarsseveen *et al.*, 2009).

Rhee *et al.* (1978) demonstrated *in vivo* that LGC form on polyester implants in rats within two days of implantation. However, from between 4-14 days the number of nuclei found within LGC increased until all MGC morphology was that of FBGC. They noted a transition in nuclear arrangement stating that 3-6 nuclei MGC⁻¹ were all LGC, 6-30 nuclei MGC⁻¹ both LGC and FBGC were present and at >30 nuclei MGC⁻¹ all were FBGC. The ability of LGC to form FBGC was also confirmed in human sarcoidosis extracts (Van Maarsseveen *et al.*, 2009) and *in vitro* with Concanavalin A (ConA) derived MGC (Möst *et al.*, 1997). However, some teams have argued that LGC and FBGC are generated in response to different cytokines. As mentioned above FBGC can be generated *in vitro* using IL-4 in combination with other cytokines while IFN γ is argued to be the key determinant for LGC formation (Byrd, 1998; McNally and Anderson, 1995; Sakai *et al.*, 2012; Takashima *et al.*, 1993)

1.3.3.1 MTB AND HIV COINFECTION

The World Health Organisation (WHO) Global Tuberculosis Report 2015 states:

"In 2014, TB killed 1.5 million people (1.1 million HIV-negative and 0.4 million HIV-positive). The toll comprised 890,000 men, 480,000 women and 140,000 children. TB now ranks alongside HIV as a leading cause of death worldwide." (Anderson *et al.*, 2015). With so many deaths occurring worldwide from TB infections it is imperative to further understand the immune system's mechanisms of combating this infection so that treatments can be augmented to compliment the immune response.

Provided the medical infrastructure and speed of diagnosis is sufficient then *Mycobacterium tuberculosis* (Mtb) infection alone is a relatively treatable condition. However, the increasing incidence of HIV and Mtb coinfection and increasing reports of antibiotic resistant Mtb strains has been flagged by the WHO as a major cause for concern (Anderson et al., 2015). Both HIV and Mtb infections have been shown to exacerbate one another. A patient infected with HIV who is also infected with the latent form of *Mycobacterium tuberculosis* is 20 times more likely to experience reactivation of the pathogen to the active form of the disease (Pawlaowski et al., 2012). Conversely, Mtb has also been implicated in accelerating the manifestation of opportunistic infections in HIV sufferers (Whalen et al., 1995).

The formation of the protective granuloma is largely mediated by CD4+ and CD8+ T-cells and their production of IFN- γ and other fusogenic cytokines (explained in more detail below) (Cooper, 2009; Lewinsohn et al., 2003). The destruction of CD4+ T-cells by HIV and subsequent dampening of the cell-mediated immunity results in a delayed containment of the bacteria which rapidly invade the lungs and tissues via their macrophage vectors (Orme et al., 1993). HIV has also been reported to increase the expression of receptors that Mtb utilises to enter their target M ϕ (Rosas-Tarco et al., 2006), dampen the ability of monocytes to produce reactive oxidative species (Spear et al., 1990) and inhibit TNF- α driven apoptosis of Mtb infected M ϕ (Patel et al., 2007).

1.3.3.2 MECHANISMS OF MTB DRUG RESISTANCE

The antibiotic revolution of the last century has been the birthing grounds for a range of antibiotic resistant strains of Mtb. Mtb is a surprisingly resilient pathogen that has gained resistance through mutations of its own genome rather than through horizontal transfer mechanisms such as plasmids and transposons (Kochi et al., 1992). WHO has defined these multiple drug resistant strains (MDR-TB) as strains resilient to the commonly used isoniazid and rifampin. MDR-TB that has also become resistant to fluoroquinolone and any of the intravenously administered anti-Mtb drugs such as amikacin, kanamycin or capreomycin have been deemed extensively drug-resistant Mtb (XDR-TB). XDR-TB pose a growing threat in the future of TB treatment, as of 2015, 105 countries have already reported the presence of XDR-TB strains (Anderson

et al., 2015). WHO also reported that MDR-TB were present in 3.3% of new TB cases and 20% of previously treated cases and that in 2014, ~190,000 people died as a result of MDR-TB (Anderson et al., 2015).

Mtb's hardiness can be attributed not just to the acquisition of beneficial mutations but also to its residual low permeability to antibiotics as a result of its mycolic acid containing cell wall (Jarlier and Nikaido, 1994). Furthermore, Mtb is immune to β -lactam based antibiotics due to its ability to produce β -lactamase to hydrolyse the β -lactam ring thus rendering the drug inactive (Wang et al., 2006). Isoniazid, one of the most common TB treating drugs, comprises of a pyridine ring and a hydrazide group that is administered in an inactive form. It is the Mtb's own catalase-peroxidase activity (KatG) that activates isoniazid which then binds with high affinity to enoyl-acyl carrier protein reductase (InhA) blocking its ability to produce the mycolic acid necessary for cell wall integrity (Rawat et al., 2003). Resistance to isoniazid has been confirmed by mutations in the Mtb's KatG to decrease affinity to the drug (Cade et al., 2010) or in the InhA promoter to increase InhA expression (Niehaus et al., 2015). InhA mutations have the added problem of conferring resistance to other structurally similar drugs such as ethionamide (Banerjee et al., 1994).

Rifampicin is a lipophilic ansamycin that has been used to treat Mtb for over 40 years. Rifampicin targets the Mtb β -subunit of RNA polymerase, once bound rifampicin inhibits the elongation of mRNA resulting in the arrest of protein synthesis (Blanchard, 1996). Rifampicin resistance has been shown to be conferred by mutations in the *rpoB* gene of Mtb which contains the code for the β -subunit of RNA polymerase. By mutating the *rpoB* sufficiently to lessen the affinity of Rifampicin but maintain activity of the β -subunit; Mtb is able to gain resistance to the drug (Telenti et al., 1993). The aminocyclitol glycoside antibiotic known as Streptomycin was the first ever antibiotic used to treat TB. As its name suggests, streptomycin was first isolated from *Streptomyces griseus* in 1943 by Albert Schatz (1920-2005) and Selman Abraham Waksman (1888-1973) (Kingston, 2004). Streptomycin is a potent inhibitor of protein synthesis as it is able to bind to the 16S rRNA of the 30S subunit of the prokaryotic ribosome and block translation initiation (Moazed and Noller, 1987). To circumvent

this inhibition, streptomycin resistant Mtb strains regularly show mutations in their *rrs* and *rpsL* genes at the coding sequences for the streptomycin binding site (Gillespie, 2002).

1.3.3.3 THE MOLECULAR BASIS OF MTB ENTRY

Mycobacterium tuberculosis typically enters via the lungs and airways where it is phagocytosed by tissue resident Langerhans macrophages (not to be mistaken with LGC) which recruit new inflammatory M ϕ and moDC. However, *M. tuberculosis* has evolved to inhibit the fusion and maturation of the phagosome with lysosomes to avoid acidification and digestion. Early work suggested that the bacterium inhibited phagolysosome maturation utilising sulphatides (Goren *et al.*, 1976) and secreted ammonia (Gordon *et al.*, 1980) to inhibit phagosome maturation. Later, Via *et al.* (1997) demonstrated that early stage phagosomes contained Rab5 and late stage phagosomes contained Rab7, however, *M. tuberculosis* containing phagosomes remained Rab5. The Rab family of GTPases are responsible for coordinating the movements of endosomes and phagosomes to lysosomes for fusion and destruction of the contents (Seto *et al.*, 2011). The mechanism for how *M. tuberculosis* inhibits the shedding of Rab5 and the integration of Rab7 is not fully understood but it is within this phagosome maturation phase that the virulent strains avoid destruction (Seto *et al.*, 2011).

Protected within the M ϕ , the bacterium is able to proliferate whereby it causes stress on the host cell or ruptures the M ϕ . The resultant damage-associated molecular patterns (DAMP) and PAMP signals released trigger the secretion of CCL2 to attract more pro-inflammatory M1. The accumulating M ϕ amass and secrete pro-inflammatory cytokines IFN γ , TNF α , IL-1 β , IL-6, IL-12 (Aranday-Cortes *et al.*, 2013; Flynn and Chan, 2001) and local Th17 cells secrete IL-17A which acts as a potent pro-fusion signal (Coury *et al.*, 2008). A granuloma forms as a result of this cocktail of cytokines with the infected macrophages in the centre, engulfed by a highly organised structure of M ϕ , LGC and external T-cells (Figure 1.6) (Guirado and Schlesinger, 2013).

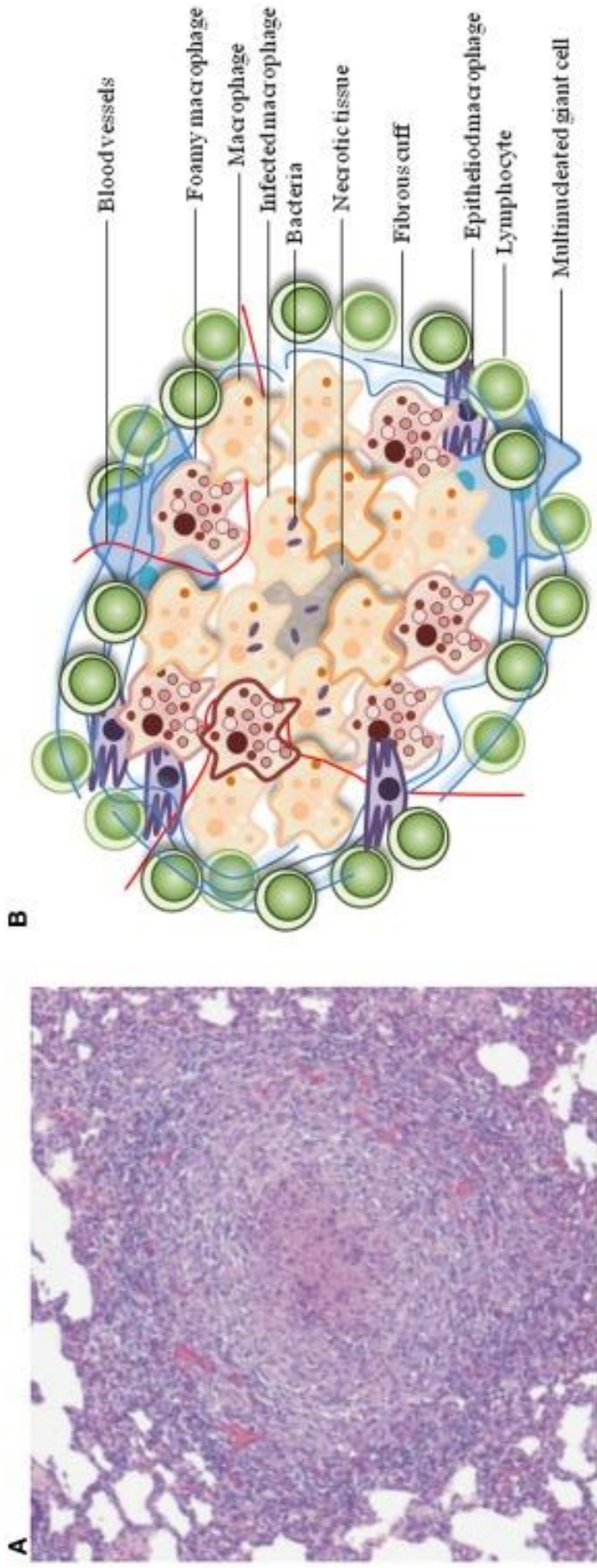


Figure 1.6: Structure of a TB Induced Granuloma

Far from being disorganised clumps of cells amassing around *Mycobacterium tuberculosis* infected macrophages; granuloma are actually highly organised immune structures that act to encapsulate and inhibit the pathogens spread.

A. A histological example of a granuloma formed in a minipig's lung. Cells stained with hematoxylin-eosin.

B. Model diagram of a granuloma. Infected Mφ release chemoattractants that attract more macrophages, NK-cells and T-cells which in turn create an IFNγ and pro-inflammatory cytokine-rich microenvironment which stimulate incoming monocytes to fuse and for MGCs to encase the infection.

From (Guirado and Schlesinger, 2013) with permissions.

The granuloma functions to encapsulate the bacterium so that it cannot spread but does not actually function to destroy the pathogen. The role of granuloma development and whether it is beneficial to the host is still highly debated; Davis and Ramakrishnan (2009) demonstrated in zebrafish that early granuloma production assisted the bacterium in spreading to newly recruited M ϕ . However, they did not analyse the effect that MGC formation and engulfment would have during the later stages of granuloma formation and their zebrafish model lacked adaptive immune cells that are important in cytokine signalling during granuloma development (Bold and Ernst, 2009). An increase in CD16⁺ monocyte populations in the bloodstream in response to TB infection or granuloma have been reported by multiple investigators (Castaño *et al.*, 2011; Lastrucci *et al.*, 2015; Park *et al.*, 2014). However, the individual contribution of the monocyte subsets towards MGC formation remains largely unknown and under-investigated and could reveal potential strategies for combating advanced-stage granuloma.

1.4 MECHANISMS OF MONOCYTE FUSION

The exact mechanism by which monocytes fuse to become MGC is still largely unknown and is likely to require the participation of multiple receptors and proteins to coordinate the *en masse* rearrangement of cytoskeletal structures and overcome the repulsive forces of the cell membranes. Homotypic monocyte fusion is a complex multistep process and can be subdivided into three key stages: competence, contact and commitment. In all three stages mentioned below, there is evidence of tetraspanin proteins forming partnerships with many of the membrane bound fusion-mediating proteins. The role and partnerships of tetraspanins will be discussed at length in the next section.

1.4.1 MONOCYTE FUSION: COMPETENCE & COMMUNICATION

In steady state when circulating in the bloodstream or patrolling the non-bone tissues; monocytes and M ϕ do not fuse. To initiate a fusion-ready state, the monocytes must first be made fusion-competent by pro-fusion cytokines. These cytokines in turn trigger the transcription and upregulation of certain genes whose products facilitate fusion. Monocyte differentiation into M ϕ has been shown to eliminate fusion

competence (Möst *et al.*, 1997). Monocyte cultured in serum containing media for 8 days to form macrophages were unable to fuse when ConA was added. However, Möst and colleagues (1997) observed that when freshly isolated monocytes were added to the M ϕ with ConA media the two cells types could fuse and form MGC. These findings suggest monocytes are the more fusion-competent of the monocyte lineage.

As previously described, monocytes can be induced to form LGC using IFN γ and FBGC in response to IL-4+IL-13. IFN γ binds to the IFN γ R which utilises the Jak1/Jak2 kinases to phosphorylate and activate the signal transducer and activator of transcription 1 (STAT1) (Figure 1.7) (O'Shea *et al.*, 2015). Phosphorylated STAT1 forms a homodimer that is able to enter the nucleus and promote the transcription of a multitude of genes by binding the IFN-gamma activated sequences (GAS) to create a fusion-competent cell (Ramana *et al.*, 2000). IL-4 and IL-13, on the other hand, are both able to bind the same receptor or their own individual receptors and utilise Jak1/Jak2/Jak3/Tyk2 kinases to activate and homodimerise STAT6 which binds a different array of genes that lead to fusion competence (Goenka and Kaplan, 2011; Wurster *et al.*, 2000). It is interesting that these two different pathways are able to facilitate fusion and form MGC with different morphological features.

IL-4/IL-13 but not IFN γ signalling are able to upregulate the expression of triggering receptor expressed by myeloid cells 2 (TREM-2) on M ϕ and moDC (Turnbull *et al.*, 2006). TREM-2 is an integral membrane receptor that is able to bind a range of anionic bacterial factors (e.g. LPS) and apoptotic signals on host cells (Hsieh *et al.*, 2009). Upon binding its ligand TREM-2 subsequently recruits DNAX activating protein of 12kD (DAP12) which possesses an immunoreceptor tyrosine-based activation motif (ITAM). Src family kinases phosphorylate the ITAM sites to recruit spleen tyrosine kinases (syk) which is phosphorylated to become activated, detach from DAP12 and activate the phosphatidylinositol 3-kinase (PI3K), NF- κ B and Akt pathways (Paradowska-Gorycka and Jurkowska, 2013). The end result is a mass upregulation of hundreds of fusion-competence genes, such as DC-STAMP and E-cadherin (Helming *et al.*, 2008).

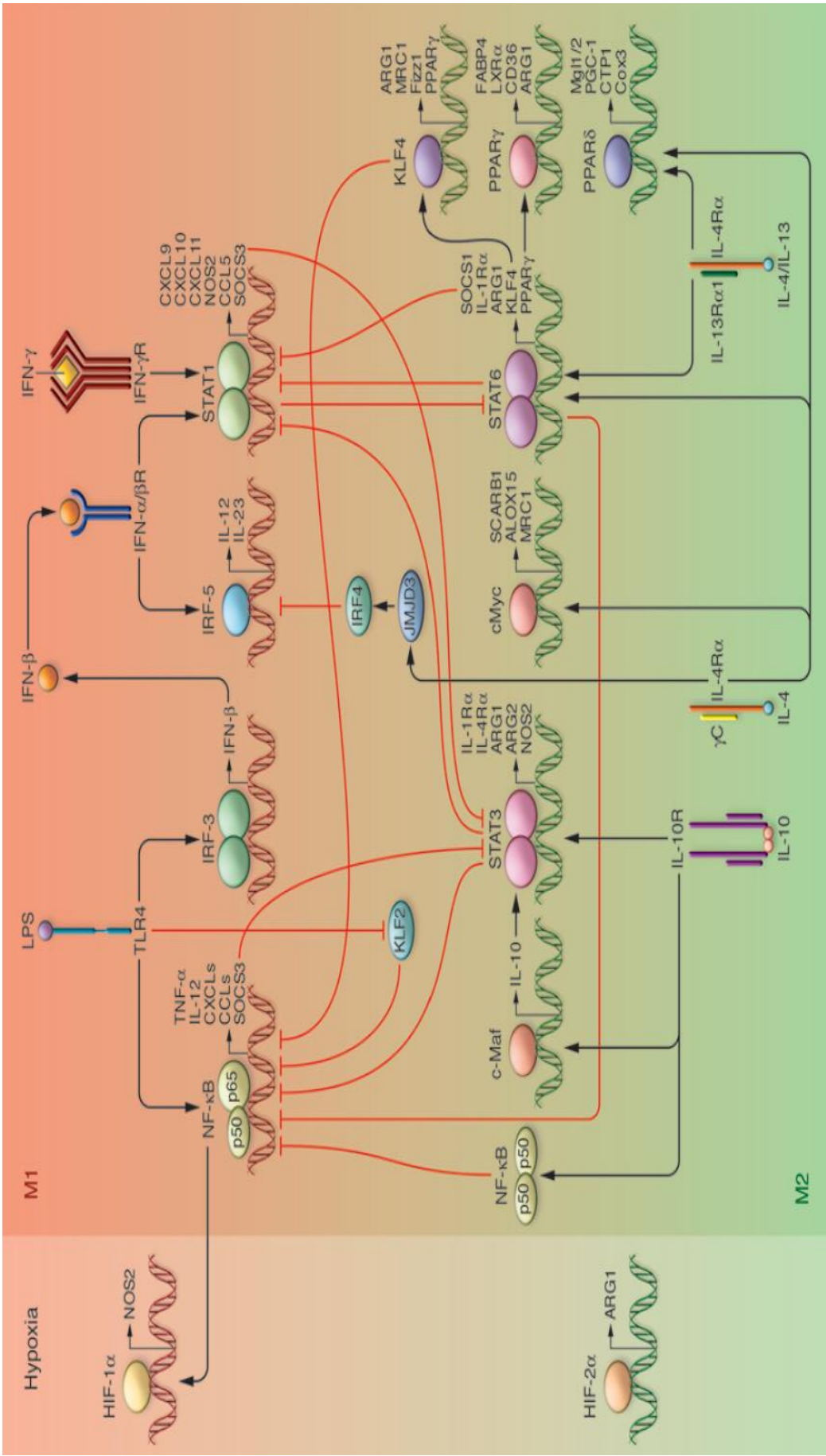


Figure 1.7: Mechanisms of Macrophage Polarisation

The myeloid transcriptome reacts to pro-inflammatory and anti-inflammatory cytokines by activating different gene promoters. M1-like stimuli such as LPS and IFN γ trigger the activation of STAT1 homodimers and NF- κ B to promote pro-inflammatory genes. M2-like signals such as IL-4, IL-10 and IL-13 result in the dimerization of STAT6 and other promoters leading transcription of anti-inflammatory genes. From (Sica and Mantovani, 2012) with permissions.

Expression of particular proteins has been observed on fusion-competent monocytes and many have proven to be essential for fusion by using blocking antibodies. Dendritic cell-specific transmembrane protein (DC-STAMP) is an integral membrane protein that has been shown using knockout mice to be essential for formation of FBGC and osteoclasts (Yagi *et al.*, 2005, 2007). Interestingly, DC-STAMP expression is controlled by different transcription factors in FBGC and osteoclasts. Yagi *et al.* (2007) demonstrated with chromatin immunoprecipitation that the transcription factors PU.1 and NF- κ B were responsible for the promotion of DC-STAMP in IL-4 derived FBGC formation. In RANKL driven osteoclast formation they demonstrated that the promoters of DC-STAMP were instead NFATc1 and c-Fos by using an NFATc1 inhibitor and c-Fos knockout mice. Despite its vital role in FBGC and osteoclast formation the mechanism by which DC-STAMP contributes to fusion is still unknown.

Matrix metalloprotease-9 (MMP-9) is a zinc dependent endopeptidase that can digest the extracellular matrix and cleave cytokines into active or inactive forms. MacLauchlan *et al.* (2009) demonstrated *in vitro* that blocking MMP-9 activity with antibodies did not arrest fusion but did act to significantly decrease the size of FBGC and % of fused nuclei. They then showed *in vivo* using MMP-9 null mice that FBGC could still form on implants but were significantly reduced in their capacity to form large FBGC (MacLauchlan *et al.*, 2009). E-cadherin is a calcium dependent transmembrane protein that contributes to cell-cell adhesion by binding adjacent E-cadherins homotypically (Moreno *et al.*, 2007) and is involved in the formation of tight junctions (Wanat *et al.*, 2015). Upon ligand binding the intracellular domain of E-cadherin recruits α - and β -catenin which facilitates actin polymerisation to link the cytoskeleton to the bound E-cadherin (Van Den Bossche *et al.*, 2009). Moreno *et al.* (2007) observed that IL-4 stimulated mouse monocytes expressed E-cadherin in a STAT6 dependent manner, they then found that anti-E-cadherin antibodies inhibited the formation of large MGC but, unlike anti-DC-STAMP antibodies, they did not arrest fusion outright. Wong and colleagues have observed that the surface expression of E-cadherin was highest in nonclassical and intermediate monocytes and lowest in the classical monocytes (unpublished data). They also observed that the expression of

DC-STAMP was significantly higher in intermediate monocytes (unpublished data), possibly implicating a heightened role of intermediate monocytes in the fusion process.

1.4.2 MONOCYTE FUSION: CONTACT AND CONTRACTION

Once a monocyte has become fusion-competent and its transcriptome modulated by pro-fusion signals it must attract other monocytes or migrate towards other fusion-competent monocytes to fuse. CCL2 is highly secreted by fusing monocytes (Khan *et al.*, 2015; Kyriakides *et al.*, 2004; Moon *et al.*, 2016). Khan *et al.* (2015) revealed with mRNA analysis that CCL2 transcription levels were 9- and 16-fold higher in M-CSF+RANKL and GM-CSF+IL-4 cultured monocytes compared to M ϕ . They also showed that FBGC and osteoclast formation was significantly reduced in CCL2 knockout mice.

Monocytes responding to CCL2 must migrate using adhesion molecules and get close to one another by utilising surface adhesion molecules such as integrins. Integrins are a family of transmembrane proteins involved in adherence and outside-to-inside cellular signalling. Integrins exist as heterodimers comprising of an α subunit and a β subunit. Different α and β subunits can dimerise to produce different integrins for different ligands. In mammals there are 24 known integrin heterodimers composed of 18 different α subunits and 8 β subunits (Hynes, 2002). Specifically, β 1 and β 2 have recently been shown to be important in FBGC formation and have been revealed to be highly expressed following IL-4 treatment by multiple studies including confocal microscopy (McNally *et al.*, 2007). The β 2 integrin lymphocyte function-associated antigen 1 (LFA-1 or α L β 2 or CD11a:CD18) and its ligand intercellular adhesion molecule 1 (ICAM-1 or CD54) have been shown to play an important role in monocyte fusion. Möst *et al.* (1990) used antibodies targeting LFA-1 and ICAM-1 to show almost complete arrest of fusion indicating their involvement in cell-cell contacts as a necessary step towards monocyte fusion.

The macrophage fusion receptor (MFR) was first observed in 1995 by Saginario and colleagues when they found that by blocking the MFR with antibodies the rat M ϕ would still aggregate and make cell clumps but were unable to fuse their membranes. It was

later reported by Han *et al.* (2000) that CD47 was the ligand for MFR and that fusion-competent Mφ upregulate their expression of both MFR, CD47 and a partner protein CD44. The current hypothetical model (Figure 1.8) is that upon MFR binding to CD47 on an adjacent monocyte, the MFR undergoes a change in quaternary structure and contracts, thus pulling the two membranes together, the CD44 molecule acts to stabilise this process and is shed upon MFR-CD47 contortion (Vignery, 2005). The formation of such tight gap junctions between monocytes and MGC has recently been confirmed by transmission electron microscopy images (Imaizumi *et al.*, 2016). Signal-regulatory protein alpha (SIRPα) is another ligand to CD47 that has been implicated in the formation of contacts between fusing monocytes (Han *et al.*, 2000; Wang and Pfenninger, 2006). The surface expression of SIRPα in intermediate and nonclassical monocytes have been shown to be twice that of classical monocytes (Wong *et al.* unpublished data) but its exact roll in fusion remains unknown.

1.4.3 MONOCYTE FUSION: COMMITMENT AND COMPLETION

Once two fusion-competent monocytes have made contact and their membranes have committed to fusion there needs to be an array of proteins facilitating cytoskeletal and lipid rearrangements as the two cells merge.

As the membranes are brought into close proximity by MFR-CD47 complexes, the presence of the CD44 partner protein allows the recruitment of cytoplasmic ezrin-radixin-moesin (ERM) proteins. ERMs have been shown to bind the cytoplasmic domain of CD44 directly and are able to polymerise actin and rearrange the local cytoskeleton to stabilise the close cell contacts. Furthermore, EWI-2 and EWI-F (named for their conserved Glu-Trp-Ile motif) are also able to recruit cytoplasmic ERM and are partners to the tetraspanin proteins CD9 and CD81 (Sala-Valdés *et al.*, 2006). CD9 and CD81 have been increasingly implicated as major organisers of fusion proteins (Charrin *et al.*, 2013; Hulme *et al.*, 2014; Parthasarathy *et al.*, 2009; Takeda *et al.*, 2003) and cell motility (Berditchevski and Odintsova, 1999; Takeda *et al.*, 2008).

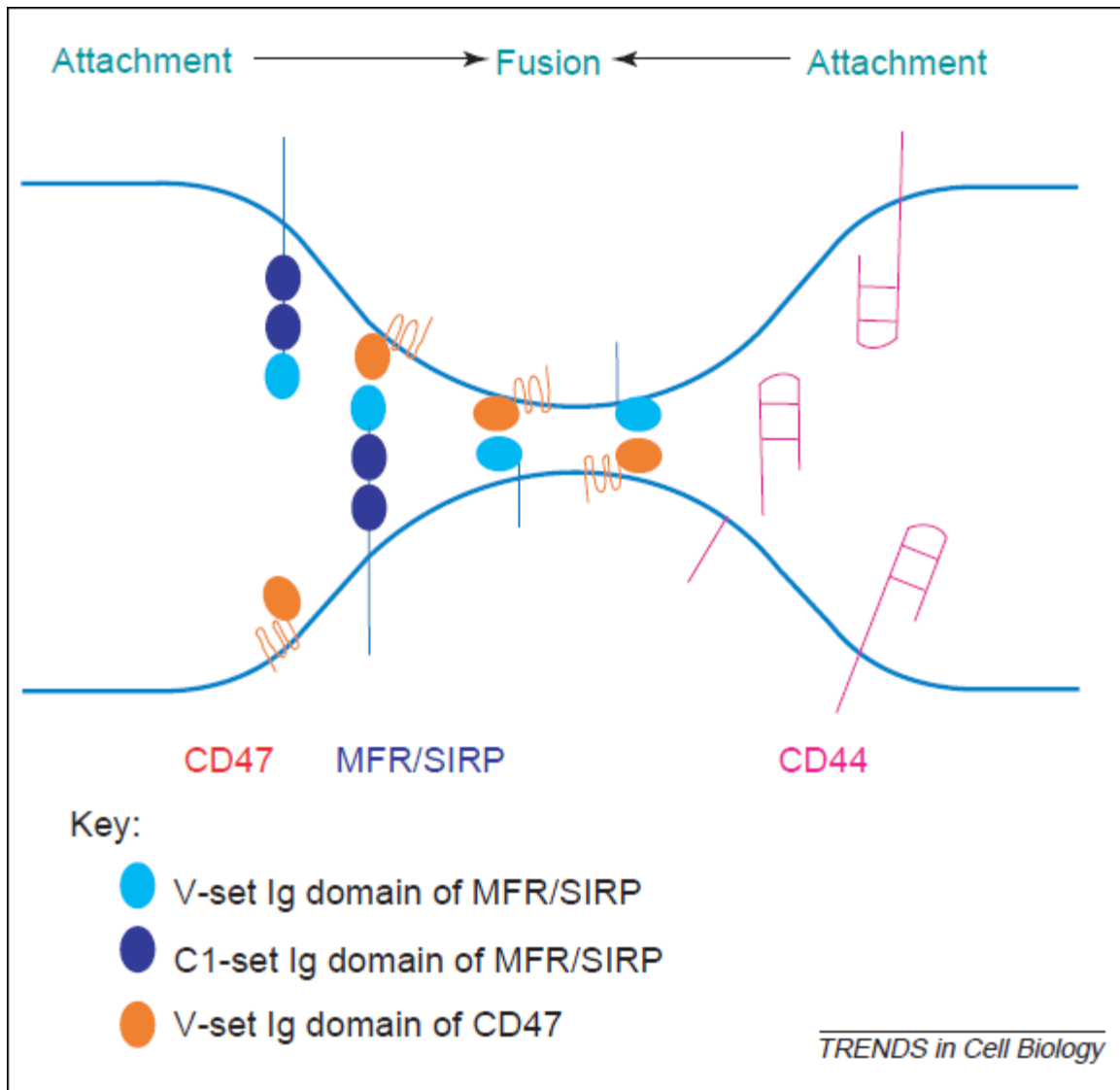


Figure 1.8: Theoretical Model of MFR-CD47 Tethering of Fusing Membranes

The MFR of a fusion competent monocyte binds to a CD47 of another monocyte. MFR-CD47 complexing favours a contraction of the two proteins to bring the two membranes closer together. CD44 acts as a partner protein and stabilises the complex and is shed once the contracted state has been achieved.

From (Vignery, 2005) with permissions.

The fusing cells not only need to mediate strong cell-cell contacts but must also establish strong contacts with the surface it is adhered to. Kitazawa *et al.* (1995) used Northern blot analysis on IL-4 treated mouse M ϕ to show that α V β 3 is upregulated in a dose-dependent manner to IL-4. α V β 3 binds vitronectin and when activated form clusters of multiple α V β 3 units that are able to activate intercellular actin cytoskeleton polymerisation (Cluzel *et al.*, 2005). α V β 3 expression has been shown to be vital for correct actin ring formation in osteoclasts for podosome formation (Izawa *et al.*, 2012; McHugh *et al.*, 2000) as well as adherence and formation of FBGC (McNally *et al.*, 2008).

P2X7 is an ATP gated cation channel that is also able to act as membrane pore (Rassendren *et al.*, 1996). P2X7 expression has been seen to increase on fusion competent monocytes stimulated with IFN γ while anti-P2X7 blocking antibodies significantly inhibited MGC formation (Falzoni *et al.*, 1995; Pellegatti *et al.*, 2011). The pore function of P2X7 has also been shown to increase the outer membrane content of phosphatidylserine (MacKenzie *et al.*, 2001), a phospholipid that is usually in the inner leaflet of the plasma membrane that, when exposed on the outer leaflet, labels a cell for apoptosis (Fadok *et al.*, 1998; Greenberg *et al.*, 2006) or fusion (Helming *et al.*, 2009). Phosphatidylserine is recognised and bound by the class B scavenger receptor CD36 (Silverstein *et al.*, 1992). Helming *et al.* (2009) demonstrated that bone marrow derived M ϕ from CD36 knockout mice were inhibited in their capacity to form FBGC but not osteoclasts. They also demonstrated that CD36 and phosphatidylserine interact directly by masking phosphatidylserine with annexin V in CD36 competent M ϕ , which inhibited fusion. CD36 was later found to be highly co-localised with the tetraspanin CD9 on M ϕ and genetic deletion of CD9 significantly reduced CD36-mediated uptake of phosphatidylserine (Huang *et al.*, 2011).

1.4.4 FUSION MECHANISMS IN ALTERNATIVE SYSTEMS

Though this thesis focuses on the fusion of monocytes to form multinucleated giant cells it does not mean that this is the only form of membrane fusion that occurs within humans. Indeed, membrane fusion is essential for the creation, development and maintenance of all Animalia. At the very creation of life, two haploid gametes must

undergo heterotypic fusion of their membranes to create a new totipotent cell; the earliest form of "life". In mammals where gestation occurs *in utero*; the developing blastocyst must gain nutrients from the mother and expel waste products into her bloodstream. To do this without evoking an immune reaction from the mother's leukocytes the blastocyst's outer cytotrophoblasts undergo homotypic fusion to form syncytiotrophoblasts (Schumacher *et al.*, 2013). This multinucleated giant cell forms a leukocyte-impenetrable layer for the blastocyst whilst allowing for the diffusion of vital nutrients. As the foetus develops myoblasts undergo homotypic fusion to generate skeletal muscle. Furthermore, within every cell, vesicles are trafficked from the endoplasmic reticulum to the surface to express integral membrane proteins or release cell signalling molecules by exocytosis. Throughout life our immune systems are bombarded by a range of pathogens including viruses. The membrane coated viruses enter host cells via membrane fusion to hijack host machinery and replicate. It is clear that membrane fusion is an important process in many stages of life and are worthy of further explanation before narrowing the focus on homotypic monocyte fusion.

To achieve fusion of two lipid bilayers all the membrane fusion events listed previously all follow a similar pathway to integration; competence, contact and commitment to fusion. The competence state requires that one or both of the fusing membranes contain proteins that can tether the two membranous bodies together. Further contacts are made between the two membranes and in some cases tethered proteins can contract to pull the membranes within the necessary ~4nm distance (Siegel, 1993; Warner and O'Shaughnessy, 2012). Although the exact mechanism of membrane integration is unknown, it is thought that once the membranes have been brought into contact the outer lipid layers mix into a transient state known as hemifusion (Kozlovsky and Kozlov, 2002; Warner and O'Shaughnessy, 2012). Through this the inner lipids flip and open up a fusion pore whereby membrane assimilation is energetically favourable.

In the case of a spermatozoon and an oocyte, the spermatozoon expresses a protein called Izumo1 (named after the Izumo-taisha shrine in Japan which honours the god

of marriage) while the oocyte expresses Izumo1's ligand; Juno (named after the Roman goddess of love and marriage) (Aguilar *et al.*, 2013; Bianchi *et al.*, 2014; Inoue *et al.*, 2005; Melcher, 2016). Before Izumo1 and Juno have made contact the spermatozoon must bypass the cumulus cells and zona pellucida protecting the oocyte. The spermatozoon releases digestive enzymes to break down the zona pellucida and in doing so releases internalised Izumo1 to the outer membrane thus establishing its fusion competence (Barros *et al.*, 1996; Krauchunas *et al.*, 2016). As the two membranes meet, multiple Izumo1 units on the spermatozoon's form a tight clamp-like association with Juno in a 1:1 ratio (Ohto *et al.*, 2016). The mechanisms of fusion thereafter are not known but the binding of Juno and Izumo1 has been shown to be essential for gamete fusion using Izumo1-targeting antibodies (Inoue *et al.*, 2005). CD9 has also been shown to play a vital role in mice using CD9 knockout mice (Kaji *et al.*, 2000) but again its exact role in gamete fusion remains elusive.

Within one week of fertilisation the blastocyst must establish a source of nutrients to survive and continue growth. Within the womb the only available source of nutrients is the mother's bloodstream. However, the mother's immune system would quickly identify the invading blastocyst and mount an immune attack. To avoid infiltration and rejection by the maternal leukocytes the blastocyst produces a multinucleated giant cell called a syncytiotrophoblast that shields it from the maternal immune system (Guleria and Sayegh, 2007; Koch and Platt, 2012). Patrolling maternal phagocytes can transmigrate between cells but they cannot migrate directly through the syncytiotrophoblast itself. The syncytiotrophoblast is produced and maintained by the fusion of cytotrophoblasts which the blastocyst produces at the uterus-blastocyst border. The syncytiotrophoblast invades the uterus epithelium to both embed the blastocyst and establish a close-contact site with the maternal capillaries for diffusion of waste and nutrients (Huppertz and Gauster, 2011).

Once the blastocyst has been completely surrounded by the uterine endometrium the invasive syncytiotrophoblast takes on a more passive role. Maintained by the fusion of more cytotrophoblasts, the single all-encompassing syncytiotrophoblast releases β -human chorionic gonadotropin (β -hCG) and human placental lactogen (hPL)

(Handschuh *et al.*, 2007). β -hCG acts to both stimulate the ovaries to release progesterone which increases angiogenesis of the uterus lining to sustain the developing foetus and attract and activate regulatory T-cells to confer immune tolerance of the developing foetus (Cole, 2010). hPL acts to increase the glucose content of the mother's bloodstream (for the developing foetus to utilise) by inhibiting maternal insulin sensitivity (Hill *et al.*, 1986).

The fusion of cytotrophoblasts with the growing syncytiotrophoblast has been shown to be largely mediated by syncytin proteins (Huppertz and Gauster, 2011; Mi *et al.*, 2000). Syncytin proteins are believed to be derived from an ancient retroviral insertion of env genes into the mammalian genome that was subsequently domesticated to facilitate *in utero* gestation. Syncytins show structural and functional similarities with modern day class I cell fusion proteins found on membrane coated viruses (Podbilewicz, 2014). Syncytin-1 is expressed on trophoblasts and interacts with human sodium-dependent neutral amino acid transporter type 1 and 2 (hASCT1/hASCT2) expressed by the syncytiotrophoblast (Lavillette *et al.*, 1998; Marin *et al.*, 2000).

Syncytin-1 has several key structural features that are vital to the fusion mechanism. The functioning unit consists of a trimer of syncytin-1 peptides; each containing a small cytoplasmic and transmembrane domain, a highly hydrophobic fusion peptide sequence proximal to a furin cleavage site (RNKR), two distal cysteine-rich motifs and a hASCT2 binding sequence (¹¹⁵-SDGGGX2DX2R⁻¹²⁵) (Gerbaud and Pidoux, 2015). The two distal cysteine rich motifs form a disulphide bond that is cleaved upon binding of trophoblast syncytin-1 to syncytiotrophoblast hASCT2. This cleavage induces a structural loop to helix change that propels the hydrophobic fusion peptide into the neighbouring membrane ~10nm away (Gerbaud and Pidoux, 2015). Once embedded the two opposing membranes are irreversibly anchored and retraction of the syncytin-1 trimer leads to membrane contortion and eventually fusion.

Syncytin-1 is an example of a domesticated retroviral membrane fusion protein, however, modern membrane coated viruses such as influenza, HIV and Ebola utilise similar proteins to facilitate membrane fusion and host cell invasion (Podbilewicz,

2014). Influenza haemagglutinin, like syncytin-1, is a class I membrane fusion protein that follows a similar mechanism to membrane fusion but shares almost no sequence similarity. Haemagglutinin forms a trimer on the viral membrane with the hydrophobic fusion peptide internalised within the trimer forming contacts with conserved charged residues (Epanand, 2003; Floyd *et al.*, 2008). When the virus is exposed to an acidic environment, such as endocytosis, the conserved charged residues are protonated which releases the fusion peptide from its internalised state (Xu and Wilson, 2011). Upon protonation the helix-loop-helix supporting the fusion peptide forms an extended α -helix that propels the fusion peptide into the nearby host membrane, tethering the viral membrane to the host endosome. It is thought that like syncytin-1, subsequent contraction of the extended haemagglutinin trimer results in merging and fusion of the two membranes and the release of viral cargo into the host cytoplasm (Xu and Wilson, 2011).

In humans at least, it is clear that there is a wide variety of fusion-mediating proteins that are utilised by different cell-types to achieve membrane fusion. The coordination of all these proteins to achieve fusion is likely to require other proteins to organise the machinery, one such family, the tetraspanins, have been implicated as the molecular organisers of fusion.

1.5 TETRASPANINS

Tetraspanins are a family of relatively small (20-50kDa; ~250 amino acids) integral membrane proteins (Maecker *et al.*, 1997; Wright and Tomlinson, 1994). Humans possess 33 tetraspanins and the family has members in other eukaryotes such as *Drosophila* and *Caenorhabditis* as well as plants, fungi (excluding yeasts) and protozoa (Henkle *et al.*, 1990; Todres *et al.*, 2000; Tomlinson and Wright, 1996). Tetraspanins have no enzymatic activity yet they are involved in a wide range of processes ranging from cell motility, microdomain organisation, viral entry, adhesion and membrane fusion (Hemler, 2003, 2005). However, in the context of this review the tetraspanins discussed will be the members involved in membrane fusion and formation of multinuclear giant cells.

1.6 TETRASPANIN STRUCTURAL FEATURES

The conservation of tetraspanins across different phyla suggests they originated early in evolution of eukaryotes (Figure 1.9) and are involved in important processes (Boucheix and Rubinstein, 2001). Key features of the tetraspanin structure include four membrane-spanning domains beginning and ending in short N- and C-termini and two extracellular domains; one small (EC1) and one large (EC2). CD37, CD63, CD82 and CD151 possess C-terminal tyrosine based internalisation motifs (Yxx ϕ) (Berditchevski, 2001) which can be recognised by adaptor coat proteins of the endocytosis pathway (Pandey, 2009). Due to the dependence of tetraspanins on the membrane to maintain structural integrity it has not yet been possible to gain a crystal structure of an entire tetraspanin. Crystal structures of the solubilised EC2 domain exist (Kitadokoro *et al.*, 2001) and the structure of the transmembrane regions have been predicted by molecular modelling (Figure 1.10) (Seigneuret, 2006).

1.6.1 EC1 & EC2

The two extracellular loops show the most sequence divergence of the whole structure, both between different tetraspanins of the same species and orthologues in different species. The EC1 and EC2 loop comprise of 13-30 and 70-140 amino acid

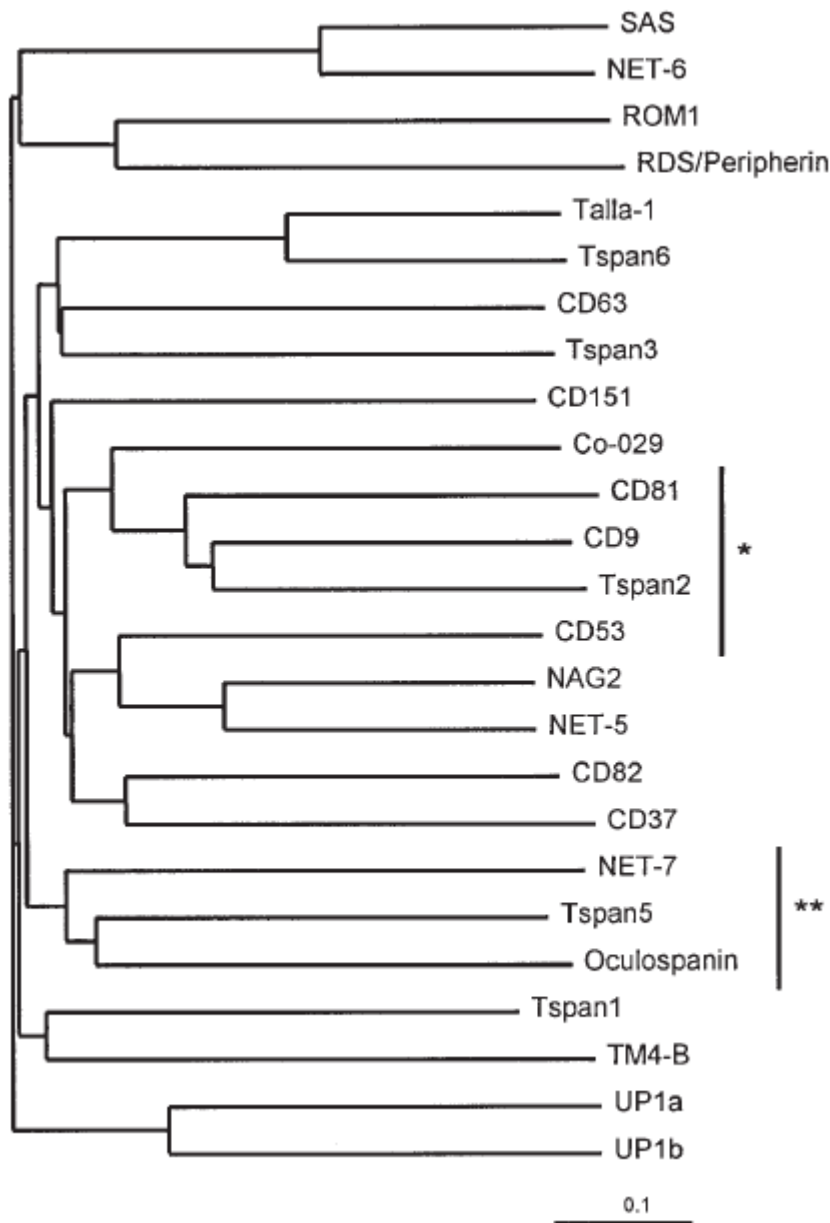


Figure 1.9: Tetraspanin Primary Structure Distance Tree

The primary amino acid sequence of each human tetraspanin above is compared and distributed to show relative divergence. Tetraspanins are grouped into branches based on their similarity and probable divergence after gene duplication. The scale-bar represents 10% amino acid difference. Tetraspanins marked with an “*” possess four cysteines in the EC2 domain, “**” possess eight and all other tetraspanins possess six.

From (Boucheix and Rubinstein, 2001) with permissions.

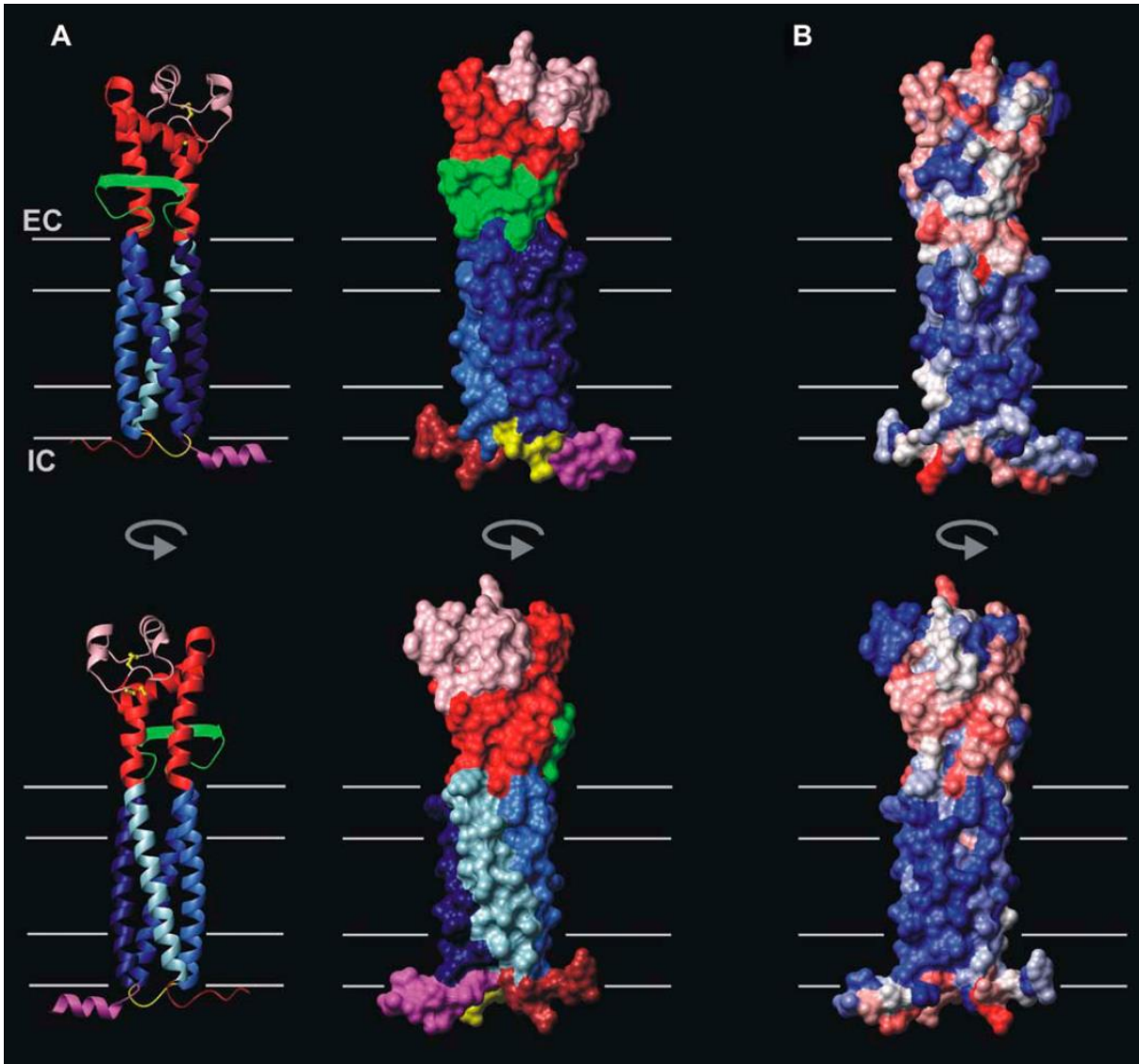


Figure 1.10: 3D Crystal Structure of CD81 with Predicted Transmembrane Regions.

A: Ribbon structure of CD81 with a rotational view showing the EC2's rigid A, B and E α -helices (red), C & D fluid α -helices (pink) and short EC1 β -strand. The EC2 domain faces the extracellular (EC) space and the N- and C- termini are intracellular (IC).

B: The surface topography (left) utilises the same colouring system as "A" and shows the spatial arrangement of the different domains with the disulphide bridges more obvious in yellow. The right sided surface topography is recoloured with highly polar residues as red and hydrophobic residues as blue.

From (Seigneuret, 2006) with permissions.

residues respectively. The EC2 domain contains the highly conserved CCG motif which interacts with another conserved Cys that resides near the 4th transmembrane region (Hemler, 2001; Parthasarathy *et al.*, 2009). A PXXC motif contains the fourth and final Cys required to form the two disulphide bonds that are a characteristic motif of tetraspanins (Stipp *et al.*, 2003). The EC2 is the most variable of the two extracellular domains and has been shown to be essential in forming associations with partner proteins to carry out functions. Kazarov *et al.* (2002) demonstrated that by deleting the QRD^{194–196} residues in the CD151 EC2 they could abrogate CD151- α 3 β 1 and - α 6 β 1 association, trafficking and inhibit cell migration. Zhu *et al.* (2002) found that deletions of the SFQ^{173–175} residues in the EC2 of CD9 of mouse oocytes completely abolished sperm-egg fusion. Furthermore, anti-tetraspanin antibodies targeting the EC2 have been used extensively to bind and interfere with tetraspanin enriched microdomain (TEM) formation and tetraspanin functions (Parthasarathy *et al.*, 2009; Takeda *et al.*, 2003; Yáñez-Mó *et al.*, 2001).

More than half of known tetraspanins possess additional cysteines in their EC2 domains that might form disulphide bridges to add stability to the structure (Hemler, 2001; Parthasarathy *et al.*, 2009). The crystal structure of CD81-EC2 was solved to 1.6Å by Kitadokoro and colleagues in 2001. They discovered the EC2 domain to be composed of five α -helices (A-E); helices A, B and E form a U-shape on one plane and C and D form a more fluid variable region. So far little has been revealed about the functions of the EC1 domain, however, Masciopinto *et al.* (2001) demonstrated that CD81-EC1 deletion results in a decreased surface expression of CD81 due to a failure to traffic the tetraspanin from the golgi to the surface.

1.6.2 THE FOUR TRANSMEMBRANE HELICES

The four transmembrane helices of the tetraspanins show notable conservation between different species; a necessary feature to allow tetraspanin-tetraspanin associations in the TEMs (Kashef *et al.*, 2012). This was demonstrated by Berditchevski *et al.* (2001) when they deleted CD151-EC2 and discovered that it could still co-localise with tetraspanins CD9, CD63 and CD81. This style of intramembrane association contrasts with the typical mechanism of transmembrane protein complex formation,

in which membrane bound proteins interact via charged extracellular domains. Helices 1, 3 and 4 contain conserved charged and polar residues e.g. Asn, Gln and Glu (Hemler, 2005) which are thought to become protonated in the membrane allowing them to interact with the lipid alkyl chains via hydrogen bonds and stabilise the structure (Gratkowski *et al.*, 2001; Zhou *et al.*, 2000).

1.6.3 PALMITOYLATED CYSTEINES

There are six conserved cysteines which act as sites of palmitoylation: four cysteines in the transmembranal helices, one N- and another C-terminal membrane-proximal cysteines. The membrane-proximal cysteine residues on the tetraspanin become palmitoylated during post-translational modification, these membrane-embedded palmitoyl groups may form hydrophobic interactions with membrane lipids to stabilise the structure (Yang *et al.*, 2002). Palmitoylation of these cysteines has been shown to be important for initial establishment of tetraspanin-tetraspanin interactions and formation of the tetraspanin web (Charrin *et al.*, 2002; Kovalenko *et al.*, 2004). The palmitoylated sites appear to stabilise the tetraspanin structure alongside the transmembrane polar residues and maintain a certain level of membrane rigidity. Deletion of the palmitoylation sites of CD151 resulted in a decrease in lateral associations with CD9 and CD63 but did not inhibit CD151 associating with its $\alpha 3\beta 1$ binding partner (Yang *et al.*, 2002). Furthermore, site-directed mutagenesis of CD9 palmitoylation sites led to a loss in its detergent resistant association to CD81 (Charrin *et al.*, 2002).

1.7 TETRASPANIN ENRICHED MICRODOMAINS AND THE "TETRASPANIN WEB"

In vivo, tetraspanins are known to co-localise with other membrane proteins and associate molecules into a TEM (Charrin *et al.*, 2003; Hemler, 2008). By generating a TEM, the tetraspanins group together proteins of similar pathways allowing proteins to work together with greater efficiency than if they were scattered throughout the membrane (Figure 1.11). This tetraspanin-facilitated organising of transmembrane proteins and with binding partners is often referred to as the "tetraspanin web" (Levy

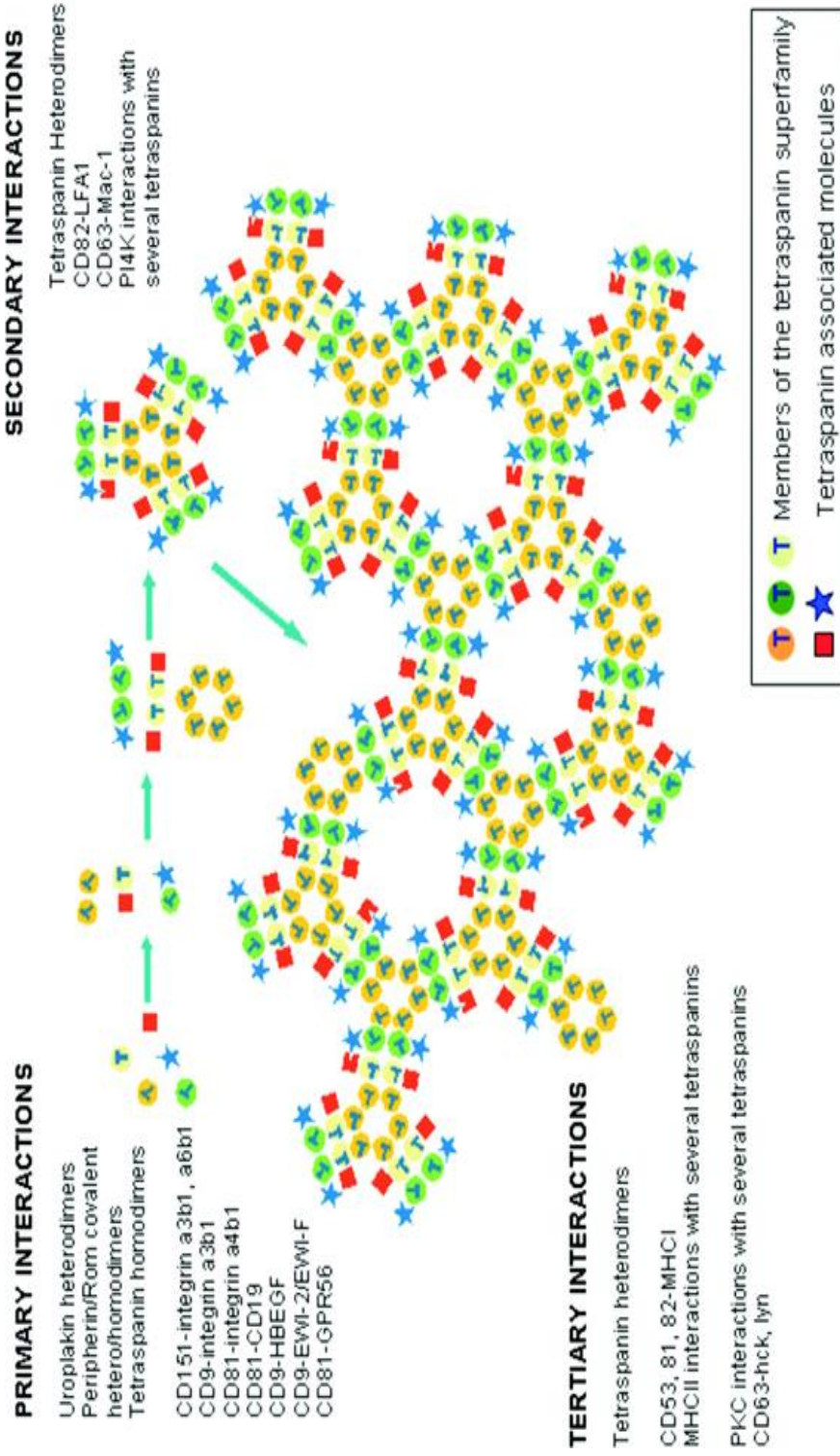


Figure 1.11: Theoretical Model for Formation of a Tetraspanin Enriched Microdomain or “Tetraspanin Web”

Tetraspanins are able to form strong primary interactions (tetraspanin-tetraspanin) via their transmembrane domains. They can also form secondary interactions by associating with certain partner proteins. Tetraspanins bind the partner proteins bound to other tetraspanins (tertiary interactions) and form stable scaffolding structures comprising of multiple tetraspanins and partner proteins; referred to as a TEM or tetraspanin web.

From (Martin et al., 2005) with permissions.

and Shoham, 2005a; Zuidsherwoude *et al.*, 2015). TEMs are not the same as lipid rafts as the two can be fractionated independently on sucrose gradients (Yang *et al.*, 2004). Furthermore, there is evidence that tetraspanins can recruit proteins from lipid rafts. Suzuki *et al.* (2009) demonstrated that CD14 and TLR4 on naïve Mφ were suspended in lipid rafts but upon LPS stimulation they were recruited by CD9 to the TEM fraction of the sucrose gradient.

The structure of TEM has been a point of growing controversy. Proteomic studies (André *et al.*, 2006) have revealed long lists of tetraspanin binding partners and multi-staining fluorescence microscopy (Nydegger *et al.*, 2006) has shown that tetraspanins co-localise with other tetraspanins in regions of the membrane leading many researchers to conclude that active TEMs exist as a vast scaffold of associated proteins (Andreu and Yáñez-Mó, 2014; Levy and Shoham, 2005b; Zöller, 2009). However, the van Sriel group used dual colour stimulated emission depletion (STED) microscopy to show that CD37, CD53, CD81 and CD82 were localised in separate clusters (~120nm in size) on the membrane of moDC. They proposed a new model for TEMs whereby tetraspanins exist in small clusters of no more than 10 tetraspanin molecules and their binding partners and that separate clusters could drift through the membrane and co-localise with other tetraspanin enriched clusters (Zuidsherwoude *et al.*, 2015).

1.8 TETRASPANINS AND FUSION

Due to their ability to organise multiple proteins and form TEMs, tetraspanins have been implicated in orchestrating cell fusion. CD9 and CD81 are among the most widely studied of the tetraspanins since the discovery that CD9 (Kaji *et al.*, 2000; Naour *et al.*, 2000) and CD81 (Rubinstein *et al.*, 2006) knockouts in mice result in sterility as the gametes are unable to fuse. Interestingly this effect seems to be cell specific as CD9 and CD81 knockouts in myoblasts fuse uncontrollably and rapidly form multinucleated syncytia (Charrin *et al.*, 2013). *In vitro* experiments utilising anti-tetraspanin antibodies to bind and interfere with CD9 and CD81 on fusing human monocytes increased the number of nuclei per MGC suggesting an enhancement in fusion. In the same experiments anti-CD63 treatment significantly decreased the

fusion index of MGC but did not affect cell adhesion or migration (Parthasarathy *et al.*, 2009; Takeda *et al.*, 2003). As the EC2 domains have been shown to be the site of many tetraspanin-partner interactions, soluble EC2 mimics have been used to bind the tetraspanin binding partners and in theory disrupt TEM formation. CD9-EC2 (Hulme *et al.*, 2014) and CD63-EC2 (Parthasarathy *et al.*, 2009) significantly inhibited ConA induced fusion of freshly isolated human monocytes.

CD9 has been shown to form partnerships with multiple fusion related proteins (Figure 1.12) such as the MFR ligand CD47 (Longhurst *et al.*, 1999) and MFR partner protein CD44 (Schmidt *et al.*, 2004; Yashiro-Ohtani *et al.*, 2000), CD36 scavenger receptor (Huang *et al.*, 2011), MMP-9 (Herr *et al.*, 2013) and EWI-2 (Stipp *et al.*, 2001). Wong and colleagues found in flow cytometric studies that CD36 was expressed highest in steady-state human classical and lowest in nonclassical monocytes while CD44 was expressed highest in classical and intermediate and only at traceable levels in the nonclassical subset (unpublished data). On a genetic level, the expression of CD9 has been shown to be linked to the expression of fusion related proteins. Mensah *et al.* (2010) found that when they cultured mouse moDC in RANKL to generate osteoclasts the moDC split into DC-STAMP^{Low} and DC-STAMP^{High} cells. They noted the DC-STAMP^{Low} cells were able to augment fusion and appeared to have internalised DC-STAMP in response to ligand binding and gaining fusion-competence. The DC-STAMP^{Low} cells showed a 1.5-fold upregulation in the transcription of CD9 and CD47. Garner *et al.* (2016) observed in human kidney cell lines that CD9 knock-down caused an 80% decrease in E-cadherin gene expression. In contrast, Huber *et al.* (2014) found that CD63 knock-downs expressed increased E-cadherin but decreased β -catenin resulting in arrested motility (Figure 1.12). It is therefore unsurprising that CD9 has been so eminent in fusion studies, however, the association of CD9 with multiple partner proteins makes it difficult to determine which specific interaction is affected by CD9 interference.

CD81 has also been shown to associate with CD36 (Heit *et al.*, 2013) and EWI-2 (Sala-Valdés *et al.*, 2006) (Figure 1.12). CD81 has been shown to associate with MFR (Wang and Pfenninger, 2006) which, when bound to CD47 on another cell, could generate

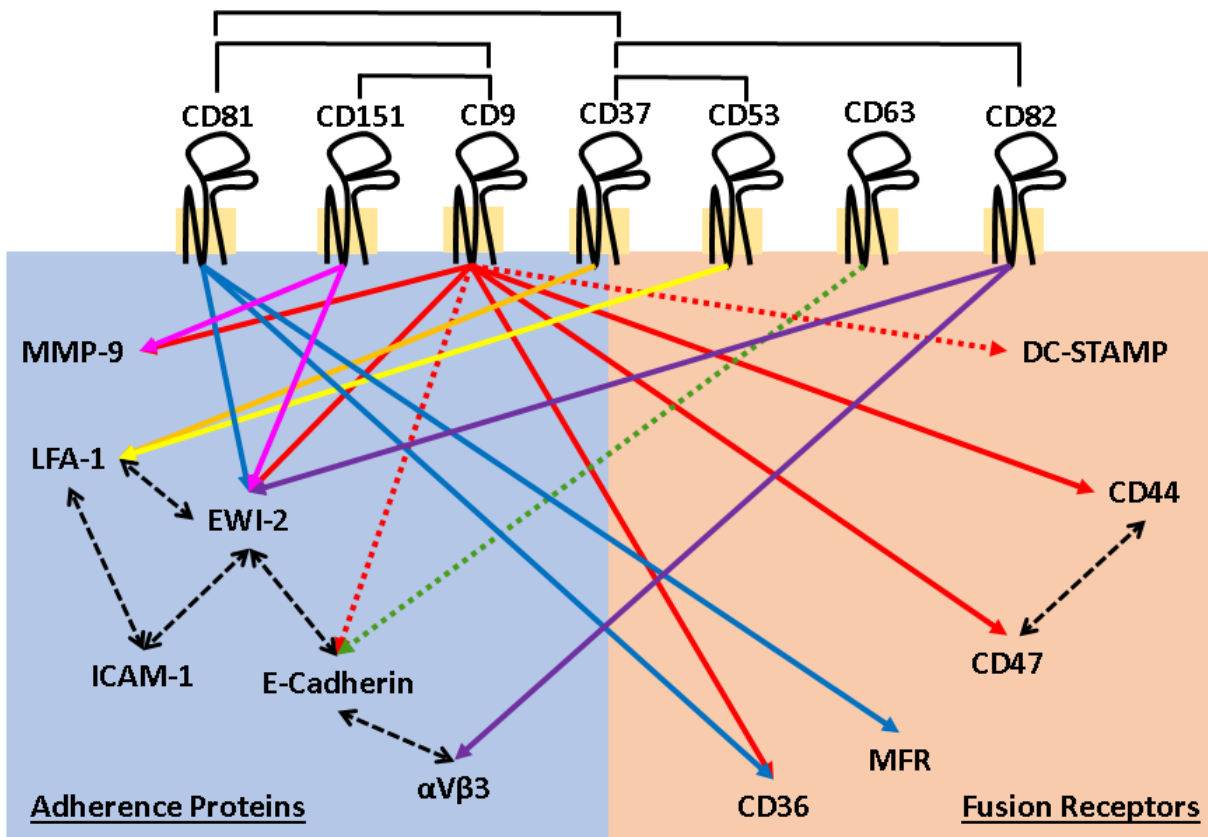


Figure 1.12: Interactions of Tetraspanins, Adherence Proteins and Fusion Receptors.

Tetraspanins are able to associate with a range of binding partners involved in adhesion (blue segment) or fusion (red segment). Tetraspanin-tetraspanin associations (white segment) allow for the formation of tetraspanin enriched microdomains containing multiple tetraspanins and binding partners to carry out cellular processes *en masse*. The coloured arrows indicate direct associations reported between a tetraspanin and an adhesion/fusion protein. The dotted coloured arrows indicate a genetic relationship between a tetraspanin and a relevant protein. Arrows for CD9, CD37, CD53, CD63, CD81, CD82 and CD151 are coloured as red, orange, yellow, green, blue, purple, pink, respectively. Filled black bars (white segment) indicate observed tetraspanin-tetraspanin interactions and dashed black arrows (blue/red segments) indicate reported interactions between adherence proteins/fusion receptors.

TEMs on opposing monocytes; however, existence of such a complex has yet to be proven. Of all the fusion proteins discussed, EWI-2 is able to associate with the widest range of tetraspanins, namely; CD9, CD81, CD82 (Zhang *et al.*, 2003) and CD151 (this interaction is thought to be indirect through CD9) (Charrin *et al.*, 2001). It seems therefore that tetraspanins play an active role in coupling adhesion proteins with actin cytoskeleton remodelling. CD82 is the only tetraspanin that has been shown to associate with and regulate $\alpha V\beta 3$ (Ruseva *et al.*, 2009); the integrin responsible for podosome integrity (McHugh *et al.*, 2000). Pique *et al.* (2000) demonstrated with CD82 overexpressed cells that increased CD82 on host cells inhibited fusion, transmission and syncytia formation by human T-cell leukaemia virus type 1 (HTLV-1).

Antibodies targeting CD151 have been shown to inhibit human sperm-egg fusion (Ziyyat *et al.*, 2006) and overexpression of CD151 in human melanoma cells significantly increased MMP-9 production and enhanced cell motility (Hong *et al.*, 2006). CD151 has also been shown to control $\beta 1$ integrin trafficking, Liu *et al.* (2007) demonstrated by mutation of the CD151 endocytosis-sorting-motif in mouse embryonic fibroblasts that cellular migration could be arrested by inhibited integrin cycling.

CD37 and CD53 share a common association with LFA-1 (Figure 1.12) and appear to both play a role in transducing apoptotic signals. The LFA-1 integrin associates with CD53 (Todros-Dawda *et al.*, 2014) and CD37 via an interaction with the $\beta 2$ unit (CD18) (Wee *et al.*, 2015). CD37 has been shown to be a transducer of apoptosis by direct phosphorylation of its N-terminal domain (Lapalombella *et al.*, 2012) whereas CD53 has been shown by a genome-wide linkage scan to be a regulator of TNF α ; an important pro-inflammatory cytokine that can activate NF- κ B transcription (Bos *et al.*, 2010). CD53 has also been suggested to be a pro-inflammatory marker as its expression was increased when monocytes were differentiated into M1 (Tippett *et al.*, 2013). Furthermore, patients suffering from recurring non-pulmonary tuberculosis were found to have a congenital defect in CD53 (Mollinedo *et al.*, 1997).

1.9 EXPRESSION OF TETRASPANINS IN MONOCYTE SUBSETS

Since monocytes were not publically classified into three subsets until 2010 there is very little published data on tetraspanin expression on monocyte subsets. Ingersoll *et al.* (2010) quantified the expression of CD9 and CD81 in CD16⁻ and CD16⁺ monocytes at steady state. They found that CD9 expression was slightly higher in CD16⁻ monocytes and CD81 was marginally higher in CD16⁺ monocytes. Furthermore, they found that CD9 was expressed as a bimodal peak in CD16⁺ monocytes. Peng *et al.* (2011) separated monocytes by their expression of the high-affinity receptor for IgE (FcεRI) and found that FcεRI^{High} cells expressed higher levels of CD9 and CD81.

Tippett *et al.* (2013) used CD14/CD16 staining to quantify CD9, CD53, CD63 and CD81 expression. CD9 and CD63 were expressed predominantly on CI and at higher intensities, they found these decreased across the subsets with NCI expressing the least. CD53 was expressed on >95% of all monocytes but surface levels were significantly different between each subset with NCI expressing the most and CI the least. CD81 was expressed on ~85% of all the subsets but was expressed significantly higher in NCI monocytes and lowest in CI. While the literature on monocyte subset expression of tetraspanins is limited, currently, there is no publications on the tetraspanin expression of fusing monocytes/Mφ.

Many questions remain about the role of tetraspanins and the individual contribution of the monocyte subsets to the formation of MGC. A greater understanding of MGC formation could aid in the development of treatments to tuberculosis and medical implant rejection.

"It's the questions we can't answer that teach us the most. They teach us how to think. If you give a man an answer, all he gains is a little fact. But give him a question and he'll look for his own answers." - Patrick Rothfuss, *The Wise Man's Fear*.

1.10 HYPOTHESES, AIMS AND OBJECTIVES

1.10.1 HYPOTHESES

Hypothesis 1: Monocyte subsets possess different propensities to fuse to form MGC.

Hypothesis 2: Monocyte subsets mediate fusion by expressing certain combinations of tetraspanins.

Hypothesis 3: The binding of anti-tetraspanin antibodies to fusion-mediating tetraspanins will abrogate or enhance fusion by interfering with their normal functions.

1.10.2 AIMS & OBJECTIVES

Aim 1: Optimise the fusion assay protocol to increase sampling sizes and automate the nuclei counting process to gain an accurate assessment of monocyte fusion.

Aim 2: Purify the monocyte subsets and quantify their individual ability to fuse.

Aim 3: Determine the surface expression of tetraspanins at steady state and when cultured in fusogenic conditions.

Aim 4: Establish which anti-tetraspanin antibodies, if any, affect the fusion of ConA treated monocytes.

CHAPTER 2: MATERIALS AND METHODS

2.1 MATERIALS

Table 1: Lab Consumables

Lab Consumable	Supplier	Cat No
0.2 ml Individual Flat Cap Tubes	Thermo Scientific Abgene	AB-0620
0.4% Trypan Blue Stain (20ml)	Sigma-Aldrich	T8154-20ML
0.5M EDTA , pH 7.3, ultra-Pure Grade, 1L	1st BASE	BUF-1051-1L-pH7.4
0.5ml Micro Tubes	Greiner, Germany	667201
1000 μ L Traditional Shaped Tip, Blue, NP Tip, Bulk, Sterile	Neptune	BITX2110.B
10X PBS Buffer	Biopolis Shared Facilities Media Preparation Unit	https://www.bsf.a-star.edu.sg/Portal/Pages/BMG/BMG
200 μ L Univ. Tip, S3 Tip,	Neptune	BITX2102
35mm Glass Bottom Petri Dish, Well Diameter 14mm, Thickness no. 0	MatTek	35-T0-14-U
96-well Clear V-Bottom, Sterile	Corning	3960
96-well plate, Tissue Culture Treated, black frame with clear flat bottom, polystyrene (#3904)	Corning™	07-200-588
Blunt Needle 18gx1.5 inch	BD - Becton Dickinson	305180
Bottle Top Vacuum Filter, 0.22 μ m	Corning	430513
Bovine Serum Albumin (BSA), lyophilized powder.	Sigma-Aldrich	A9418
Cell Scraper 23cm	Nunc	NNU 179693-PK

Centrifuge Tube 50ml Blue Cap	BD Falcon – Becton Dickinson	35 2070
Centrifuge Tube 50ml Blue Cap	BD Falcon - Becton Dickinson	35 2070
Centrifuge tube, 15ml, Racked	Greiner, Germany	188261
Concanavalin A, Type IV-S, Lyophilized powder	Sigma-Aldrich	C5275
Disposable Haemocytometer C-Chip Neubauer	NanoEnTek, Korea	DHC-N01
PBS (10x) without Ca ²⁺ or Mg ²⁺	Lonza	17-515Q
Fetal Calf/ Bovine Serum (FCS), Heat Inactivated	Gibco™ Thermo Scientific	10082147
Ficoll-Paque™ PLUS	GE Healthcare Life Sciences	17-1440-02
Human AB Serum (HS)	Innovative Research Inc	IPLA-SERAB
IMDM with L-glutamine, Phenol Red & HEPES	Lonza	12-722F
8-Chamber Lab-Tek II Slide System	Nunc	NNU 154534-PK
Latex 12" Powder Free Gloves, Large	Faith Touch	GL-LT-12PFDT-L
MACS Separation LD Columns	Miltenyi Biotec	130-042-901
Micro Tubes 1.5ml Snaplock	Axygen Scientific	MCT-150-C
Microscope Round Cover Glass Ø13mm	Paul Marienfeld, Germany	01 115 30
Parafilm 2in X 250ft Roll	VWR	52858-076
Paraformaldehyde powder, 95%	Sigma-Aldrich	158127-500G
Penicillin-Streptomycin (10,000 units ml ⁻¹ & 10mg ml ⁻¹)	Biological Industries	03-031-1B
Pipet 10ml Single Wrapped	BD Falcon - Becton Dickinson	35 7551

Pipet 25ml Single Wrapped	BD Falcon - Becton Dickinson	35 7525
Pipet 5ml Single Wrapped	BD Falcon - Becton Dickinson	35 7543
Pipette Tip Reload System, 0.1-10ul	QSP	QSP T104RL-Q-PK
Sodium Azide (NaN ₃), ≥99.5%	Sigma-Aldrich	S2002
Syringe 20cc Luer-Lok	BD - Becton Dickinson	300141
Tally Counter	Heinz, Germany	2131 803
Tissue Cell culture plate 24-well sterile with lid	Greiner, Germany	662160

2.1.1 CELL SAMPLES

All experiments were carried out on monocytes derived from human blood collected in ethylenediaminetetraacetic acid (EDTA) anticoagulant at a final concentration of 1.5mg/ml. For experiments with unpurified monocytes and for peripheral monocyte tetraspanin expression, Human mononuclear phagocytes were obtained from peripheral blood taken from healthy volunteers with ethics approval from the South Sheffield Research Ethics Committee [07/Q2305/7]. For all experiments using purified monocyte subsets, cells were obtained from apheresis 'cones' donated by the Singapore Health Sciences Authority from anonymous platelet donors in Singapore. Apheresis cones contain $400-1200 \times 10^6$ PBMCs cone⁻¹, of which; $67.78 \pm 8.63\%$ lymphocytes, 24.62 ± 8.94 monocytes, $4.99 \pm 2.59\%$ neutrophils, $2.22 \pm 0.72\%$ basophils and $0.39 \pm 0.49\%$ eosinophils (Néron *et al.*, 2007; Pfeiffer *et al.*, 2013). Singapore samples were handled with the guidelines directed by the National University of Singapore Institutional Review Board [NUS-IRB 09-256].

2.1.2 MEDIA, BUFFERS & SOLUTIONS

Iscove's Modified Dulbecco's Medium (IMDM) & cIMDM

All IMDM variants contained $3.996 \mu\text{M}$ L-glutamine, $40.755 \mu\text{M}$ phenol red pH indicator and 25.001mM HEPES. For tissue culture complete IMDM (cIMDM) was made by combining 470ml IMDM + 25ml pooled human blood group AB Serum + 5ml Penicillin-

Streptomycin (p/s) solution to make a solution containing 5%(v/v) HS and 1% (v/v) p/s.

1xPhosphate Buffered Saline (1xPBS) pH7.3

1xPBS was used for washing cells that had not been fixed yet and for general washing of fixed cells. 10xPBS pH7.3 was purchased from the in-house Biopolis Shared Facilities Media Preparation Unit and diluted to 1xPBS by combining 100ml 10xPBS to 900ml MilliQ water in tissue culture conditions.

1xPhosphate Buffered Saline pH7.3 without Ca²⁺ or Mg²⁺ (1xPBSw/o)

PBSw/o was used for making PBSE, MACS & FACS buffers and for washing detached cells. 10xDPBS pH7.3 without Ca²⁺ or Mg²⁺ was diluted by adding 100ml to 900ml MilliQ water in tissue culture conditions.

1x Phosphate Buffered Saline + 2mM EDTA (PBSE) pH7.3

PBSE was used for detaching cells non-enzymatically, for washing detached cells and for making MACS & FACS buffers. 3.2ml of 0.5M EDTA was added to 796.8ml of 1xPBSw/o pH7.3 in tissue culture conditions.

4% Paraformaldehyde (PFA)

For 1L of 4% (v/v) PFA, 800ml of 1xPBS pH7.3 was added to a glass beaker on a magnetic stirrer plate in a fume hood. The liquid was slowly heated to ~60°C whilst stirring with a magnetic flea. 40g of 95% (w/v) paraformaldehyde powder was added to the warmed 1xPBS. To completely dissolve the powder; 1M NaOH was added drop by drop until the solution went clear. The magnetic flea was removed and the solution was allowed to cool in the fume hood before it was topped up to 1000ml with 1xPBS. The solution was vacuum filtered using a 0.22µm bottle top vacuum filter. The pH was adjusted to 7.3 before aliquoting the solution into 15ml tubes. The 4% (v/v) PFA was refrigerated at 4°C and discarded after a month, spare tubes were frozen and stored at -20°C.

Nuclei/Actin Staining Solution

For every 1ml of staining solution required: 1µl of a 3mg ml⁻¹ DAPI stock and 5µl of 0.2mg ml⁻¹ phalloidin-TRITC was added to 994µl 1xPBS to give a final concentration of 3µg ml⁻¹ DAPI and 1µg ml⁻¹ phalloidin-TRITC.

10x Red Blood Cell Lysis Solution (10x RBC Lysis Solution)

10x RBC lysis solution was made by combining 16.6g of NH₄Cl, 2g KHCO₃, 400µl of 0.5M EDTA pH7.3 and MilliQ water added to 200ml. 25ml of the 10x RBC lysis solution was then combined with 225ml MilliQ water in sterile conditions to make a working 1x RBC lysis solution and stored at 4°C for up to 3 months.

Magnetic-Activated Cell Sorting (MACS) Buffer

MACS buffer contained 0.5% (w/v) of BSA powder in 1xPBSE. The solution was vacuum filtered (0.22µm) and stored at 4°C and opened only in sterile conditions.

Fluorescence-Activated Cell Sorting (FACS) Buffer

FACS buffer was made by combining 450ml PBSE, 25ml foetal calf serum (FCS), 25ml human serum (HS) and 0.5g sodium azide (NaN₃) to make a solution containing 1xPBS, 2mM EDTA, 5% (w/v) FCS, 5% (v/v) HS and 0.1% (w/v) NaN₃. The solution was vacuum filtered (0.22µm) and stored at 4°C.

Concanavalin A (ConA)

5mg of lyophilised ConA from *Canavalia ensiformis* (Jack bean) was reconstituted in 1ml of 1xPBS, according to the manufacturer's instructions. The 5mg ml⁻¹ solution was aliquoted into 20µl stocks and frozen at -20°C and once thawed, the aliquots were never refrozen but were refrigerated at 4°C for up to 1 month. Fusion media contained 10µg ml⁻¹ ConA in cIMDM.

ConA has been used in multiple studies to induce reproducible homotypic fusion of monocytes (Hulme et al., 2014; Kasugai et al., 2009; Maltesen et al., 2010; Möst et al., 1990; Parthasarathy et al., 2009; Takashima et al., 1993; Takeda et al., 2003; Zhu et al., 2007). The exact mechanism of ConA facilitated fusion is currently unknown,

however, it has been shown that ConA triggers a release of fusion initiating cytokines from mouse M ϕ e.g. IFN γ , TNF- α , IL-1 β and IL-4 (Sodhi et al., 2007; Wang et al., 2012). In 2000, Suen and colleagues showed that ConA induced mitochondrial clustering, release of cytochrome c and apoptosis in murine PU5-1.8 macrophages. Apoptosis has already been established as a vitally important defence in Mtb infections and is thought to play a role in killing infected M ϕ whilst priming nearby M ϕ against the pathogen (Bocchino et al., 2005; Kelly et al., 2008; Lee et al., 2009; Mustafa et al., 2008; Patel et al., 2007). Though the exact mechanism of ConA in the proceeding experiments cannot be confirmed, it is arguably a sufficiently reproducible and obtainable means of inducing monocyte fusion.

MilliQ Water

MilliQ water was produced in-house using a Direct-Q[®] water purification system. To ensure sterility, bottled MilliQ water was autoclaved at 121°C for 15mins at 15psi where after it was only opened in tissue culture conditions.

2.1.3 ANTIBODIES & MARKERS

Antibodies used are all anti-human antibodies.

Table 2: Monocyte Negative-Selection: Magnetic Bead-Antibodies

Target	Conjugate	Isotype	Clone	Retailer	Cat No
Monocyte Isolation Kit II	n/a	n/a	n/a	Miltenyi Biotec	130-091-153
Fc γ R-blocking reagent	n/a	n/a	n/a	Miltenyi Biotec	130-091-765
Non-monocyte depletion cocktail	Magnetic Bead	n/a	n/a	Miltenyi Biotec	130-091-765
CD3	Magnetic Bead	n/a	n/a	Miltenyi Biotec	130-097-43
CD19	Magnetic Bead	n/a	n/a	Miltenyi Biotec	130-097-055

Table 3: FACS: Monocyte Sorting Antibodies

Target	Conjugate	Isotype	Clone	Retailer	Cat No
CD14	eFluor450	IgG1, κ	61D3	eBioscience	48-0149-42
CD16	PE-Cy7	IgG1, κ	3G8	BD Biosciences	560918
CD14	PE-CF594	IgG2b, κ	M ϕ P9	BD Biosciences	562334
CD16	PE-Vio770	IgM	VEP13	Miltenyi Biotec	130-100-432
CD56	APC	IgG2b, κ	NCAM16.2	BD Biosciences	341027
CD9	Biotin	IgG1	MEM-61	Abcam	ab28094
Streptavidin	APC-Cy7	n/a	n/a	Biolegend	405208
CD9	FITC	IgG1, κ	HI9a	Biolegend	312104
CD36	FITC	IgG2a, κ	AC106	Miltenyi Biotec	130-095-470

Table 4: Flow Cytometry: Anti-Tetraspanin Positive Reporter Antibodies

Target	Conjugate	Isotype	Clone	Retailer	Cat No
LIVE/DEAD Blue	DAPI	n/a	n/a	ThermoFisher	L23105
CD9	Biotin	IgG1	MEM-61	Abcam	ab28094
Streptavidin	APC-Cy7	n/a	n/a	Biolegend	405208
CD37	APC	IgG1, κ	MB-1	eBioscience	17-0379-41
CD53	CF405M (Pacific Blue)	IgG1	HI29	Abcam	ab115895
CD63	PerCP	IgG1	MEM259	Abcam	ab77227
CD81	AF700	IgG1, κ	1D6	Novus	NB100-65805AF700
CD82	PE	IgG1	B-L2	Abcam	ab27338
CD151	FITC	IgG1	11G5a	Abcam	ab33316

Table 5: Flow Cytometry: Anti-Tetraspanin Isotype Control Antibodies

Target	Conjugate	Isotype	Clone	Retailer	Cat No
CD9 (Iso)	IgG1-Biotin	IgG1, κ	P3.6.2.8.1	eBioscience	13-4714-85
CD37 (Iso)	APC	IgG1, κ	MOPC-21	Biolegend	400122
CD53 (Iso)	CF405M	IgG1, κ	ICIG1	Abcam	ab126026
CD63 (Iso)	PerCP	IgG1, κ	ICIG1	Abcam	ab118658
CD81 (Iso)	AF700	IgG1, κ	MOPC-21	BD Biosciences	557882
CD82 (Iso)	PE	IgG1, κ	P3.6.2.8.1	eBioscience	12-4714-42
CD151 (Iso)	FITC	IgG1, κ	P3.6.2.8.1	eBioscience	11-4714-42

Table 6: Fluorescence Microscopy

Target	Stain	Retailer	Cat No
DNA	DAPI	ThermoFisher	D1306
DNA	Hoechst (H333342)	ThermoFisher	H3570
DNA	Propidium Iodide	ThermoFisher	P3566
F-Actin	NH3 (IgM)	ThermoFisher	MA1-80729
F-Actin	TRITC	ThermoFisher	R415
2° reporter for NH3 (Anti-mouse Antibodies)	Anti-Mouse Polyvalent Immunoglobulins (G,A,M)-FITC antibody produced in goat	Sigma-Aldrich	F1010

Table 7: Other Marker Reagents

Name	Used in	Retailer	Cat No
AbC™ Anti-Mouse Bead Kit	Flow Cytometry, Compensation	ThermoFisher	A10344
ArC™ Amine Reactive Compensation Bead Kit	Flow Cytometry, Compensation	ThermoFisher	A10346

8 Peak Rainbow Beads	Flow Cytometry, Quality Control	BioLegend	422903
Cell Dissociation Solution (enzyme-free)	Cell Detachment	ThermoFisher	13151014

Table 8: Fusion Assay: Anti-Tetraspanin Phenotyping Antibodies

Target	Stock Conc	Isotype	Clone	Retailer	Cat No
IgG1 LEAF™ (Isotype)	1mg ml ⁻¹	IgG1,κ	MOPC-21	Biolegend	400153
CD9	1.4mg ml ⁻¹	IgG1	602.29	Prof Peter Andrews, University of Sheffield	n/a
CD37	1.17mg ml ⁻¹	IgG2A,κ	WR17	Professor Martin Glennie, University of Southampton	n/a
CD53	1mg ml ⁻¹	IgG1	MEM-53	Abcam	ab667
CD63	2.3mg ml ⁻¹	IgG1	H5C6	Developmental Studies Hybridoma Bank, Iowa, USA	n/a
CD81	1mg ml ⁻¹	IgG1	1D6	Abcam	ab35026
CD82	1mg ml ⁻¹	IgG1	B-L2	Abcam	ab47153
CD151	1.6mg ml ⁻¹	IgG1	14A2.H1	Prof Leonie Ashman, University of Newcastle, Australia.	n/a

Table 9: Software

Software (Version)	Used For	Source
FIJI ImageJ (1.50e)	Viewing, optimisation and analysis of images taken by the Olympus microscopes.	http://fiji.sc/#download
FACSDiva™	Recording of all flow cytometry data to produce .fcs files.	https://www.bdbiosciences.com/us/instruments/research/software/flow-cytometry-acquisition/bd-facsdiva-software/m/111112/overview
FlowJo (10)	Analysis of all .fcs files generated by FACSDiva™ during flow cytometry	http://www.flowjo.com/download-newest-version/
GraphPad Prism (6.04)	Displaying data as graphs and all statistical analysis	http://www.graphpad.com/scientific-software/prism/
MetaMorph (7.8.3.0)	Image acquisition on Olympus microscopes	https://www.moleculardevices.com/systems/metamorph-research-imaging/metamorph-microscopy-automation-and-image-analysis-software

2.2 METHODS

2.2.1 PRIMARY CELL PREPARATION

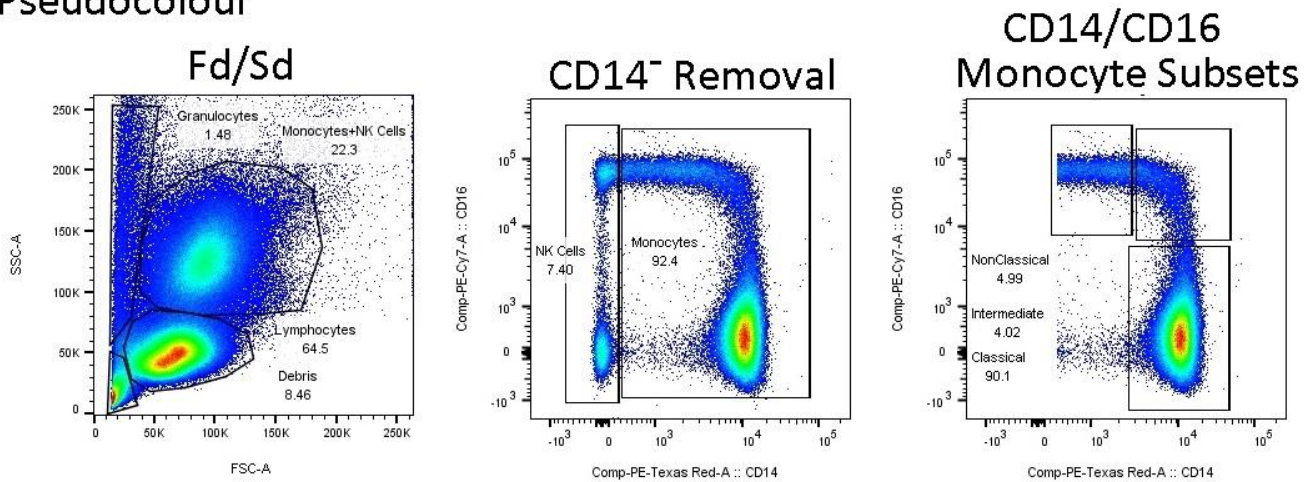
PBMC Extraction from Blood

Human blood from apheresis cones or obtained in-house by venepuncture was diluted 1:1 in PBSE. 30ml of diluted blood was gently layered on top of 15ml Ficoll-Paque PLUS in a 50ml Falcon tube. The blood was then fractionated by density centrifugation at 2000xg for 20min at room temperature with no braking so as not to disturb the layers. The top plasma layer was removed by aspiration before the white PBMC layer was transferred into a fresh 50ml falcon tube and washed of platelets by filling completely with PBSE and centrifuging at 480g, 5min at room temperature. The supernatant was aspirated and the cell pellet resuspended in 5mL 1xRBC-lysis solution and incubated at room temperature for 5min before being topped up to 50ml with PBSE and centrifuged at 480g, 5min at room temperature. From this point, every effort was made to keep the cells and solutions on ice until cells were seeded (as described below), to minimise marker internalisation. Cell density was determined using a disposable haemocytometer (NanoEntek C-Chip) using exclusion of 0.04% Trypan Blue solution to assess cell viability.

2.2.1.1 PURIFICATION OF MONOCYTES BY ADHERENCE

PBMCs were resuspended in cIMDM to 1×10^7 PBMCs ml^{-1} and seeded on 8-chamber Lab-Tek II slides or black framed 96-well plates at 2.2×10^6 and 1×10^6 PBMCs well^{-1} respectively. The slides or plates were incubated for 2hrs at 37°C, 5% CO₂ to allow the monocytes to adhere. The liquid phase was then removed and cells washed three times with 1xPBS that had been warmed to 37°C, to remove non-adherent cells. Fusion assays were performed immediately after this step (see "2.2.3 Fusion Assay"). As the Lab-Tek II chambers are 70mm² and the plate wells are all 31.65mm² and assuming that, on average, 15% of the PBMCs will be monocytes, this would result in $\sim 3.3 \times 10^5$ and $\sim 1.5 \times 10^5$ monocytes well^{-1} (4714 and 4739 monocytes mm^{-2} respectively). Within PBMCs, $21.6 \pm 8.83\%$ of cells were monocytes (Figure 2.1), of these $87.13 \pm 4.38\%$ were classical (Cl), $6.41 \pm 1.43\%$ intermediate (Int) and $5.18 \pm 2.25\%$ nonclassical monocytes (NCI) (N=9).

Pseudocolour



Contour

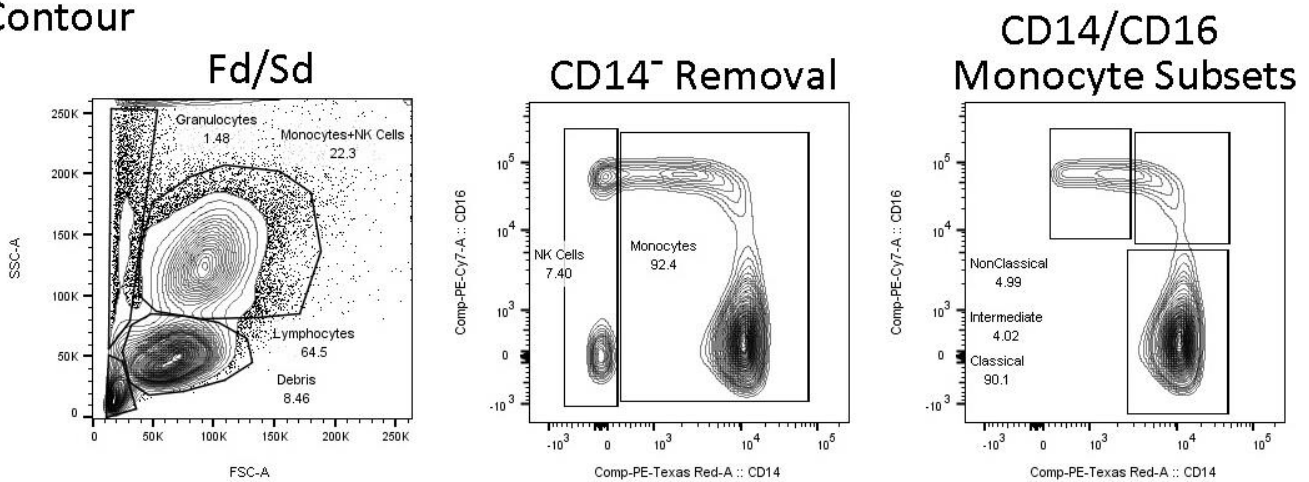


Figure 2.1: Components of PBMCs Isolated from Human Blood

Flow cytometric analysis of the cellular components within PBMCs before adhesion purification; both pseudocolour and contour graphs are shown above for the same data.

Left: Granulocytes show a low forward scatter due to their small size and high side scatter due to their internal granule complexity. Monocytes and NK-cells are similar in size and granularity and the lymphocytes are the smallest living population with low forward and side scatter.

Middle: NK-cells and any remaining non-monocyte components can be gated out from monocytes by their low CD14 expression.

Right: The remaining cells are all monocytes and can be split up into Classical (CD14++CD16-), Intermediate (CD14++CD16+) and Nonclassical (CD14+CD16++). In 9 donors $21.60 \pm 8.83\%$ of cells were monocytes, of these $87.13 \pm 4.38\%$ were Classical, $6.41 \pm 1.43\%$ Intermediate and $5.18 \pm 2.25\%$ were Nonclassical monocytes.

2.2.1.2 ISOLATION OF MONOCYTES BY MAGNETIC-ACTIVATED CELL SORTING USING NEGATIVE-SELECTION

For every 1×10^8 PBMCs, 200 μ l MACS-buffer and 80 μ l Fc γ R-blocking reagent was added and the cells were incubated for 5min at 4°C. Then a cocktail containing 100 μ l MACS-buffer, 50 μ l non-monocyte depletion cocktail, 45 μ l anti-CD3-beads (B-cell targeting) and 45 μ l anti-CD19-beads (T-cell targeting) were added and the cell suspension. *N.B.* For non-monocyte cell depletion, the antibody cocktail contained anti-CD7, anti-CD56, anti-CD123 and glycophorin-A to target CD8+ T-cells, NK-cells, stem cells and erythrocyte precursors, respectively. The cells were refrigerated for 15min at 4°C with gentle resuspension at 5min intervals. The suspension was topped up to 10ml with MACS-buffer before centrifuging for 5min at 480g and resuspended in 1ml MACS-buffer. An LD column was placed in the MACS magnetic separator and equilibrated with 2ml MACS-buffer. The cells were then added to the column when depleted the column was washed at least twice with 1ml MACS-buffer. Total monocytes were collected from the flow-through and counted using a haemocytometer as previously described. MACs-enriched cells contained $68.74 \pm 9.73\%$ monocytes (Figure 2.2); of these $79.71 \pm 6.70\%$ were CI, $8.77 \pm 2.80\%$ Int and $10.57 \pm 4.49\%$ NCI monocytes (N=21).

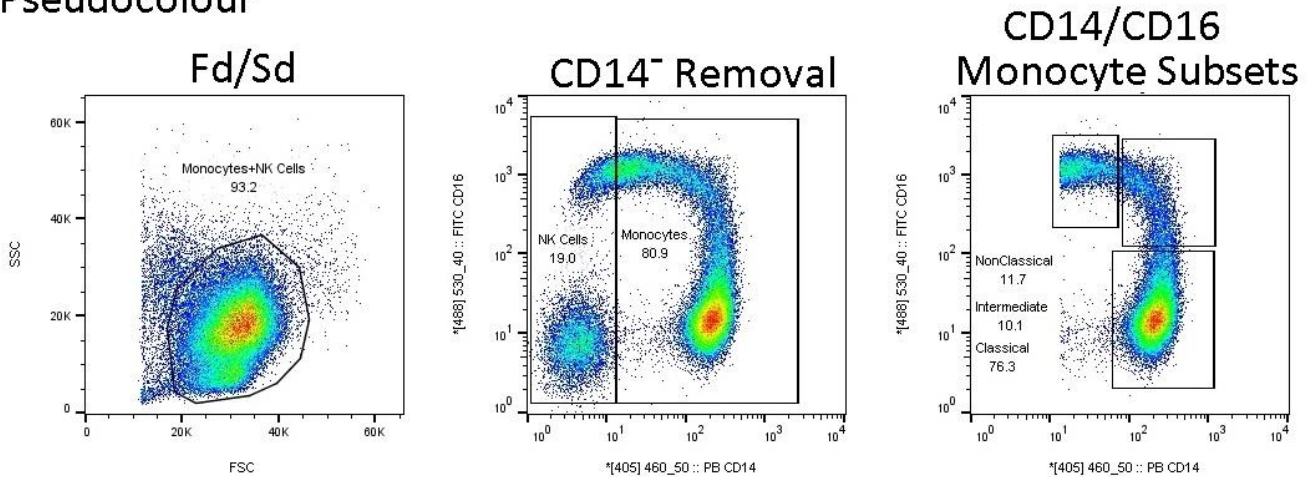
2.2.1.3 SORTING MONOCYTE SUBSETS USING FLUORESCENCE-ACTIVATED CELL SORTING

After counting, the desired number of total monocytes was placed in a new tube and pelleted by centrifugation for 5min at 480g before being labelled depending on the experiment they were used in.

FACS 1: Monocyte Subsets for Phenotyping Experiments

For every 1×10^7 monocytes; a cocktail containing 8 μ l anti-CD14-eFluor450, 12 μ l anti-CD16-FITC, 6 μ l anti-CD56-APC (NK-cell targeting) and 10 μ l MACS-buffer was made before rapidly resuspending the pellet in the cocktail. The cell suspension was refrigerated for 15min at 4°C and at 5min intervals the cells were gently resuspended. The suspension was topped up to 10ml with MACS-buffer before centrifuging for 5min at 480g and resuspended in MACS-buffer to a cell density of 12×10^6 monocytes ml⁻¹.

Pseudocolour



Contour

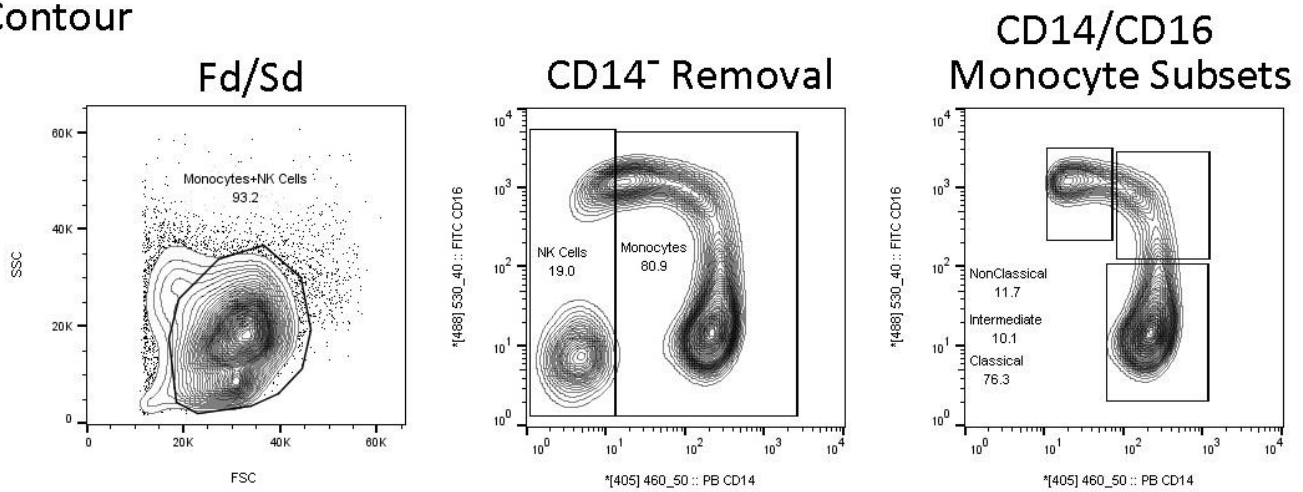


Figure 2.2: Components of MACs Isolated Cells from Human Blood

Flow cytometric analysis of the cellular components within MACs isolated cells; both pseudocolour and contour graphs are shown above for the same data. The same gating strategy as Figure 2.1 has been used. After MACs purification the granulocyte and lymphocyte population were depleted dramatically and the monocyte population became the major cell type of the suspension. In 21 donors MACs enriched cells comprised of $68.74 \pm 9.73\%$ monocytes, of these $79.71 \pm 6.70\%$ were Classical, $8.77 \pm 2.80\%$ Intermediate and $10.57 \pm 4.49\%$ Nonclassical monocytes.

This cell suspension was stored and transported in the dark on ice to the SING Flow Cytometry Facility.

FACS 1 Gating Strategy

Cells were gated using their forward and side (FSC-A/SSC-A) scatter characteristics (Figure 2.3). Singlet monocytes were selected by consecutive FSC-A/FSC-W and SSC-A/SSC-W gating and CD56^{Low}CD14^{Low-High} monocytes were gated to ignore contaminating NK-cells and gated again by their CD14-eFlour450/CD16-FITC binding into monocyte subsets: Cl (CD14⁺⁺CD16⁻), Int (CD14⁺⁺CD16⁺) and NCI (CD14⁺CD16⁺⁺). To maintain reproducibility, subsets were always gated with equal sized square gates with perpendicular borders. Subsets were collected into 5ml polypropylene tubes containing 0.5ml cIMDM. A post-sort check was conducted on 100 cells in every subset to ensure that the purity was $\geq 99\%$. Cells were stored on ice until collection was complete. Subsets were then counted as described above (see "2.2.1 PBMC Extraction from Blood") and diluted accordingly in cIMDM. A post-sort check was conducted on every sorted sample by the operator to ensure $\geq 98\%$ purity was maintained.

FACS 2: Monocyte Subsets for MGC Flow Cytometric Analysis

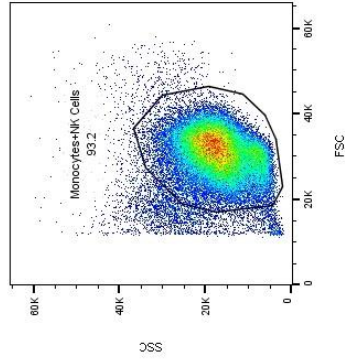
A different set of antibodies and conjugates was used to sort monocytes for flow cytometry experiments to avoid fluorescence emission overlaps in the panel. For 1×10^6 monocytes, cells were rapidly resuspended in a cocktail containing 1 μ l anti-CD14-PE-C594, 2.3 μ l anti-CD16-PE-Vio770 and 47 μ l MACS. The cells were then treated in the same way as described above.

FACS 2 Gating Strategy

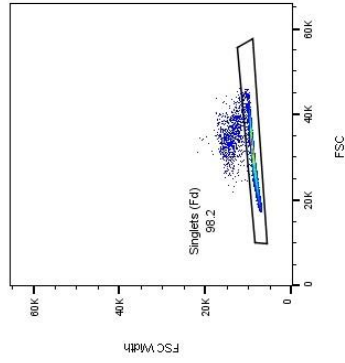
The same gating strategy as FACS 1 was applied but with the alternative CD14 and CD16 fluorophore channels in place.

Pseudocolour

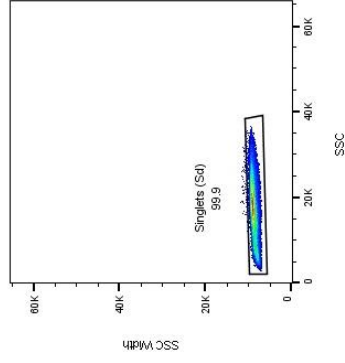
Fd/Sd



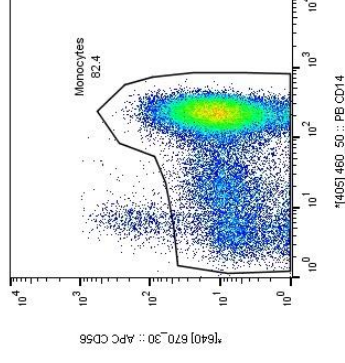
Singlet (Fd-A/Fd-W)



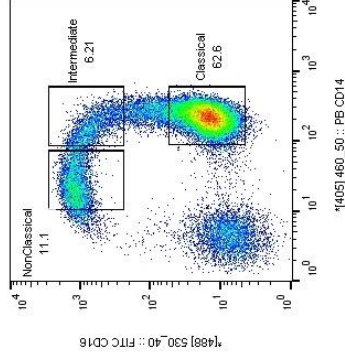
Singlet (Sd-A/Sd-W)



CD56+ NK Removal

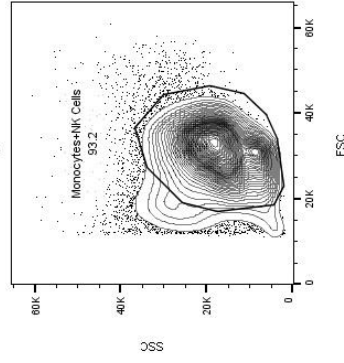


CD14/CD16 Monocyte Subsets

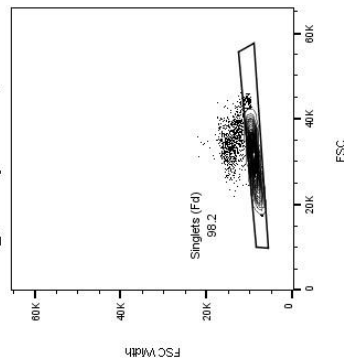


Contour

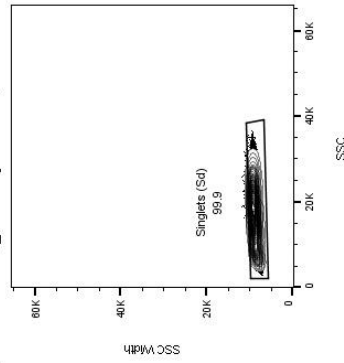
Fd/Sd



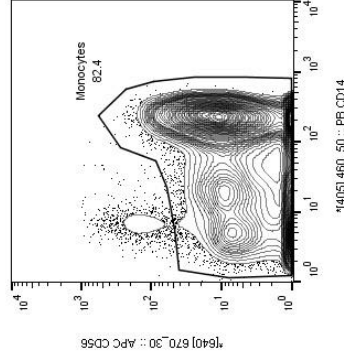
Singlet (Fd-A/Fd-W)



Singlet (Sd-A/Sd-W)



CD56+ NK Removal



CD14/CD16 Monocyte Subsets

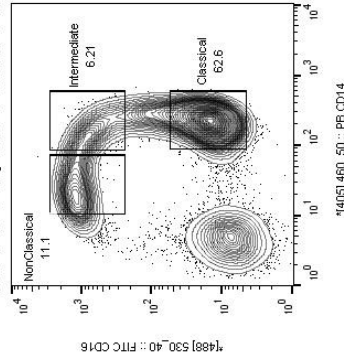


Figure 2.3: FACS Gating Strategy of Monocyte Subsets from MACs Isolated Cells

Pseudocolour and contour graphs showing the FACS gating strategy used to purify monocyte subsets. First, monocytes were broadly selected by their FSC-A/SSC-A scatter, from this population singlets were selected by sequential FSC-A/FSC-W and SSC-A/SSC-W selection. Note: Forward scatter (FSC) is a direct measure of cell size, side-scatter (SSC) is a measure in the internal cellular complexity/granularity. The cells were then presented in a CD14/CD56 dot plot and NK-cells (CD14^{low}CD56^{high}) were gated out using the section shown. Finally Classical (CD14⁺⁺CD16⁻), Intermediate (CD14⁺⁺CD16⁺) and Nonclassical (CD14⁺⁺CD16⁺⁺) monocytes were gated using 3 equally sized gates that had their borders strictly aligned with each other in an inverted 'L'-shape. After sorting an aliquot from each tube of collected subset cells was quality checked to ensure ≥99% purity was maintained.

FACS 3: Monocyte Subsets for Classical CD9 Low vs High Fusion Assay

For every 1×10^6 monocytes, cells were first resuspended in a mixture of 0.18 μl anti-CD14-eFluor450, 0.7 μl anti-CD16-PE-Cy7 and 49 μl MACS buffer then split accordingly. Cells were labelled for CD9 either directly or indirectly.

Direct Labelling of CD9: 2.5 μl anti-CD9-FITC per 1×10^6 monocytes was added to the cell suspension, then incubated for 30 min at 4°C in the dark before being washed by topping up the wells with MACS buffer and spinning for 5 min at 480g. Cells were resuspended in MACS-buffer to a cell density of 12×10^6 monocytes ml^{-1} for sorting.

Direct labelling of CD36: CD36 was also used as a substitute marker for CD9 as the markers appeared to co-express in CI monocytes (Figure 2.4). 3 μl anti-CD36-FITC was added to the cell suspension for every 1×10^6 monocytes and incubated and washed as previously described.

Indirect Labelling of CD9: 0.4 μl anti-CD9-Biotin was added, incubated and washed as described in direct labelling then the cell pellet was resuspended in 0.4 μl Streptavidin-APC-Cy7 for every 1×10^6 monocytes and made up to 50 μl with MACS buffer. After incubation and washing cells were resuspended for FACS as previously described.

FACS 3 Gating Strategy

A CD9-APC-Cy7 CD36-FITC double stained sample was used to set up the gating. Cells were gated into singlets, NK-cells removed and monocyte subsets allocated as outlined in "FACS 1 Gating Strategy" and Figure 2.3. The CI ($\text{CD14}^{++}\text{CD16}^{-}$) subset was displayed into a dot plot. The $\text{CD9}^{\text{Lo}}/\text{CD36}^{\text{Lo}}$ and $\text{CD9}^{\text{Hi}}/\text{CD36}^{\text{Hi}}$ populations were gated as the lowest 25% and the highest 25% of the MFI readings respectively (see Figure 2.4). Once the gates had been set the single stained cells were loaded and sorted. Cells were collected and stored as previously described.

2.2.2 FLOW CYTOMETRIC ANALYSIS OF TETRASPANINS

A 10-marker panel was developed that could identify the three monocyte subsets, quantify the expression of all seven tetraspanins of interest and detect cell viability all in one sample. The panel consisted of a LIVE/DEAD Blue dye, two monocyte subset markers (anti-CD14- PE-CF594 & anti-CD16- PE-Vio770) and seven tetraspanin markers

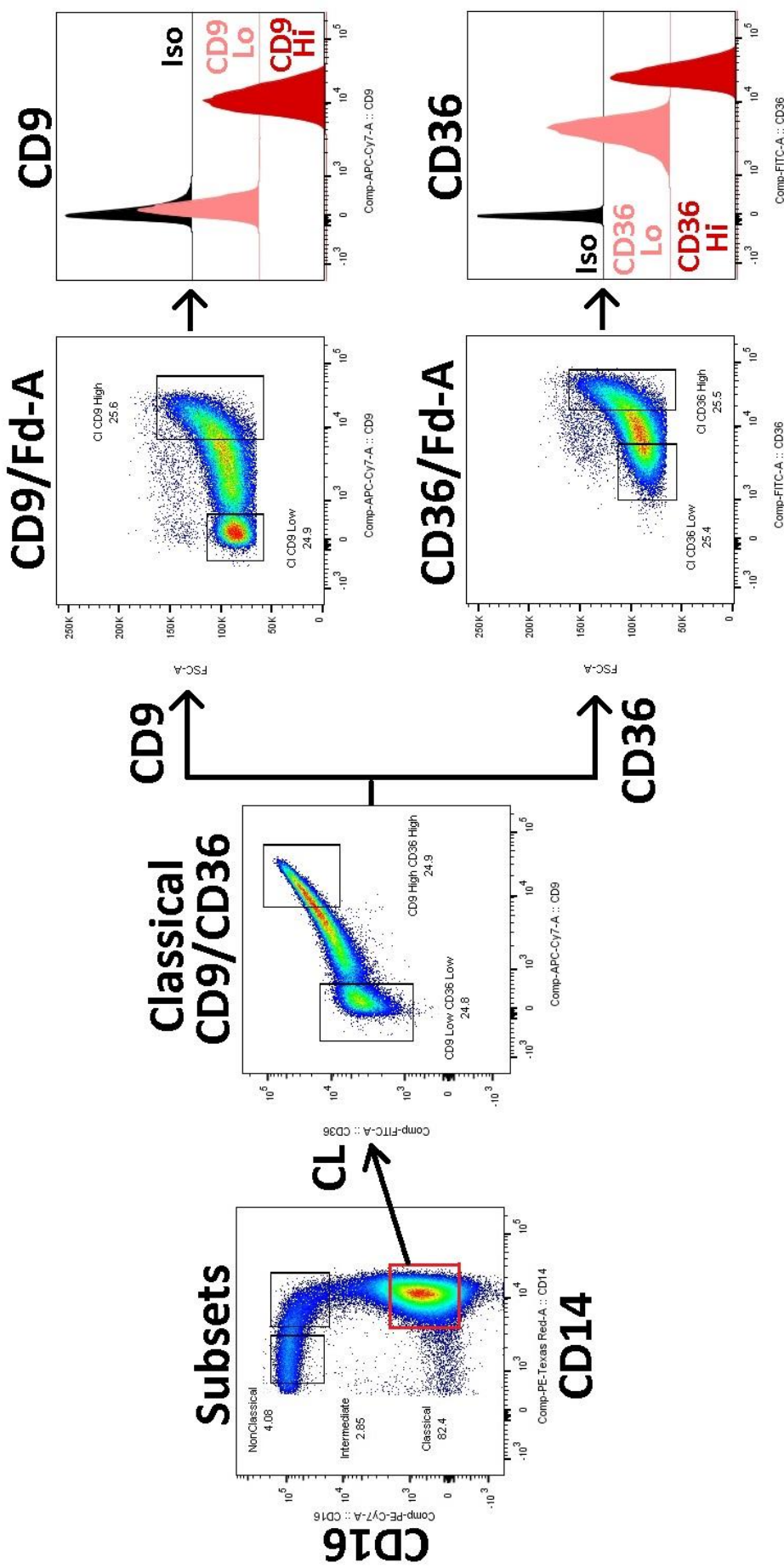


Figure 2.4: FACS Gating Strategy of CD9^{Low}CD36^{Low} and CD9^{High}CD36^{High} Classical Monocytes
 After undergoing the same FACS gating strategy as described in Figure 2.3 the Classical (CD14⁺⁺CD16⁻) subset was drilled down and using a small sample of double stained cells (both CD9-APC-Cy7 and CD36-FITC) the upper and lower 25% limits of CD9/CD36 expression were set. The cells to be sorted were single stained but due to the correlation between CD9 and CD36 expression CD9^{High} cells were CD36^{High} and *vice versa* thus allowing single staining to sort for either population.

(anti-CD9-Biotin, anti-CD37-APC, anti-CD53-CF405M, anti-CD63-PerCP, anti-CD81-Alexa Fluor 700, anti-CD82-PE, anti-CD151-FITC). Streptavidin-APC-Cy7 was used as the secondary reporter for CD9-Biotin and all anti-tetraspanin antibodies had an IgG1 isotype equivalent in a separate sample. Each antibody was individually titrated to ascertain the concentration for optimum binding and reporting (data not shown).

2.2.2.1 STAINING FRESHLY ISOLATED PERIPHERAL BLOOD MONOCYTES FOR FLOW CYTOMETRY

PBMCs from in-house volunteer donors were pelleted and washed with PBS in a 15ml Falcon tube (480g, 5min at room temperature) and resuspended in 1ml PBS + 1 μ l LIVE/DEAD Blue dye and incubated for 30min in the dark at room temperature. Excess dye was removed by adding 2mls of FACS buffer before cells were pelleted (480g, 5min at room temperature) and washed again in 1ml FACS buffer. The PBMC pellet was resuspended in 200 μ l FACS buffer containing 1 μ l anti-CD14-PE-C594 and 2.3 μ l anti-CD16-PE-Vio770 per million cells. PBMCs were refrigerated at 4°C for 30min in the dark, topped up to 3ml with FACS Buffer and centrifuged (480g, 5min at room temperature). The pellet was washed in 1ml FACS buffer, spun again and resuspended to a suitable density to allow the PBMCs to be seeded in v-bottomed wells on a 96-well plate at 1x10⁶ PBMCs well⁻¹. Hereafter PBMCs were split into positive and isotype. The following master mixtures were made up and the PBMCs were rapidly resuspended in them before incubation for 30min, 4°C, in the dark.

Positive Panel (for 1x10⁶ PBMCs): 0.4 μ l anti-CD9-Biotin, 5 μ l anti-CD37-APC, 1.5 μ l anti-CD53-CF405M, 10 μ l anti-CD63-PerCP, 5 μ l anti-CD81-Alexa Fluor 700, 5 μ l anti-CD82-PE, 10 μ l anti-CD151-FITC and 13.1 μ l FACS buffer.

Isotype Panel (for 1x10⁶ PBMCs): 0.4 μ l IgG1-Biotin, 5 μ l IgG1-APC, 2.4 μ l IgG1-CF405M, 2.4 μ l IgG1-PerCP, 6 μ l IgG1-Alexa Fluor 700, 1.2 μ l IgG1-PE, 2 μ l IgG1-FITC and 30.6 μ l FACS buffer.

The PBMCs were washed with FACS buffer and pelleted (480g, 5min at room temperature). A mixed secondary antibodies solution was made by adding 0.8 μ l streptavidin-APC-Cy7 to 60 μ l FACS buffer and 30 μ l of this solution was added to both the positive and isotype pellets. PBMCs were incubated for 20min, 4°C, in the dark before a final wash and resuspended in 150 μ l FACS buffer and transferred into 1.1ml

FACS tubes and stored on ice to be taken to the SIgN Flow Cytometry Facility and analysed on a BD LSRII 5-Laser analyser.

2.2.2.2 FLUORESCENCE COMPENSATION

A compensation matrix was generated on FACSDiva before any flow cytometric analysis was conducted (excluding any observations where only one fluorophore was used). Antibody compensation beads were prepared by combining 1 drop each of negative and capture anti-mouse Fc compensation beads into a 1.1ml FACS tube that was labelled with a specific antibody (one tube for every antibody-fluorophore used). Each tube then had its own 1µl of antibody added and rapidly mixed by pipette, these tubes were incubated in the dark on ice for 5min before adding 200µl of FACS buffer.

ArC beads were used for the LIVE/DEAD Blue stain as the dye targets amines and is unreactive to Fc targeting mechanisms. ArC beads were prepared by adding 1 drop of capture ArC compensation beads into a 1.5ml Eppendorf tube and allowed to warm to room temperature for 5min. 1µl of LIVE/DEAD Blue dye was added to the ArC beads and mixed rapidly by pipette before being incubated at room temperature in the dark for 30min. 1ml of PBS was added to the tube before it was spun at 300g for 5min. The liquid phase was carefully removed and 200µl FACS buffer was used to resuspend the bead pellet. 1 drop of negative ArC beads was added before briefly vortexing the tube and running the beads through flow.

Rainbow beads were run as a separate sample alongside any quantitative flow cytometric analysis to verify instrument performance and allow readings to be standardised between long periods of use.

2.2.2.3 MONOCYTES CULTURED FOR 4 HRS IN IMDM VS IMDM+CONA

Monocyte subsets obtained from FACS 2 sorting strategy were seeded at 0.25×10^6 monocytes well⁻¹ (positive, isotype & unstained) in a u-shaped 96-well plate in either 200µl cIMDM or 200µl cIMDM + 10µg ml⁻¹ ConA. The plate was incubated for 4hrs at 37°C, 5% CO₂. The plate was centrifuged at 500g for 5min before the liquid phase was removed from the wells. 200µl of cold cell dissociation solution was added to each

well and the plate placed on ice for 30min. By repeatedly pipetting up and down in each well the highly adherent cells were removed from the plate walls before being spun (500g, 5min), resuspended in 200µl ice-cold PBSE and transferred into new wells and pelleted again. A stock LIVE/DEAD Blue solution was made by adding 2µl of LIVE/DEAD Blue dye to 1500µl 1xPBS and 200µl was added to each of the isotype and positive pellets and 1xPBS alone was added to the unstained wells. After 20min incubation at room temperature in the dark, the cells were pelleted and washed once in 200µl FACS buffer to remove excess dye and pelleted once more before adding the positive or isotype antibodies. Antibody master mixes were made as outlined below on ice:

Positive Panel (for 1.5×10^6 monocytes): 1.2µl anti-CD9-Biotin, 15µl anti-CD37-APC, 4.5µl anti-CD53-CF405M, 30µl anti-CD63-PerCP, 15µl anti-CD81-Alexa Fluor 700, 15µl anti-CD82-PE, 30µl anti-CD151-FITC and 189.3µl FACS buffer.

Isotype Panel (for 1.5×10^6 monocytes): 1.2µl IgG1-Biotin, 15µl IgG1-APC, 7.2µl IgG1-CF405M, 7.2µl IgG1-PerCP, 18µl IgG1-Alexa Fluor 700, 3.6µl IgG1-PE, 6µl IgG1-FITC and 241.8µl FACS buffer.

50µl of the corresponding master mix was added to the six positive or six isotype wells and refrigerated for 30min at 4°C in the dark. Wells were topped up with 150µl of FACS buffer and spun at 500g for 5min to pellet the cells, washed with 200µl FACS buffer and pelleted again. A master mix containing 2.8µl streptavidin-APC-Cy7 + 597.2µl FACS buffer was made and 50µl was added to each of the positive and isotype wells (unstained cells were resuspended in FACS buffer alone). The cells were refrigerated for 20min at 4°C in the dark before being topped up with 150µl of FACS buffer and spun at 500g for 5min to pellet the cells. After a final wash with 200µl FACS buffer the cells were pelleted, resuspended in 150µl FACS buffer and transferred into 1.1ml FACS tubes and stored on ice to be taken to the SING Flow Cytometry Facility and analysed on a BD LSRII 5-Laser analyser (Figure 2.5).

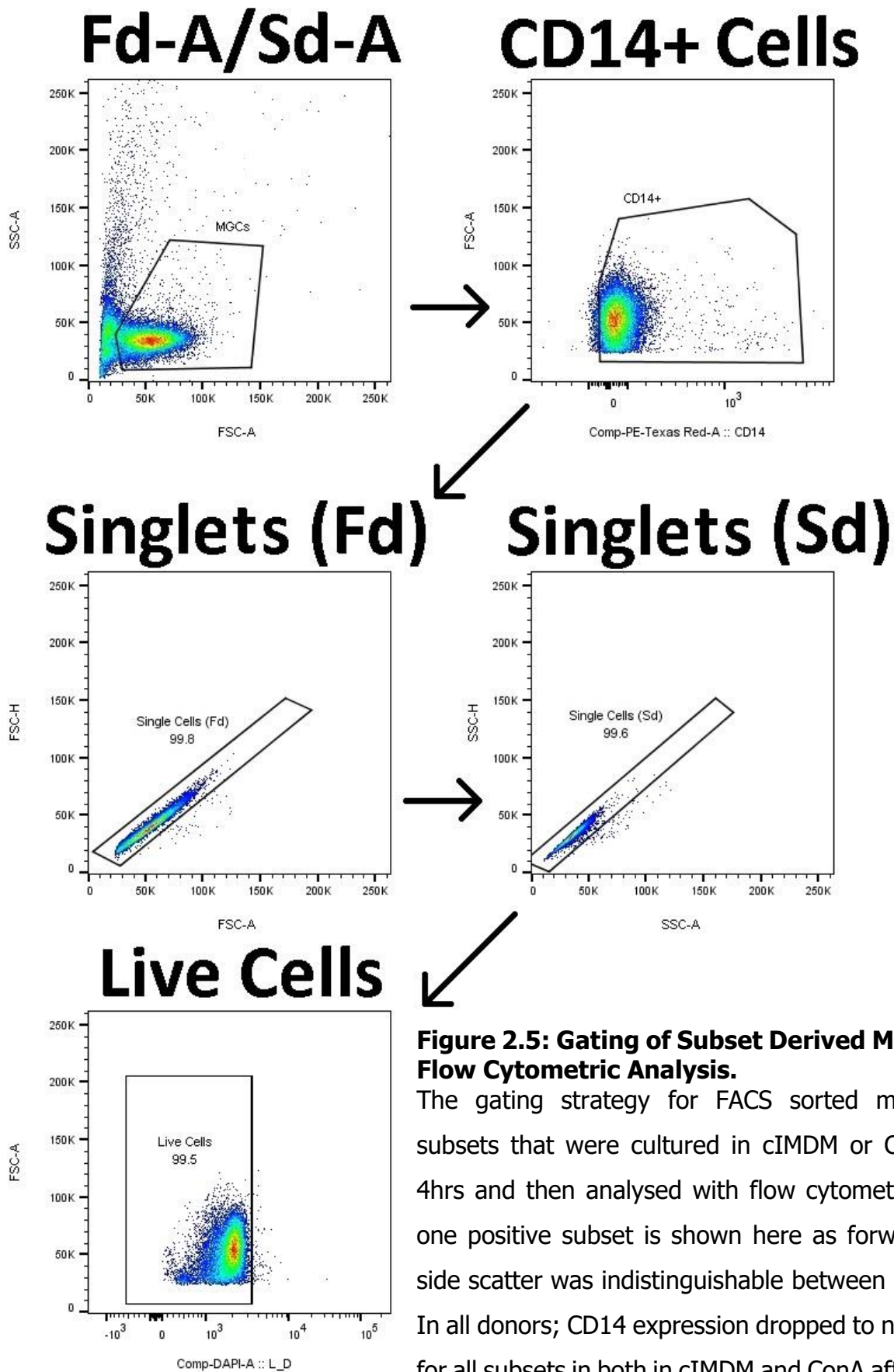


Figure 2.5: Gating of Subset Derived MGCs for Flow Cytometric Analysis.

The gating strategy for FACS sorted monocyte subsets that were cultured in cIMDM or ConA for 4hrs and then analysed with flow cytometry. Only one positive subset is shown here as forward and side scatter was indistinguishable between subsets. In all donors; CD14 expression dropped to near zero for all subsets in both in cIMDM and ConA after 4hrs.

2.2.3 FUSION ASSAYS

Fusion assays were carried out on total monocytes and FACS 1 sorted subsets. Monocytes were resuspended in cIMDM to 1.5×10^6 monocytes ml^{-1} and 100 μl of this cell suspension was seeded per well in a 96-well plate to give 1.5×10^5 monocytes well^{-1} . Where relevant, 100 μl of cIMDM containing 2xConA ($20 \mu\text{g ml}^{-1}$) and 2xanti-tetraspanin antibodies ($20 \mu\text{g ml}^{-1}$) was added to the each well. This way, monocytes were always cultured at a density of 4740 monocytes mm^{-2} unless specified otherwise. Monocytes were incubated at 37°C in 5% CO_2 for 72hrs in all total, subset and anti-tetraspanin antibody assays. For the fusion kinetics analysis and Luminex™ ELISA samples individual time-points were taken at 24hrs, 48hrs and 72hrs.

Fixing Lab-Tek II slides: The media was discarded before the cells were washed with pre-warmed (37°C) 1xPBS, aspirated, fixed and permeabilised by adding ~200 μl of 100% (v/v) acetone. Cells were left to fix and permeabilise for 5min in 100% (v/v) acetone before being bathed in a glass tank containing 500ml of 1xPBS which was refrigerated at 4°C until staining could be performed.

For the fusion kinetics samples & Luminex™ ELISA: At the specific time-points the media in the well was collected and put into separate 1ml tubes for ELISA analysis. The tubes were spun at 3000g for 5min to pellet any cells/debris and two 75 μl aliquots were taken from the resultant liquid phase and placed into PCR tubes and stored at -20°C. The cells in the wells were fixed as outlined below.

For all other assays: The media was discarded before the cells were washed with pre-warmed (37°C) 1xPBS, aspirated, fixed by adding 100 μl of pre-warmed 4% (v/v) PFA and incubated at 37°C, 20 min, 5% CO_2 . The wells were aspirated and washed with 200 μl PBS and stored at 4°C in the dark until the day before imaging, cells were always stained and imaged within one week of fixing.

2.2.4 STAINING CELLS FOR FLUORESCENCE MICROSCOPY

2.2.4.1 STAINING LAB-TEK II SLIDES:

This staining protocol was only used on total monocytes in Chapter 3. Unless specified otherwise, all staining for fluorescence microscopy was performed using the "Optimised Staining of 96-Well Plates" protocol below.

Lab-Tek II slides were removed from the 1xPBS tank and excess liquid was aspirated. Each chamber was stained with 100 μ l of a nuclei/actin staining solution (containing 1 μ g ml⁻¹ propidium iodide and 20 μ g ml⁻¹ NH₃ anti-F-actin primary antibody. For 1ml of stain 14.3 μ l of 1.4mg ml⁻¹ NH₃ antibody + 1 μ l of 1mg ml⁻¹ propidium iodide was added to 984.7 μ l 1xPBS. Slides were refrigerated for 30min at 4°C in the dark, then the chambers were washed with 1xPBS. A secondary staining solution was made containing 4 μ g ml⁻¹ goat anti-mouse polyvalent immunoglobulins with a FITC label. 100 μ l of the secondary stain was added to each chamber and refrigerated for 30min at 4°C in the dark. Chambers were then aspirated, washed with 1xPBS and the Lab-Tek II frame was removed as per the manufacturer's instructions and mounted with a few drops of 1xPBS and a glass coverslip fixed in place with nail varnish. Slides were imaged immediately after staining.

2.2.4.2 OPTIMISED STAINING OF 96-WELL PLATES:

PBS was aspirated from the wells and fixed cells (see "2.2.3 Fusion Assays") were stained with 50 μ l of nuclei/actin staining solution (containing 3 μ g ml⁻¹ DAPI and 1 μ g ml⁻¹ Phalloidin-TRITC). Cells were left to stain overnight at 4°C in the dark. Prior to imaging, the staining solution was aspirated and wells were washed with PBS, aspirated and resuspended in 200 μ l PBS and taken to the Institute of Molecular and Cell Biology (IMCB) microscope facility.

2.2.5 FLUORESCENCE IMAGING

An Olympus IX83 inverted microscope running MetaMorph was used for image acquisition. Each well was imaged at 4x magnification in a 4x4 grid, 0 μ m spacing between images with DAPI and TRITC channels then imaged again at 10x magnification in a 4x4 grid, 200 μ m spacing with DAPI, TRITC and brightfield channels. All images were taken at 16-Bit scale with Binning at 2, Gain 2 (1x) and the autofocus set to \pm 60 μ m. The exposure of each fluorophore was set by finding a particularly MGC dense region in one of the wells and adjusting the exposure so that the 16-bit scale slider on the left never saturated to more than \sim 95-98%. The stringency of these parameters was maintained so that the downstream macros and calculations based on pixel size/value were accurate and reproducible.

2.2.6 IMAGE OPTIMISATION

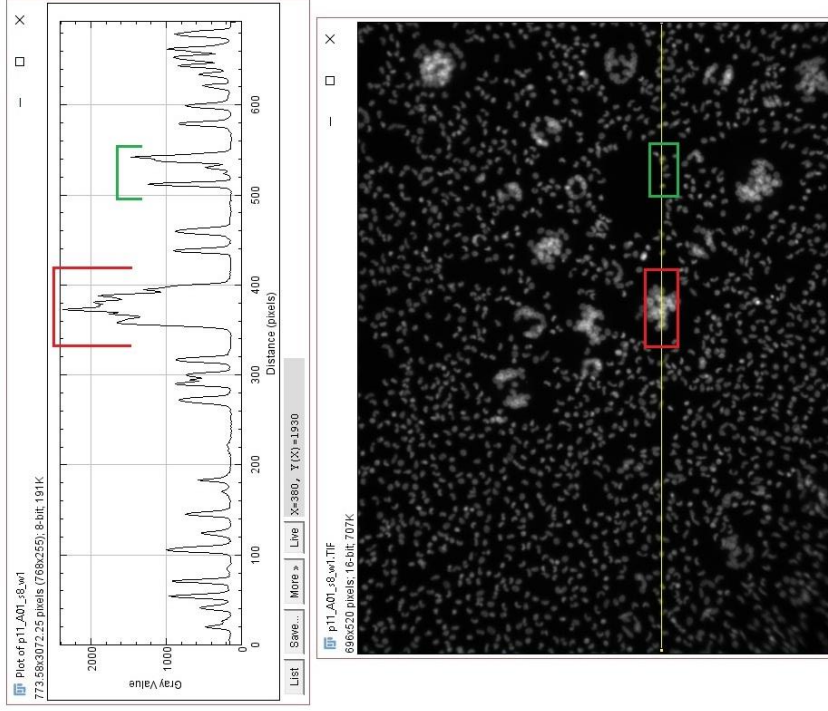
Raw image files were arranged into a Stack on FIJI ImageJ and a Hyperstack was generated. The channels were then split apart (Image>Color>Split Channels) from the Hyperstack and each was individually background reduced (Process>Subtract Background...), inadequate background removal from the DAPI channel led to poor macro sensitivity during counting (see Figure 2.6). The Stacks were then combined again (Image>Color>Merge Channels...) and converted to an RGB format (Type>RGB Color) so that each view could be saved as a Tiff file for future analysis.

The 4x images were collaged on FIJI ImageJ by creating a stack of all the images in a chosen well then aligned and combined (Plugins>Stitching>Grid/Collection Stitching). The 4x well collages were used to give an overall view of the fusion in the well. Four representative 10x images were selected for each well (covering a total area of 2.6mm²) and arranged into a separate stack with the other conditions for image analysis. The ordering of the sample images in the stack was noted on a spreadsheet so that each image in a stack did not have an obvious label that would detail the condition; this way double-blind analysis could be carried out.

2.2.7 IMAGE ANALYSIS

MGCs were identified from the image Stack on FIJI ImageJ and freehand outlines were drawn around each MGC with >3 nuclei or more to make "Region Of Interest" (ROI) coordinates that could be saved alongside the Stack files. The stack and ROI list file were mounted onto ImageJ, the Stack was split up into its three colour channels (Image>Color>Split Channels) and all but the DAPI channel were closed. The DAPI stack and ROI lists were used in conjunction with the corresponding macro below to count the nuclei per MGC, measure MGC area and count the total number of nuclei per view. Despite efforts to automate the designation of MGC type there was no reliable method other than manually scoring the MGCs for morphological features (see Figure 2.7).

Before Background Reduction



After Background Reduction

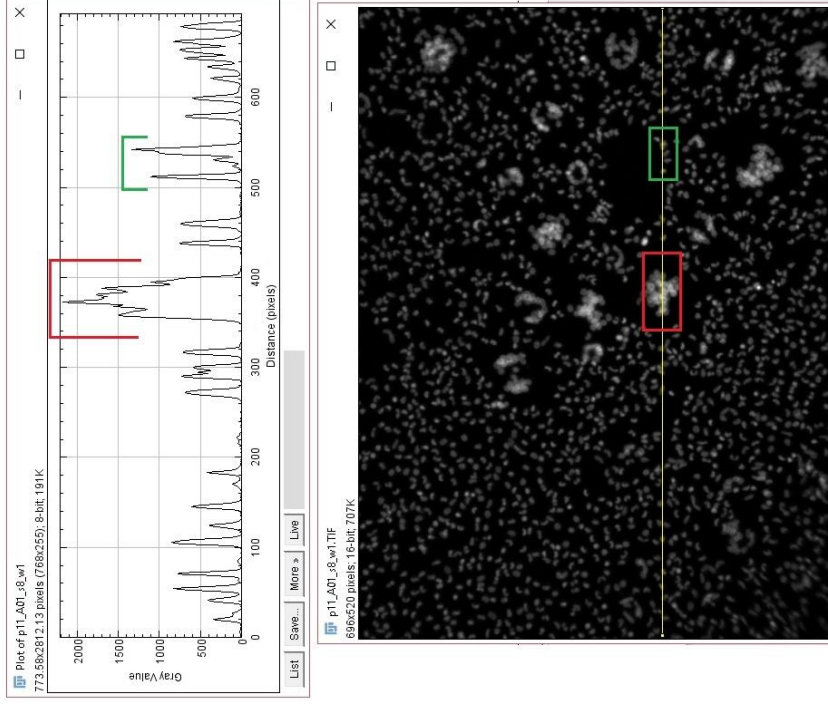


Figure 2.6: Effect of Background Reduction on Image Channel Noise

Each image taken was composed of three 'channels' – Red, Green and Blue. As DAPI was the nuclear label it was necessary to reduce background signal in the blue channel so that the counting macro could identify signal peaks with the highest accuracy. Above are two nuclear images and signal plots before and after background reduction. On the left signal plot the background noise in the dark "negative" regions are high (~180 on the Gray Scale). The positive signal for each nuclei bisected along the yellow line is represented as a peak (green box) with stacked/overlaid nuclei (red box) producing a cumulative signal. After background reduction the signal plot on the right has almost no noise but there is no loss of positive signal from the nuclei. The image on the right would now be optimised for the counting macros.

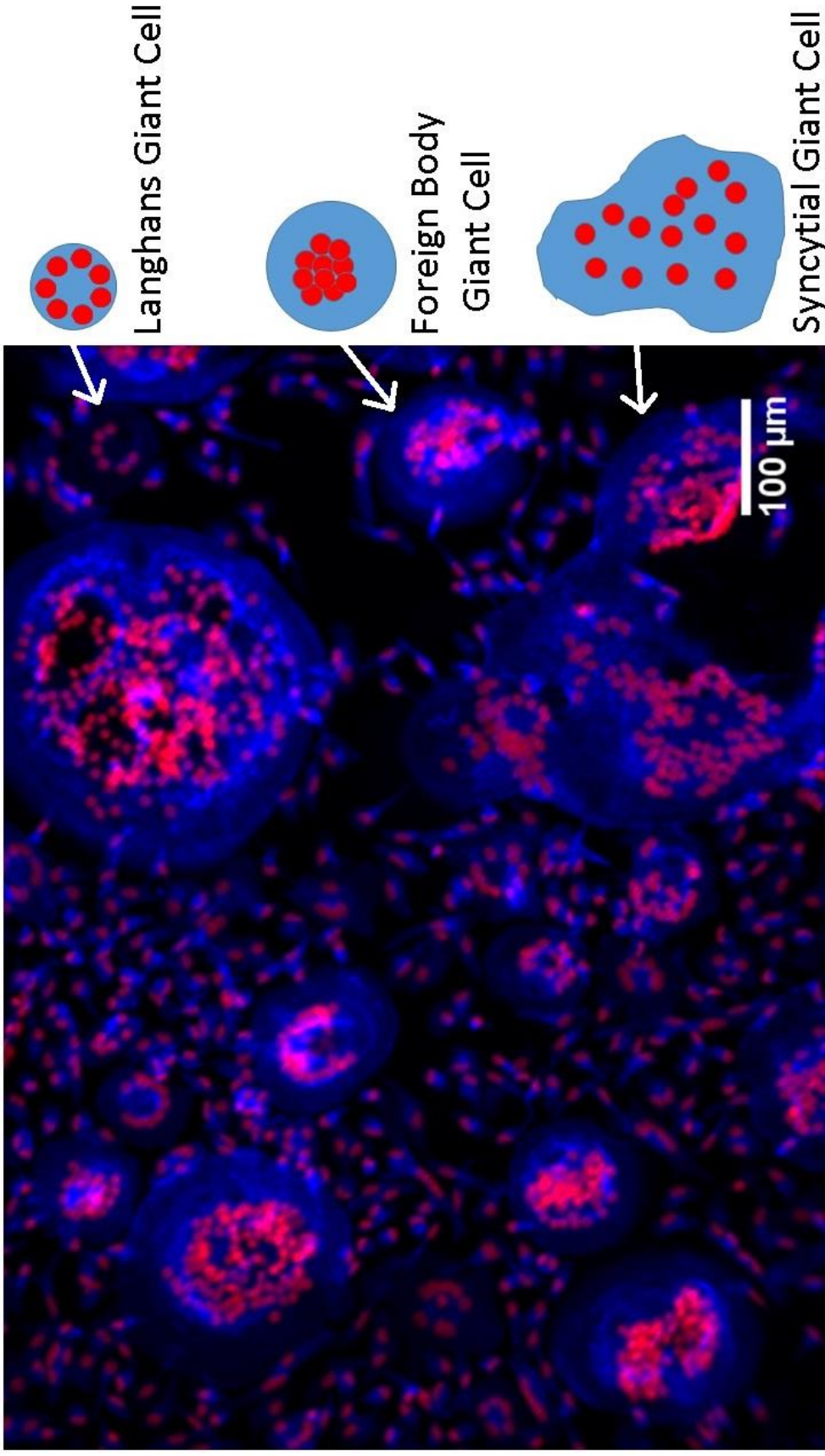


Figure 2.7: Morphologies of the Three MGC Types Observed During Fusion Assays.

An example 10x image with red nuclei channel, blue actin channel and 100μm scale bar. Langhans giant cells (LGCs) can be identified by their horse-shoe or ring-shaped nuclei arrangement and are typically the smallest in size. Foreign body giant cells (FBGCs) are larger and contain more nuclei in a stacked central cluster in the centre. Syncytial giant cells (SGCs) are by far the largest, have heterogeneous spreading of the membrane and the nuclei within are unevenly distributed.

The three MGCs observed were:

Table 10: MGC Types

Type	Key Morphological Features
Langhans Giant Cell (LGC) Type 1	Ring or horse-shoe arrangement of the nuclei, typically containing 3-18 nuclei, small surface area and roundish shape. Actin staining typically consistent.
Foreign Body Giant Cell (FBGC) Type 2	Stacked ball of nuclei at the centre, typically containing 20-80 nuclei, medium surface area and roundish shape. Actin staining typically consistent.
Syncytial Giant Cell (SGC) Type 3	Disorganised spread of nuclei, occasional circular clumps evident where large MGCs have potentially fused, 80-600 nuclei, very large surface area and no apparent shape. Actin staining shows patches of high and low staining.

In the course of this study three morphologically distinct MGC types (see Table 10: MGC Types) were observed when human monocytes were cultured in ConA for 1-3 days. Currently there are no known surface markers to differentiate LGC, FBGC and SGC. Soluble markers such as cathepsin K and tartrate-resistant acid phosphatase were once thought to be produced solely by osteoclasts but even these have been scrutinised and shown to be a feature common to other types of MGC (Park et al., 2013). It has been suggested previously that in vivo FBGC could form from further enlargement and fusion events of LGC (Rhee et al., 1978). Studies of implants in animal models (Barbeck et al., 2016; Chappuis et al., 2015) and human granuloma biopsies (Okamoto et al., 2003) has shown that LGC typically accumulate at the early stages of investigation with increasing incidence of FBGC over time.

While LGC and FBGC are reported to show some organisation of their nuclei and membrane perimeter, the SGC are classified as such due to their disorganised nuclei and asymmetrically spread shape. This vast cellular structure is structurally similar with the syncytiotrophoblast found encasing mammalian blastocysts (Huppertz and Gauster, 2011). The SGC represents the largest and most aggressively fused of the three MGC types. Through using these morphological classifications we hope to identify if any of the monocyte subsets show any predisposition to forming any of these MGC types.

2.2.7.1 MACROS FOR ANALYSING IMAGES

For each DAPI stack to be analysed the Noise Tolerance was set, a handful of MGC ROIs were selected within the stack and the individual noise tolerance (Process>Find Maxima...) for each was ascertained. This usually ranged between 3-10 and once a 'best-fit' value had been found it was recorded and used henceforth for any macro on that stack to maintain consistency.

Nuclei per MGC

```
n= roiManager("count");

for(i=0; i<n; i++){
    roiManager("select", i);
    //wait(200);
    run("Find Maxima...", "noise=NUMBER output=Count exclude");
    run("Find Maxima...", "noise=NUMBER output=[Point Selection]");
}
```

N.B. "**NUMBER**" was replaced with the appropriate Noise Tolerance number ascertained by the maxima testing described above. The results window produced will have a list of all the MGCs in their order in the ROI list and the number of nuclei detected in each.

Number of Pixels per MGC

```
n= roiManager("count");

for(i=0; i<n; i++){
    roiManager("select", i);
    {run("Measure");
    run("Add Selection...");}
```

The raw output for this macro was a list of the number of Pixels within each MGC in the ROI list, this was later converted into MGC Area using the calculations below.

Total Number of Nuclei per View

```
s= nSlices;

for(i=1; i<=s; i++){
    setSlice(i);
    //wait(200);
    run("Find Maxima...", "noise= NUMBER output=Count exclude");
    run("Find Maxima...", "noise= NUMBER output=[Point Selection]");
```

N.B. "**NUMBER**" was replaced with the appropriate Noise Tolerance number ascertained by the maxima testing described above. The counts generated from this show the total number of nuclei per image i.e. both fused or single cell.

The results from all the macros was entered into a spreadsheet template that would convert all the raw macro data into useful values using the formulas below.

2.2.8 FUSION ASSAY MATHEMATICS & EQUATIONS

Median Nuclei per MGC

The number of Nuclei per MGC in any given condition typically possessed a positive skew whereby smaller 3-8 nuclei MGCs were far more common than larger ≥ 20 nuclei MGCs. The median was therefore used to describe the average size of a giant cell in any given condition.

Single Cells & Fused Nuclei

By having both the Total Number of Nuclei per View and a list of all the Nuclei per MGC; the number of single cells per condition could be deduced:

$$\text{Single cells} = \text{Total No of Nuclei per View} - \sum (\text{Nuclei per MGC})$$

Fusion Index (FI)

The FI expresses the fusibility of cells in a given condition, the higher the FI the more cells have committed to fusion. FI was generated by dividing the number of fused nuclei by the total number of nuclei and expressed as a percentage.

$$FI = \left(\frac{\text{Fused Nuclei}}{\text{Total Nuclei}} \right) \times 100$$

Converting Pixels per MGC to MGC Area

Each 10x image taken on the microscope was 696 (width) by 520 (height) pixels. The width and height of each pixel was 1.35189 μm and so the area of each pixel and the area of each MGC could be calculated:

$$\begin{aligned} \text{Pixel Area} &= (\text{Pixel Width} \times \text{Height}) = (1.35189\mu\text{m} \times 1.35189\mu\text{m}) \\ &= 1.827606572\mu\text{m}^2 \end{aligned}$$

Therefore:

$$\text{MGC Area } (\mu\text{m}^2) = \text{Pixel Area } (1.827606572\mu\text{m}^2) \times \text{No of Pixels in MGC}$$

% of Well Covered by MGCs

% of well covered by MGCs was generated by taking the sum of all the MGC area (μm^2) values recorded for a given condition and dividing it by the total number of the views analysed multiplied by the area of one view (μm^2) and expressing it as a percentage.

$$\% \text{ Of Well Engulfed} = \left(\frac{\sum \text{MGC Area per Condition}}{(\text{No of Views Counted} \times \text{Area per View})} \right) \times 100$$

Calculating the Percentage of Single, Fused, and Detached Cells

The number of fused and single cells were calculated as shown in "Single Cells & Fused Nuclei", to convert the values into a percentage and ascertain the amount of detached cells:

- A. $\text{Total Nuclei per Well} = \left(\frac{\sum \text{All Nuclei in a Condition}}{\text{Number of Views Analysed}} \right) \times \left(\frac{\text{Total Well Area } (31.65\text{mm}^2)}{\text{Area of a View } (0.661\text{mm}^2)} \right)$
- B. $\text{Fused Nuclei per Well} = \left(\frac{\sum \text{Fused Nuclei in a Condition}}{\text{Number of Views Analysed}} \right) \times \left(\frac{\text{Total Well Area } (31.65\text{mm}^2)}{\text{Area of a View } (0.661\text{mm}^2)} \right)$
- C. $\text{Single Cells per Well} = (\text{Total Nuclei per Well} - \text{Fused Nuclei per Well})$
- D. $\text{Detached Cells per Well} = \text{Cells Seeded per well} - \text{Total Nuclei per Well}$

As nuclei could only exist in 3 states (single cell, fused nuclei or detached cell) **B**, **C** and **D** could all be expressed as a percentage of the Cells Seeded per well.

$$\% \text{ Fused Cells} = \left(\frac{\text{Fused Nuclei per Well}}{\text{Cells Seeded per well}} \right) \times 100$$

$$\% \text{ Single Cells} = \left(\frac{\text{Single Cells per Well}}{\text{Cells Seeded per well}} \right) \times 100$$

$$\% \text{ Detached Cells} = \left(\frac{\text{Detached Cells per Well}}{\text{Cells Seeded per well}} \right) \times 100$$

Whereby:

$$(\% \text{ Fused Cells} + \% \text{ Single Cells} + \% \text{ Detached Cells}) = 100\%$$

Calculating the Percentage of LGC, FBGC and SGC

The sum of the nuclei in each of the three types of MGCs was totalled for each condition tested in a spreadsheet. The Total LGC/FBGC/SGC Nuclei per Well was calculated in the same way as Fused Nuclei per well (**B**) by instead substituting "Fused Nuclei in a Condition" with "Total LGC/FBGC/SGC in a Condition". The Total LGC/FBGC/SGC Nuclei per Well could then be expressed as a percentage of the Fused Nuclei per Well.

e.g.

$$\text{LGC Nuclei per Well} = \left(\frac{\sum \text{LGC Nuclei in a Condition}}{\text{Number of Views Analysed}} \right) \times \left(\frac{\text{Total Well Area (31.65mm}^2\text{)}}{\text{Area of a View (0.661mm}^2\text{)}} \right)$$

$$\% \text{ of Fused Nuceli in LGCs} = \left(\frac{\text{LGC Nuclei per Well}}{\text{Fused Nuceli per Well}} \right) \times 100$$

Statistics

All statistical analysis were conducted in GraphPad Prism (6.04) and the appropriate tests are noted in the legend of each figure. In all graphs the "N=x" value represents the number of different donor repeats in the experiment and the standard error of the mean (SEM) is reported in all graphs where $N \geq 3$. After performing the calculations described previously, the results for each parameter was tested with an analysis of variance (ANOVA) or a Kruskal-Wallis test for results that were integers or percentages respectively. Afterwards an appropriate post-hoc test (described below) was selected to compare the values of interest. An ANOVA assumes a parametric distribution of

integer values (e.g. MFI or MGC area in μm^2) and detects if there is a dominant member of three or more samples. The Kruskal-Wallis test is designed for non-parametric and pure numbers such as percentages (e.g. fusion index or % surface covered by MGCs) and reports if one or more conditions is dominating over the others.

As the primary statistics tests only measure the variance between the conditions post-hoc tests were conducted to make direct paired comparisons (e.g. control vs condition 1). A Dunnett's post-hoc test was run after an ANOVA to compare the average of the control samples to that of the other samples. A Dunn's post hoc test was used in conjunction with a Kruskal-Wallis test to conduct pairwise comparisons based on rank sum between individual samples to a control sample. A Tukey post hoc test was used after an ANOVA to compare the mean values of different time-points whereby all possible combinations are compared and reported.

A Fishers LSD post hoc test was conducted after an ANOVA to compare the expression of tetraspanins between the monocyte subsets. Because the fluoresce index is different for each anti-tetraspanin antibody reporter, it is only accurate to compare the significant differences between the same antibody reporter itself on different subsets or in different conditions. Therefore, in the Fishers LSD each comparison stands alone, the means are pooled and square rooted and this value becomes an assumed SD. A comparison is then run to see if group differences exceed this pooled SD. All stars (*) mentioned hereafter refer to the following scale of significance:

ns: $p \geq 0.05$ * $p \leq 0.05$ ** $p \leq 0.01$ *** $p \leq 0.001$ **** $p \leq 0.0001$

2.2.9 ADHESION ASSAY

The adhesion assay protocol was adapted and optimised from an experiment conducted by Lisa Mauracher. Monocyte seeding densities (0.5×10^5 , 1.0×10^5 & 1.5×10^5 monocytes well^{-1}) and incubations times (1, 2, 4, 6hrs) were all tested and the following protocol generated from the optimal results (data not shown).

Total Monocytes from in-house venepuncture donors were resuspended to a density of 5×10^5 monocytes ml^{-1} in cIMDM. 100 μl of cell suspension was added to each well in a clear bottomed black framed 96-well plate to give 0.5×10^5 monocytes well^{-1} . 3ml

of 2xConA media ($20\mu\text{g ml}^{-1}$ ConA) was made by adding $12\mu\text{l}$ of 5mg ml^{-1} ConA solution to $2988\mu\text{l}$ cIMDM, this was then subdivided into 9 tubes containing $300\mu\text{l}$ each. Anti-tetraspanin antibodies were added at double concentration ($20\mu\text{g ml}^{-1}$) to the corresponding tube of $300\mu\text{l}$ 2xConA media. $100\mu\text{l}$ of the 2xConA 2xtetraspanin antibody cIMDM was added to each of the corresponding wells (containing $100\mu\text{l}$ of seeded monocytes) to bring ConA and antibodies to 1x concentration ($10\mu\text{g ml}^{-1}$) and induce fusion conditions. Control wells containing cIMDM without ConA and ConA+IgG1 were also prepared with each assay. Once placed in the incubator at 37°C , 5% CO_2 the cells were left to adhere for 2 hours. Media was aspirated and $200\mu\text{l}$ of 1xPBS (pre-warmed to 37°C) was added to the wells, then drawn up and down at a steady speed at the North, South, West & East of the well to ensure non-adherent cells were removed before fixing. The PBS was aspirated and $100\mu\text{l}$ of 4% (v/v) PFA (pre-warmed to 37°C) was added to each well and the plate was returned to the incubator for 20min. The 4% (v/v) PFA was removed and wells were washed with 1xPBS, the plates were stored at 4°C until they could be stained and imaged.

The liquid phase was aspirated prior to staining. A $10\mu\text{g ml}^{-1}$ Hoechst 33342 staining solution was made, for every 1ml of staining solution; $1\mu\text{l}$ of 10mg ml^{-1} Hoechst 33342 was added to $999\mu\text{l}$ 1xPBS. $50\mu\text{l}$ of the solution was added to each well and the plate was left in the dark at room temperature for 15min. The staining solution was

```
setAutoThreshold("Otsu dark");  
run("Analyze Particles...", "size=4-400 circularity=0.00-1.00 show=Nothing display  
summarize");  
close();
```

aspirated and cells resuspended in $200\mu\text{l}$ 1xPBS and taken to the Institute of Molecular and Cell Biology (IMCB) microscope facility. An Olympus IX83 inverted microscope running MetaMorph was used to take the images. Automated microscope acquisition was performed as outlined in "Fluorescence Imaging" above but only 4x images in the DAPI channel were collected. Images obtained were analysed with the following macro in ImageJ FIJI to count cell numbers:

2.2.10 TANDEM FLUORESCENCE-SCANNING ELECTRON MICROSCOPY (FLU-SEM) OF MGCS

Subset monocytes from FACS 1 were resuspended in cIMDM to 3.65×10^6 monocytes ml^{-1} and 200 μl of cell suspension was seeded onto a 35mm glass bottom petri dish (well diameter 14mm, glass thickness no. 0) to give a cell density of ~ 4740 monocytes mm^{-2} . After 1hr incubation at 37°C at 5% CO_2 to allow the monocytes to adhere the dish was filled with 2ml cIMDM + 1xConA ($10\mu\text{g ml}^{-1}$) and returned to the incubator for 72 hrs. 3 μl of 10mg ml^{-1} Hoechst 33342 was added to 2997 μl cIMDM to make 3ml of Hoechst stain media ($10\mu\text{g ml}^{-1}$) which was warmed to 37°C . 1ml of the warm Hoechst stain media was added directly into the already present 2ml of culture media in the three dishes thus diluting the final concentration of Hoechst 33342 to $3.3\mu\text{g ml}^{-1}$. At the same time the glass well was marked with a small downwards facing triangle using the pipette tip to create an arbitrary 12 o'clock marking. The dish was incubated for 1hr to allow the Hoechst to permeate the cells. The dishes were then taken to the IMCB microscope facility and mounted on the IX83 equipped with an environment chamber. The cells were maintained at 37°C and 5% CO_2 throughout the imaging. The triangular mark made on the dish was aligned at the 12 o'clock of the camera and the wells were raster scanned in a 5x5 grid below the mark at 20x magnification (DAPI and brightfield channels). After imaging, the plates were handed over to Mr Benoît Malleret for fixation and preparation for SEM.

The subsequent stages were all performed by Mr Benoît Malleret, Miss Tan Suat Hoon and Mr Lu Thong Beng of the Electron Microscopy Unit, National University of Singapore:

The media was aspirated and the cells were then fixed in a suspension with 2.5% (w/v) glutaraldehyde in a 0.1M phosphate buffer for 1hr (pH 7.4) at room temperature. Then the cells are washed twice in 1xPBS. The glass well at the centre of the dish was carefully removed using a diamond-tipped glass cutter to be handled as a glass coverslip. After post-fixation with 1% (w/v) osmium tetroxide (Ted Pella Inc., USA) at room temperature for 1 hour, cells were washed in deionised water and dehydrated with a graded series of ethanol starting at 25% (v/v) to 100% (v/v) and critical point dried (CPD 030, Bal-Tec, Liechtenstein). The glass coverslip with the dry

cells on it was laid on an adhesive film on an SEM sample holder. This was firmly touched with another adhesive sample holder and pulled away. The surface on which the cells were grown and the adhesive surface were coated with 5nm of gold by sputter coating in a high-vacuum sputtering device (SCD005 sputter coater, Bal-Tec, Liechtenstein). The coated samples were examined with a field emission scanning electron microscope (JSM-6701F, JEOL, Japan) at an acceleration voltage of 8kV using the in-lens secondary electron detector.

Combining Tandem Flu-SEM Images

The fluorescence images taken at 20x magnification were collaged into a larger “map” image using ImageJ FIJI (Plugins>Stitching>Grid/Collection Stitching). The brightfield map was compared with the low magnification SEM images to identify the location of the high magnification images. The appropriate high magnification SEM images and 20x magnification DAPI images were then matched, cropped (Image>Crop) and merged (Image>Color>Merge Channels...).

2.2.11 LUMINEX® ELISA OF FUSION ASSAY SUPERNATANTS

Frozen Sample Preparation: The 24, 48 & 72hr supernatants from the fusion kinetics study stored at -80°C were thawed and 10µl aliquots were taken to be diluted before analysis. 24hr samples remained undiluted, 48hr samples were 2x diluted (10µl sample + 10µl cIMDM) and 72hr samples were 3x diluted (10µl sample + 20µl cIMDM). Samples and media were handled and stored on ice.

ELISA was carried out on the Luminex® platform by Miss Esther Mok and an in-house team following the protocol below:

Diluted samples were quantified for: CCL2 (MCP-1), CCL3 (MIP-1α), RANTES, IL-1α, IL-1β, TNFα, IL-6, IL-17A, IL-4, IL-10, IL-13, GM-CSF, IL-3, IFNγ & VEGF. Luminex® bead-based multiplex assays are based on Luminex® xMAP® technology and they are designed to simultaneously measure multiple specific protein targets in a single sample. Customized human 9- and 15-plex kits (Merck Millipore, cat# HCYTOMAG-60K) were measured with DropArray™-bead plates (Curiox).

9-plex: Human GM-CSF, IFNγ, IL-10, IL-6, IL-13, IL-1α, IL-1β, IL-4, and TNFα.

15-plex: Human GM-CSF, IFN γ , IL-10, IL-6, IL-13, IL-17A, IL-1 α , IL-1 β , IL-3, IL-4, CCL2, CCL3, RANTES, TNF α and VEGF

Using DropArray-bead plates, samples or standards were incubated with fluorescent-coded magnetic beads, which had been pre-coated with respective capture antibodies. After an overnight incubation at 4°C with shaking, plates were washed twice with wash buffer. Biotinylated detection antibodies were incubated with the complex for 1 hour and subsequently streptavidin-PE was added and incubated for another 30 min. Plates were washed twice again, and beads were re-suspended with sheath fluid in PCR plates before reading on the Luminex analyzer FLEXMAP® 3D (Merck Millipore). Data acquisition was done using xPONENT® 4.0 (Luminex) acquisition software and data analysis was done using Bio-Plex Manager® 6.1.1 (Bio-Rad). Standard curves were generated with a 5-parameter logistic algorithm which provided a better fit than a 4-parameter logistic when the response curve was asymmetrical/non- sigmoidal. Lastly, a report was generated with values for both MFI and concentration data.

CHAPTER 3: TOTAL MONOCYTE FUSION

3.1 RESULTS

3.1.1 OPTIMISATION OF THE FUSION ASSAY

At the beginning of the study the protocols and techniques used were developed by previous PhD students, Dr Marzieh Fanaei and Dr Varadarajan Parthasarathy. These techniques relied on a monocyte purification method that did not separate subsets and was too slow for the testing of multiple tetraspanins in the subsets.

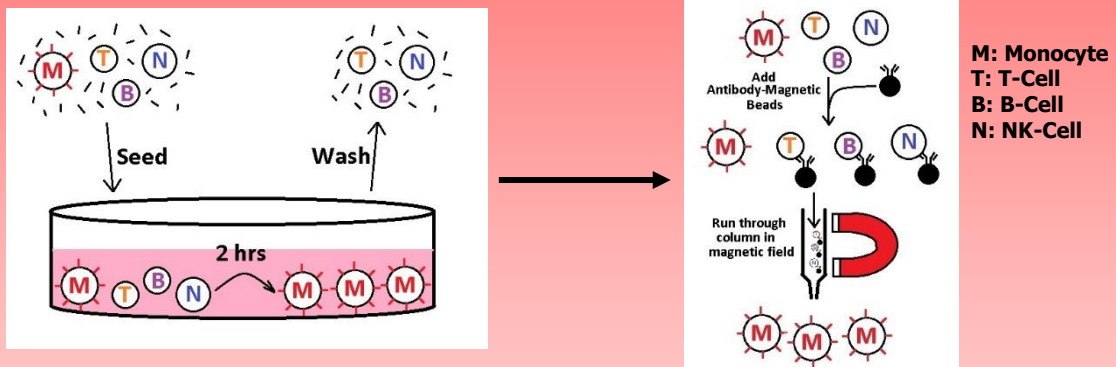
Monocyte Purification

Initially, monocyte purification relied on the adhesive properties of monocytes (see "2.2.1.1 Materials and Methods" for details). While MGCs could be generated reproducibly with this method, it is flawed in three ways. Firstly, the adherence technique assumes that all monocytes are equally adherent, but later studies with isolated subsets showed that this is not the case. Intermediate monocytes were the least adherent yet were the most aggressive fusers of the subsets. Secondly, the adherence method meant that PBMCs were seeded directly into the well at a predetermined density but after washing the exact number of monocytes present in each well was not known and prone to donor variation. Thirdly, the adherence method is subject to contamination with platelets and lymphocytes which are also able to adhere within the 2hr incubation time. The presence of lymphocytes and platelets could alter the fusion behaviour of the monocytes.

The monocyte purification protocol was improved by utilising a negative selection method (see Figure 3.1) which was able to remove non-monocytic cells directly using antibodies bound to magnetic beads (MACS purification). The resultant monocyte suspension could be counted and seeded accurately, possessed a high purity and all three monocyte subsets were enriched equally. It is also worthy of note that for later subset work; apheresis cones were used as the source of monocytes as they contained $400-1500 \times 10^6$ PMBCs of which 40-50% were typically monocytes. In-house venepuncture donors in the UK and Singapore were limited to ~550ml and 40ml

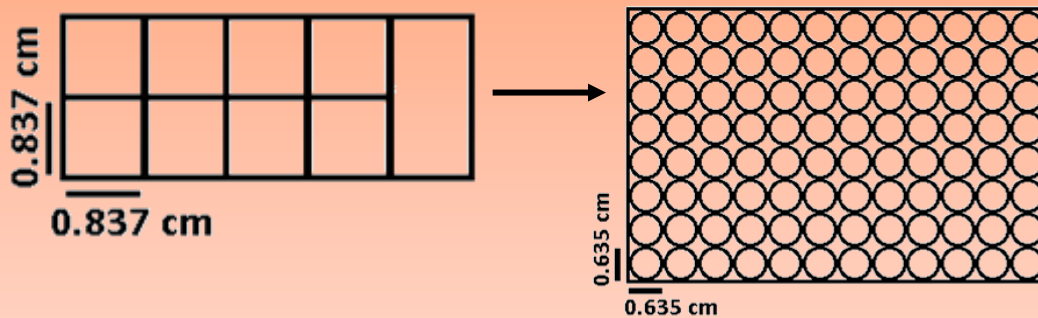
Figure 3.1: Optimisation of Fusion Assay

A) Monocyte Purification



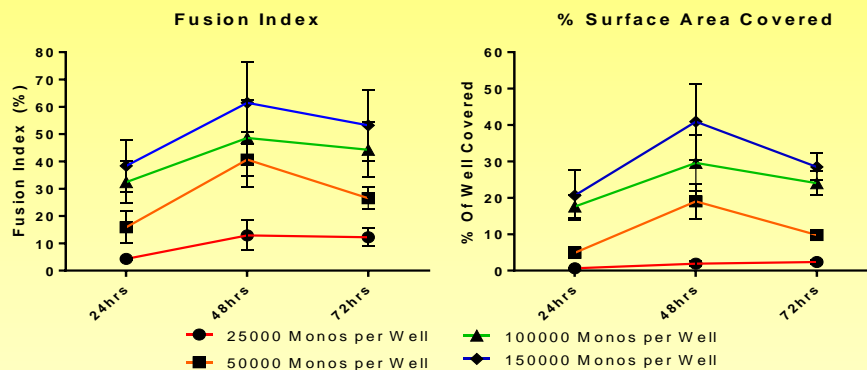
Original Technique (Left): Monocytes were purified using adherence purification. PBMCs were seeded in media and incubated for 2hrs then washed with warm media to remove non-adherent cells. Issues: Final cell number of monocytes is unknown, contamination levels are relatively high, non-adherent monocytes are washed away.
Optimised Technique (Right): Negative selection using an antibody-magnetic bead cocktail that targets all leukocytes except monocytes. The resultant suspension of monocytes are high purity, can be counted and seeded to a high accuracy and there is no loss of non-adherent monocytes.

B) Cell Culture Container



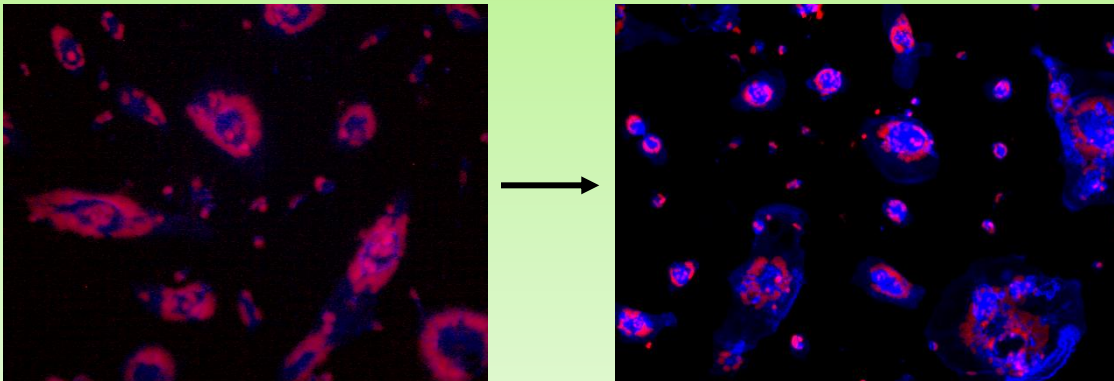
Original Technique (Left): Monocytes were seeded onto glass 8-chamber Lab-Tek II slides. Issues: High cell number required per condition, only 8 chambers per slide, (see "Fixing & Staining" and "Imaging" below).
Optimised Technique (Right): Black-frame 96-well plate. Advantages: Fewer cells required per condition as plate well area (31.65mm²) is 2.2x smaller than the Lab-Tek II chamber (70mm²), up to 96 conditions per plate available, (see "Fixing & Staining" and "Imaging" below).

C) Culture Conditions



Once the magnetic enrichment method was adapted it was possible to count and seed the monocytes to a very high degree of accuracy. A range of seeding densities and culture times were compared for 96-well plates to find the optimum culture conditions. 150,000 cells fixed at 72hrs was chosen as the optimum test conditions as the FI was at the ideal 50% mark and between 48-72hrs the variation between recordings seemed to lessen. N=4, Mean±SEM. All conditions in cIMDM+10ug ml⁻¹ ConA.

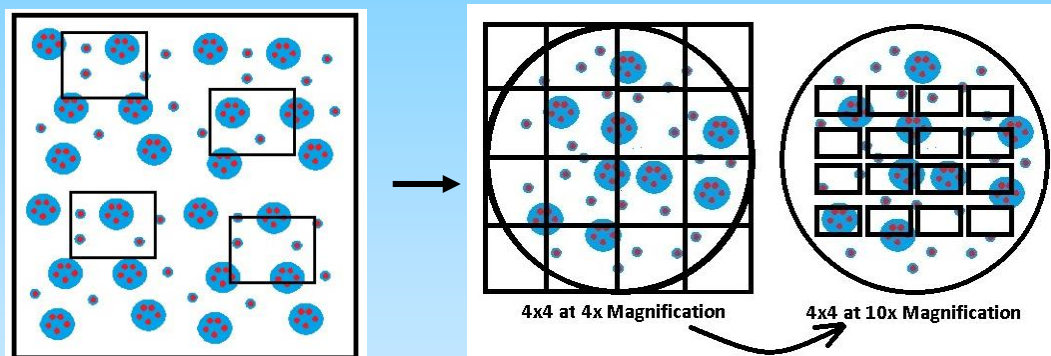
D) Fixing & Staining



Original Technique (Left): Lab-Tek II slides were fixed and permeabilized with acetone and stained with DAPI+NH3 (anti-F-actin) and after washing counterstained with an anti-IgM-GFP secondary. This robust protocol meant that MGCs would often rupture giving poor resolution of the membrane borders and lots of background artefacts.

Optimised Technique (Right): In the 96-well plates a gentler protocol was developed to maximise preservation and resolution. Warmed 4% PFA was used to fix before adding a high affinity Phalloidin-TRITC and DAPI overnight stain.

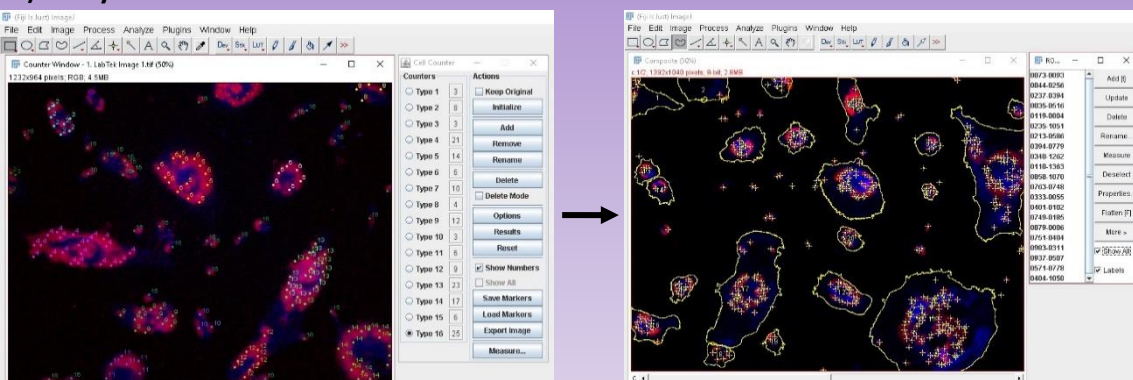
E) Imaging



Original Technique (Left): Each "Site" had to be manually chosen and imaged in a Lab-Tek II chamber. Disadvantages: user bias, slow (30-40 images hour⁻¹), only a few sample images per condition.

Optimised Technique (Right): The plate dimensions were calibrated to the microscope so that the computer could raster scan the whole well at 4x to generate a "well map" then subsequently take 16 sample images equally spaced at 10x for analysis. The automated protocol possessed an autofocus option allowing high resolution images to be taken much faster than before (~720 images hour⁻¹).

F) Analysis



Original Technique (Left): Images were counted individually by manually selecting each nuclei using the ImageJ FIJI "Cell Counter". Disadvantages: Slow, user bias, no way to measure MGC area.

Optimised Technique (Right): By creating a stack on ImageJ FIJI and drawing ROI boundaries on each MGC a macro could be used to instantaneously count all the nuclei in each MGC and measure the area of each. Advantages: Rapid, higher throughput, more parameters recorded, ROIs and macros can be saved and reused/reanalysed.

respectively and averaged at 1.2×10^6 PBMCs ml^{-1} of blood of which 20-30% were monocytes.

Cell Culture Conditions

The 8-chamber Lab-Tek II slide had a culture surface area of 70mm^2 and early experiments utilising adherence purification required 2.2×10^6 PBMCs to be seeded in each well. 96-well plates could accommodate many more conditions than the 8-chambered Lab-Tek II slides and due to the lower surface area (31.65mm^2), each well required 2.2x fewer cells and lower reagent quantities per condition. The black wall 96-well plates also had the added advantages of low background fluorescence and were compatible with automated imaging protocols on the microscope (see "Imaging" below).

Once it was established that the MACS beads significantly enriched the monocyte population (Figure 2.1 & 2.1) and could be seeded to an accurate density, it was essential to compare the effects that seeding density and total culture time in ConA media had on fusion (see Figure 3.1). By 48hrs total monocytes reached a peak for both Fusion Index (FI) and % coverage, with increasing seeding densities resulting in higher values for each parameter. Interestingly, by 72hrs the values decreased slightly but the variability of each parameter also decreased (FI: $38 \pm 90\% \rightarrow 61 \pm 15\% \rightarrow 53 \pm 13\%$; % covered: $21 \pm 70\% \rightarrow 41 \pm 10\% \rightarrow 29 \pm 40\%$). It was decided that 150,000 monocytes well^{-1} for 72hrs yielded the most reproducible results in most parameters and provided a sub-maximal ($\sim 50\%$) FI. Thus allowing subsequent treatments (e.g. with antibodies) to either increase or decrease the FI.

Fixing and staining

The initial protocol utilised acetone to both fix and permeabilise the cells to the glass coverslip before washing and staining with DAPI and an anti-actin antibody (NH3) and an anti-mouse GFP secondary antibody. The resultant images showed poor resolution between grouped nuclei, low resolution of the MGC membrane borders and multiple membranous artefacts and evidence of ruptured MGCs (see Figure 3.1). The use of 96-well plates made acetone a poor fixative/permeabilisation reagent as it would

dissolve the plastic and so pre-warmed 4% (w/v) PFA was substituted. Initially 0.1% (v/v) Triton-X100 was used to permeabilise the cells but again membrane fragments were evident and overnight staining without any permeabilisation proved effective, so the permeabilisation stage was removed. DAPI was maintained as the nuclear stain but the NH3 antibody which required secondary staining was replaced with phalloidin-TRITC. With this method, fixed cells could be stained in one batch without an additional wash and secondary stain that could cause cells to rupture.

Imaging

Initially, after focusing and exposure settings were adjusted, four 10x images were taken randomly for each chamber of the Lab-Tek II slides using a fluorescence microscope. Thus there were not many images per condition and any "site" choice could be subject to bias. As the slide was moved manually by hand and the focusing would often need readjusting this method also did not have a sufficient output. At an average speed of 30-40 images hour⁻¹ it was not feasible to take more sample images without somehow increasing the image output. The 96-well plate was compatible with an automated plate-holder on an Olympus IX83 inverted microscope and MetaMorph software allowed automated imaging to be conducted. The autofocus function meant that image resolution was always maximised in every image and could be performed far faster than manual adjustment. A personalised acquisition set-up was made so that settings could be reused and make imaging reproducible. The set-up included an initial well mapping phase where 16 images per well were taken for every well in 4x magnification. These images were later combined into a montage to give an overall impression of the fusion in each well and to observe if MGCs were distributed uniformly on the well surface. A subsequent scan at 10x magnification was conducted; 16 equally spaced sample images per well were taken throughout the well. These higher magnification images would be the images for analysis and counting. The new automated plate method removed all human bias in choosing sites and was able to acquire 18-24x more images per hour; averaging at ~720 images hour⁻¹.

Analysis

Previously, images were analysed individually by counting the number of nuclei in each MGC and then counting the single cells that had not fused. With these values it was possible to calculate the "Median Number of Nuclei per MGC" and "Fusion Index" (see "2.2.8 Fusion Assay Mathematics & Equations"). The original protocol was similar to that developed by Annette Gasser and Johannes Möst (Gasser and Möst, 1999); where 300-400 nuclei from each condition were analysed and every MGC had to contain ≥ 3 nuclei. The problem with such a technique is that not all images obtained were of a uniform number of nuclei so some conditions called for more images to be analysed than others leading to disproportionate sampling. Furthermore, the analysis only took into account the number of the nuclei in each MGC and whether it was in a fused or unfused state. By measuring a fixed number of images on a calibrated microscope it was possible to ascertain the area analysed. In this way each analysis consisted of four images covering 0.66mm^2 totalling an area of 2.65mm^2 (8.4% of the 31.65mm^2 well). The total number of nuclei analysed across the four images averaged at 2400 nuclei; a 6-fold increase in the number of nuclei analysed as suggested by Gasser and Möst.

Region of Interest (ROI) borders were drawn around each MGC and these coordinate files could be saved and recalled at any time – a function essential for the analysis macros developed later. The ROIs also allowed the number of pixels within each border to be counted which could then be easily converted into an area thus allowing direct measurement of MGC area and % surface covered by MGCs. The biggest challenge by far was in the automation of the counting. With the images arranged into stacks combined with the ROI files and the specific acquisition settings it was then possible to develop a macro that would systematically count the peaks in fluorescence generated by each nuclei (see "2.2.7.1 Macros for Analysing Images"). Manually counting the nuclei, it was possible to count $\sim 5,000$ nuclei per hour, the counting macro was able to count $\sim 65,000$ nuclei per hour; a ~ 13 fold increase in output. The other two macros generated counted all the nuclei in each image and listed the number of pixels in each MGC ROI so that further calculations could be conducted

(Figure 3.1 "Analysis"). The final addition to the analysis was a manual allocation of MGC type based on the morphology of the MGCs observed.

Conclusion of Optimisation:

Quantitatively, the optimised protocol produced monocytes of a greater purity (3.18-fold higher purity), required 2.2x fewer cells per condition, could acquire images ~18-24x faster, analyse ~6x more nuclei per condition and count nuclei ~13x faster than before. The greater output and larger sampling sizes ensured that results were representative and the ROI files to facilitate post hoc reanalysis of images.

3.1.2 FUSION KINETICS OF TOTAL MONOCYTES

Fusion of monocytes relies on the ability of the cells to adhere to a surface, migrate to one another, make contact and merge membranes (Aguilar *et al.*, 2013). The adherence purification method meant that exact monocyte seeding numbers were always estimated as a percentage of the total PBMCs and there was always the possibility that low-adherence monocytes were washed away. With the new optimised protocol it was possible to count and seed monocytes at an exact density to generate a reproducible film of fusible monocytes. It was therefore essential to find out how the monocyte density affected the rate and outcomes of fusion over time.

Figure 3.2 shows the changes in fusion parameters of 4 donors at 24hrs, 48hrs and 72hrs through a range of seeding densities (0.25×10^5 , 0.50×10^5 , 1.00×10^5 and 1.50×10^5 total monocytes well⁻¹). It is evident in all four parameters that an increase in monocyte seeding density increases the number of nuclei per MGC, the size (area) of the MGCs and the percentage of fused nuclei and area of the well covered by MGCs.

Within 24hrs fusion was evident at all monocyte densities cultured in ConA. Controls cultured without ConA (not shown) showed no evidence of fusion. With the exception of 0.25×10^5 total monocytes well⁻¹ (which only produced a small increase), all other seeding densities increased notably in FI, MGC area and % coverage between 24hrs and 48hrs. Curiously, the same conditions that showed a sharp increase in these values between 24hrs to 48hrs subsequently showed a decrease from 48hrs to 72hrs.

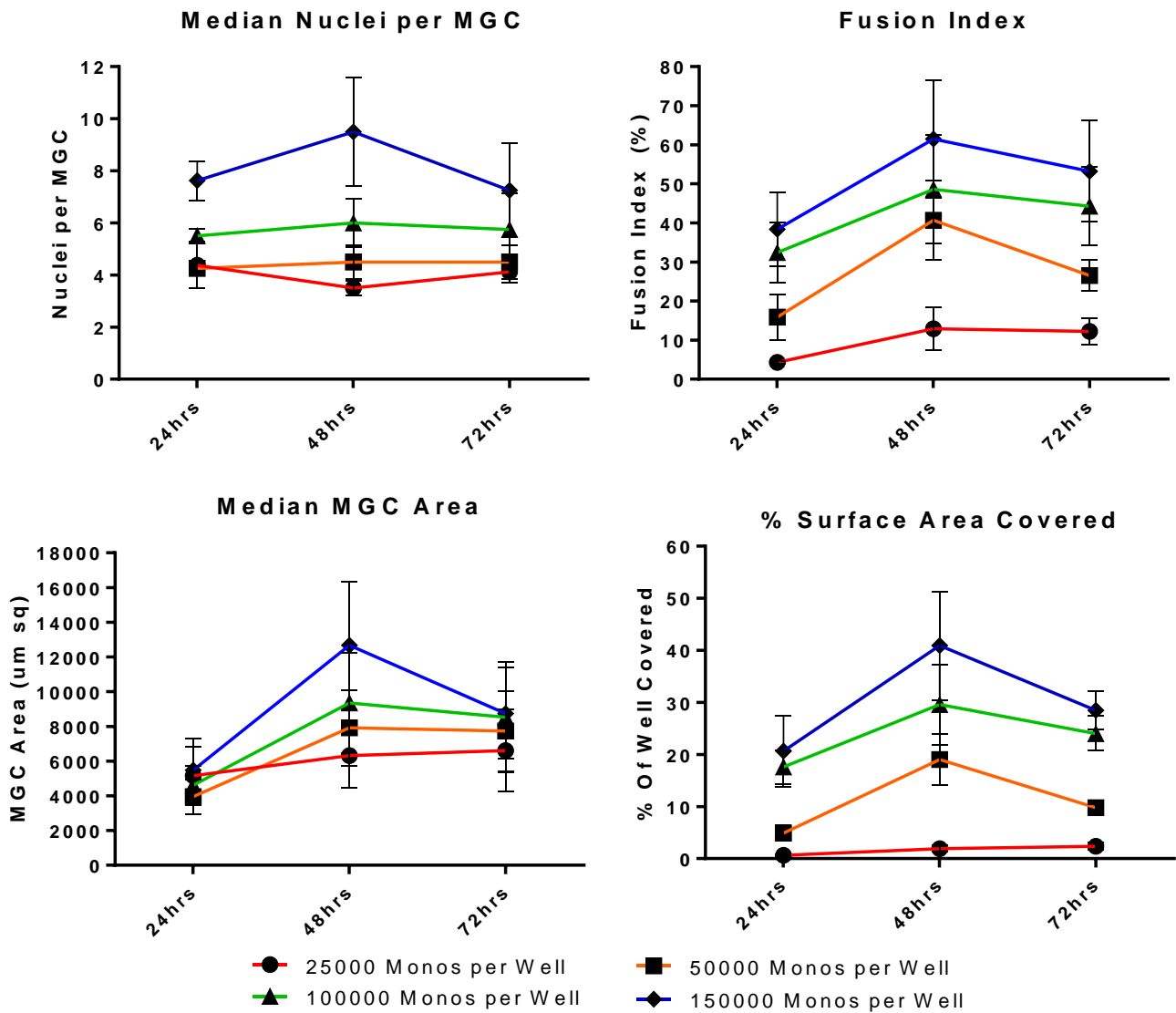


Figure 3.2: Fusion Kinetics of Total Monocytes.

Total monocytes from the same donors were purified using the optimised protocols, seeded at different densities and fixed at 24hrs, 48hrs and 72hrs. Overall, an increasing seeding density produced an increase in all parameters observed. There was no fusion evident in the cIMDM only time points. N=4, Mean±SEM for all points.

It may be worth noting that the standard errors for readings taken at 48hrs were markedly larger than those recorded at 72hrs. When 0.25×10^5 monocytes were seeded per well a more consistent increase from 24hrs to 72hrs was observed.

The median nuclei per MGC measure showed the least dramatic changes and only the 1.50×10^5 total monocytes well⁻¹ samples showed any distinct increase (7.6 to 9.5 nuclei per MGC) from 24hrs to 48hrs. At 24hrs the median area of MGCs cultured in all seeding densities was approximately the same ($\sim 4550 \mu\text{m}^2$) but by 48hrs they showed an increasing size with an increasing seeding density, therefore the MGC size is positively correlated with the seeding density.

Figure 3.3 shows the types of MGCs produced as a percentage of the fused nuclei at each of the time points. When seeded at the lowest density (0.25×10^5 monocytes well⁻¹) there is exclusive formation of LGCs up to 48hrs and FBGCs are only generated by 72hrs. Thereafter there is a positive correlation between seeding density and the formation of larger FBGCs and LGCs. Between 0.50×10^5 and 1.00×10^5 monocytes well⁻¹, there is a dramatic increase in the formation of FBGCs and SGCs formed within 24hrs. At 0.50×10^5 monocytes well⁻¹ a population containing all three MGCs (LGC: 70.45%, FBGC: 7.38%, SGC: 22.18%) did not occur until 48hrs. A similar distribution of all three MGCs (LGC: 71.65%, FBGC: 15.40%, SGC: 12.95%) was achieved in only 24hrs when monocytes were seeded at double the density.

When comparing time points between Figure 3.2 and Figure 3.3 it is evident that an increase in the formation of larger FBGCs and SGCs results in an increase in the FI, MGC median area and % coverage. The formation of SGCs seemed to have a threshold for the seeding density across all the time points observed. No SGCs were evident in any well seeded with 0.25×10^5 monocytes well⁻¹. Between 48-72hrs the percentage of SGCs in all higher monocyte densities in Figure 3.3 show a decrease; similar to that of the parameters in Figure 3.2. Like the FI, MGC median area and % surface covered the formation of SGCs in all cell densities seemed to be maximal at 48hrs. There was no evidence of fusion in all control wells cultures in cIMDM alone.

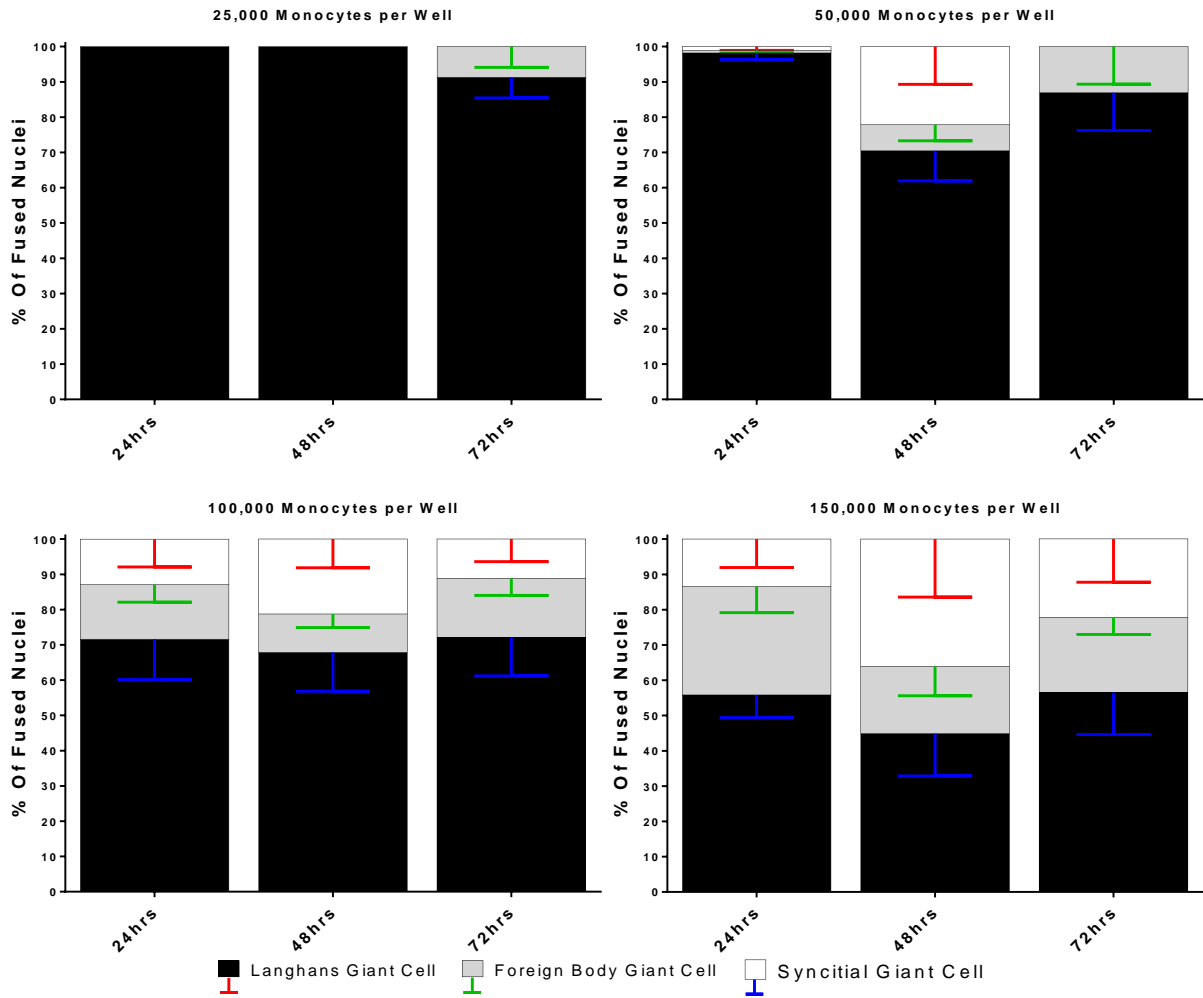


Figure 3.3: MGC Types Generated from Fusion Kinetics Analysis of MACS Purified Total Monocytes.

The types of MGC generated in the fusion kinetics study on total monocytes were allocated into either Langerhans, Foreign Body or Syncytial Giant cells. The nuclei counted in each type is expressed above as a percentage of all the fused nuclei analysed. N=4, Mean±SEM for all points.

3.1.3 ADHERENCE OF TOTAL MONOCYTES CULTURED IN ANTI-TETRASPANIN ANTIBODIES

As tetraspanins have been shown to partner with integrins and mediate cellular adhesion (Kazarov *et al.*, 2002; Liu *et al.*, 2007) it was essential to test if the antibodies could inhibit adhesion to the well surface. If anti-tetraspanin antibodies inhibit initial adherence this would inhibit fusion and give false-positive fusion inhibition results.

There was no significant difference in the initial adherence of total monocytes in all wells containing either IgG1 control or anti-tetraspanin antibodies when ConA was present (Figure 3.4). Monocytes grown in the absence of ConA showed a 40.73% decrease in adherence (compared to ConA+IgG1 control). There was no significant difference between ConA+IgG1 and ConA only wells. From these results it is clear that the anti-tetraspanin antibodies do not interfere with the initial adherence of monocytes in the first 2hrs after seeding.

3.1.4 COMPARISON OF FUSION FROM ADHERENCE AND MACS PURIFIED TOTAL MONOCYTES.

Anti-tetraspanin antibodies were used on both adherence purified total monocytes and MACS isolated total monocytes. Previous studies have predominantly been conducted on adherence purified monocytes and have not been analysed with high throughput automated techniques or have MGC types assessed.

Figure 3.5a and Figure 3.5b show a selection of sample images of MGCs generated from either adherence or MACS purified total monocytes from a single donor and cultured in ConA and IgG1 or an anti-tetraspanin antibody. Figure 3.6a and Figure 3.6b show the fusion parameters from all the donors analysed and Figure 3.7 shows the MGC types generated. It is clear that there are differences in MGC formation between the two purification techniques. All parameters in MACS purified cells were higher than the adherence purified monocyte equivalents. Furthermore, the distribution of the types of MGCs found in the ConA+IgG1 controls is different between the two purification methods. The LGC population decreases by -50.15%, the FBGC remains almost the same with a -0.65% difference and the SGC type increases by

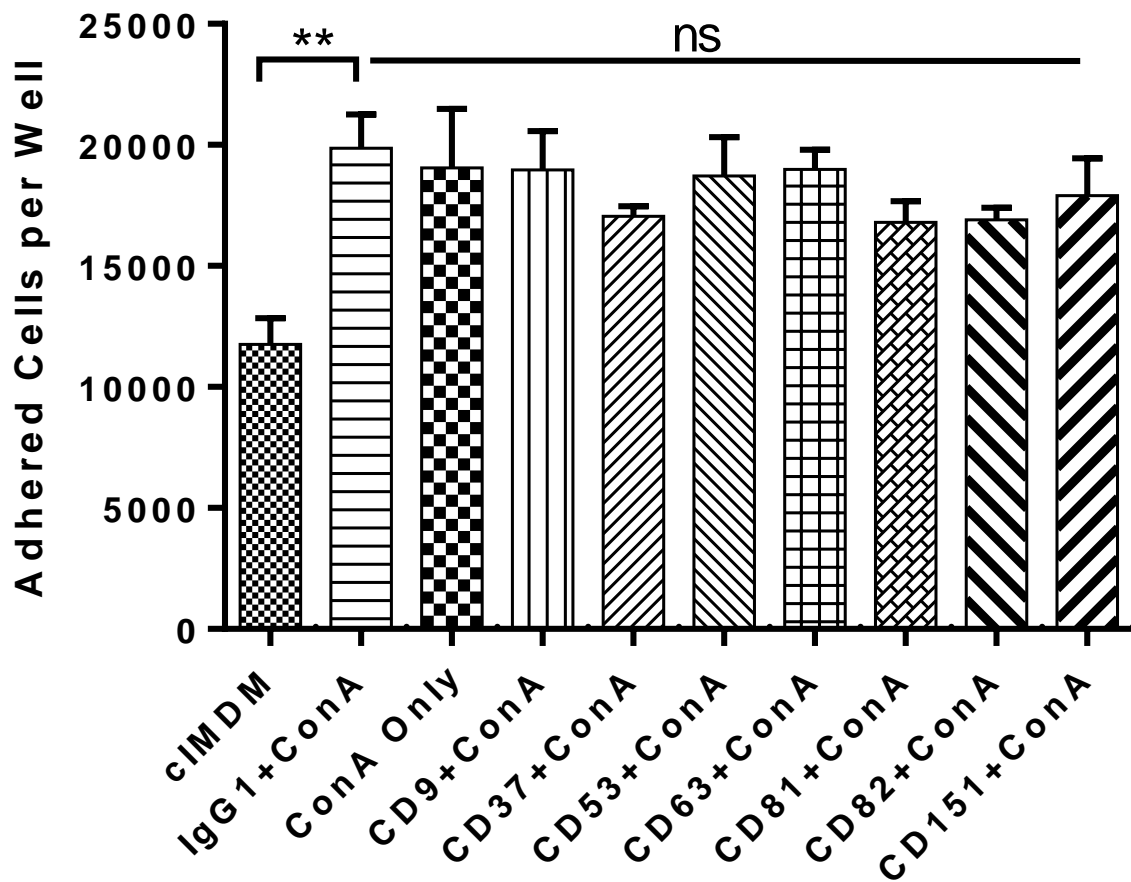


Figure 3.4: Total Monocyte Adherence after 2hr Incubation with Anti-Tetraspanin Antibodies.

The number of total cells counted in a 96-well plate well after being seeded with 50,000 total monocytes in media containing cIMDM, cIMDM+ConA or cIMDM+Antibody (IgG1 or tetraspanin) and incubated for 2hrs to allow cells to adhere. Bars represent the mean±SEM. Each donor performed in triplicate, N=4, tested with a Dunnett's 1-Way ANOVA.

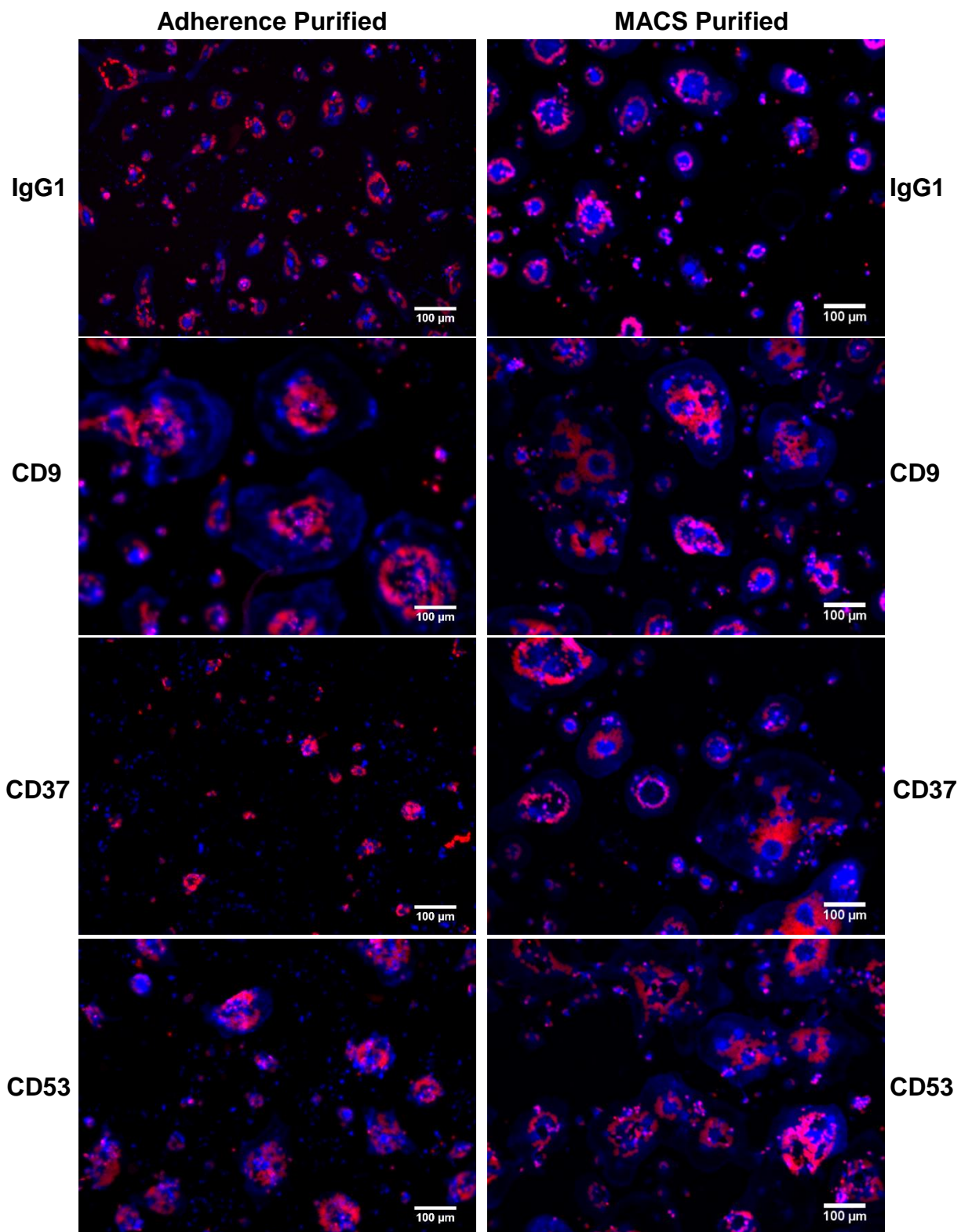


Figure 3.5a: Sample 10x Images from Fusion Assays (Part 1/2)

The left column contains images from adherence purified monocytes, the right column are image from the MACS purified monocytes. All conditions contain cIMDM containing $10\mu\text{g ml}^{-1}$ ConA and $10\mu\text{g ml}^{-1}$ of an IgG1 control or an anti- tetraspanin antibody. Scale bars are all $100\mu\text{m}$.

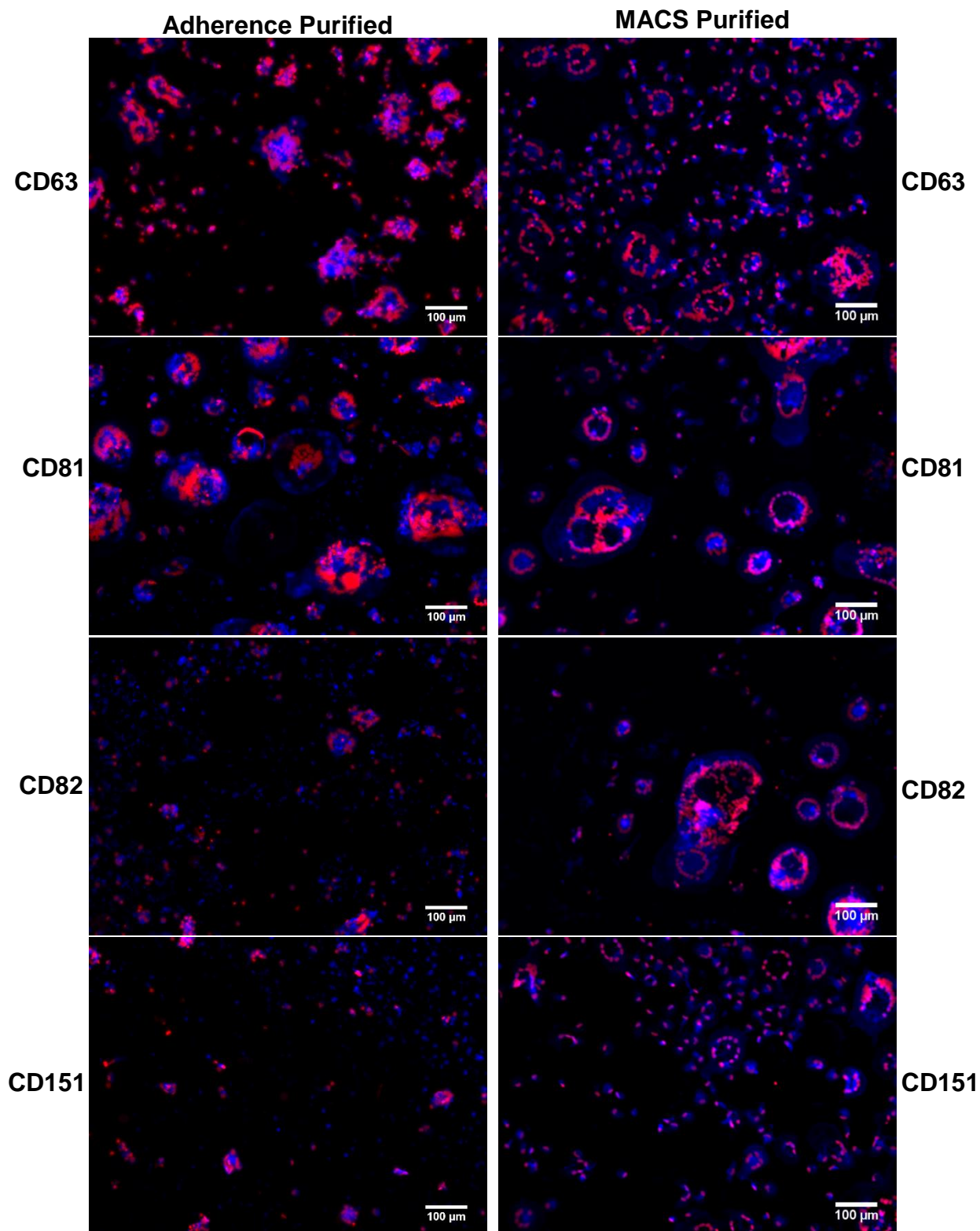


Figure 3.5b: Sample 10x Images from Fusion Assays (Part 2/2)

The left column contains images from adherence purified monocytes, the right column are image from the MACS purified monocytes. All conditions contain cIMDM containing $10\mu\text{g ml}^{-1}$ ConA and $10\mu\text{g ml}^{-1}$ of an IgG1 control or an anti- tetraspanin antibody. Scale bars are all $100\mu\text{m}$.

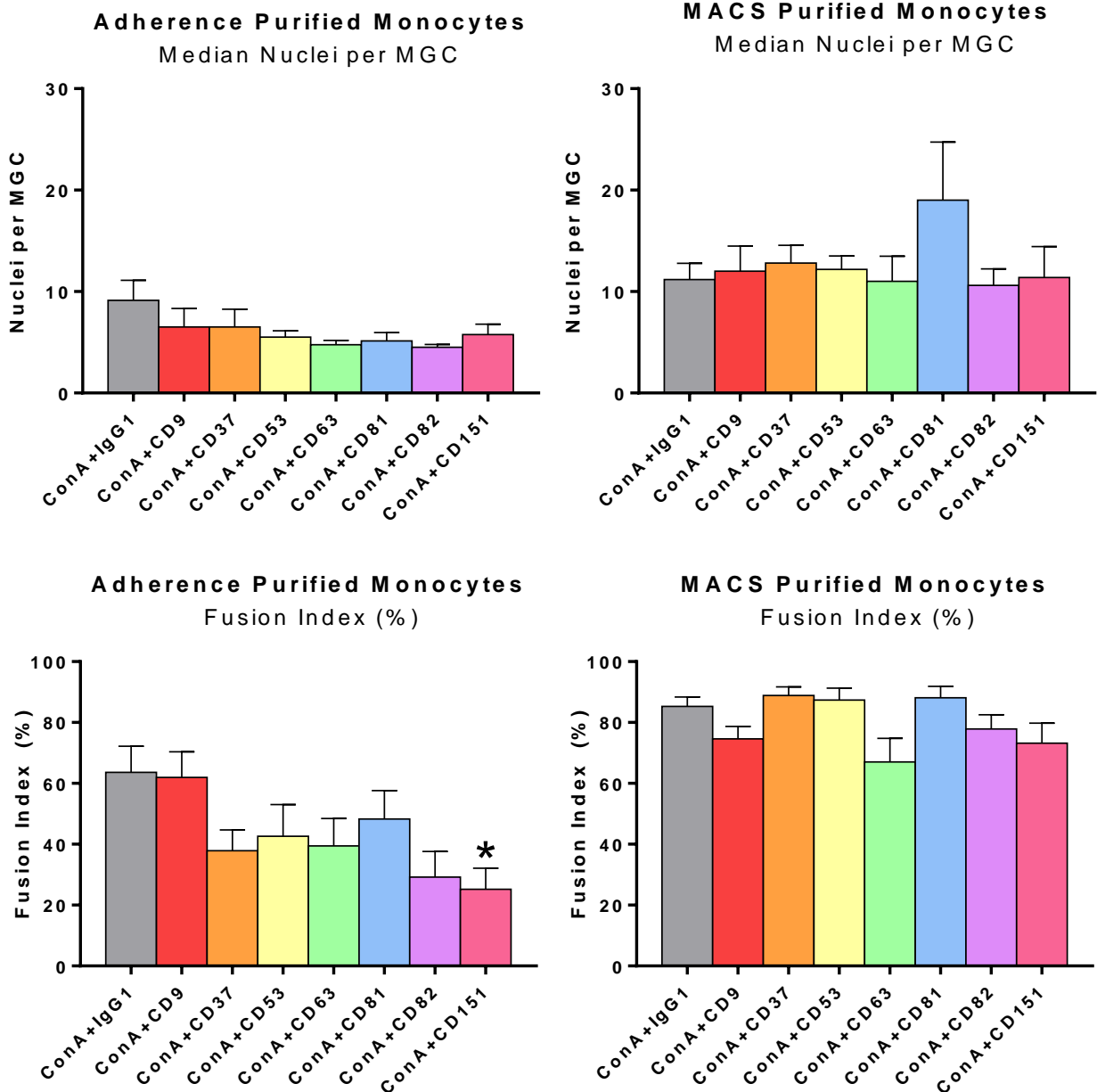


Figure 3.6a: Comparison of Fusion Results from Adherence and MACS Purified Monocytes (Part 1/2)

The Median Nuclei per MGC and Fusion Index results from total monocytes purified by adherence (left) and MACS (right) cultured for 72hrs in ConA media and corresponding anti- tetraspanin antibody. Bars represent the mean±SEM. N=4 for Adherence graphs and N=5 for MACS graphs, tested with a Dunn's multiple comparison test with all column means compared to IgG1+ConA control.

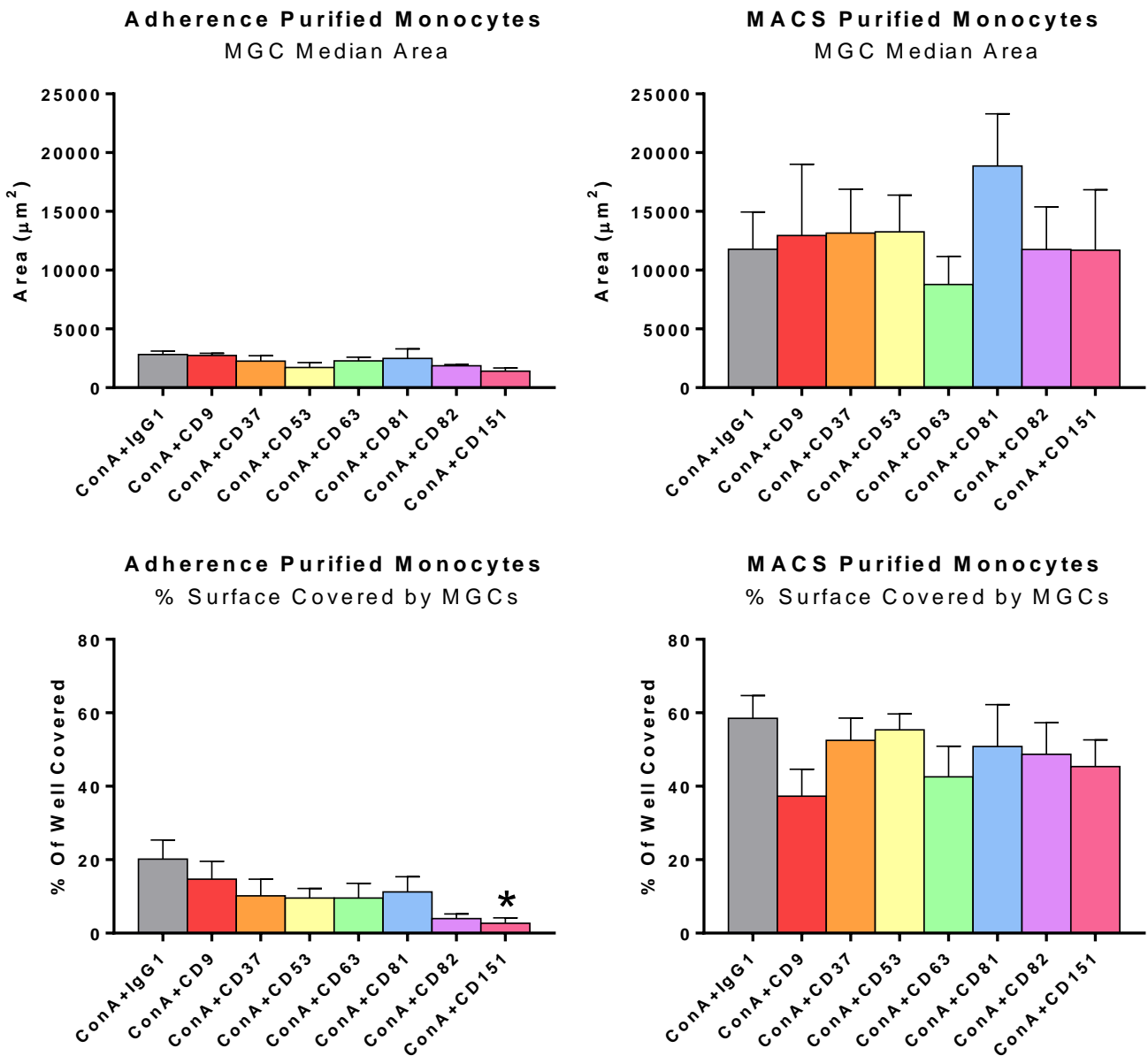


Figure 3.6b: Comparison of Fusion Results from Adherence and MACS Purified Monocytes (Part 2/2)

The MGC Median Area and % of Well Covered results from total monocytes purified by adhesion (left) and MACS (right) cultured for 72hrs in ConA media and corresponding anti-tetraspanin antibody. Bars represent the mean±SEM. N=4 for Adherence graphs and N=5 for MACS graphs, tested with a Dunn's multiple comparison test with all column means compared to IgG1+ConA control.

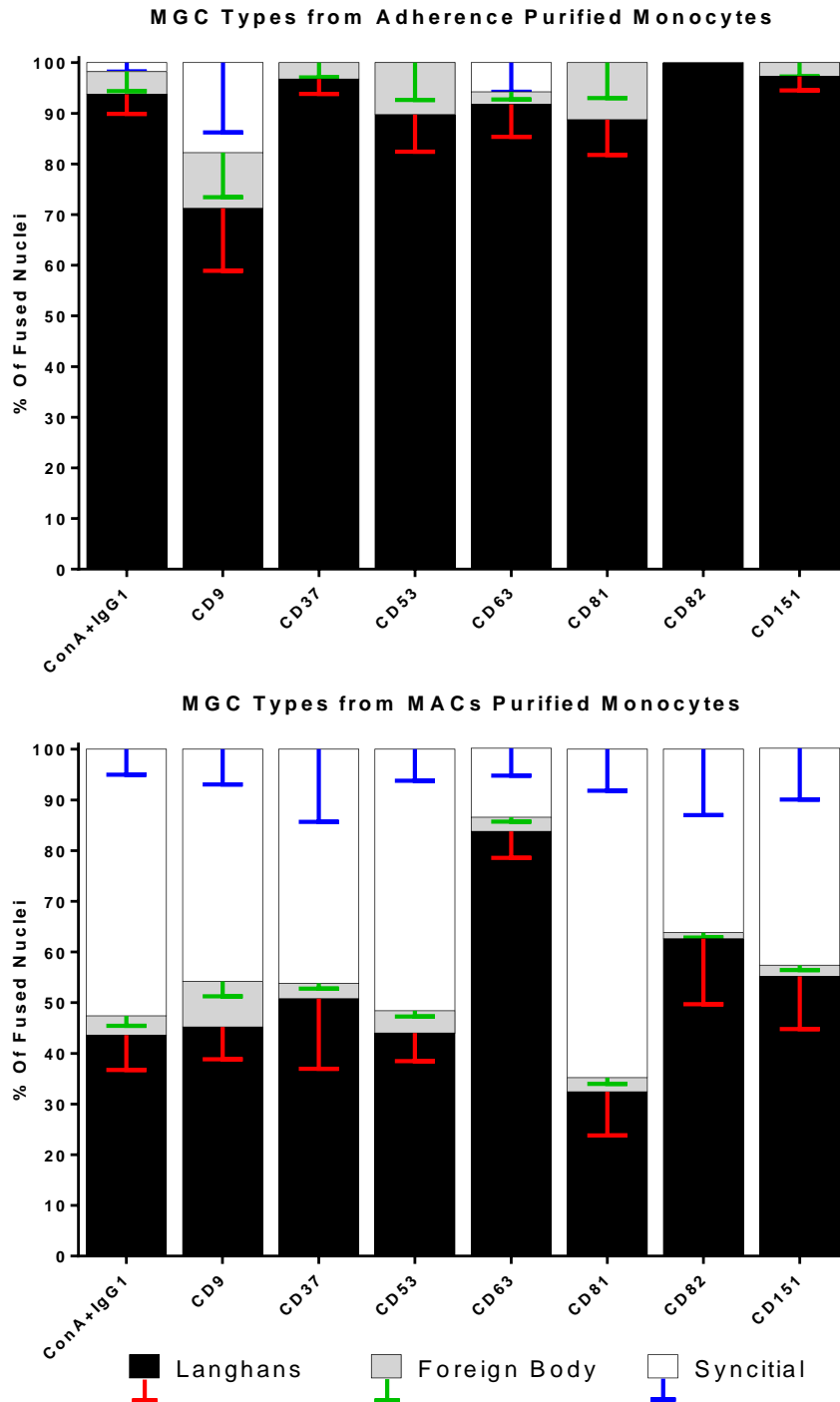


Figure 3.7: MGC Types Generated from Adherence or MACs Purified Total Monocytes.

The MGC types generated from total monocytes purified by adherence (top) or MACS (bottom) cultured for 72hrs in ConA media and corresponding anti-tetraspanin antibody. Fused nuclei were tallied into either LGC, FBGC or SGC depending on what MGC type they were found in and expressed as a percentage of all fused nuclei. Bars represent the mean±SEM. N=4 for adherence graphs and N=5 for MACS graphs. Tested with a Dunn’s multiple comparison test; comparing the mean ranks of each MGC type to the IgG1+ConA control.

+50.75%. From this it is clear that the MACS purification method produces monocytes with a greater potential for forming larger MGCs.

For median nuclei per MGC, the Kruskal-Wallis test showed there was no significant differences between the IgG1 control and the anti-tetraspanin antibodies in either purification method. Both methods produced similar values for the control samples with 9.13 and 11.20 nuclei per MGC for adherence and MACS purification respectively. In the MACS monocytes anti-CD81 antibody showed an increase to 19.00 nuclei per MGC, however; this was not significant.

The FI for the IgG1 controls was lower in the adherence purified monocytes (63.63%) than for the MACS monocytes (85.32%). However, the adherence purified monocytes showed a significant reduction in FI when cultured in anti-CD151 ($P=0.037$) but a similar effect was not observed in MACS monocytes. For MACS monocytes only anti-CD63 antibody caused a reduction in the FI (67.04%; $P=0.4891$), however, it was not found to be significant.

MGC derived from adherence purified monocytes were notably smaller than the MACS derived MGCs ($2,824\mu\text{m}^2$ vs $11,783\mu\text{m}^2$). The median area of the MGCs for the adherence purified monocytes remains relatively unchanged in the presence of any anti-tetraspanin antibody and show no significant difference to the control.

The % surface covered by MGCs was 2.9x greater when MACS purified monocytes (58.52%) were used compared to adherence purified monocytes (20.18%) for IgG1 controls. The only statistically significant decrease was from anti-CD151 (2.68% at $P=0.0292$) for adherence purified monocytes. Anti-CD82 also showed a decrease (3.98%) but was not significant.

Comparing the MGC types (Figure 3.7) formed from adherence and MACS purified monocytes it is apparent that the MACS purified monocytes are able to form far more of the larger SGCs. Of the fused nuclei analysed within the IgG1 controls; the adherence purified monocytes produced a LGC:FBGC:SGC ratio of

93.75%:4.50%:1.75% compared to the 43.60%:3.80%:52.60% of the MACS purified monocytes. The most obvious change in the MGC distribution for adherence purified monocytes came from the addition of anti-CD9 (71.25%:11.00%:17.75%) but the Dunn's test returned all comparisons as insignificant ($P>0.9999$). Though not statistically significant; the addition of antibodies targeting CD37, CD53, CD81, CD82 & CD151 were sufficient to eliminate the presence of any SGCs from the adherence purified cells. Anti-CD82 in particular produced MGCs that were only LGC type.

With the addition of anti-CD63 to the fusion media the MACS purified monocytes committed 3.9x fewer nuclei to the SGC population (52.60%→13.40% for IgG1→anti-CD63) to an almost significant difference ($P=0.0798$). Anti-CD63 also caused nearly double the number of nuclei in the LGC population (43.60%→83.80%; $P=0.0559$). Addition of anti-CD81 produced the lowest number of nuclei located in LGCs (32.40%, $P>0.9999$) and the highest amount of SGCs (64.80%, $P>0.9999$). The addition of any of the other tetraspanin antibodies to the fusion media did not produce any statistically observable changes in fusion, nor was it sufficient to completely eliminate the presence of any of the MGC types.

3.1.5 FUSION OF ADHERENCE PURIFIED TOTAL MONOCYTES CULTURED WITH DUAL ANTI-TETRASPANIN ANTIBODIES

Tetraspanins have been reported to possess a high degree of redundancy with one another. It is therefore possible that the removal of one tetraspanin can be compensated by another. Furthermore, many studies report tetraspanin interact in heterotypic groups (Mazurov *et al.*, 2013) in which correct couplings could lead to the formation of a fusion-mediating TEM. By binding pairs of tetraspanins at the same time it could elucidate some of the interactions between tetraspanins in a fusion setting; be they additive, compensatory, inhibitory or null.

There was no significant increases or decreases in the median number of nuclei per MGC (Figure 3.8a) for any combination of antibodies when compared to the IgG1 control (red stars) or the single antibody equivalents (black stars). However, the FI, MGC Area and % coverage (Figures 3.8b-c) were more sensitive to double anti-

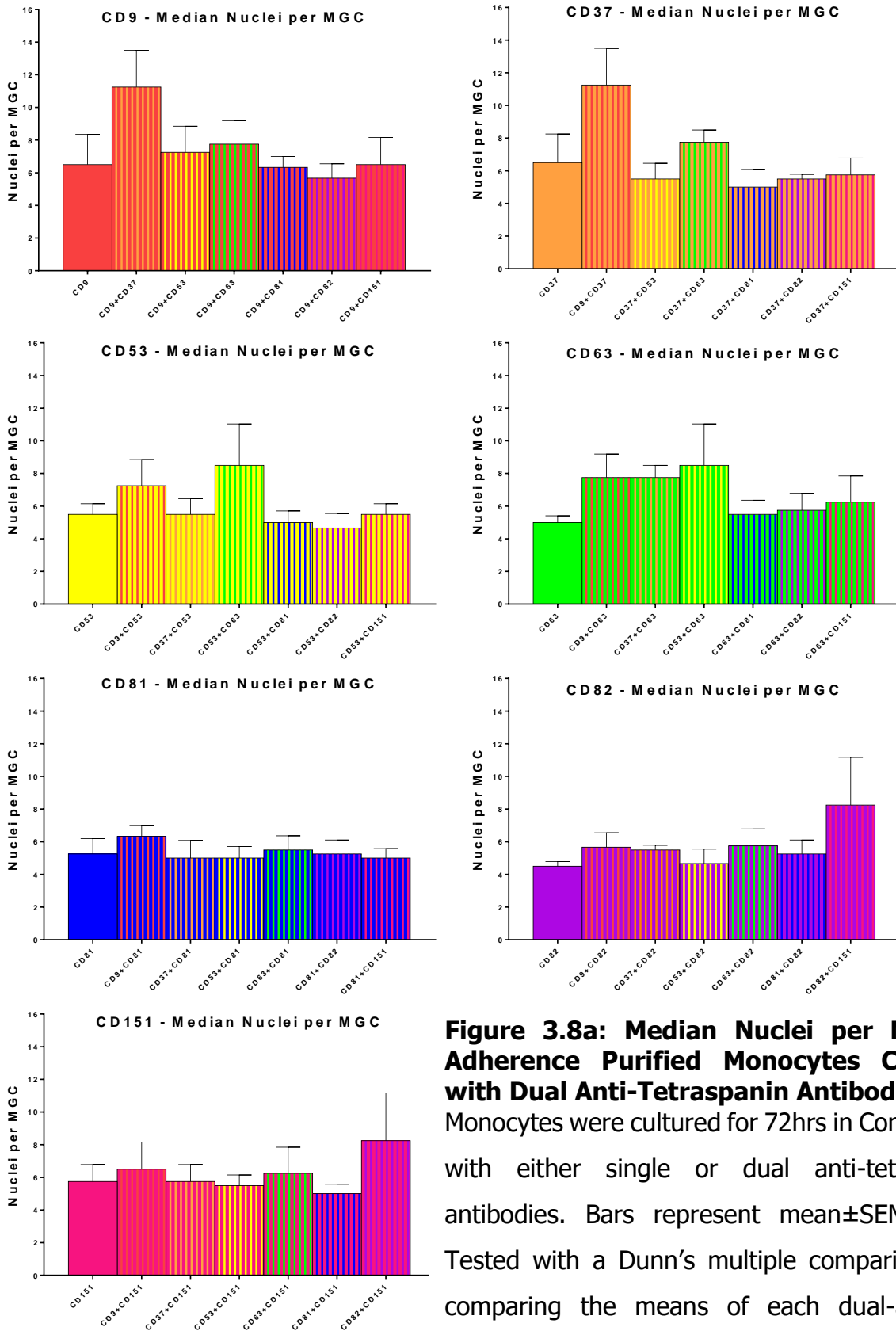


Figure 3.8a: Median Nuclei per MGC of Adherence Purified Monocytes Cultured with Dual Anti-Tetraspanin Antibodies. Monocytes were cultured for 72hrs in ConA media with either single or dual anti-tetraspanin antibodies. Bars represent mean±SEM, N=4. Tested with a Dunn’s multiple comparison test comparing the means of each dual-antibody treatment to the single antibody treatment (black stars) or to the IgG1 control (red stars; 8.75nu MGC⁻¹).

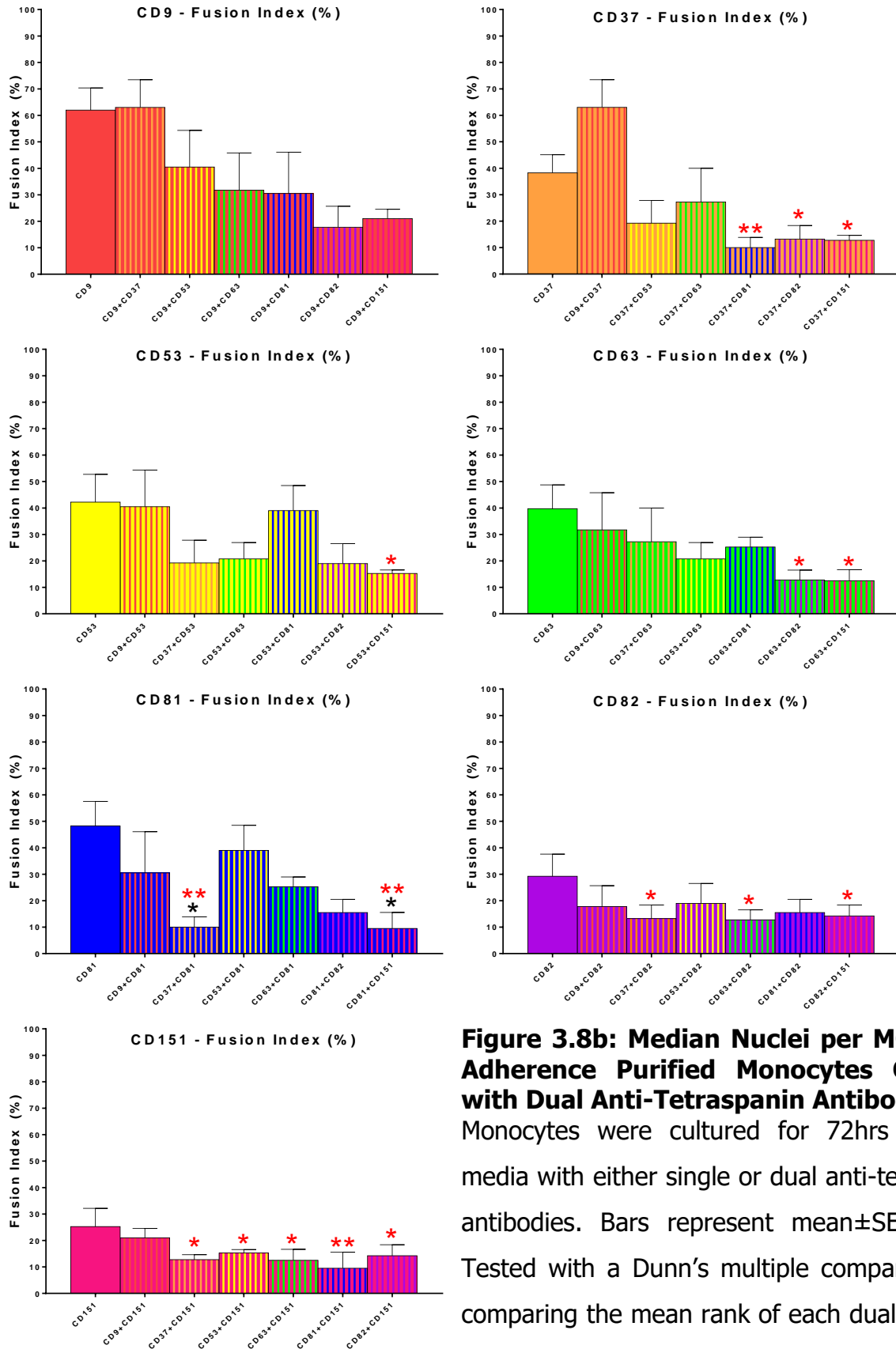


Figure 3.8b: Median Nuclei per MGC from Adherence Purified Monocytes Cultured with Dual Anti-Tetraspanin Antibodies. Monocytes were cultured for 72hrs in ConA media with either single or dual anti-tetraspanin antibodies. Bars represent mean±SEM, N=4. Tested with a Dunn's multiple comparison test comparing the mean rank of each dual-antibody treatment to the single antibody treatment (black stars) or to the IgG1 control (red stars; 61.75%).

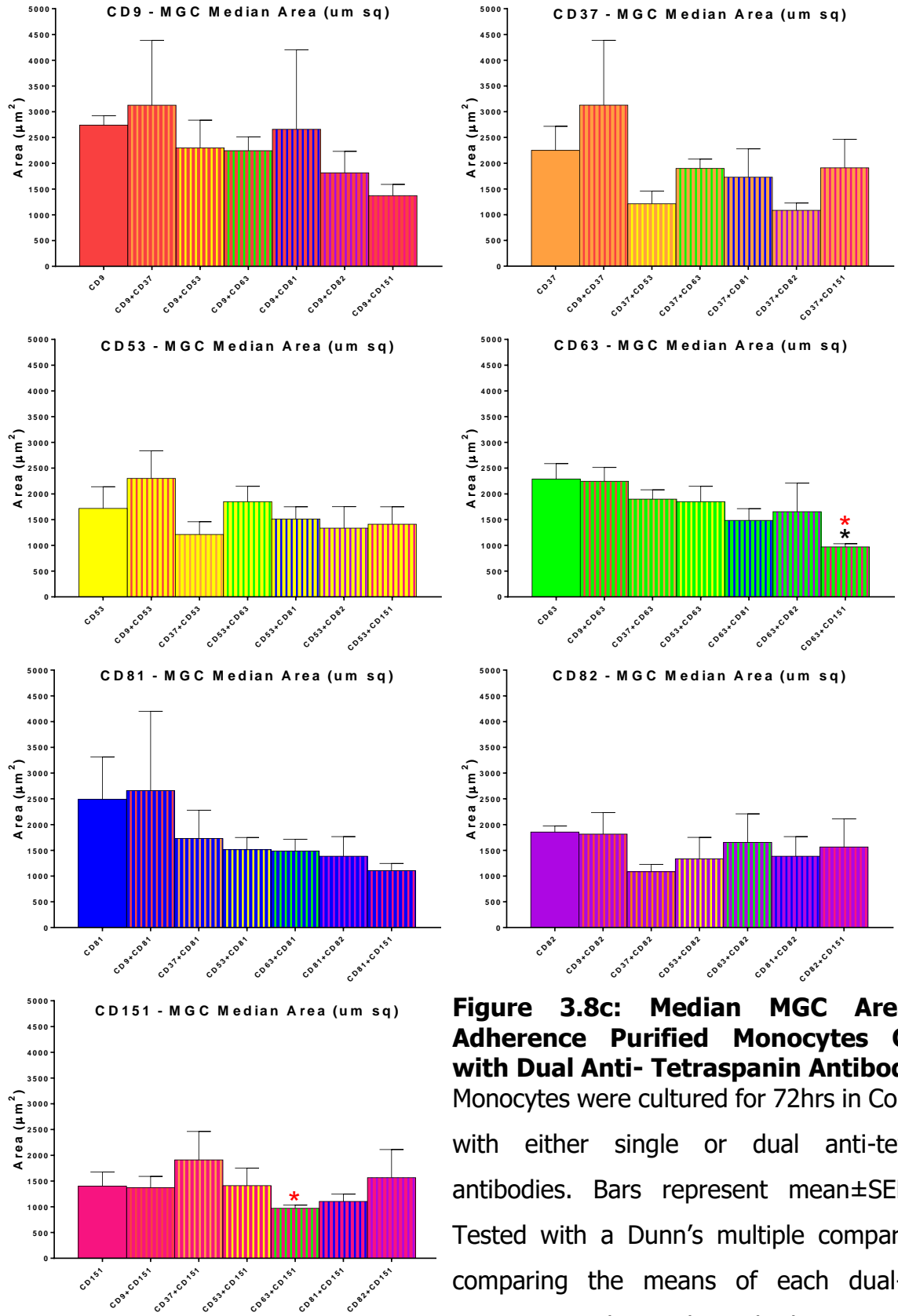


Figure 3.8c: Median MGC Area from Adherence Purified Monocytes Cultured with Dual Anti- Tetraspanin Antibodies. Monocytes were cultured for 72hrs in ConA media with either single or dual anti-tetraspanin antibodies. Bars represent mean±SEM, N=4. Tested with a Dunn’s multiple comparison test comparing the means of each dual-antibody treatment to the single antibody treatment (black stars) or to the IgG1 control (red stars; 2511um²).

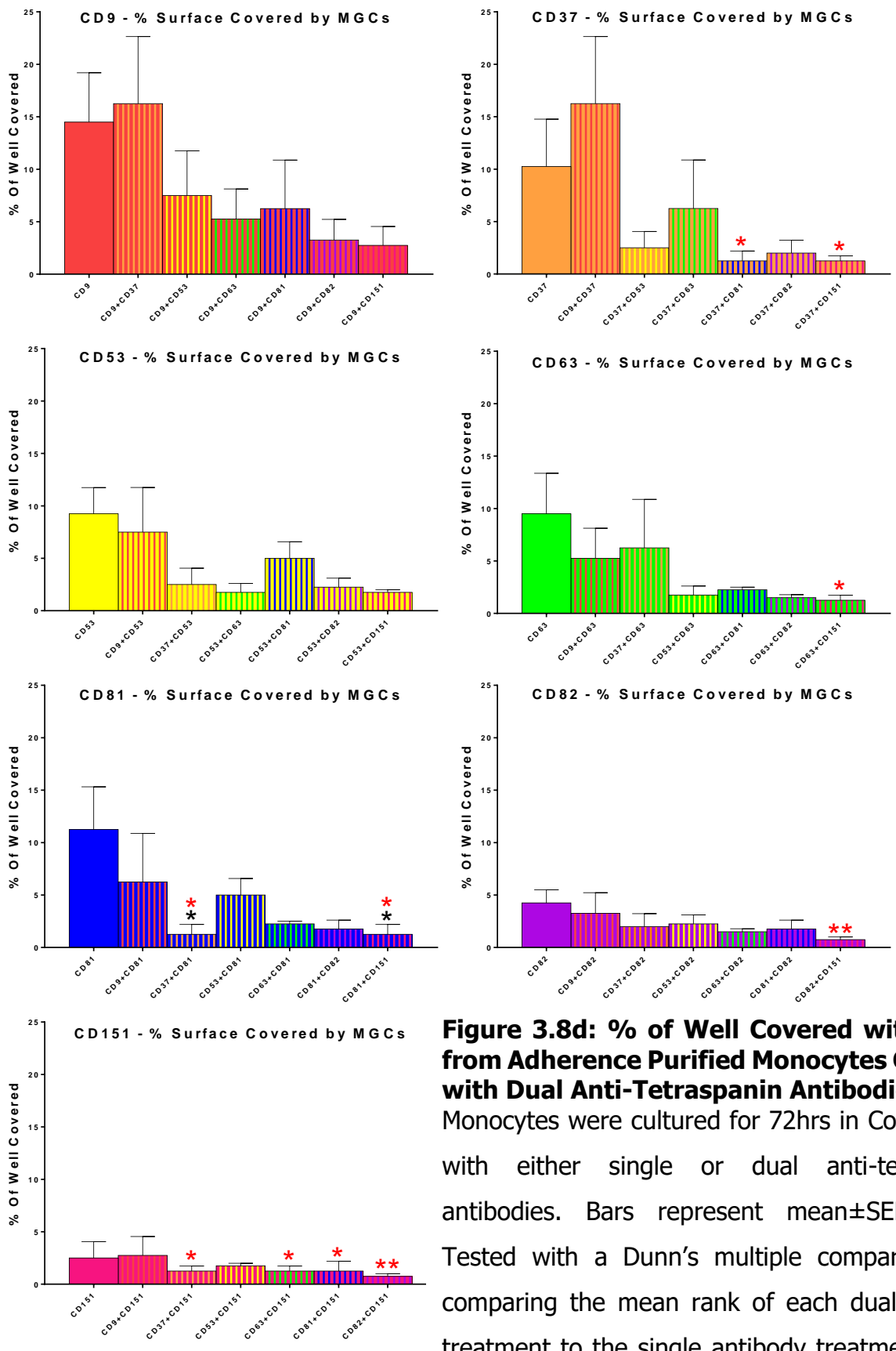


Figure 3.8d: % of Well Covered with MGCs from Adherence Purified Monocytes Cultured with Dual Anti-Tetraspanin Antibodies. Monocytes were cultured for 72hrs in ConA media with either single or dual anti-tetraspanin antibodies. Bars represent mean±SEM, N=4. Tested with a Dunn's multiple comparison test comparing the mean rank of each dual-antibody treatment to the single antibody treatment (black stars) or to the IgG1 control (red stars; 19.13%).

tetraspanin antibody treatment than median nuclei per MGC. Overall, anti-CD82 alone had the lowest median nuclei per MGC at 4.5 nuclei per MGC ($P=0.2252$). The population distributions for anti-CD82 in Figure 3.9 shows that the presence of anti-CD82 in any combination other than with anti-CD9 was sufficient to completely impede the formation of FBGCs and SGCs.

Anti-CD9+anti-CD37 was the only combinational treatment that was similar to the IgG1 control (IgG1: 8.75nu MGC⁻¹, 61.75% FI, 2511 μm^2 , 19.13% covered vs anti-CD9+anti-CD37: 11.25nu MGC⁻¹, 63.00%, 3127 μm^2 , 16.25% covered). All other anti-tetraspanin antibody combinations produced considerable decreases in fusion parameters compared to the single antibodies alone. Anti-CD9+anti-CD37 treatment also produced similar results to anti-CD9 alone treatment in all parameters except the number of nuclei per MGC. In Figure 3.9 addition of anti-CD9+anti-CD37 is sufficient to cause a significant decrease in the % nuclei in LGCs (87.75%) compared to anti-CD36 alone (96.75%) as a result of more FBGCs and SGCs are forming.

The lowest FI, MGC area and % coverage for a single antibody treatment was anti-CD151 at 25.25%, 1402 μm^2 and 2.50% respectively. Only 6 of the 21 double anti-tetraspanin treatments possessed FI above anti-CD151 (four of which contained anti-CD9), the remaining 15 combinations were all less than any of the single anti-tetraspanin antibody treatments. Anti-CD81+anti-CD151 was ranked the most inhibitory; possessing the lowest FI (9.5%), third smallest MGC area (1103 μm^2) and second lowest % covered (1.25%). Anti-CD82 had the second lowest rank amongst the single antibody treatments with a FI of 29.25% and when combined with anti-CD151 resulted in a FI that was lower than both (14.25%).

Anti-CD151 double antibody treatments had the lowest collective FI with anti-CD9+anti-CD151 being the only combination above 20% FI. With the exception of anti-CD9+anti-CD151 all other anti-CD151 containing combinations were ranked in the bottom 8 of the FI and bottom 7 of the % surface covered. These showed significant reductions compared to the IgG1 control (red stars, Figure 3.8b & 3.8d,

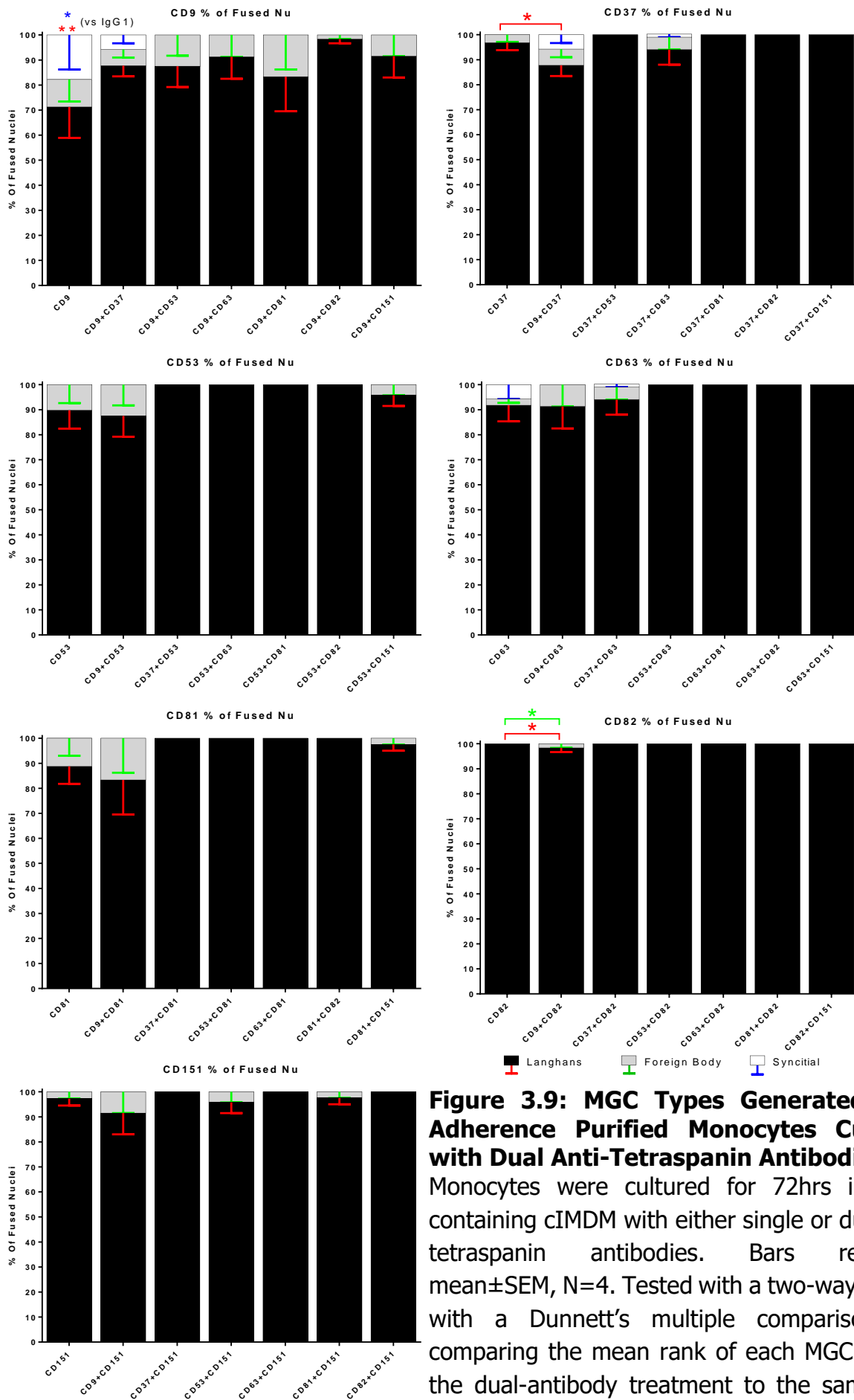


Figure 3.9: MGC Types Generated from Adherence Purified Monocytes Cultured with Dual Anti-Tetraspanin Antibodies.

Monocytes were cultured for 72hrs in ConA containing cIMDM with either single or dual anti-tetraspanin antibodies. Bars represent mean±SEM, N=4. Tested with a two-way ANOVA with a Dunnett's multiple comparison test comparing the mean rank of each MGC type of the dual-antibody treatment to the same MGC type of the equivalent single antibody treatment or IgG1. Red stars: LGCs, Green: FBGCs & Blue: SGCs.

anti-CD151 graph). Antibody combinations containing anti-CD82 showed an inhibiting effect similar to anti-CD151, but to a lesser extent.

Curiously, anti-CD81 produced the second highest FI (48.25%) of the single antibody treatments yet anti-CD81 was also present in the two lowest FI treatments: anti-CD81+anti-CD151 (9.50%) and anti-CD37+anti-CD81 (10.00%). Compared to anti-CD81 alone, the Dunn's test reported significant reductions in anti-CD81+anti-CD151 ($P=0.0431$) and anti-CD37+anti-CD81 ($P=0.0459$) treatments. Compared to the original IgG1 control (red stars) these reductions were even more significant ($P=0.0039$ and $P=0.0053$ respectively). The % coverage reflects the same trend as the FI with anti-CD81+anti-CD151 and anti-CD37+anti-CD81 both producing only 1.25% coverage (both $P=0.0392$) compared anti-CD81 alone (11.25%). Thus the combining of anti-CD37 or anti-CD151 produced a % coverage that was lesser than any of the single antibody equivalents (anti-CD37: 10.25%, anti-CD151: 2.50% and IgG1: 19.13%).

As a group, anti-CD9 and its combinations collectively produced the largest MGCs by area. Anti-CD9+anti-CD37 were the biggest of all single and double antibody conditions ($3127\mu\text{m}^2$) with anti-CD9+anti-CD151 ($1373\mu\text{m}^2$) being the smallest of the group. The smallest MGCs out of all the conditions tested were in anti-CD63+anti-CD151 ($970\mu\text{m}^2$). In Figure 3.9 anti-CD9 was the only condition (single or double) to produce a significant decrease in the % of LGC nuclei ($P=0.0037$) and an increase in the SGC nuclei ($P=0.0495$) compared to IgG1. Whereas anti-CD63+anti-CD151 was the only condition to cause significant decrease in the MGC area compared to both anti-CD63 alone ($P=0.0284$) or IgG1 ($P=0.0113$).

3.2 DISCUSSION

The Optimised Protocol Produces Purer Monocytes and Larger Sample Sizes

Previous studies on the fusion of monocytes have used an adhesion purification method but this runs the risk of variable contamination with cytokine-producing lymphocytes. T-cells and NK-cells have been shown to be responsive to ConA which causes differentiation, activation and cytokine release (Lei and Chang, 2009; Takashima *et al.*, 1993; Wang *et al.*, 2012). T-cells and NK-cells are selectively removed in the MACS method. Figure 2.1 and Figure 2.2 show that the MACS purification effectively removed the granulocyte and lymphocyte populations. However, in the "CD14- removal" plots it is clear that MACS treatment was not sufficient to remove the NK-cell population. Studies have shown that ConA is able to activate NK-cells to produce IFN γ which is known to initiate fusion.

The use of FACs or positive selection MACS to purify monocytes may produce greater purities but the goal of the optimisation reported here was to increase purity with minimal interference to the monocytes themselves. Binding of large beads or antibody-fluorophore conjugates could alter the fusion behaviour of the monocytes and give false results.

Different strategies were attempted to automate the selection of MGC borders and type but none were sufficient to match manual selection. When performing a threshold adjustment and subsequent watershed on the actin images it was still not possible to separate MGCs effectively. There were many images that contained overlapping, touching or partly-stained MGCs or even non-fused cell aggregates. The uniformity of actin staining was less consistent for SGC (such as those seen in Figure 2.6) which have regions of low actin. It is possible that because of the sheer size of the SGCs that at the single z-slice is unable to capture enough actin fluorescence signal for parts of the MGC structure that are particularly raised above the surface of the well. In 2014 Pegoraro and colleagues published a paper describing an automated MGC analysis method using confocal microscopy and the PerkinElmer program 'Acapella 2.7' to select *Burkholderia* infected giant cells. Unfortunately, such an advanced image

analysis program was unavailable to us and an equivalent plugin on ImageJ was not found. Though time consuming, manual ROI selection of MGCs was the only way to ensure accurate selection of MGCs and identification of MGC type.

The automation of the imaging removed any user bias and allowed low-magnification maps to be made by collaging the 4x images. For the first time it was possible to see the distribution of giant cells in the well and showed that, on some occasions, the distribution was uneven. If the wells contained an even distribution of MGCs and single cells then the sample images selected for counting were #5-8 to bisect the well from one side to the other. In cases of extremely uneven distribution an alternative row/column of sample images was selected that best represented the total population. Though this approach does confer some sample bias it was deemed to be the best method for generating a representative sample population for unevenly distributed wells.

The stacking of nuclei particularly in FBGCs posed an issue for the automated counting macro. As the nuclei get closer or overlap the fluorescence signal stacks (see red box in Figure 2.5) and the resolution of individual peaks is lessened. Using background reduction and ensuring that the pixels were not saturated prior to imaging; ensured that the resolution between the signal peaks was maximised. The automated technique for counting nuclei gave a 6-fold increase in nuclei counted per condition and further removed user bias.

The More the Merrier; Fusion Parameters Increase with Increasing Monocyte Seeding Numbers

The apparent increase in all fusion parameters in Figure 3.2 when monocyte seeding density was increased can be explained by two features of fusion. Firstly, the number of monocyte-monocyte contacts will increase with increasing cell density. This increases the chance that direct contact between monocytes will occur as they randomly patrol the well surface. Secondly, with more monocytes present in the well the concentration of fusion-triggering cytokines may go up faster. Though the exact mechanism of ConA directed fusion is still unknown, it has been shown that ConA

triggers a release of fusion initiating cytokines e.g. IFN γ , TNF- α , IL-1 β and IL-4 (Sodhi *et al.*, 2007; Wang *et al.*, 2012). With more monocytes present the concentration of these cytokines will accumulate faster in the media and therefore trigger fusion at a faster rate.

The median nuclei per MGC is a commonly used parameter in MGC experiments (Coury *et al.*, 2008; Harkel *et al.*, 2015; Kondo *et al.*, 2009). In the kinetics experiments (Figure 3.2), there was no significant change in the median nuclei per MGC throughout all the time points observed. The lack of change in this particular parameter could be a consequence of the large sampling size. MGC populations were almost exclusively positively skewed, with smaller (3-8 nuclei) MGCs being the most prevalent and larger MGCs being less common. As the seeding density is increased there is an increase in the MGC size across all three time points but little change between time points. It is possible that though there are larger MGCs present in the sample population at later time points, they are not affecting the median because the smaller MGCs are far more numerous. The median area of MGCs for example is another median measurement but because the differences in MGC area are often in hundreds to thousands of square micrometres; changes in the median are far more apparent.

For the other parameters there are initial increases between 24-48hrs but then a plateau or decline in measurements between 48-72hrs. There is no evidence in the literature or in the images obtained that fusion is a reversible process. It is more likely that at 48hrs the smaller MGCs are reaching peak activity and are then moving and fusing with one another, thus appear similar to SGCs. This would account for the higher number of SGCs at 48hrs in all densities in Figure 3.3. At 72hrs when the media has been depleted it is possible that the MGCs are less motile and stop moving over and across one another which would give fewer false counts of SGCs. Another possibility is that after 48hrs, the larger MGCs become unstable and rupture either prior or during the washing and fixing stage and so they are not present in the 72hrs images. The parameters for the lowest seeded density (0.25×10^5 monocytes well⁻¹) in Figure 3.2 do not show the post-48hrs decline in values. This could mean that there

is some sort of negative feedback occurring in the higher densities which is why the parameters decrease in the higher seeding densities.

Based on the results from the kinetics experiments it was decided that 1.50×10^5 monocytes well⁻¹ was the preferable seeding density for future assays because it produced higher values in all the measured parameters. This would mean that when fusion was inhibited or enhanced by anti-tetraspanin antibodies the change from the control would be apparent.

Anti-Tetraspanin Antibodies Do Not Affect Initial Adherence

The adhesion assay (Figure 3.4) showed that anti-tetraspanin antibodies did not affect the early monocyte behaviour in any observable way. However, even if adherence machinery is not affected this is not to say that other processes such as migration (which also utilises integrins and other proteins that complex with tetraspanins) are not affected. If for example the monocytes could adhere but an anti-tetraspanin antibody inhibits the ability for the monocyte to migrate then fusion would also be inhibited, leading to a false negative result.

Despite the seeding density for the adhesion assay being 50,000 monocytes per well, only approximately 20,000 monocytes were recorded per well (a ~40% return). It could be that when the wells were washed and fixed at 2hrs many weakly adhered monocytes were washed off thus reducing the final count. It is unlikely to be a point of concern as all the controls and anti-tetraspanin antibody wells all produced consistent results in all triplicates and produced consistent cell counts across all ConA-containing conditions.

The results of the adherence assay highlights a serious pitfall of the adherence purification method. In the absence of ConA, significantly fewer monocytes remained adhered to the well after 2hrs. The adherence purification method requires that wells be washed after 2hrs to remove adherent leukocytes but in Figure 3.4 we see that washing and fixing at this time results in substantial monocyte loss. The loss of these lesser-adherent monocytes could potentially have a big influence on the results of

fusion as the monocyte density will be lowered and there is no way to know if these monocytes have low adherence properties but are highly influential to the fusion process.

MACS Purification Enhanced the Fusion Potential of Monocytes

The MACS purified cells produced for more fusion, bigger MGCs, higher % coverage, greater SGC populations and less significant changes in response to anti-tetraspanin antibodies. It could be that the monocyte density is so high compared to the adherence purified cells (as what is seeded remains in the well) that the fusion has reached a saturated state. If the monocyte density was so high that monocytes and MGCs were in constant contact then fusion would occur to a greater extent than for the adherence purified cells and vast SGCs would form more often. Not only is the density of the seeded monocytes potentially higher in the MACS method but the presence of NK-Cells is higher (Figure 2.2). As potent producers of GM-CSF and TNF α it is possible that the NK-cells are becoming activated by ConA or ConA-induced monocyte cytokines to greatly enhance the fusion of the monocytes and produce more SGCs. It is likely that there is a lower number of monocytes in the adherence purified well due to the washing of non-adherent monocytes and this is why the fusion parameters are lesser than that of the $\sim 3x$ purer MACS monocytes. The greater degree of fusion caused by either the higher density of monocytes or the presence of NK-cells could be saturating and thus masking the effects of the anti-tetraspanin antibodies on the fusion parameters.

In both purification methods the addition of any of the anti-tetraspanins antibodies was not sufficient to completely arrest fusion and in most cases had subtle or little effect. Although the antibodies were added in saturated amounts it is possible that the monocytes endocytose and degrade any bound tetraspanins and express new functioning tetraspanins to replace them, though this would still show reduced fusion potential to the control. It is possible that the lack of any effect is because there are varying degrees of redundancy amongst the tetraspanins and that the effect of binding one tetraspanin using an antibody is being masked by the contributions of other tetraspanins involved in organising the fusion machinery.

CD63 and CD81 Altered the MGC Types Formed From MACS Cells

Though the number of nuclei per MGC (Figure 3.6a) for the IgG1 controls did not differ very much between purification methods the median area of the MGCs showed a 4-fold difference. This could be attributed to the more varied distribution of MGC types, particularly in the MACS derived MGCs (Figure 3.7). The increased presence of larger SGCs could increase the average area of the MGCs while the presence of multiple smaller LGCs would keep the median number of nuclei down. Furthermore, the unit measurement of MGC area had a much larger range in measurement (typically $800\mu\text{m}^2$ - $60,000\mu\text{m}^2$) compared to the number of nuclei per MGC (typically 3-150nuclei per MGC) and therefore it is more sensitive to change/shifts in the median value. The presence of the much larger SGCs in the MACS purified cells is possibly the cause of this overall increase.

For the MACS purified monocytes, the apparent decrease in MGC area for anti-CD63 and increase for anti-CD81 in Figure 3.6b seems linked to the equivalent decrease/increase in the SGC population in Figure 3.7. It seems that the anti-CD63 and anti-CD151 antibodies are inhibiting the formation of the larger SGCs to an extent that causes the median area and FI to decrease. CD81 had the opposite effect whereby the increase in the larger SGC population seemingly triggered an increase in the median nuclei per MGC and median area. These results are in accordance with previous studies which observed inhibition of fusion with the addition of anti-CD63 or anti-CD151 and enhancement with anti-CD81 (Parthasarathy *et al.*, 2009; Takeda *et al.*, 2003).

Antibodies Targeting CD9 Had No Significant Effect on Fusion

Anti-CD9 antibodies are well documented as causing significant enhancement of fusion in other assays, however, for the adherence purified monocytes only small increases in the SGC population were observed and there were no significant changes in the fusion parameters. The MACS purified monocytes produced no apparent changes to the distribution of MGCs or the fusion parameters in the presence of anti-CD9. Takeda and colleagues (2003) demonstrated that anti-CD9 antibodies enhanced fusion of

monocytes in their experiments, however, they used Bu16 [IgG2a] and MM2/57 [IgG2b κ] antibodies whereas our antibody was a 602.29 [IgG1]. It is likely that the different antibodies bind the EC2 at different sites and therefore some may block associations with partner proteins while others may lock them into active conformations.

CD9 is expressed by other leukocytes of the immune system and as the adherence method relies on washing off non-adherent cells so it is possible that anti-CD9 may also target and influence contaminating leukocytes. The contamination of the adherence wells with T-cells could be of particular concern. Both ConA (Wands *et al.*, 1976) and anti-CD9 (Tai *et al.*, 1996) have been shown to have an effect on T-cells so it is not fully clear if these results are due to anti-tetraspanin and ConA affecting the fusion of monocytes or responses from contaminating T-cells.

Combinational Anti-Tetraspanin Antibody Treatment Greatly Inhibited Fusion

The combining of two anti-tetraspanins antibodies together generally resulted in a greater reduction in fusion parameters. However, anti-CD9 was present in the antibody combination treatments that scored highest in the fusion parameters. CD9 has been reported as a fusion inhibitor (Takeda *et al.*, 2003) so antibody interference should enhance fusion. Anti-CD9 single antibody treatment did not show an increase in the FI or % coverage above that of the IgG1 control but the presence of an anti-CD9 antibody in the treatment did predominantly act to lessen the inhibitory effect of some of the other antibodies to a degree. While the presence of some of the anti-tetraspanin antibodies e.g. anti-CD151 may act to inhibit fusion by binding the respective tetraspanin's EC2 domain and blocking binding partners and TEM formation, anti-CD9 binding is somehow enhancing fusion enough to overcome the negative effect to an extent. It could be that when CD9 is removed from the TEM its binding partners are freed up to participate in fusion. Alternatively, CD9 could be sequestering other tetraspanins and their binding partners thus making fusion initiation unfavourable and when CD9 is bound by anti-CD9 it frees up these tetraspanins and allows them to form a fusion TEM.

CD81 is also reported as a restrictor of fusion and other reports show increased fusion with anti-CD81 antibodies (Takeda *et al.*, 2003) but our results do not reflect such an effect. Furthermore, anti-CD81 was present in the antibody combination that produced the greatest inhibitory effect (anti-CD81+anti-CD151). As CD81 and CD151 have both been shown to associate with EWI-2 (Charrin *et al.*, 2001; Sala-Valdés *et al.*, 2006) to facilitate actin polymerisation at the site of adhesion complexes the extreme loss in fusion when these tetraspanins as targeted together could be a result of EWI-2 interference. Anti-CD151 and anti-CD82 were both potent inhibitors of fusion and when used in combination with other tetraspanins had the biggest negative effect on fusion. The presence of anti-CD82 or anti-CD151 were sufficient to reduce even the higher-fusing anti-CD9 conditions down to their lower limits. Just like CD81 and CD151; CD82 has been shown to associate with EWI-2 (Zhang *et al.*, 2003). Furthermore, CD151 and CD82 are well documented as a facilitators of migration via associations with integrins (Berditchevski and Odintsova, 1999; Yáñez-Mó *et al.*, 2001) so it is uncertain whether their interaction with the cells acts to slow/arrest migration or inhibit the formation of a fusion TEM.

Anti-CD37, anti-CD53 and anti-CD63 produced very similar effects in the fusion parameters as single antibodies but when used in combination with each other they produced an additive negative effect together. This could imply that they share a degree of redundancy with each other or that they form homotypic tetraspanin partnerships with each other during fusion. As CD37 and CD53 have both been shown to associate with LFA-1 and CD63 with E-cadherin it is possible that the negative additive effect is a result of the anti-tetraspanin antibodies removing available adhesion proteins from the TEM. Furthermore, CD37, CD53, CD81 and CD82 have previously been shown on leukocytes to form associations via MHC class II proteins (Angelisova *et al.*, 1994) so it is possible they form a similar TEM during fusion.

Conclusion

To what level of involvement do tetraspanins have in the fusion process of monocytes is still an elusive question. These experiments in total monocytes purified with two

common methods has shown that monocyte purity plays a big part in the outcome of fusion and can mask inhibitory effects of the anti-tetraspanin antibodies. While anti-CD82 and anti-CD151 in adherence purified monocytes and anti-CD63 in MACS purified monocytes seem to be the most potent inhibitors of fusion; the results are still unclear. Furthermore, the contribution of the different monocyte subsets to the fusion process is still unknown and whether they would react equally to the anti-tetraspanin antibodies is still to be seen. To further understand the role of tetraspanins in monocyte fusion the monocyte subsets need to be separated to high purity, quantify their tetraspanin surface expression and analyse their potential to form MGCs.

CHAPTER 4: MONOCYTE SUBSET FUSION

4.1 INTRODUCTION

Previous studies in MGC formation have either been conducted *in vivo* on mice (Skokos *et al.*, 2011; Yang *et al.*, 2014b), or *in vitro* in mouse cell lines (Levaot *et al.*, 2015; Verma *et al.*, 2014) and total human monocytes (McNally and Anderson, 1995; McNally *et al.*, 1996; Möst *et al.*, 1997). However, mice are lacking in the Int monocyte subsets and so do not possess the three subsets seen in humans. Total human monocyte studies do not provide any insight into the individual contribution of the subsets toward fusion. Furthermore, the percentage of each subset population is variable between donors and so changes in subset distributions may affect the results of fusion experiments. In Chapter 3 it was evident that other contaminating leukocytes were often present in the fusion assays when purified by adherence or MACS and so an accurate assessment of monocyte behaviour could not be made. The monocytes used in the current chapter were FACS sorted to a high purity ($\geq 99\%$) by depleting non-monocyte leukocytes with MACS, anti-CD56 to FACS-deplete NK-cells (Figure 2.3) and stringent gating of subsets using CD14 and CD16 expression.

4.2 FUSOGENIC PROPERTIES OF MONOCYTE SUBSETS

In the experiments described in Chapter 3, the total monocyte purity was unlikely to be constant because the adherence and MACS purification methods had varying levels of leukocyte contamination. With FACS sorted subsets the purity is $\approx 100\%$ so it is possible to calculate the contributions of the seeded monocytes to the final result. Figure 4.1 shows what percentage of the monocytes (from the original 1.5×10^5 monocytes seeded well⁻¹) committed to fusion or was not found in the final images and so classified as detached/dead. Of the initially seeded cells, a surprisingly large percentage (67-77%) were classified as detached/dead after 72hrs ConA treatment. This is equivalent to a loss of 105000, 115500 and 100500 cells well⁻¹ for CI, Int and NCI monocytes respectively.

The numbers of cells that remained as adherent single cells were almost equal in CI (24.73%) and NCI (23.45%) monocytes which were ~ 1.9 -fold higher than Int

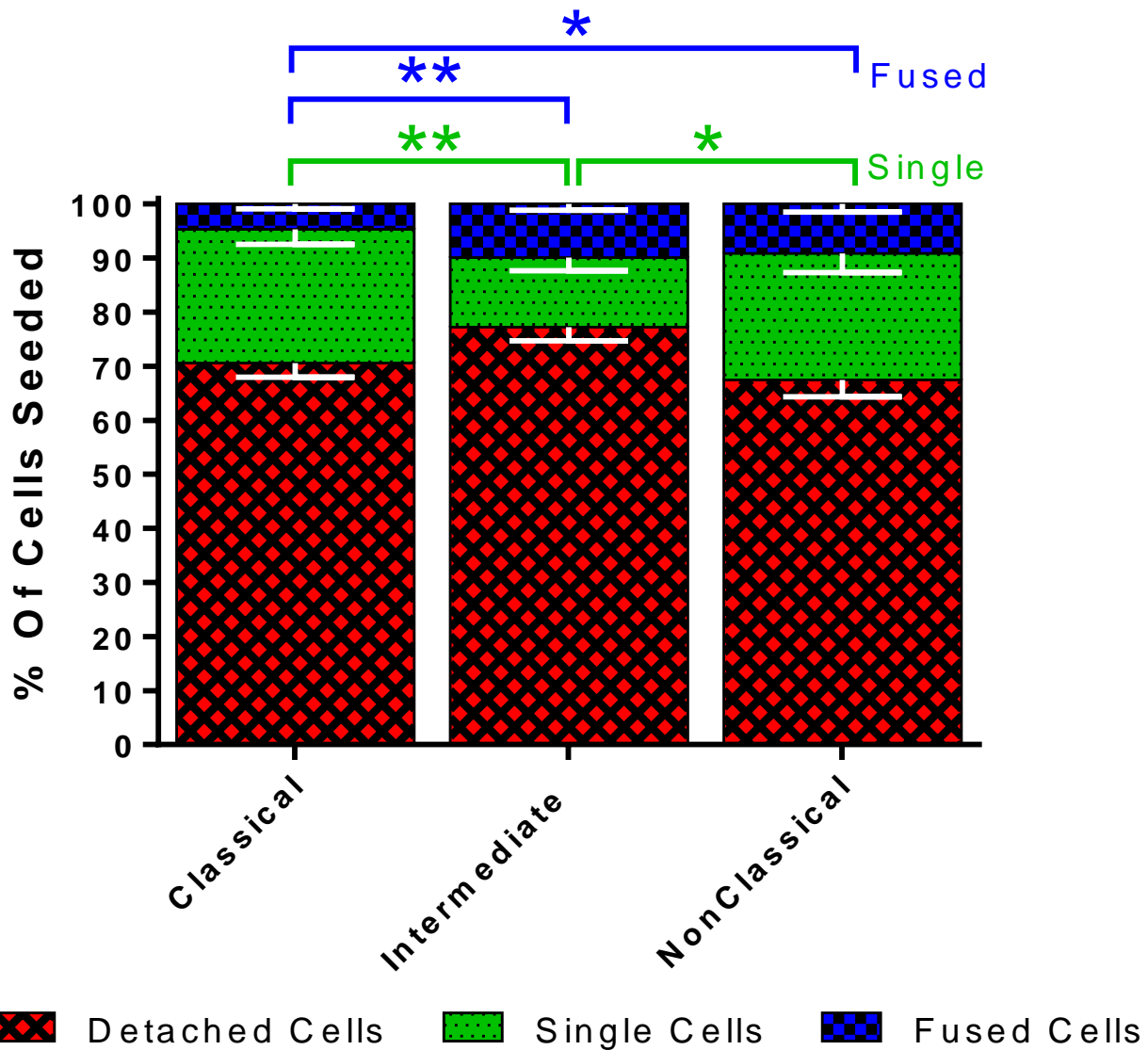


Figure 4.1: Monocyte Subset Contributions During Fusion.

As FACS purified monocytes were ~100% pure it is possible to calculate from the sample population data what the relative contribution of each subset during MGC formation. After 72hrs culture in ConA media the nuclei of the 1.5×10^5 monocytes seeded in every well were recorded as: within a single cell, within an MGC as a fused cell, or as not present (i.e. a dead or detached cell). Bars represent mean \pm SEM, N=25, tested by a Kruskal-Wallis test with Dunn's multiple comparisons tests comparing the means of percentage of each subset to the different nuclear locations.

(12.86%) monocytes. The Dunn's test reported significant differences comparing the single cell population of the Int monocytes to the CI ($P=0.0019$) and NCI ($P=0.0358$) monocytes. Of the fused cells the Int (9.92%; $P=0.0021$) and NCI (9.13%; $P=0.0348$) subsets committed ~ 2 -times more cells to fusion compared to the CI monocytes (4.72%). This is equivalent to every 1 in 21 CI monocytes, 1 in 10 Int and 1 in 11 NCI monocytes committing to fusion.

4.3 SUBSET CONTRIBUTIONS TO FUSION

Monocyte subsets when isolated and cultured in ConA for 72hrs at the same density show very different propensities to fusion (Figure 4.2 and Figure 4.3). Surprisingly, the most abundant subset – the CI monocytes ($79.71 \pm 6.70\%$ of monocytes) - had the lowest values in all 4 fusion parameters: median nuclei per MGC (4.78 nuclei MGC^{-1}), fusion index (19.50%), MGC Area ($2372 \mu\text{m}^2$) and % coverage (11.28%). The fusion index for Int monocytes was significantly higher than the CI ($P < 0.0001$) and notably higher than the NCI ($P=0.0929$). The MGC area for Int monocytes was on average 2.4-fold larger than CI ($P < 0.0001$) and 1.9-fold larger than NCI monocytes ($P=0.0175$). The only significant difference between the CI and NCI subsets in Figure 4.2 was in the % coverage. CI derived MGC showed significantly reduced coverage compared to both NCI ($P=0.0357$) and Int ($P=0.0002$) derived MGC.

Fused nuclei were counted as being in LGC, FBGC or SGC (see Figure 2.7) and populations of each MGC type is shown in Figure 4.4. CI monocytes were significantly more likely to contribute to the formation of LGC (79.51%) compared to NCI (55.33%; $P=0.0122$) and Int monocytes (43.44%; $P < 0.0001$). Compared to the CI monocytes, the Int had a significantly greater propensity to form FBGC ($P=0.0018$), with Int committing 2.14-fold more cells to FBGC than CI. Int (15.49%; $P=0.0005$) and NCI monocytes (15.98%; $P=0.0185$) were ~ 12 -fold more likely to commit to SGC formation compared to CI monocytes (1.34%). Overall it is clear that despite being smaller components of the total monocyte population, the NCI and Int monocytes are able to fuse to a greater extent than CI monocytes. They are also able to form more of the larger FBGC and SGC than the CI monocytes. Whether these differences are due to differential tetraspanin expression or other factors is yet to be revealed.

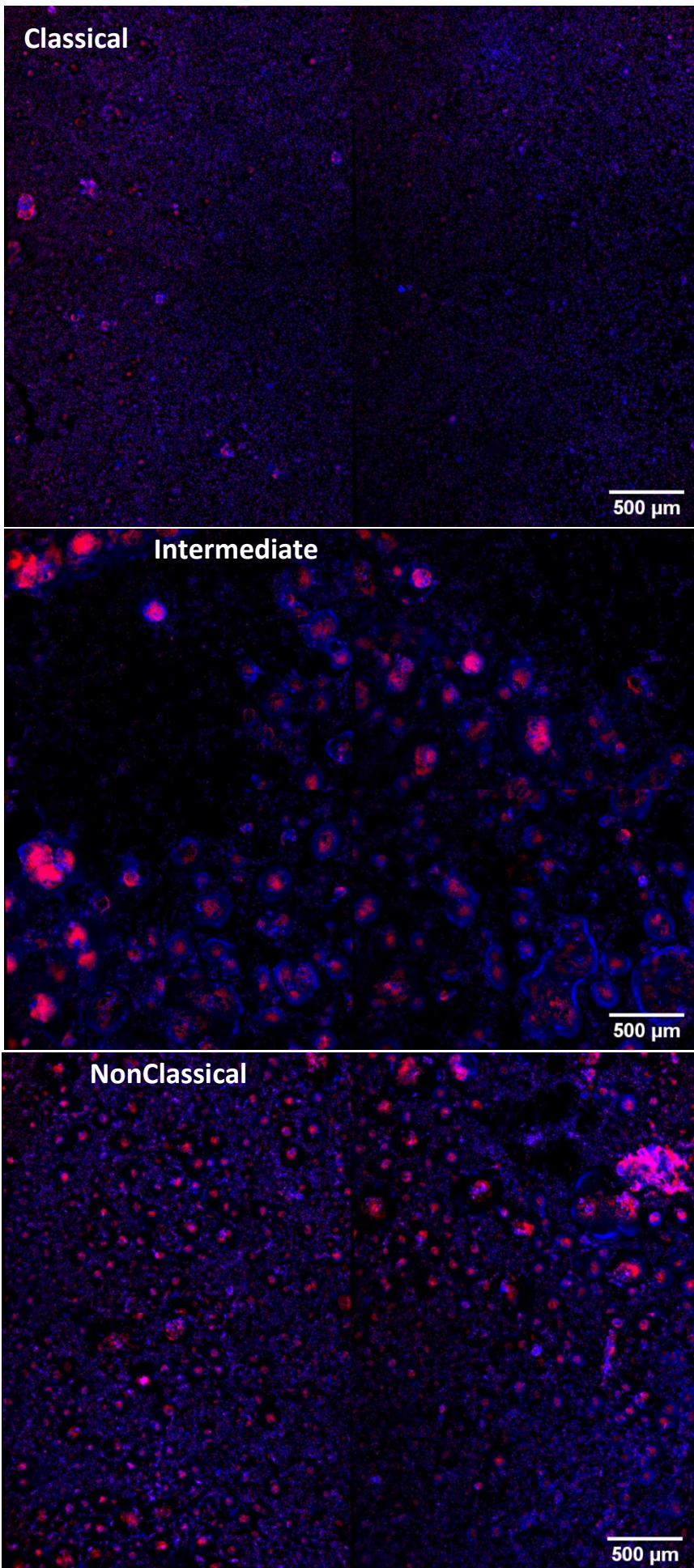


Figure 4.2: Fluorescence Microscopy of Monocyte Subset Derived MGCs.

Three representative montages containing four images taken at 4x magnification of each of the monocyte subsets from one donor after 72hrs ConA treatment. Red = Nuclei, Blue = F-Actin.

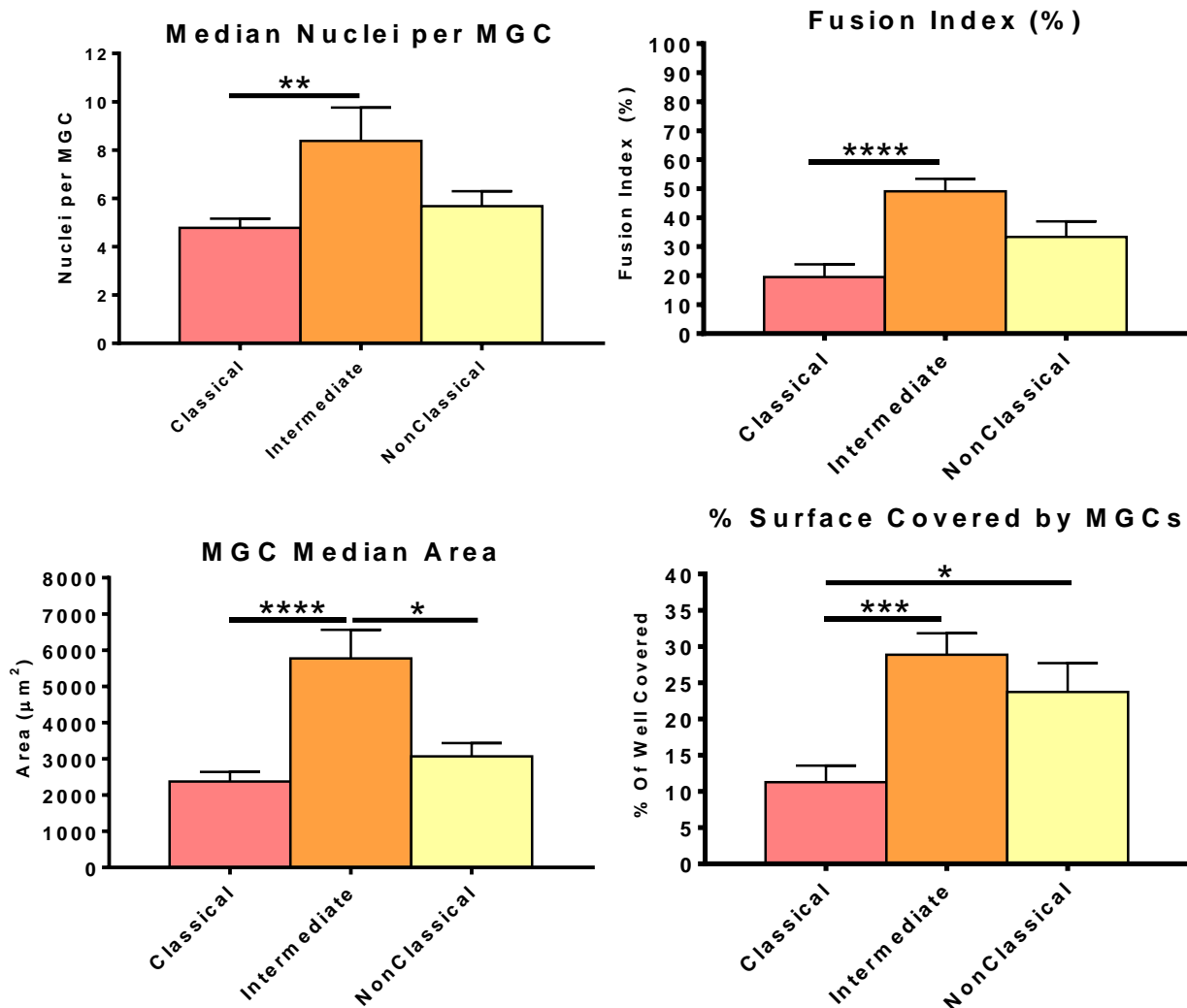


Figure 4.3: Fusion Parameters for Monocyte Subset Fusion.

Monocytes were sorted into subsets by FACS and seeded at an exact density of 1.5×10^5 monocytes well⁻¹ and incubated for 72hrs in $10 \mu\text{gml}^{-1}$ ConA to induce fusion. After fluorescence imaging the four parameters above were generated from the resultant data. Bars represent mean \pm SEM, N=25, tested by a Kruskal-Wallis test with Dunn's multiple comparisons tests comparing the mean of each subset against one another.

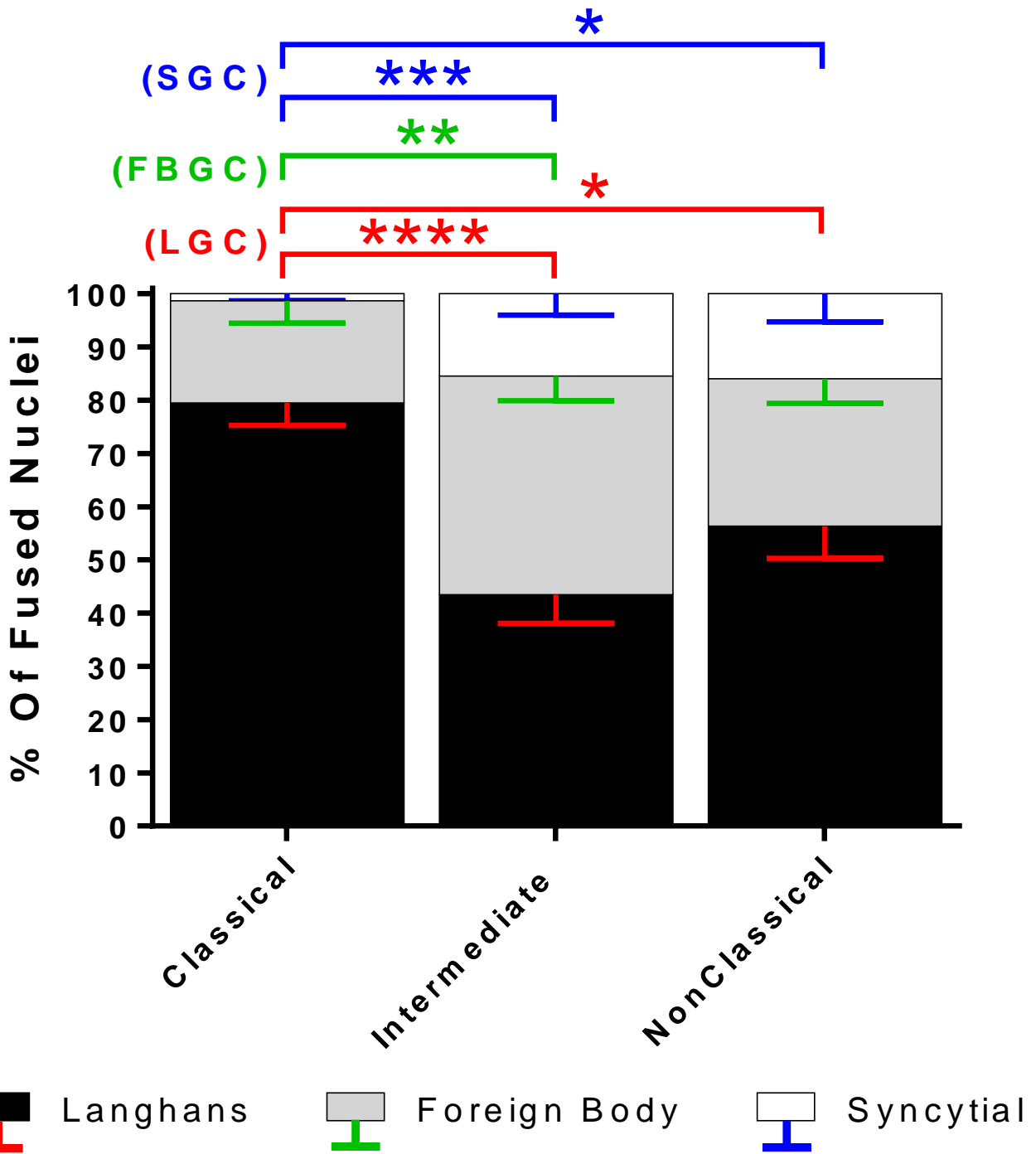


Figure 4.4: MGC Types Generated from FACS Purified Monocyte Subsets. Nuclei inside each type of MGC is shown as a percentage of the total nuclei within fused cells. Bars represent mean \pm SEM, N=25, all parameters were tested with a Kruskal-Wallis test with Dunn's multiple comparisons tests comparing the means of the same MGC type with that of the other subsets.

4.4 FLUORESCENCE-SCANNING ELECTRON MICROSCOPY OF MONOCYTE SUBSETS

It is clear from the fluorescence microscopy images that the three monocyte subsets have different propensities to produce the different MGC types. While fluorescent microscopy is sufficient for designation of MGC type, it does not reveal the high-detail 3-dimensional features of the membrane. Therefore, scanning electron microscopy (SEM) was used to visualise the surface features of the MGC, sometimes in tandem with fluorescence microscopy to show the location of the multiple nuclei.

SEM revealed that larger more developed MGC produce large filamentous networks and possess ruffled membranes (Figure 4.5a-c). Surrounding the central dome that holds the multiple nuclei is a wide, flat bed of filaments which look to be tightly anchoring the MGC to the surface. Figure 4.5c.1-2 shows a section of an MGC where the fixing and dehydration process has caused these fibres to break and lift off that allows us to see how thick these fibres are. The MGC surface is not a smooth structure but appears flaky and ruffled. Two monocytes in Figures 4.5a1-2 and 4.5a5-6 can be seen to be tightly bound by the MGC membrane and perhaps are being pulled into the structure. Figure 4.5c3 shows two NCI monocytes moving towards the MGC, possibly to fuse.

In all subsets, MGC seemed to exist as either flattened dome structures (Figures 4.5a.1, 4.5b.1 & 4.5c.1) or had the appearance of fried-eggs where they would be predominantly flat with a yolk-like bulge in the centre (Figures 4.5b.3, 4.5b.5 & 4.5c.4).

These bulbous structures were more regularly observed in the SEM images of Int and NCI derived MGC but previous fluorescent images did not reveal similar structures. Particularly in the Int and NCI derived MGC, there were examples of very large distorted bulges but such structures were not observed in the CI-derived MGC. The CI MGC typically consisted of smaller MGC (Figure 4.5a.3-4) clustered together with fewer large MGC. The Int MGC were dominated by vast MGC which required very low magnifications for SEM. The NCI MGC were the most varied in MGC size but many of the images showed damage from the fixing and dehydrating steps.

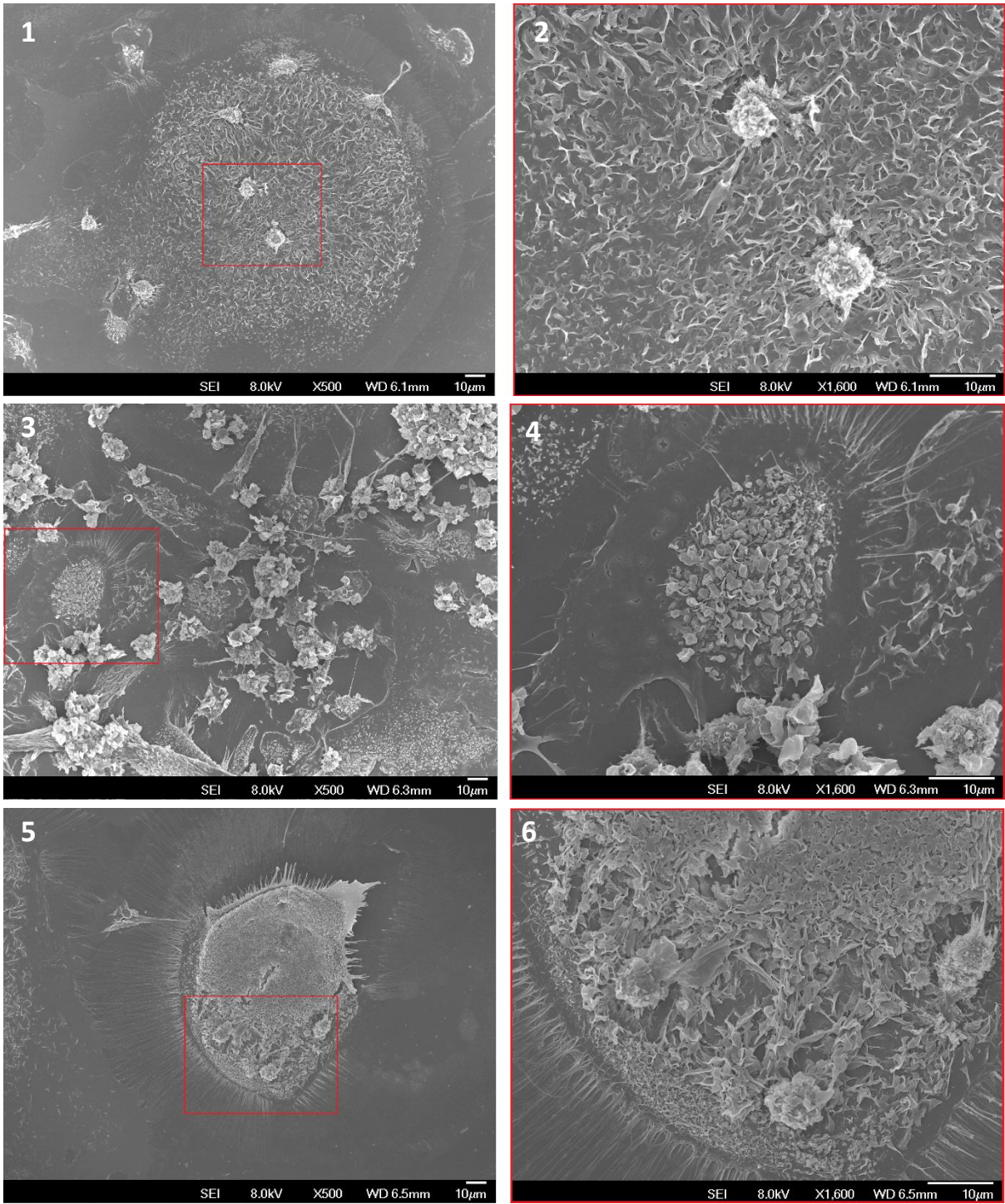


Figure 4.5a: SEM of Classical Monocyte Derived MGCs.

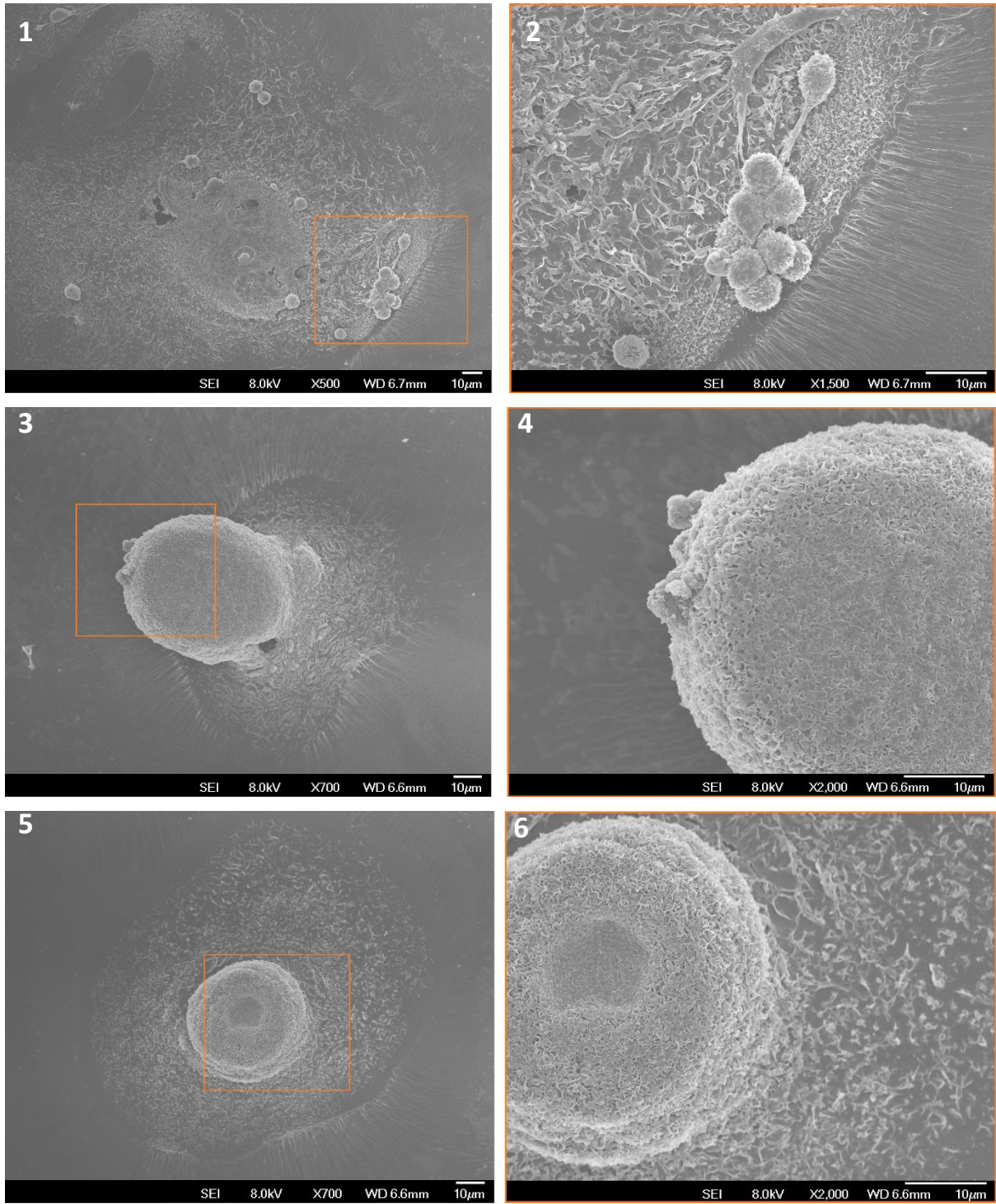


Figure 4.5b: SEM of Intermediate Monocyte Derived MGCs.

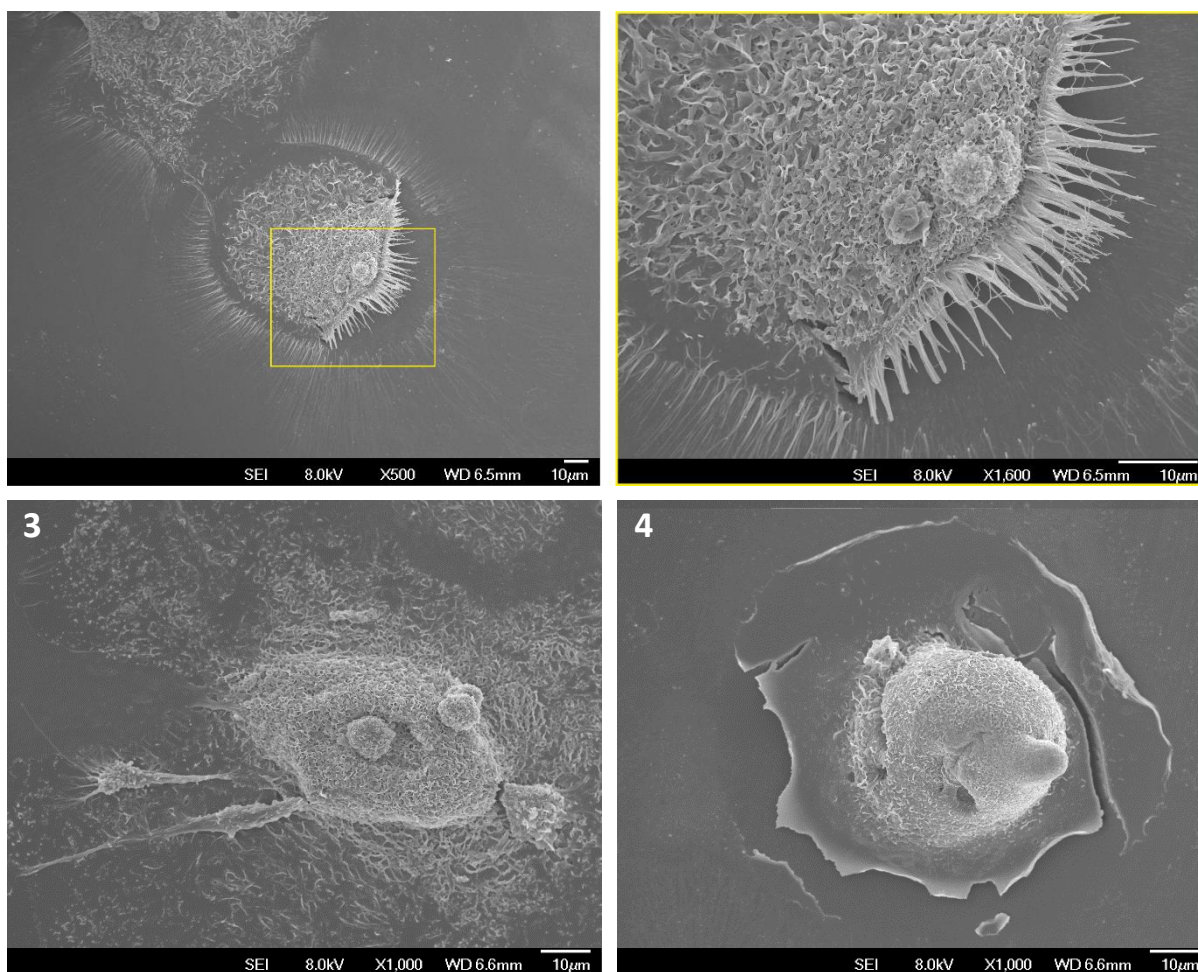


Figure 4.5c: SEM of NonClassical Monocyte Derived MGCs.

Figure 4.5a-c show a collection of scanning Electron Microscopy images of subset derived MGCs. Low magnification Images are shown on the left and the coloured box inside show the high-magnification image on the right. The cells of these images were purified with FACS and allowed to fuse for 72hrs before being sent to the SEM unit for fixing and imaging. Electron voltages, magnification, working distance (WD) and scale bars shown at the foot of each image.

Figure 4.6.a-c show three example images from tandem fluorescence-scanning electron microscopy (Flu-SEM). They were each conducted on MGC derived from each of the subsets with the nuclear images overlaid. Figure 4.6.a&c possess ring-like nuclear arrangements typical of LGC while the Int MGC shows a tight nuclear dome in the centre and a cluster of nuclei in the centre typical of FBGC.

4.5 FUSION KINETICS OF MONOCYTE SUBSETS

The subsets were investigated at different time points to analyse the progression of fusion over time and to provide samples for ELISA analysis of the cytokine signals (see Chapter 5).

In less than 24hrs of culture in ConA media, all subsets were able to produce MGC containing ≥ 3 nuclei (Figure 4.7). By 24hrs the Int subset had covered 3.2-fold more of the well surface (30.52%) in MGC than the CI (9.54%) and 7.7-fold more than the NCI subsets (3.96%). At 24hrs the NCI subset produces slightly lower values than the CI subset in all fusion parameters shown in Figure 4.7 but by 72hrs the NCI increase in fusion beyond the CI.

MGC from Int and CI subsets appear to reach a steady-state in the fusion parameters from 48hrs onwards whereas the NCI continue to increase in all parameters. Between 24-48hrs the Int had a significant increase in MGC area ($P=0.0005$, Figure 4.7) which coincided with a 12.64% increase in the FBGC population (Figure 4.9). Between the same two time points; NCI had a significant increase in fusion index ($P=0.0450$, Figure 4.7) which matched with the +3.62% increase in fused cells and -6.80% decrease in single cells (Figure 4.8). As with the total monocytes, the median nuclei per MGC did not change significantly over the 72hr period for any of the subsets.

By 24hrs there was a significant difference between the number of fused nuclei between Int (14.32%) and NCI (3.21%; $P=0.0194$) but not with the CI (5.74%; $P=0.1555$).

By 48hrs the Int have the lowest number of unfused single cells (8.60%) compared to CI (26.18%, $P=0.0126$) and NCI (21.50%, $P=0.0175$) and in turn the highest FI (52.87%). By 72hrs the difference in remaining single cells became even greater (Int vs CI $P=0.0021$; vs NCI $P=0.0030$). At 24hrs the number of detached cells appears

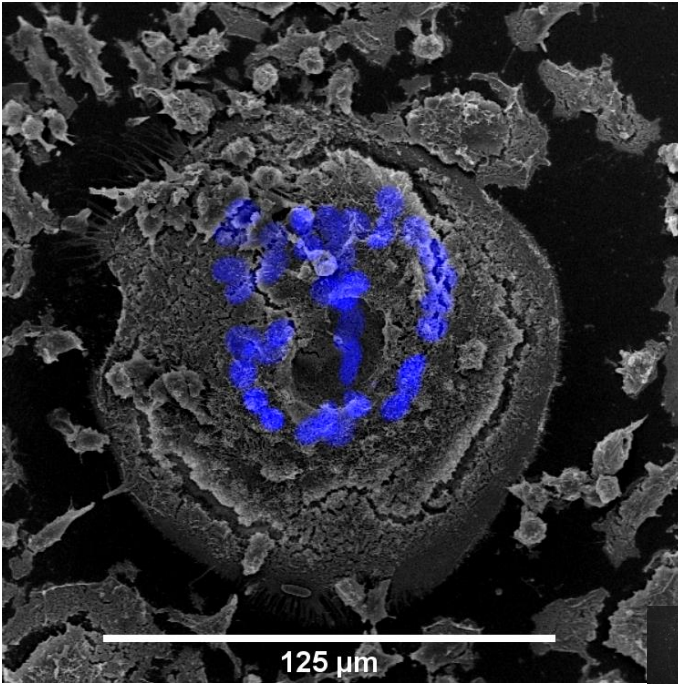
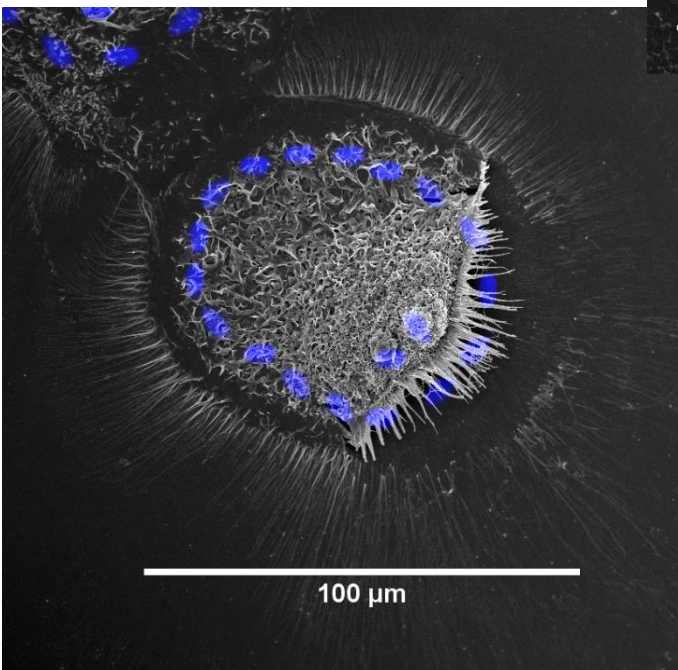
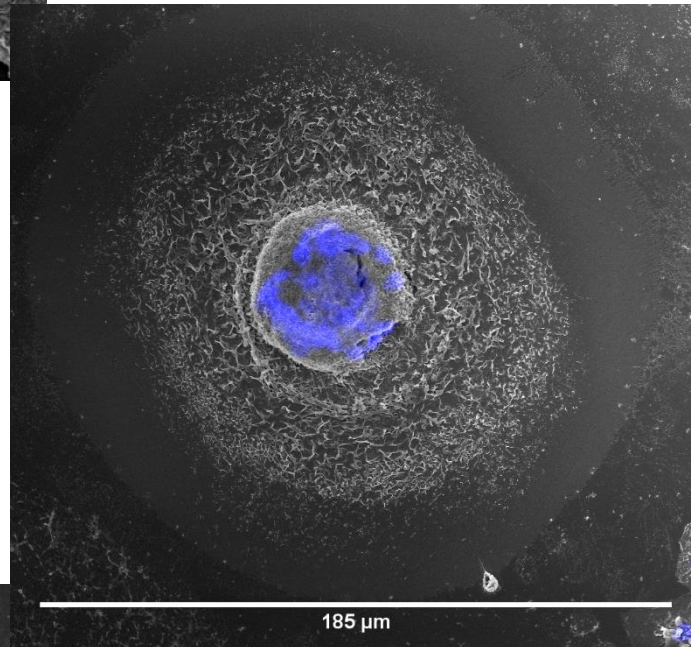


Figure 4.6: Flu-SEM Images of Nuclear Arrangement Within MGCs.

Utilising the same protocol as Figure 4.5, subsets MGCs were generated and prior to SEM fixing and imaging the cells were stained with Hoechst and the well raster scanned so that the MGCs imaged in SEM could be located and the nuclear channel overlaid onto the image. Above: Classical, Right: Intermediate, Below: Nonclassical derived MGCs with scale bars and nuclei shown in blue.



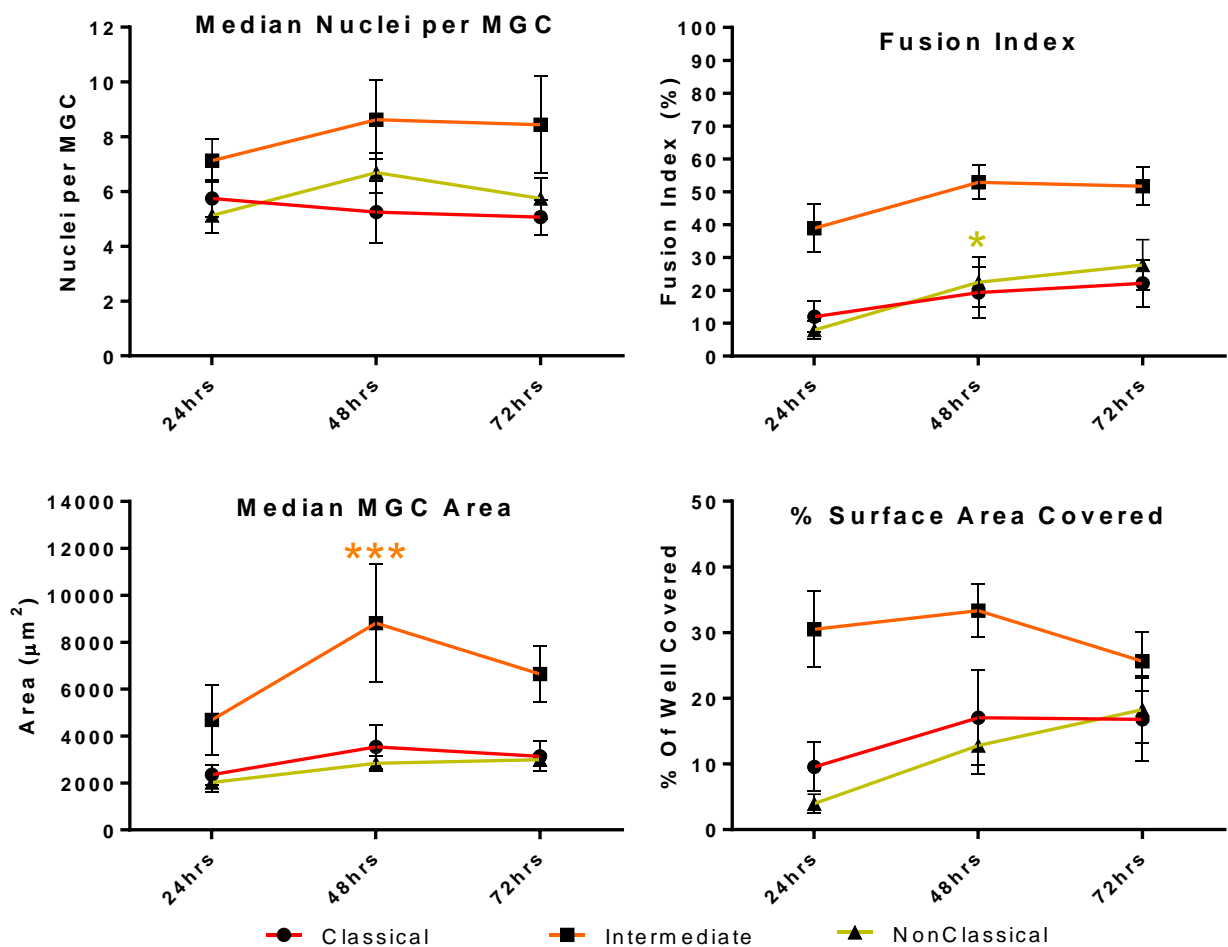


Figure 4.7: Fusion Kinetics of Monocyte Subsets.

FACS purified monocytes were seeded at 1.5×10^5 monocytes well⁻¹ and incubated for 24hrs, 48hrs and 72hrs in $10 \mu\text{gml}^{-1}$ ConA to induce fusion. **Red lines with circles:** classical, **orange lines with squares:** intermediate and **yellow lines with triangles;** nonclassical monocyte derived MGCs. Each point represents mean \pm SEM, N=8, all parameters were tested with a two-way ANOVA with a Tukey's multiple comparisons tests comparing each subset time-point to the previous one (e.g. MGC Median Area: intermediate 48hrs vs intermediate 24hrs shows "****" ($P < 0.0005$) significance). Comparison of monocyte subsets to each other is covered at the end-point, in Figure 4.3.

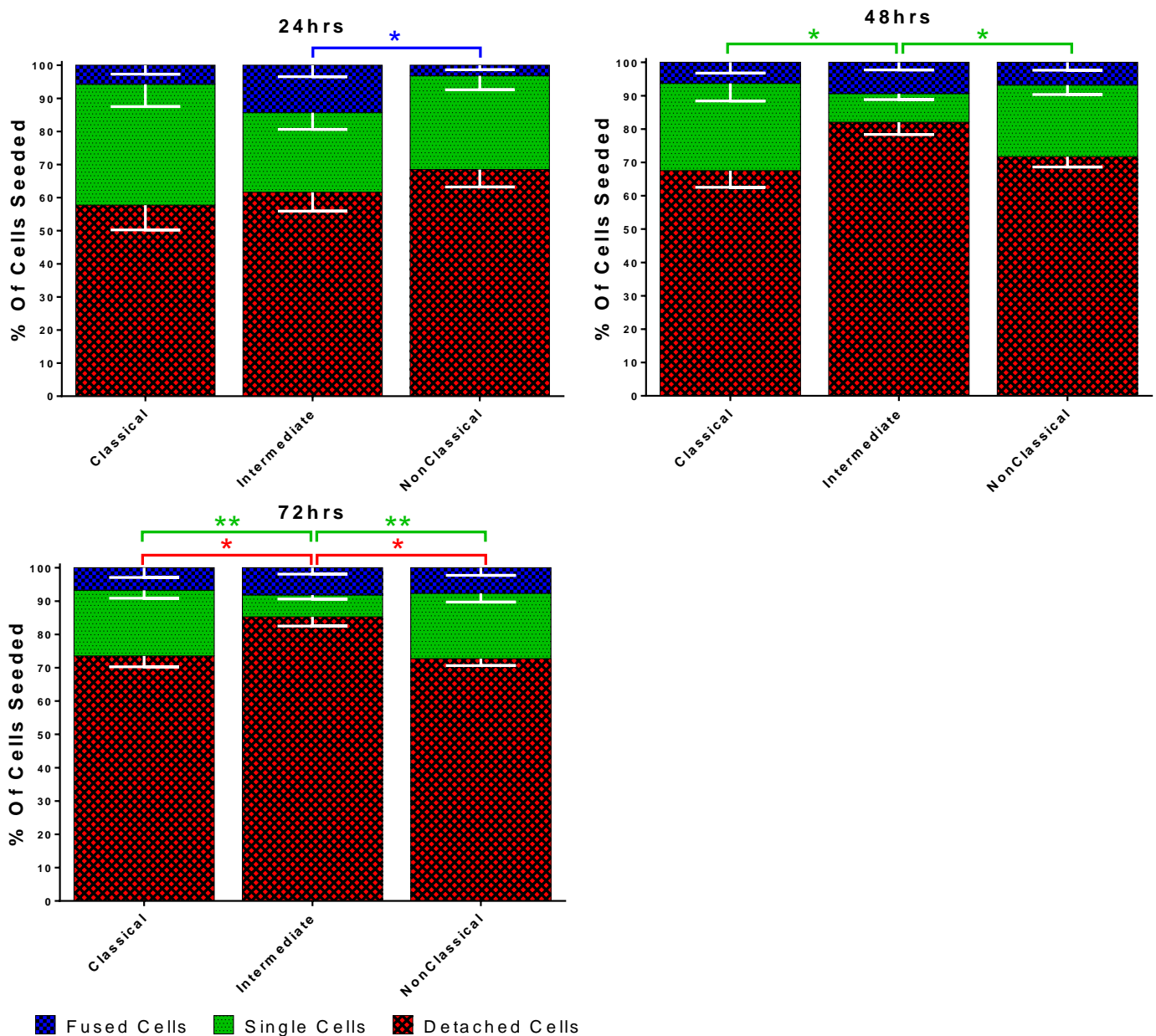


Figure 4.8: Subset Fusion Kinetics - Nuclear State Analysis.

At each of the time-points in the subset fusion kinetics experiment the 'state' of each nuclei was calculated and analysed above. Bars represent mean±SEM, N=8, all time-points were tested with a Kruskal-Wallis test with Dunn's multiple comparisons tests comparing the means of the same nuclei 'state' within the same time-point against the other subset means. e.g. 24hrs intermediate fused nuclei vs 24hrs nonclassical fused nuclei. Red stars: detached cells, green stars: single cells and blue stars: fused cells.

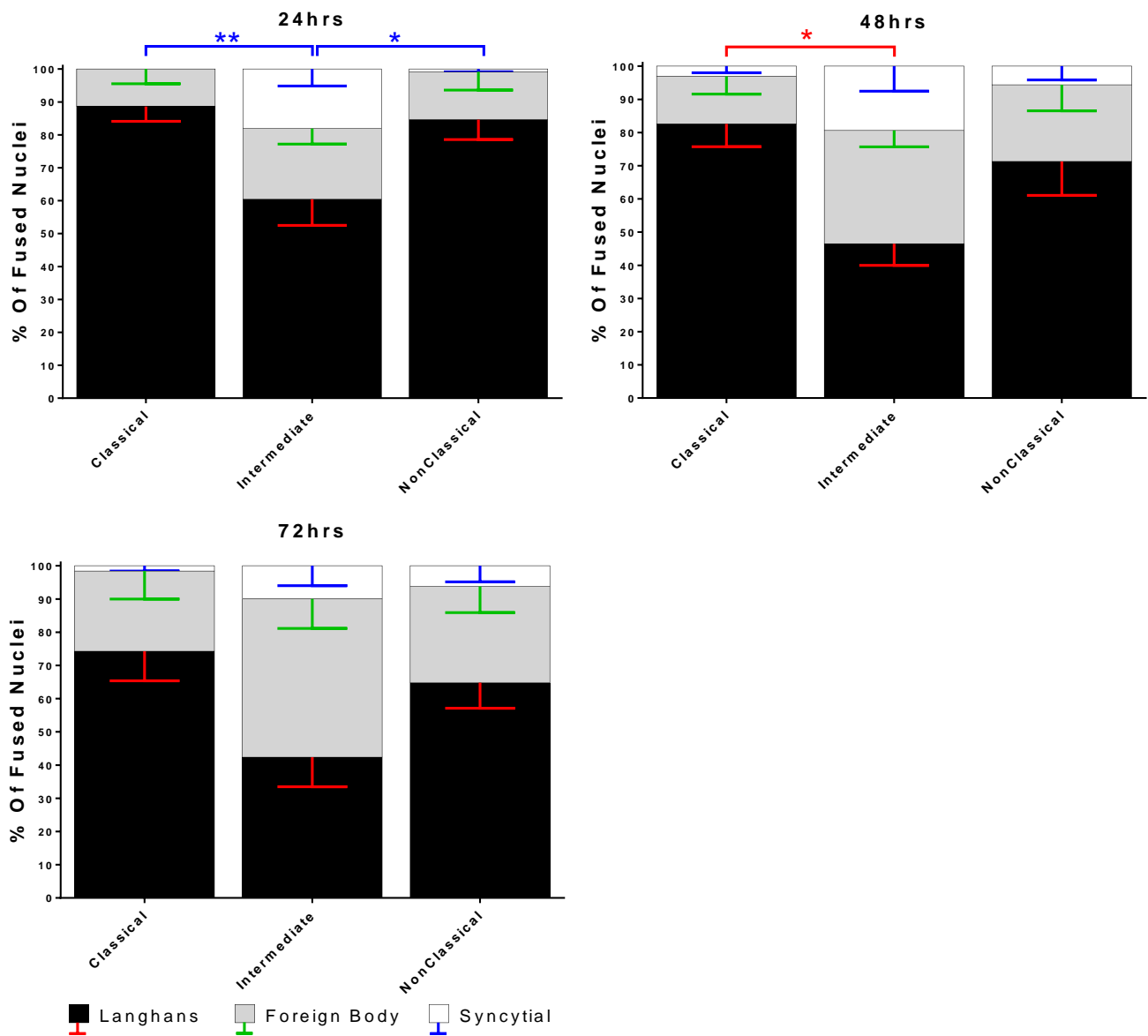


Figure 4.9: Subset Fusion Kinetics – MGC Type Analysis.

At each of the time-points in the subset fusion kinetics experiment the nuclei counted inside each MGC was tallied into one of three observed MGC types and presented as a percentage of the fused nuclei counted. Bars represent mean±SEM, N=8, all time-points were tested with a Kruskal-Wallis test with Dunn’s multiple comparisons tests comparing the means of the same MGC type within the same time-point against the other subset means. e.g. 24hrs classical LGC vs 24hrs intermediate LGC. Red stars: LGC nuclei, green stars: FBGC nuclei and blue stars: SGC nuclei.

almost the same between the three subsets. However, at 48hrs the difference between the detached populations of CI and Int monocytes is almost significant ($P=0.0777$). After 72hrs the Int has a significantly higher number of detached cells (85.27%) compared to CI (73.52%, $P=0.0486$) and Int (72.70%, $P=0.0296$) groups.

Confusingly, the fused population of the Int subset decreases from 24-72hrs but increases in both the CI and NCI subsets (Figure 4.7: CI: +1.01%, Int: -6.15% & NCI: +1.01%). In Figure 4.9 the distributions of the different MGC types are significantly different within 24hrs. Only the Int subset was able to produce significantly more SGC than CI ($P=0.0034$) and NCI ($P=0.0145$) subsets. Not until 48hrs did all three subsets possess all three MGC types to some degree. At 48hrs the Int monocytes had significantly less LGC (46.50%; $P=0.0262$) than the CI monocytes (82.61%). By 72hrs the population distributions in Figures 4.8 and 4.9 were comparable with Figures 4.3 and 4.4 respectively.

4.6 ANALYSIS OF CYTOKINE PRODUCTION BY MONOCYTE SUBSETS UNDERGOING FUSION

Fusion competent monocytes secrete chemoattractants and cytokines to augment fusion and differentiation (see 1.3.1-1.3.3). As the subsets showed different propensities to fusion it is possible that they secrete a different array of cytokines in response to gaining fusion-competence. The supernatants from the fusion kinetics samples were collected at 24, 48 and 72hrs for analysis of the cytokines produced by the monocyte subsets during fusion.

Figure 4.10a shows the unstimulated vs ConA stimulated comparison at each time point to ascertain which cytokines were upregulated in fusogenic conditions. Figure 4.10b compares the ConA-stimulated conditions between different time points within the same subset to show how cytokine secretion changed over time. Figure 4.10c compares the levels of each cytokine between the three subsets at the same time points to ascertain if the differences in fusion parameters shown in Figures 4.7, 4.8 and 4.9 were directly correlated with the cytokine signals.

CCL2, IL-6, TNF α , CCL3, IL-1 β , GM-CSF and IL-1 α were the most highly secreted cytokines (>1000pg ml⁻¹). IFN γ , IL-10, IL-13, IL-4, IL-17A, IL-3 and VEGF were all

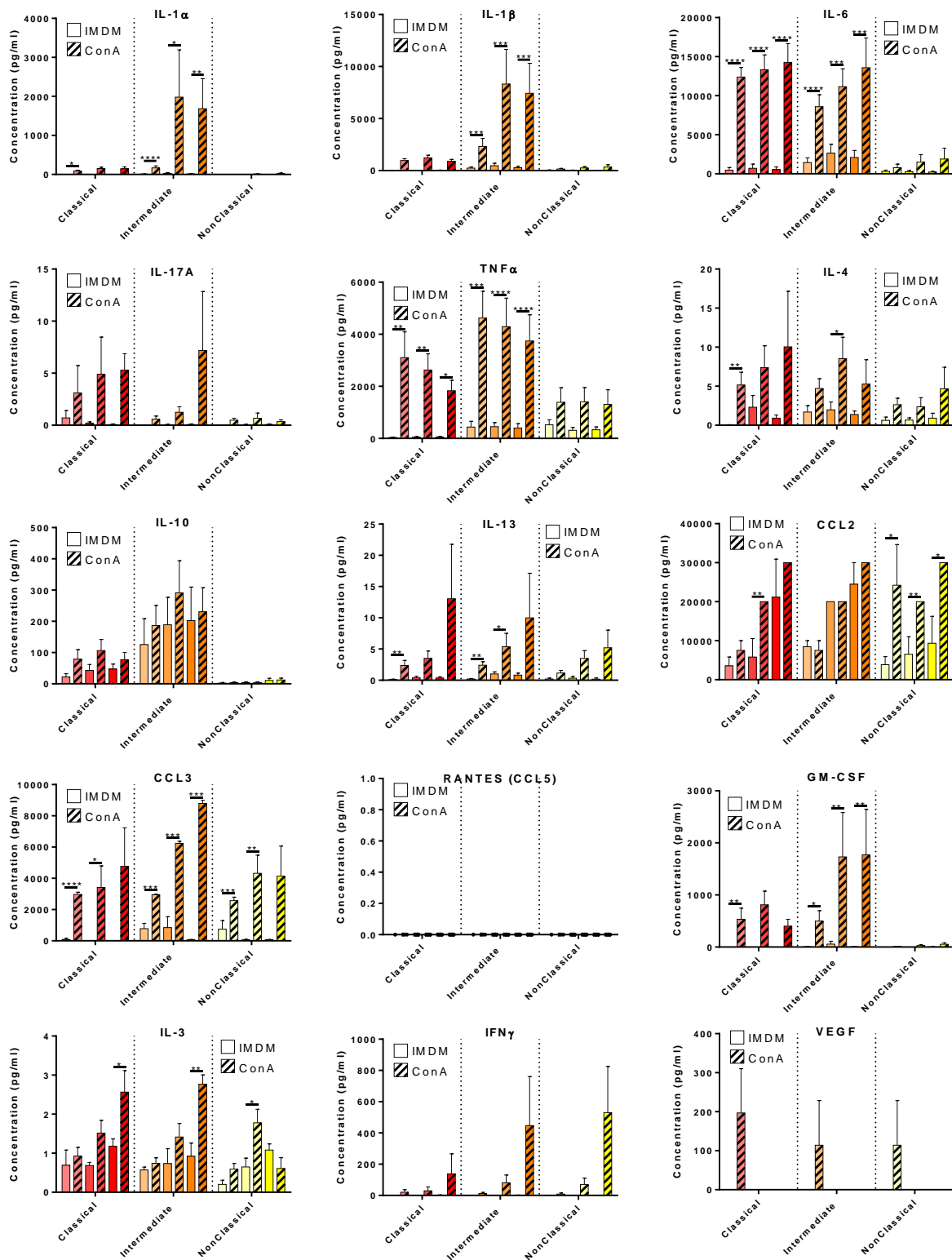


Figure 4.10a: Fusion Cytokines - Comparison of Subsets Cultured in -ConA vs +ConA.

Supernatants from the subset kinetics cultures were collected and analysed by ELISA for 15 targets of interest. Clear bars: -ConA, striped bars: +ConA; with each time point (24, 48, 72hrs) presented in adjacent pairs. Bars represent mean \pm SEM, N=8, all tested with a two-way ANOVA with a Sidak's multiple comparison test comparing the means of -ConA vs +ConA of the same time point within each subset.

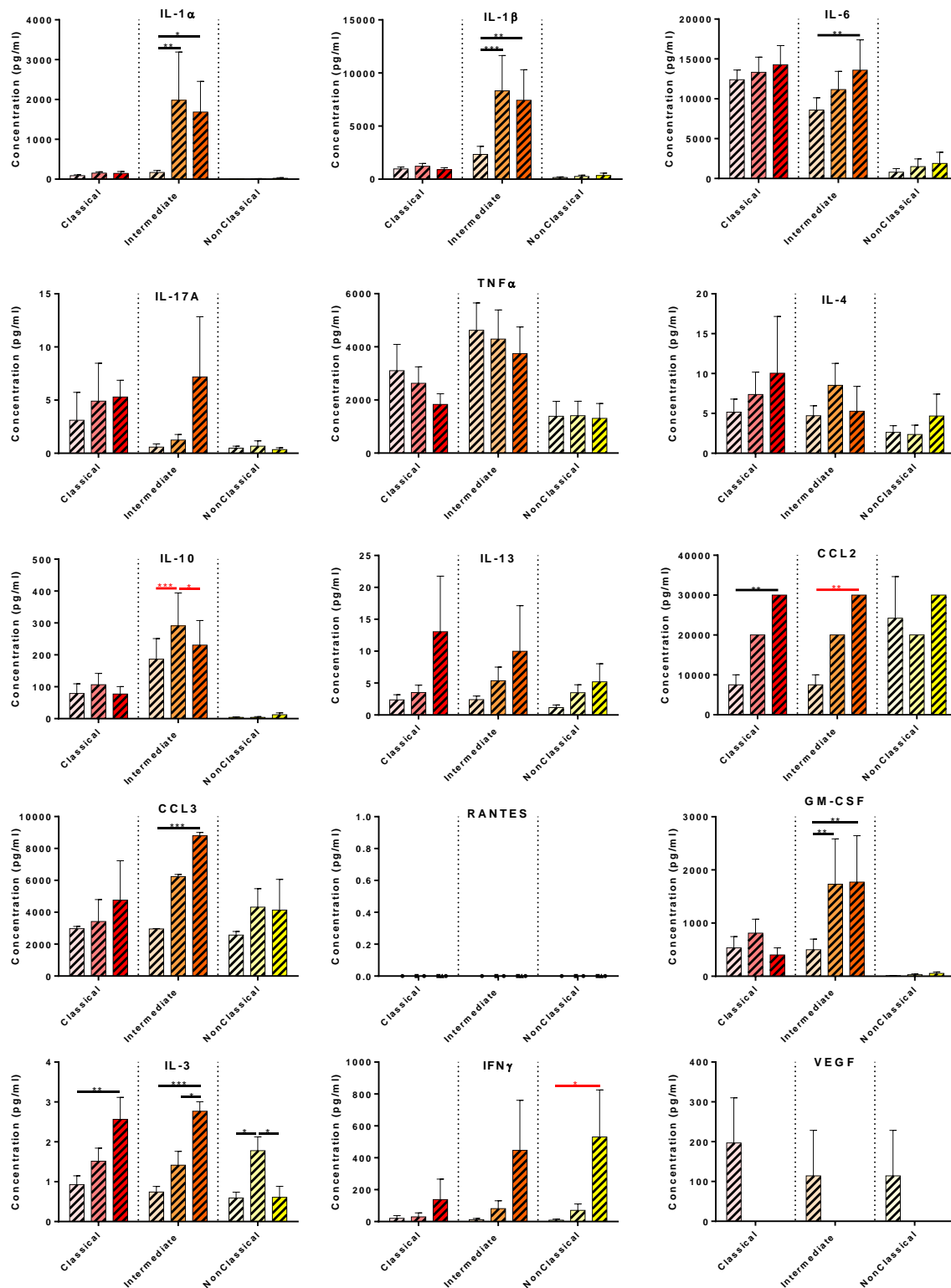


Figure 4.10b: Fusion Cytokines - Comparison of Different Time Points for Subsets Cultured in ConA.

Only the +ConA samples from Figure 4.10a are shown above; arranged in 24, 48 and 72hrs for each subset. Bars represent mean \pm SEM, N=8, all tested with a two-way ANOVA with a Tukey's multiple comparison test comparing the means of the different time points within each subset. Red bars/stars are for samples that did not show any significant differences between -ConA and +ConA in Figure 4.10a.

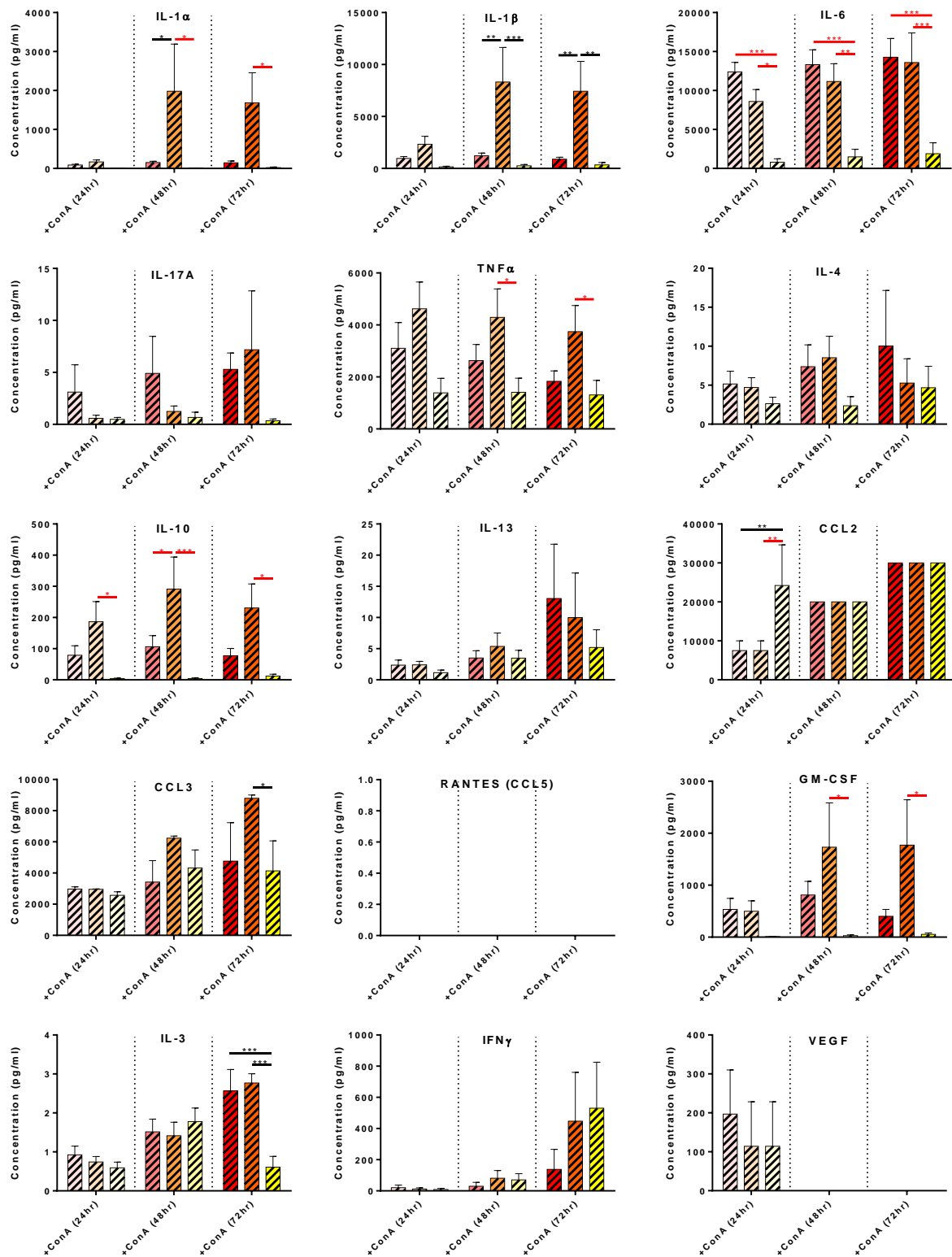


Figure 4.10c: Fusion Cytokines – Comparison of Subsets Cultured in ConA at Different Time Points.

Only the +ConA samples from Figure 4.10a are shown above; arranged into subsets at the same time point. Bars represent mean \pm SEM, N=8, all tested with a two-way ANOVA and Tukey's multiple comparison test comparing the means of each subset against one another at the same time point. Red bars/stars are for samples that did not show any significant differences between -ConA and +ConA in Figure 4.10a.

<1000pg ml⁻¹ and RANTES was undetectable. There was no significant difference between the ConA and unstimulated time points for IL-17A, IL-10, RANTES, IFN γ and VEGF. The NCI subset was particularly low in both conditions for IL-1 α , IL-1 β , IL-6, TNF α , IL-4, IL-13 and GM-CSF at all time points.

The pro-inflammatory cytokines IL-1 α and IL-1 β were significantly higher in the ConA Int time points (Figure 4.10a) and peaked in secretion at 48hrs (Figure 10b). Within 24hrs IL-6 was ~27-times higher in Cl+ConA cells than the no ConA equivalent ($P < 0.0001$) and ~6-times higher in Int+ConA ($P < 0.0001$). The Int+ConA increased significantly ($P = 0.0402$) between 24-72hrs and by the last time point both Cl+ConA (14,269pg ml⁻¹; $P = 0.0001$) and Int+ConA (13,586pg ml⁻¹; $P = 0.0003$) were significantly higher than NCI+ConA (1,888pg ml⁻¹). TNF α was another fast responding pro-inflammatory cytokine; at 24hrs the Cl+ConA and Int+ConA were 85 and 11-times higher (Cl: 3105pg ml⁻¹; $P = 0.0044$. Int: 4620pg ml⁻¹; $P = 0.0001$) than the no ConA equivalent (Cl: 36pg ml⁻¹. Int: 438pg ml⁻¹). TNF α decreased over each time point in the Cl+ConA and Int+ConA samples but remained stable from 24-72hrs in NCI+ConA. IL-17A is relatively low compared to the other pro-inflammatory cytokines (no sample exceeded 6.04pg ml⁻¹).

The concentrations of the anti-inflammatory cytokines (IL-4, IL-10 and IL-13) were all relatively low compared to the pro-inflammatory cytokines. IL-10 was the highest to be secreted but showed no significant difference between the ConA and no ConA conditions at any time point. IL-4 and IL-13 was significantly higher in ConA containing Cl samples by 24hrs ($P = 0.0019$ & $P = 0.0025$ respectively). Both cytokines generally increased over the time points but a significant difference between the subsets was not observed.

CCL2 was highly secreted in both no ConA and ConA conditions for Cl and Int monocytes. NCI+ConA samples were significantly higher in CCL2 at all three time points compared to the no ConA equivalents (24hrs: $P = 0.0201$; 48hrs: $P = 0.0066$; 72hrs: $P = 0.0416$). CCL2 seemingly increased over time from 24-72hrs for all ConA treated subsets, however, the samples were saturated beyond the detection limit of the ELISA beads (0.632-10004pg ml⁻¹) from 48hrs onwards. CCL3 is rapidly secreted by all three subsets containing ConA and remain significantly higher than the no ConA

samples at every time point. Only the Int+ConA increased significantly across all the time points (24-72hrs: $P=0.0007$; Figure 4.10b). By 72hrs the Int+ConA (3744pg ml^{-1}) supernatant contained a far greater concentration of CCL3 than NCI+ConA (1305pg ml^{-1} ; $P=0.0291$) and CI+ConA (1831pg ml^{-1} ; $P=0.0645$). RANTES was not detected in any condition for any donor within the $366\text{-}9961\text{pg ml}^{-1}$ range.

Within 24hrs the CI and Int monocytes cultured with ConA contained significantly higher GM-CSF than the no ConA equivalents (CI: 534pg ml^{-1} ; $P=0.0085$; Int: 500pg ml^{-1} ; $P=0.0158$). The CI+ConA GM-CSF concentration does not change significantly after the 24hrs time point. However, the Int+ConA increase GM-CSF concentration 3.5-fold between 24-48hrs where it plateaus until 72hrs at $1731\text{-}1770\text{pg ml}^{-1}$ ($P=0.0038$). In contrast, IFN γ was a more delayed cytokine response and increased across the time points peaking at 72hrs. The concentration of IFN γ increased rapidly between 48-72hrs in the ConA containing Int and NCI samples and by 72hrs were 3.3- and 3.9-fold higher than the CI+ConA respectfully. IL-3 was secreted in very low concentrations compared to other cytokines (Figure 4.10a) but significant increases were observed across all the time points (Figure 4.10b) for ConA cultured CI (24-72hrs: $P=0.0028$) and Int (24-72hrs: $P=0.0004$) samples. VEGF was only detected in 50% of the ConA containing samples at 24hrs and subsequent time points did not test positive for any VEGF presence. The VEGF detection range ($393\text{-}9999\text{pg ml}^{-1}$) suggests that the assay is relatively insensitive to low concentrations compared to other cytokines.

4.7 MONOCYTE SUBSETS CULTURED WITH ANTI-TETRASPANIN ANTIBODIES

It is possible that the high-fusing Int and NCI monocytes express a particular pattern of tetraspanins compared to CI monocytes. In Chapter 3 the presence of other leukocytes in the isolated cells makes it difficult to ascertain whether the anti-tetraspanin antibodies were directly targeting the monocytes or the contaminating cells to affect fusion behaviour. Anti-tetraspanin antibodies have been tested on total monocytes but here we observe their effect on purified individual subsets. From Figure 4.11a-c alone it is clear that the purified monocyte subsets not only fuse differently to total monocytes but also react to anti-tetraspanin antibodies differently. The CI and NCI subsets remain largely unaffected by most of the antibody treatments and the

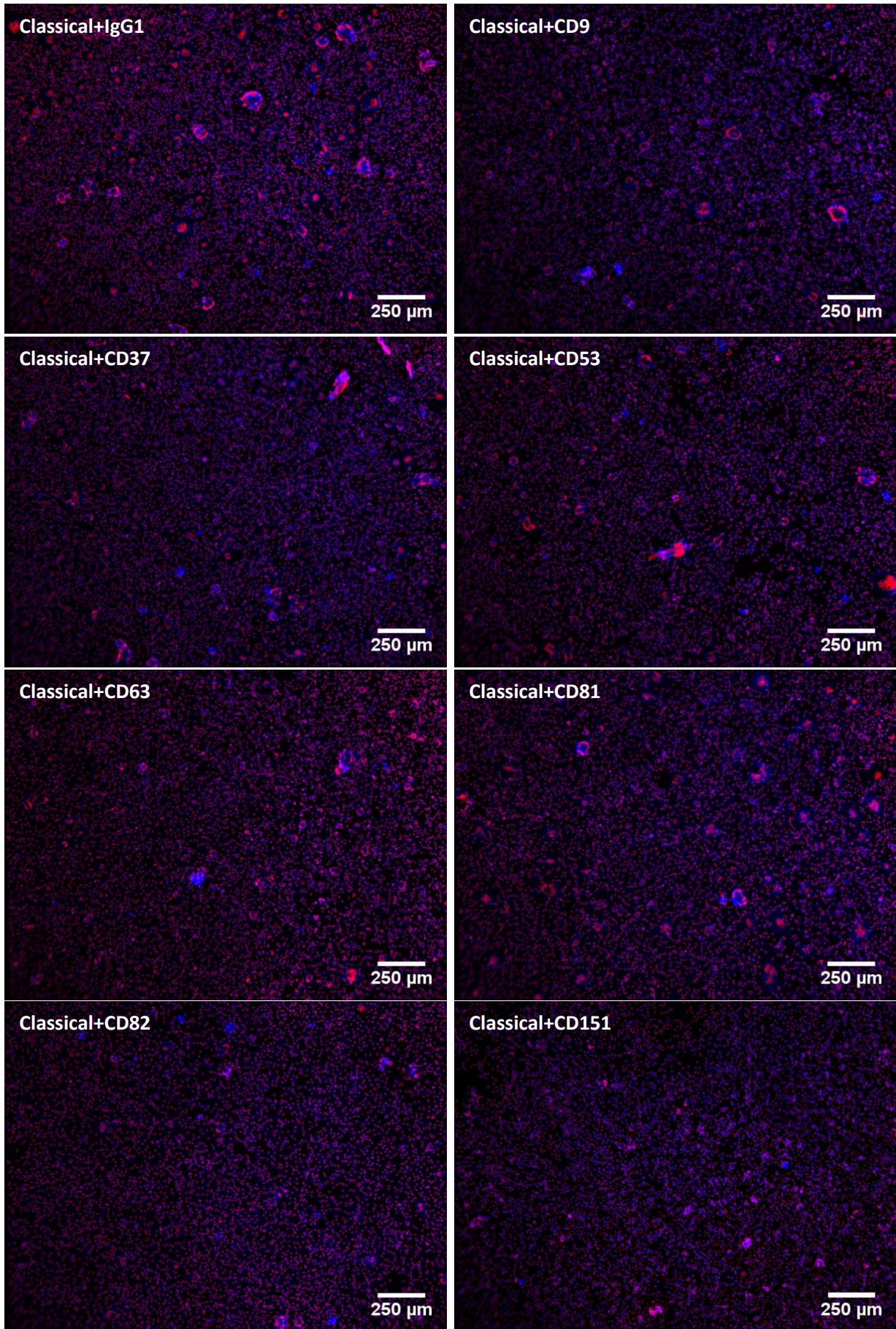


Figure 4.11a: Fluorescence Microscopy of Classical Monocyte Derived MGCs Cultured with Anti-Tetraspanin Antibodies.

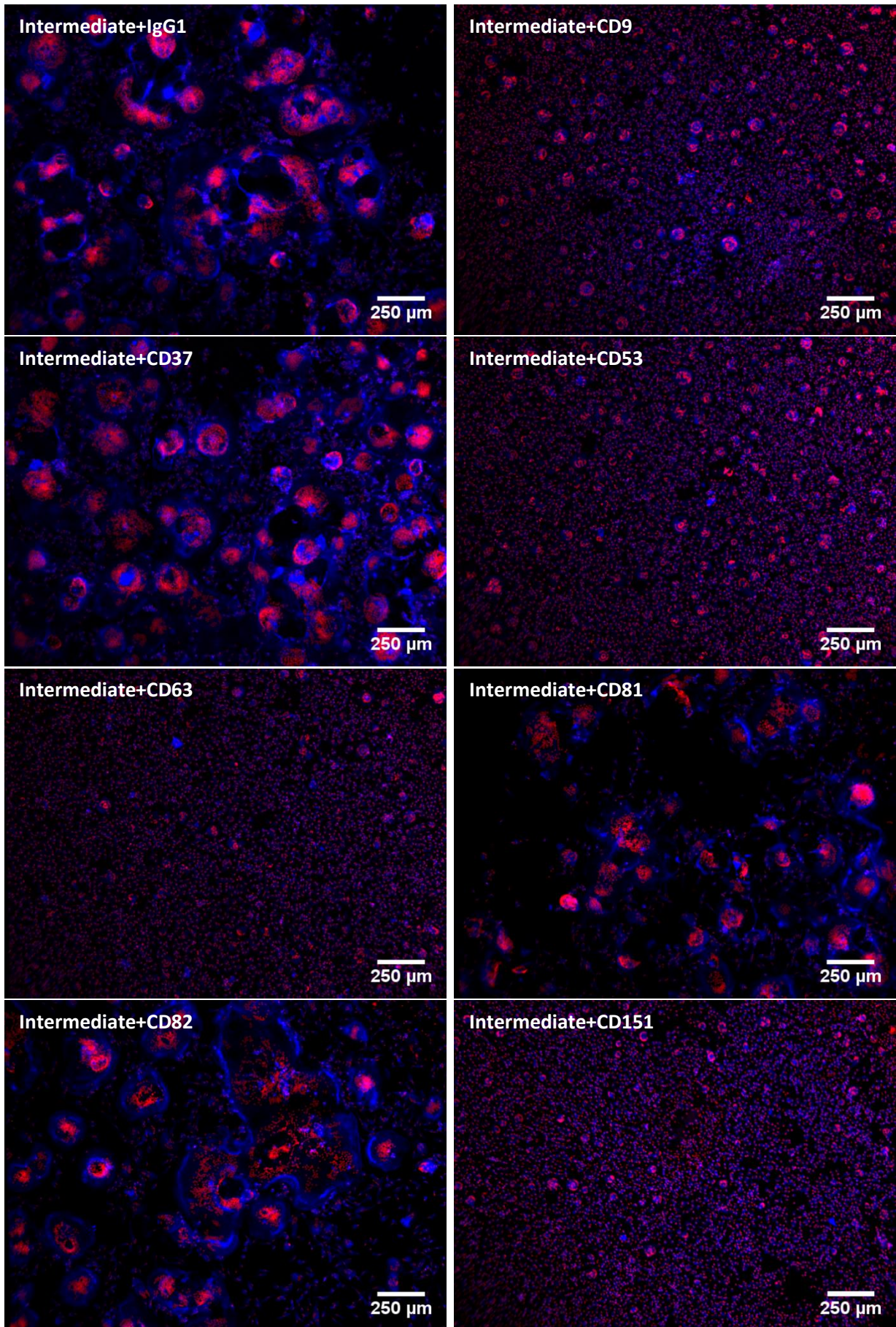


Figure 4.11b: Fluorescence Microscopy of Intermediate Monocyte Derived MGCs Cultured with Anti- Tetraspanin Antibodies.

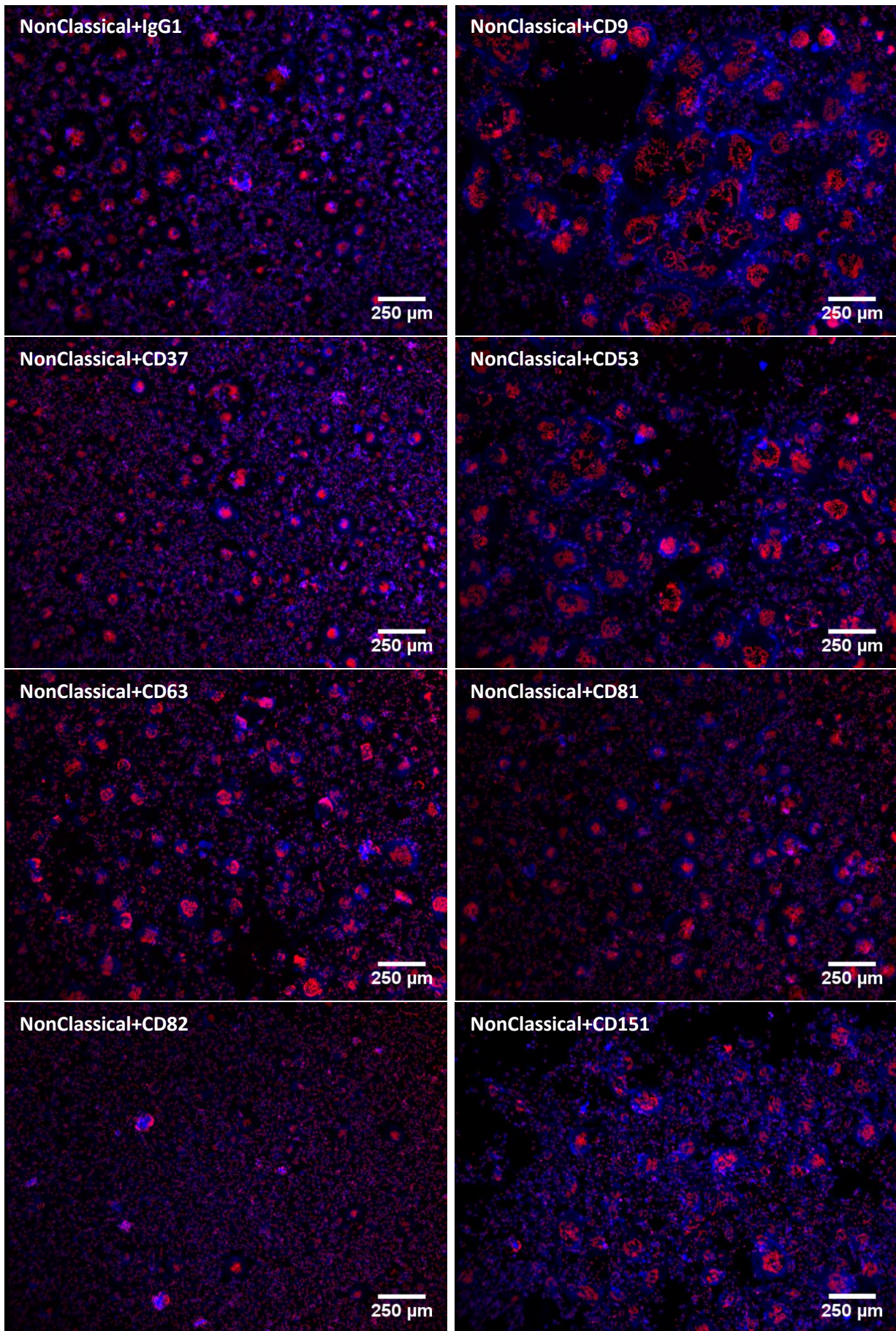


Figure 4.11c: Fluorescence Microscopy of NonClassical Monocyte Derived MGCs Cultured with Anti-Tetraspanins Antibodies.

Figure 4.11a-c: Fluorescence Microscopy of Monocyte Subset Derived MGCs Cultured with Anti-Tetraspanin Antibodies.

Figures 4.11a-c each show a representative image taken at 4x magnification of each of the monocyte subsets from the same donor after 72hrs ConA + IgG1 or an anti-tetraspanin antibody treatment. Red = Nuclei, Blue = F-Actin.

majority of the MGC produced are LGC. The Int monocytes produce larger and more regular MGC than the CI but anti-CD9, anti-CD53, anti-CD63 and anti-CD151 seem to inhibit the fusion down to a CI-like level.

Figure 4.12 summarises the data collected from 3-8 donors (8 donors tested with IgG1, anti-CD9 & anti-CD151, 4 donors with anti-CD37 & anti-CD63, 3 donors with anti-CD53, anti-CD81 & anti-CD82). While the CI monocytes remain largely unchanged in their fusion parameters by the addition of anti-tetraspanin antibodies, the Int monocytes reacted significantly to the addition of certain anti-tetraspanin antibodies. Anti-CD63 was sufficient to significantly reduce the median nuclei MGC⁻¹ (P=0.0347), fusion index (P=0.0444), MGC area (P=0.0136) and % coverage (P=0.0406) of Int monocytes compared to the IgG1 control. Anti-CD53 produced similar reductions in the fusion parameters but with only three donor repeats, however, this was not sufficient to obtain statistical significance in all parameters. Anti-CD151 produced significant decreases in the MGC area (P=0.0149) and % coverage (P=0.0406) and notable decreases in the fusion index and median number of nuclei MGC⁻¹. The addition of anti-CD9 caused a decrease in the fusion index (P= 0.1528) and a significant decrease in the Int % coverage (P=0.0331).

The decrease in Int FI for the Int monocytes with the addition of anti-CD9 seems to be due to the decrease in the number of fused cells and the increase in the number of adherent single cells in Figure 4.13. Similarly, anti-CD53, anti-CD63 and anti-CD151 also seem to decrease the number of cells committing to fusion while increasing the number of adherent single cells compared to the Int IgG1 control. For the CI and NCI subsets anti-CD9, anti-CD53, anti-CD63 and anti-CD151 did not greatly affect the number of fused cells as it did for the Int. There were however, notable reductions in the number of adherent cells for NCI monocytes cultured with anti-CD9, anti-CD53, anti-CD63 and anti-CD151 (Figure 4.13). The reductions in the fusion parameters in Figure 4.12 are proportional to the increase in the formation of the smaller LGC and decrease in the larger FBGC and SGC of Int monocytes cultured in anti-CD9, anti-CD53, anti-CD63 and anti-CD151. Anti-CD63 in particular showed significant reductions in the formation of FBGC (5.70%; P=0.0494) and a significant increase in

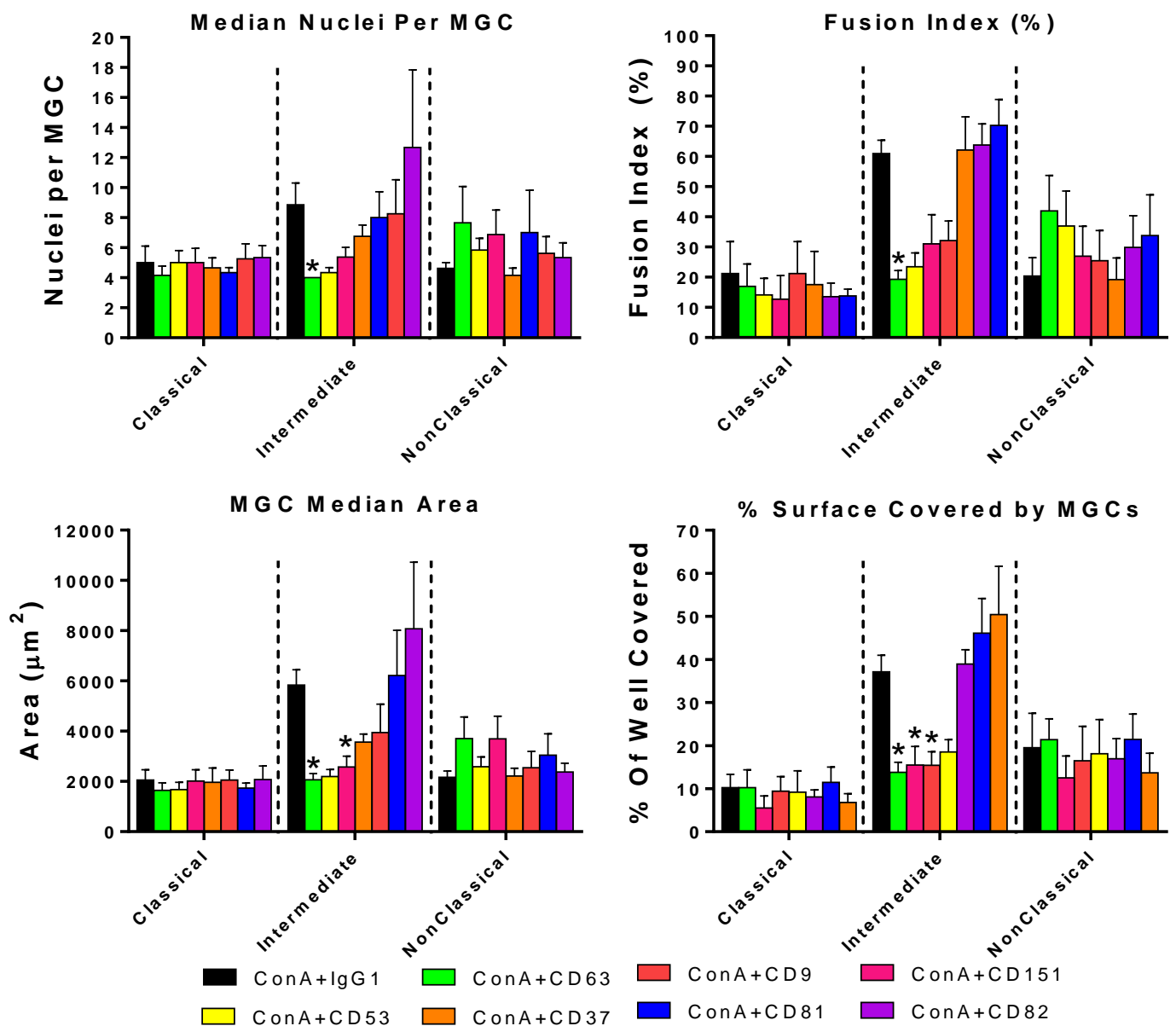


Figure 4.12: Fusion Parameters for Monocyte Subsets Cultured with Anti-Tetraspanin Antibodies.

FACS purified monocyte subsets were cultured in media containing ConA and either an anti-tetraspanin antibody or IgG1 control for 72hrs. Bars represent mean \pm SEM, N=3-8, all parameters were tested with a Kruskal-Wallis test (data was non-Gaussian) and a Dunn's multiple comparisons tests comparing the anti-tetraspanin antibody means against the IgG1 control within each subset. As the intermediate subset showed the most response to antibody treatment the columns have been arranged into ascending order for each parameter for intermediates.

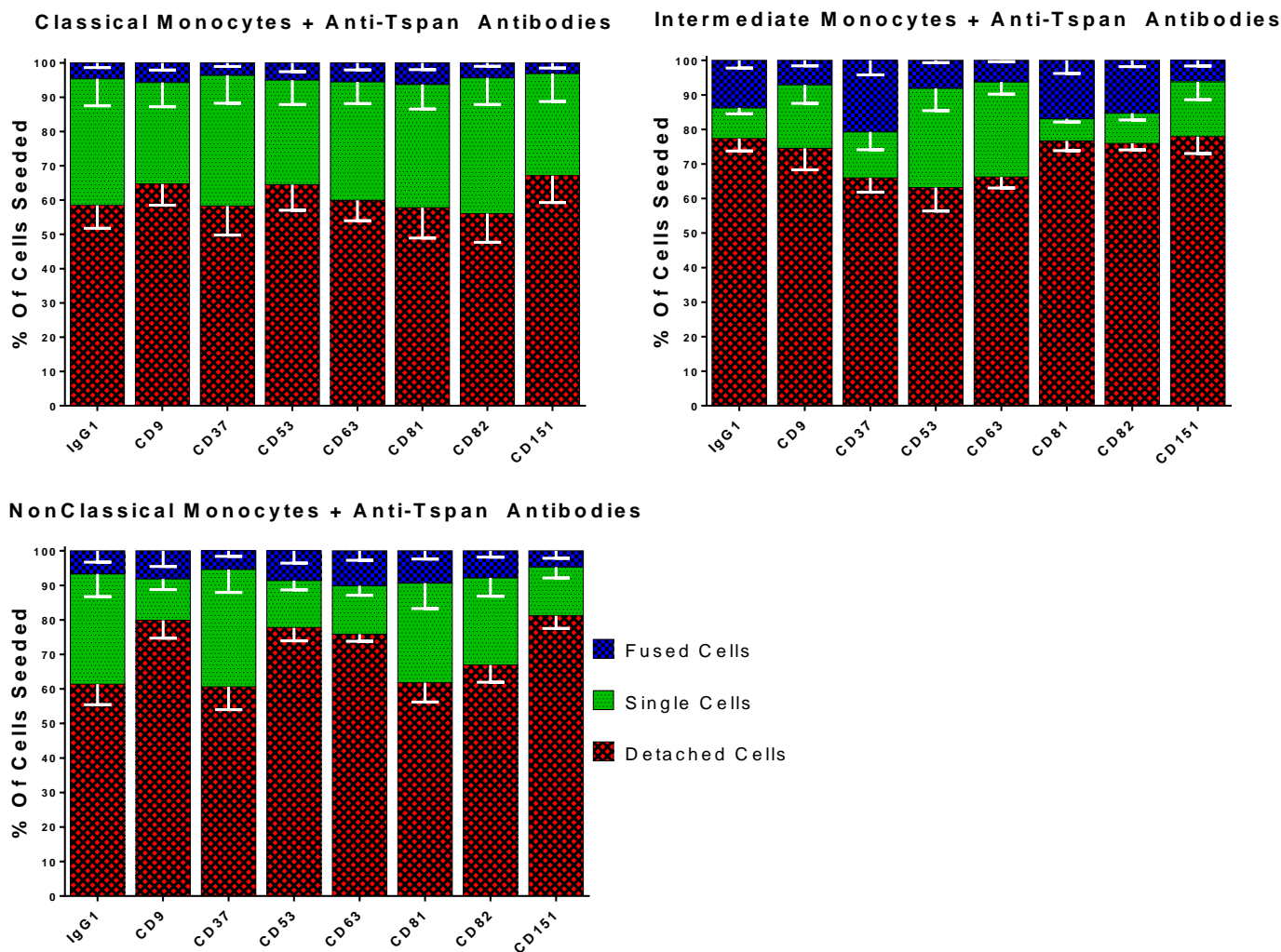


Figure 4.13: Monocyte Subsets Cultured with Anti-Tetraspanin Antibodies - Nuclear State Analysis.

The 'state' of each nuclei is summarised for each subset cultured for 72hrs in ConA media containing either IgG1 control or an anti-tetraspanin antibody. Bars represent mean±SEM, N=3-8, all time-points were tested with a Kruskal-Wallis test with Dunn's multiple comparisons tests comparing the means of the same nuclei 'state' within the same subset's IgG1 control.

the LGC (94.30%; $P=0.0340$) population compared to the IgG1 control (LGC: 26.94% & FBGC: 55.09%).

The CI and NCI subsets when cultured with anti-CD37 did not change from their respective controls (Figure 4.13), however, the Int fused cell population increased 1.51-fold from the control with the addition of anti-CD37. The increase in the SGC population for Int cultured with anti-CD37 in Figure 4.14 could be the cause of the increased fused cell counts in Figure 4.13. In Int the addition of anti-CD81 resulted in a 3.34-fold increase in the SGC population, the highest recorded in all conditions but did not affect the fusion parameters significantly. Unlike the total monocytes experiments anti-CD82 had little effect on any of the individual monocyte subsets in the fusion parameters, fused/single cell analysis or MGC type.

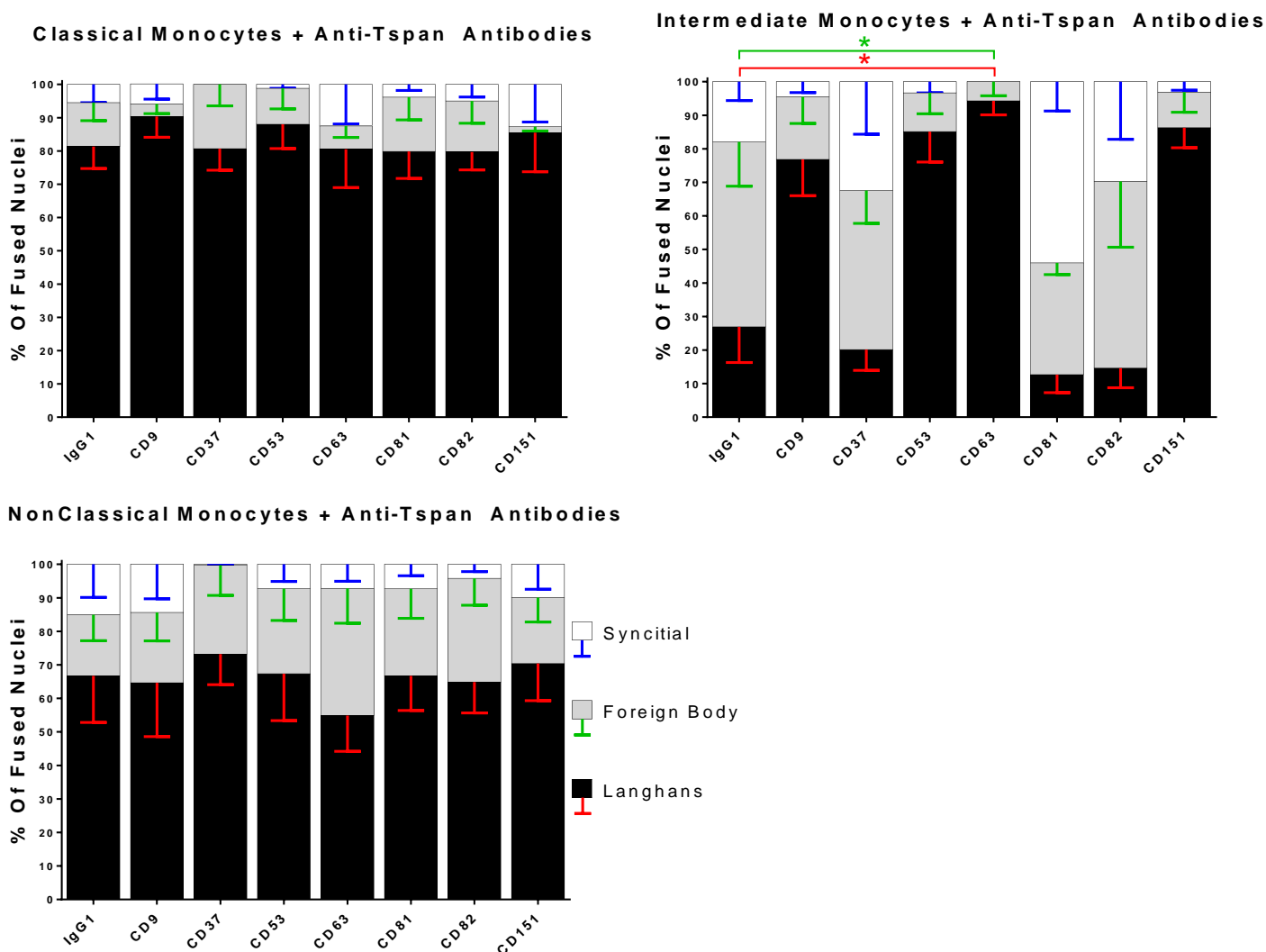


Figure 4.14: Monocyte Subsets Cultured with Anti-Tetraspanin Antibodies – MGC Type.

All the nuclei counted inside each MGC from the anti-tetraspanin experiments were tallied into one of three observed MGC types and presented as a percentage of the fused nuclei counted. Bars represent mean±SEM, N=3-8, all time-points were tested with a Kruskal-Wallis test with Dunn’s multiple comparisons tests comparing ‘like’ MGC types between the anti-tetraspanin conditions and the IgG1 control. Red stars: LGC nuclei, green stars: FBGC nuclei and blue stars: SGC nuclei.

4.8 DISCUSSION:

Monocyte Subsets Possess Different Predispositions to Fusion.

Previous studies have always tested monocytes as a total population and not sorted the subsets prior to the induction of fusion. Unlike the experiments performed in Chapter 3, there are no blood-derived leukocyte contaminants present in these experiments because FACS produces tightly selected subsets devoid of NK-cells or T-cells.

CI monocytes are typically ~17-fold and ~8.5-fold more numerous in the bloodstream than Int and NCI monocytes in healthy donors. Multiple studies have shown an expansion of the Int and NCI subsets during fusion-related inflammatory diseases such as tuberculosis (Castaño *et al.*, 2011), Crohn's disease (Grip *et al.*, 2007), hepatitis B (Zhang *et al.*, 2011a) and rheumatoid arthritis (Rossol *et al.*, 2012). The increase in these subsets could be an immune response to increase the number of fusion-ready monocytes in the blood to facilitate the formation of MGC in the tissues.

Figure 4.1 revealed that the subsets each commit different proportions to fusion. Furthermore, the subsets produced different ratios of LGC, FBGC and SGC compared to one another. This could indicate that the three subsets have distinct roles in regards to fusion which would have important implications on the development of treatments for the rejection of prosthesis and treating granulomatous masses. These findings are also a cautionary note for the study of fusion in mice because murine models only possess CI and NCI monocytes but not the highest fusing Int monocytes. Fusion is an irreversible commitment of monocytes and there has been no evidence in the literature or in these experiments that MGC can revert to single cells. MGC are relatively short lived cells and so any monocytes committed to fusion are lost from circulation. It is possible that the high-fusing Int and NCI monocytes are less prevalent in the bloodstream to avoid over-reactions to fusion-promoting signals which could otherwise be more detrimental than beneficial to the host.

Fusion Index Is Not an Accurate Measurement of Subset Fusibility

Fusion index (Figure 4.3) has long been a standard measurement of fusion; it is the ratio of nuclei in fused cells to total nuclei counted in a sample. For total monocyte work, this has always been adequate but by analysing the relative contributions of the subsets to fusion (Figure 4.1) it is clear that the fusion index can be misleading. For example, all three subsets produced a different fusion index but in Figure 4.1 it is clear that the subsets retain different numbers of adherent single cells (green segment). The higher the number of these single cells compared to the fused nuclei - the lower the FI. Int and NCI appear to have almost identical numbers of fused nuclei (blue segment) but because the Int monocytes retain less adherent single cells the fusion index increases and gives a somewhat misinformed view on the fusion behaviour. Fusion index is still a useful method of quantifying fusion between monocytes of a similar origin (e.g. Cl vs Cl) but due to the differing adherence properties of the subsets the fusion index must be considered with caution. It is therefore important to consider other measurements such as the ratio of nuclei in detached/single/fused cells, the MGC types formed and the % coverage. The % well covered in MGC was far more representative than FI for analysing the propensity of a subset to undergo fusion. The % coverage just analysed the total area of the well covered by MGC independent of what type of MGC it was or how many nuclei it contained or how many single cells remained unfused.

The Majority of Seeded Cells Detached or Died – Are Monocytes Committing Suicide To Attract More To Their Funeral?

Of the initially seeded 1.5×10^5 monocytes well⁻¹, a surprisingly high number of cells did not fuse or remain adhered as single cells. It is possible that a large number of single cells detach prior to the fixing stage. The larger MGC are tightly adhered but could instead rupture prior to fixing resulting in their loss from the analysed images. It is possible that only a small number of cells within each subset is fusion-competent and that Int and NCI subsets possess more of these cells. The remaining single cells appeared to detach slowly over time which could indicate that if a monocyte for whatever reason does not commit to fusion then it either detaches to patrol elsewhere or dies.

ConA has been shown to be internalised by monocytes and its internalisation in hepatomas triggers apoptosis via mitochondrial autophagy and release of cytochrome c (Li *et al.*, 2011; Liu *et al.*, 2009; Sodhi *et al.*, 2007). Many studies have supported a pro-inflammatory role of apoptosis via the release of internal IL-1 α and IL-1 β (Hogquist *et al.*, 1991; Sarih *et al.*, 1993). The massive loss of monocyte cell numbers over time (Figure 4.8) and the increase in pro-apoptotic cytokines such as IFN γ , IL1 β and TNF α (Figure 4.10a) could indicate that some monocytes undergo apoptosis to generate a cytokine signature that promotes fusion. In accordance with this, Sodhi *et al.* (2007) observed that ConA enhanced the expression of TLR and adaptor protein MyD88 in murine M ϕ which are both components of the NF- κ B pathway (Figure 1.3 and Figure 1.7). Furthermore, Kelly *et al.* (2008) observed that after TB infected M ϕ undergo apoptosis they trigger apoptosis of bystander M ϕ that are not infected with TB. Wong and colleagues have shown that the CD16+ monocyte subsets are more susceptible to apoptosis than the CI monocytes (Zhao *et al.*, 2010). In persistent TB infections, the phagocytosed pathogen arrests lysosome-phagosome fusion and generates anti-apoptotic mediators to allow it to proliferate within the host cell. Successful apoptosis in TB infections is thought to confer an anti-proliferative outcome (Bocchino *et al.*, 2005; Lee *et al.*, 2009). Though it is just speculation, apoptosis could play an important part in generating fusion-promoting microenvironments.

In vivo fresh monocytes would be constantly recruited from the bloodstream to the source of fusion (be it a foreign body or TB infection), however, in this *in vitro* model there is only one initial input of monocytes. It is important to keep this in mind as this model is limited to a finite number of monocytes in the well, of which the majority seemed to detach. Thus the level of fusion *in vivo* could potentially be much greater than that seen here. For our experiments, subset monocytes had to be sourced from apheresis cones to gain sufficient numbers of Int and NCI monocytes through FACS. It therefore not possible to arrange subsequent monocyte 'seeding' time-points from the same donor such as the technique demonstrated by Möst *et al.* (1997).

Subset Derived MGC All Possess Ruffled Membranes and a Network of Securing Filaments

SEM was able to show in high resolution that many MGC are tethered down by networks of long filaments. Using confocal microscopy, DeFife *et al.* (1999) also observed these microfilaments in FBGC but not M ϕ and found them to be composed predominantly of F-actin. These filamentous structures could be a trait of particularly late-stage MGC that have low motility and high adherence to allow them to form a secure podosome on the surface to secrete digestive molecules. Smaller early-stage MGC may not have these large filamentous networks to allow a greater degree of mobility. *In vivo* these long filaments may also act not only as a strong tethering system but as 'tracks' to reel in wandering monocytes for fusion. It is unclear whether these filaments are a particular feature of glass-adhered MGC or if they are also present on plastic or in tissues.

The bulbous structures commonly observed in the Int and NCI MGC were not observed in any detail in the fluorescence images. Furthermore, in larger MGC the central 'nuclear compartment' of the MGC stained notably weaker with the phalloidin stain indicating a lower abundance of F-actin. DeFife *et al.* (1999) found that late stage FBGC (10 days culture with IL-13) had FBGC with weak central F-actin staining as the clusters of nuclei were instead supported with networks of microtubules and Int filaments. If these bulbous structures found in the SEM images are indeed composed of tubulin and Int filaments then they would not be apparent in the phalloidin stained fluorescence images. Alternatively they appear to be elevated off of the MGC structure and so they could be out of focus of the fluorescence microscope. The fixing and dehydrating treatments seemed to be very damaging to the MGC especially the larger ones (Figure 4.5c.4). It is unclear whether some of the structures are representative of the MGC morphology or if they are just distortions produced by the sample preparation techniques.

Ruffled membranes is a morphological feature typically found on osteoclasts (Quinn and Schepetkin, 2009; Xia and Triffitt, 2006; Yagi *et al.*, 2005) though some have reported this morphology on FBGC (Athanasou and Quinn, 1990; Milde *et al.*, 2015; Saginario *et al.*, 1995). Milde *et al.* (2015) suggested that these ruffled membranes

grant MGC a greater phagocytic ability, particularly with complement-opsonised targets. In Figure 4.5a2 we see the ruffled membrane of an MGC interacting with two Cl monocytes. It is possible that this image shows the beginnings of endocytosis/fusion of these two monocytes prior to their incorporation into the MGC structure.

Though Flu-SEM allows the nuclei arrangements to be overlaid over the SEM images it is still subject to user bias and error as the techniques are conducted independently of one another. Furthermore, Flu-SEM was only carried out in one z-frame so it only produced a 2D image of the nuclei which is inadequate for analysing nuclear stacking. Transmission electron microscopy would be far more effective at capturing all the layers of MGC from the external surfaces to the internal arrangement of the nuclei and even digestive vesicles being secreted at the well surface.

ConA Treatment Produces MGC Formed From Monocytes Not M ϕ :

In the fusion kinetics study all three subsets were able to fuse and form MGC within 24hrs. Multiple studies state that MGC form from "the fusion of macrophages", however, freshly isolated monocytes typically take 5-8 days of differentiation in GM-CSF/M-CSF (Ohradanova-Repic *et al.*, 2016) and other factors to form M ϕ . The freshly isolated monocytes were able to fuse in less than 24hrs, indicating that fusion was initiated and facilitated by monocytes not macrophages. This is in accordance with the findings of Möst *et al.* (1997) who found that freshly isolated monocytes were able to form MGC but cultured M ϕ could not.

NCI monocytes were slow to start in fusion and possessed the lowest fusion parameters of all the subsets at 24hrs. However, by the final 72hr time point they overtook the low-fusing Cl. The plateauing of the fusion parameters in the high-fusing Int after 48hrs also suggests that they have reached their maximal fusion potential. 72hrs is therefore an ideal end point for all the fusion assays though it is not clear if by 72hrs the lack of further fusion is due to a lack of monocytes, lack of nutrients in the media, excess waste in the media or negative feedback from the MGC.

LGC Are Precursors to FBGC and SGC

There was a relationship between the median MGC area and the abundance of larger FBGC and SGC within the same time points. The smaller LGC typically range from 3-15 nuclei per MGC with an area of 1044-8599 μm^2 , when the larger FBGC and SGC become more abundant there is a big increase in the median MGC area. At the earliest time points the majority of MGC were LGC and the appearance of larger FBGC and SGC increases as time increases. As the FBGC and SGC increase the LGC population decreases; this supports the notion that the three MGC types are not distinct and that the larger MGC are later stages of the smaller LGC. The ability for LGC to develop into FBGC has been observed *in vivo* on rat implants (Rhee *et al.*, 1978) in humans suffering from sarcoidosis (Van Maarsseveen *et al.*, 2009) and *in vitro* with ConA (Möst *et al.*, 1997). Presently MGC classification is based predominantly on morphology so until markers of the different MGC are found, such conclusions can only be speculative.

ConA Produced A Strong Pro-Inflammatory and Pro-Apoptotic Response in CI and Int Monocytes.

Within the first 24hrs of culture in ConA the CI and Int monocytes reacted by secreting high levels of IL-6 and TNF α . TNF α is able to both induce the transcription of GAS genes via the NF- κ B pathway and is also an inducer of apoptosis (Wajant *et al.*, 2003). Thereafter, by 48hrs the detectable levels IL-1 α and IL-1 β were at their highest in the CI and Int subsets but were virtually undetectable in the NCI subset. Monocytes and M ϕ have been shown to release internal stores of IL-1 derivatives during apoptosis (Hogquist *et al.*, 1991; Sarih *et al.*, 1993). Following this, Figure 4.8 shows that between 24-48hrs there is a large increase in the number of dead cells for the CI and Int subsets but less so for the NCI. These cytokine patterns suggest that the CI and Int subsets could be generating a pro-apoptotic microenvironment in the first 24-48hrs following which the Int subset responds by forming larger FBGC and SGC whereas the CI forms smaller LGC. The NCI subset does not secrete pro-apoptotic cytokines but does secrete the highest levels of IFN γ by 72hrs suggesting that activation of NCI fusion is mediated by a different pathway to the other two subsets.

ConA Induced Rapid Secretion of Pro-Fusion Cytokines IFN γ , IL4, IL-17A, IL-13 and IL-3.

FBGC have been shown to form in response to combinations of IL-4, GM-CSF, IL-3 and IL-13 (DeFife *et al.*, 1997; McNally and Anderson, 1995) while LGC form more favourably in response to IFN γ and IL-17A (Byrd, 1998; Coury *et al.*, 2008; McNally and Anderson, 1995; Sakai *et al.*, 2012; Takashima *et al.*, 1993). Compared to the concentrations of pro-inflammatory cytokines the secreted levels of IL-4, IL-3, IL-13 and IL-17A were minute. However, pro-fusion cytokines have been shown to be effective at very low concentrations. MGC have been generated *in vitro* with IL-4 at concentrations of 15ng ml⁻¹ (McNally and Anderson, 2014) to 10ng ml⁻¹ (Moreno *et al.*, 2007). DeFife *et al.* (1997) titrated IL-4 and IL-13 and found MGC to develop at concentrations as low as 1ng ml⁻¹. IL-17A is a potent stimulator of fusion and has shown to be effective at 1ng ml⁻¹ (Kotake *et al.*, 1999). IL-3 was shown by McNally and Anderson (1995) to develop small MGC at 10ng ml⁻¹ and the addition of IL-4 had an additive effect on the size of the MGC produced. Therefore, despite the apparently low concentrations of IL-3, IL-4, IL-13 and IL-17A, they are all detected at biologically effective concentrations and perhaps are initiating fusion at the earlier time points (24-48hrs).

GM-CSF is routinely used to differentiate monocytes into M1-like M ϕ and was secreted at quite high levels in CI and Int subsets cultured in ConA. It's likely that the presence of pro-inflammatory cytokines such as IL-6 and TNF α at 24hrs were triggering the transcription and secretion of other cytokines such as GM-CSF at 48hrs. From CI to NCI the expression of the GM-CSF receptor decreases and the M-CSF receptor increases (Figure 1.1) (Martinez *et al.*, 2006). Though M-CSF was not tested in these samples it is possible that the NCI monocytes were utilising M-CSF over GM-CSF signalling in accordance with their respective receptor expression. Sakai *et al.* (2012) measured IFN γ and found concentrations of 10ng ml⁻¹ to be sufficient to induce fusion. However, their cultures also contained cytokine producing T-cells. Möst *et al.* (1990) used anti-IFN γ antibodies to demonstrate that IFN γ is essential in MGC formation. Our results show that within 24hrs IFN γ was secreted at concentrations exceeding 10ng ml⁻¹ and increased through each time point peaking at 72hrs. At 72hrs time point the

concentration of IFN γ was highest in the Int and NCI subsets. At the same 72hr time-point the Int and NCI possessed the highest % coverage of MGC (Figure 4.7) suggesting that IFN γ is a later stage pro-fusion cytokine.

ConA Stimulated CCL2 & CCL3 Cytokine Secretion

CCL2, CCL3 and RANTES are secreted by monocytes and M ϕ to attract leukocytes to sites of inflammation (Moriuchi *et al.*, 1997; Ueda *et al.*, 1994; Widmer *et al.*, 1993). RANTES is produced in sites of viral infection and is secreted to attract cytotoxic T-cells, NK-cells and DC (Crawford *et al.*, 2011). There was no detectable level of RANTES in both ConA and untreated wells for any of the subsets at any time-point. Therefore it seems that none of the monocyte subsets utilise RANTES signalling during fusion. The secreted levels of CCL2 on the other hand were so high in both ConA and unstimulated conditions that by 48hrs it exceeded the ELISA detection limit for some samples. CCL2 is secreted not just by leukocytes but also endothelial cells, smooth muscle cells and fibroblasts and is a potent chemoattractant for monocytes towards sites of inflammation (Deshmane *et al.*, 2009).

Like CCL2, CCL3 is secreted by multiple cells types to attract monocytes and other leukocytes and is particularly upregulated in monocytes and M ϕ in response to LPS detection (Menten *et al.*, 2002). Compared to untreated wells CCL3 was detected at significantly higher concentrations in ConA cultured cells as early as 24hrs. Unlike CCL2; CCL3 was not produced secreted in large quantities in the untreated wells suggesting its secretion was ConA specific.

Only Int Monocytes Were Responsive to Anti-Tetraspanin Antibodies

Previous studies utilising anti-tetraspanin antibodies have always been conducted on total monocytes. The total monocyte work in Chapter 3 did not replicate the results published by other research groups, however, to date no study has used FACS to isolate monocyte subsets to absolute purity. In the anti-tetraspanin antibody assays conducted on subset monocytes it is clear that the subsets not only fuse differently but react to the anti-tetraspanin antibodies differently. This has important implications for the previous work that has reported on the effects of these antibodies in total

monocytes as it appears that the significant effects are primarily a result of the Int monocytes.

Anti-CD9, anti-CD53, anti-CD63 and anti-CD151 abrogated fusion in Int monocytes but their effects were almost negligible on CI and NCI monocytes. Firstly, addition of any one of these antibodies to the fusion media of Int was sufficient to reduce the FI, MGC area and % coverage to half their respective readings in the IgG1 control (Figure 4.12). Secondly, these four anti-tetraspanin antibodies greatly reduced the population of fused nuclei (Figure 4.13) while increasing the number of single cells. Finally, anti-CD9, anti-CD53, anti-CD63 and anti-CD151 caused drastic reductions in the FBGC and SGC populations, instead favouring the formation of smaller LGC (Figure 4.14), however, this effect was not observed in the CI and NCI subset.

Conclusion:

Int monocytes, despite being up only 5-8% of the monocyte population, have the greatest potential to fuse and form large MGC. In the kinetics study, we have shown that Int monocytes are the first to form MGC of the three subsets. The ELISA data revealed that compared to the other subsets the Int secrete high levels of pro-apoptotic and pro-inflammatory cytokines and release high levels of chemokines to recruit more monocytes for fusion. The Int monocytes showed a greater potential to form larger FBGC and SGC. However, addition of anti-tetraspanin antibodies targeting CD9, CD53, CD63 and CD151 was sufficient to reduce measured fusion parameters and MGC populations of Int to that of CI monocytes. A greater understanding of the expression of tetraspanins on monocyte subsets may reveal why Int monocytes are so fusogenic and why these select anti-tetraspanin antibodies are able to limit their fusion potential.

CHAPTER 5: TETRASPANIN EXPRESSION IN MONOCYTE SUBSETS

5.1 INTRODUCTION

Monocyte subsets are able to fuse to form MGC but the rates of fusion and the types of MGC produced are different in each subset (see Chapter 4). Furthermore certain anti-tetraspanin antibodies are able to affect the fusion outcomes of the high-fusing Int subset more than the NCI and CI subsets. It has been suggested that tetraspanins play a vital role in establishing fusion-facilitating TEMs (Hemler, 2003). This model has been supported by multiple studies utilising mouse knock outs, antibody-interference and soluble EC2 proteins that all act to disrupt the formation of a functioning TEM.

Knock outs in mouse gametes have shown that CD9 (Kaji *et al.*, 2000; Naour *et al.*, 2000) and CD81 (Rubinstein *et al.*, 2006) play a vital role in gamete cell fusion in mice. Whereas human sperm-egg fusion can be blocked using CD151 targeting antibodies (Ziyyat *et al.*, 2006). Anti-CD63 has been shown to greatly inhibit the fusion of human monocytes (Parthasarathy *et al.*, 2009; Takeda *et al.*, 2003). CD53 is a regulator of TNF α (Bos *et al.*, 2010), in Chapter 4 TNF α was highly secreted in high-fusing Int and anti-CD53 antibodies subdued their ability to fuse. CD37 is able to transduce apoptotic signals (Lapalombella *et al.*, 2012) which from the cytokine patterns in Chapter 4 appeared to be an important step in fusion initiation. CD82 has been shown to play an important role in virus induced syncytium formation (Daenke *et al.*, 1999; Hildreth, 1998; Hildreth *et al.*, 1997). An understanding of the surface expression of these tetraspanins on monocyte subsets may reveal differences in the tetraspanin stoichiometry that could be responsible for their differing fusion potentials.

5.2 RESULTS

5.2.1 SURFACE EXPRESSION OF TETRASPANINS ON HUMAN MONOCYTE SUBSETS.

Figure 5.1 shows the relative intensity of the surface expression of tetraspanins on the different monocyte subsets and the percentage of cells positive for each tetraspanin. CD53 was expressed on 100% of cells in all subsets but was significantly different in the level of expression between all subsets (MFI CI: 3185, Int: 4734 & NCI: 4147). High percentage expression was also observed in CD81 (78-90%) and CD82 (92-99%). CD81 expression levels were very similar on all subsets but for CD82, the CI monocytes (MFI: 1671) expressed higher levels than the Int and NCI subsets (MFI: 954; $P=0.0037$ and 827; $P=0.0007$). Compared to the expression of the other tetraspanins, CD63 and CD151 were expressed on a minority of monocytes (CD63: 5-8% & CD151: 41-51%). The MFI readings were also very low and no significant difference between the subsets was found. The percentage of monocytes expressing CD37 was significantly lower in the CI (47%) subset than the Int (78%; $P<0.0001$) and NCI (65%; $P=0.0193$) monocytes. However, there was no significant difference between the MFIs of the CD37 positive subsets. CD9 was expressed significantly higher in CI monocytes, however, as the histograms in Figure 5.2 show, CD9 was expressed as a bimodal population in CI monocytes. The CD9^{low} population consisted of 76.77% of the CI monocytes and the remaining 23.23% were termed the CD9^{high} population. Expression of CD9 in the Int subset was positively skewed (59% positive for CD9) and the NCI showed a Gaussian distribution but with only 28% positive for CD9. The MFI for the CD9-positive cells was significantly lower in the NCI (MFI: 349) compared to the Int (MFI: 1174; $P=0.0009$) but not compared to the CI (MFI: 804; $P=0.0635$).

Figure 5.3 shows the co-expression of the 7 tetraspanins compared to each other. The degree of correlation of expression of two tetraspanins is shown by a shift of the dots to the upper-right region of the panel. As the CI (red) monocytes are the most abundant in the PBMCs they are the most prominent population on the graphs. The CD9 row shows small shifts indicative of correlated expression of CD9/CD81 and

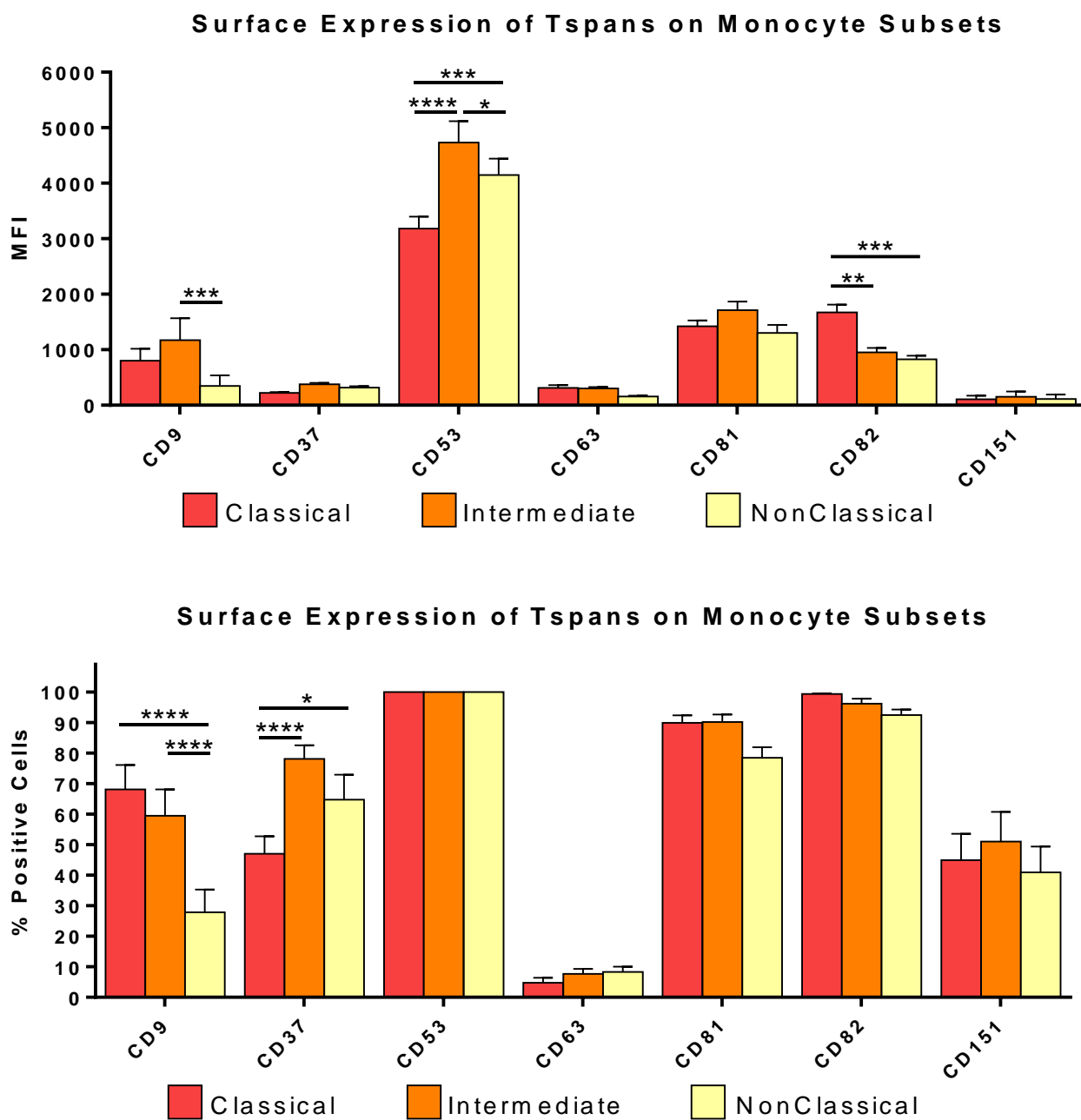


Figure 5.1: Surface Expression of Tetraspanins on Human Monocyte Subsets.

Freshly isolated human PBMCs were stained with a 10-antibody panel and their surface tetraspanin expression was analysed on a flow cytometer. MFI and percentage positive graphs are shown above for each tetraspanin detected on the monocytes subsets. Bars represent the mean±SEM, N=10. Tested with a two-way ANOVA with an Uncorrected Fisher’s LSD post-hoc test to compare column means.

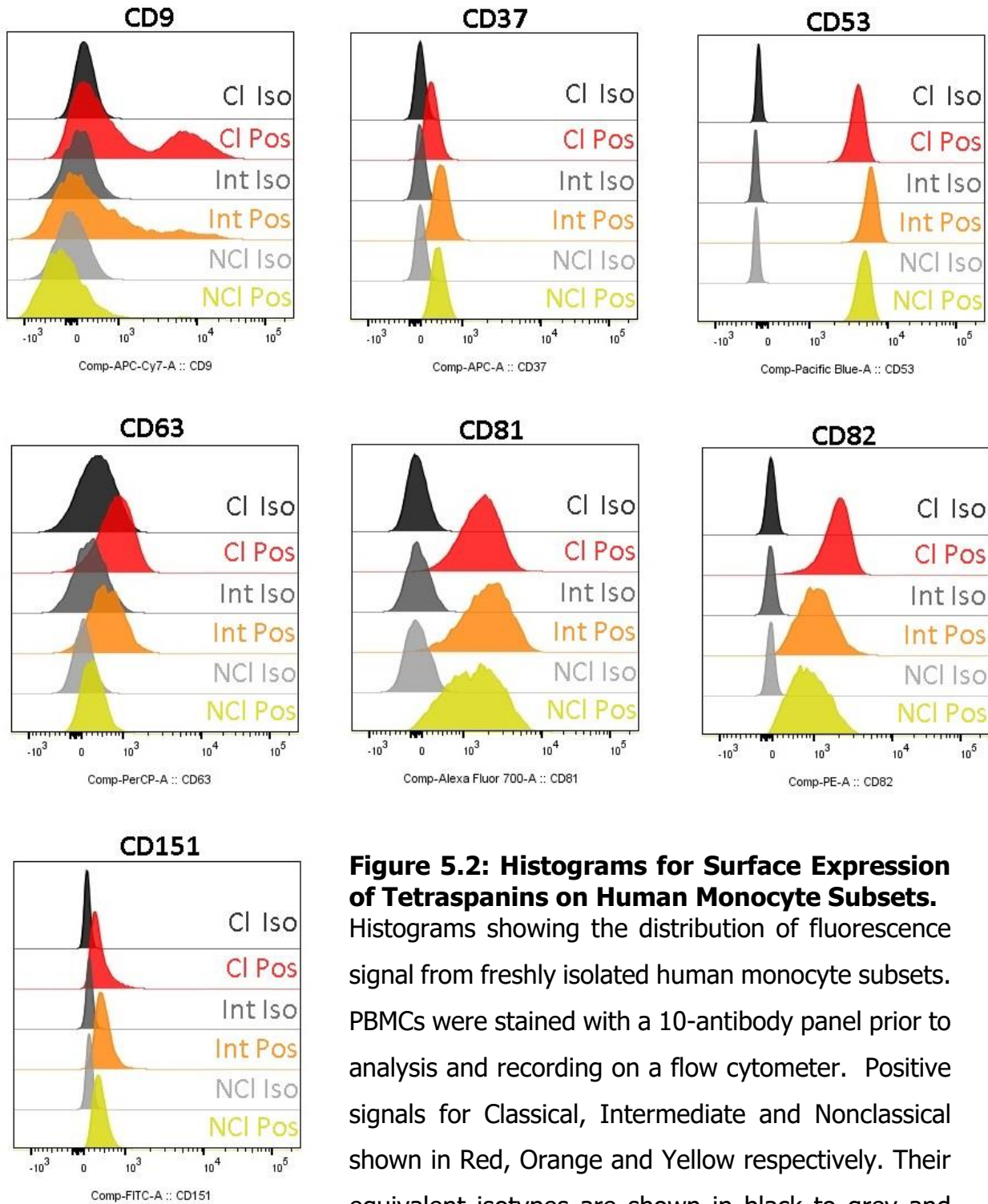


Figure 5.2: Histograms for Surface Expression of Tetraspanins on Human Monocyte Subsets. Histograms showing the distribution of fluorescence signal from freshly isolated human monocyte subsets. PBMCs were stained with a 10-antibody panel prior to analysis and recording on a flow cytometer. Positive signals for Classical, Intermediate and Nonclassical shown in Red, Orange and Yellow respectively. Their equivalent isotypes are shown in black to grey and represent the background/nil signal.

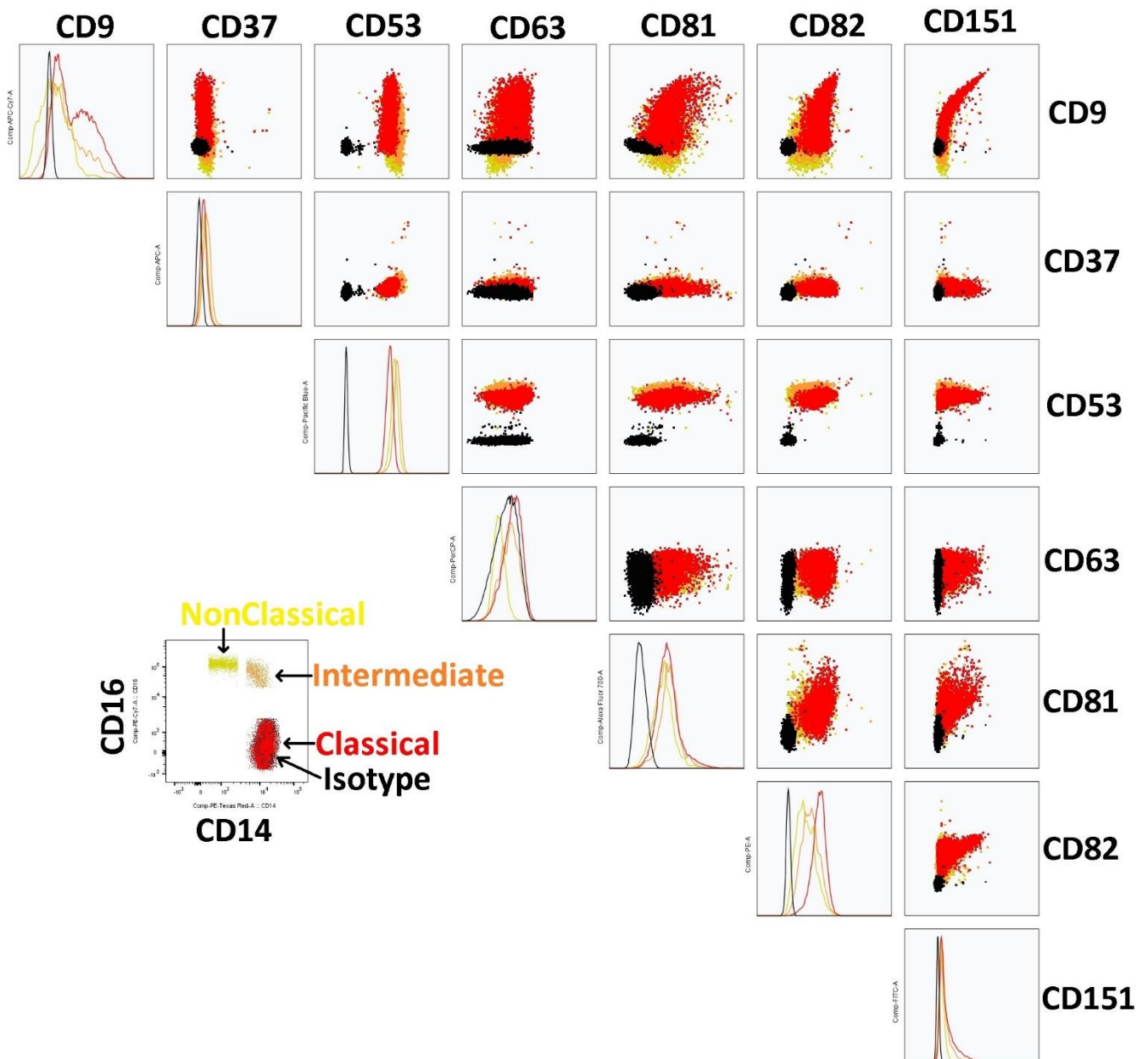


Figure 5.3: Tetraspanin Co-Expression on Human Monocyte Subsets.

Dot plots showing the co-expression of CD9, CD37, CD53, CD63, CD81, CD82 and CD151 on freshly isolated monocyte subsets. Classical, Intermediate and NonClassical shown as dots in Red, Orange and Yellow respectively. An isotype control is shown in black. Note that CD9 was the only tetraspanin in the histograms to show a bimodal peak of expression and that co-expression of two tetraspanins results in a shift of dots to the top right of the respective plot (e.g.CD9/CD151).

CD9/CD82 in the CI subset, and a strong positive correlation between CD9/CD151. CD82/CD151 also appear to have correlated expression in CI monocytes.

5.2.2 COMPARISON OF CD9^{LOW} AND CD9^{HIGH} CLASSICAL MONOCYTES

Multiple studies have reported that CD9 is an important component in the fusion machinery. The bimodal distribution of CD9 expression in CI monocytes in Figure 5.2 and the co-expression of CD9/CD151 (Figure 5.3) led us to believe there may be a subset of tetraspanin-high CI monocytes that could have a unique role in the fusion process.

The CI monocytes from Figure 5.1 were gated into CD9^{Low} (76.77% of CI) or CD9^{High} (23.23% of CI) (Figure 2.4) and the MFI values of the other tetraspanins were compared (Figure 5.4). In Figure 5.4 it is clear that even though the CD9^{High} population comprises only 1/4th of the CI monocytes, it is significantly higher in CD9 (MFI: 5545) than CD9^{Low} (MFI: 560; $P < 0.0001$). CD63 and CD81 had MFI values 1.52-fold higher ($P = 0.6643$) and 1.40-fold higher ($P = 0.1210$) in CD9^{High} compared to CD9^{Low} CI. CD151 was 6.56-fold higher expressed in CD9^{High} (MFI: 479) than CD9^{Low} (MFI: 73; $P = 0.2434$), in Figure 5.5 it is clear that the CD9^{High} CI monocytes are positively skewed for CD151 expression.

Though not statistically significant, the CD9^{High} CI monocytes appeared to consist of a small population of tetraspanin-rich monocytes. To see if there was a difference in their fusion behaviour the two populations were sorted by FACs into either total CI (CI monocytes that had not been separated further), CD9^{Low} or CD9^{High} CI monocytes (Figure 5.6 and 5.7). Initially, CD9^{Low} and CD9^{High} CI were sorted using the indirect anti-CD9 label that was used in flow cytometry (anti-CD9-biotin + streptavidin-APC-Cy7). Later a direct anti-CD9-FITC was used as a control to see if indirect labelling was having an effect. Compared to the CD9^{Low} cells, the CD9^{High} CI monocytes purified with the biotin-streptavidin conjugate (B-S); produced MGC with 1.5-fold more nuclei per MGC ($P = 0.0692$), 2.3-fold MGC area ($P = 0.0718$), had a 5.2-fold higher fusion index ($P = 0.0219$) and 6.1-fold higher % coverage ($P = 0.0219$). The MGC types produced from each population (Figure 5.7) show that the CD9^{Low} (B-S) produced

Surface Expression of Tspan on Classical Monocytes

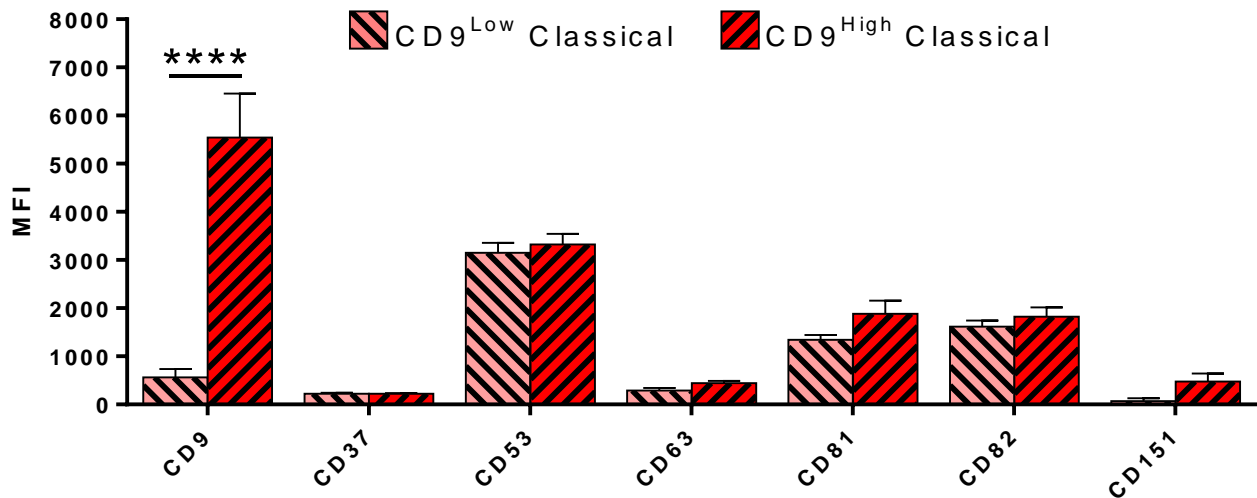


Figure 5.4: Surface Expression of Tetraspanins on CD9^{Low} vs CD9^{High} Classical Monocytes

Classical monocytes possess a CD9^{Low} and CD9^{High} population in freshly isolated monocytes. To see if there was a correlation between CD9 expression and expression of other tetraspanin markers the CD9^{Low} and CD9^{High} classicals were gated and the MFIs of other tetraspanins displayed. Bars represent the mean \pm SEM, N=10. Tested with a two-way ANOVA with an Uncorrected Fisher's LSD post-hoc test to compare column means.

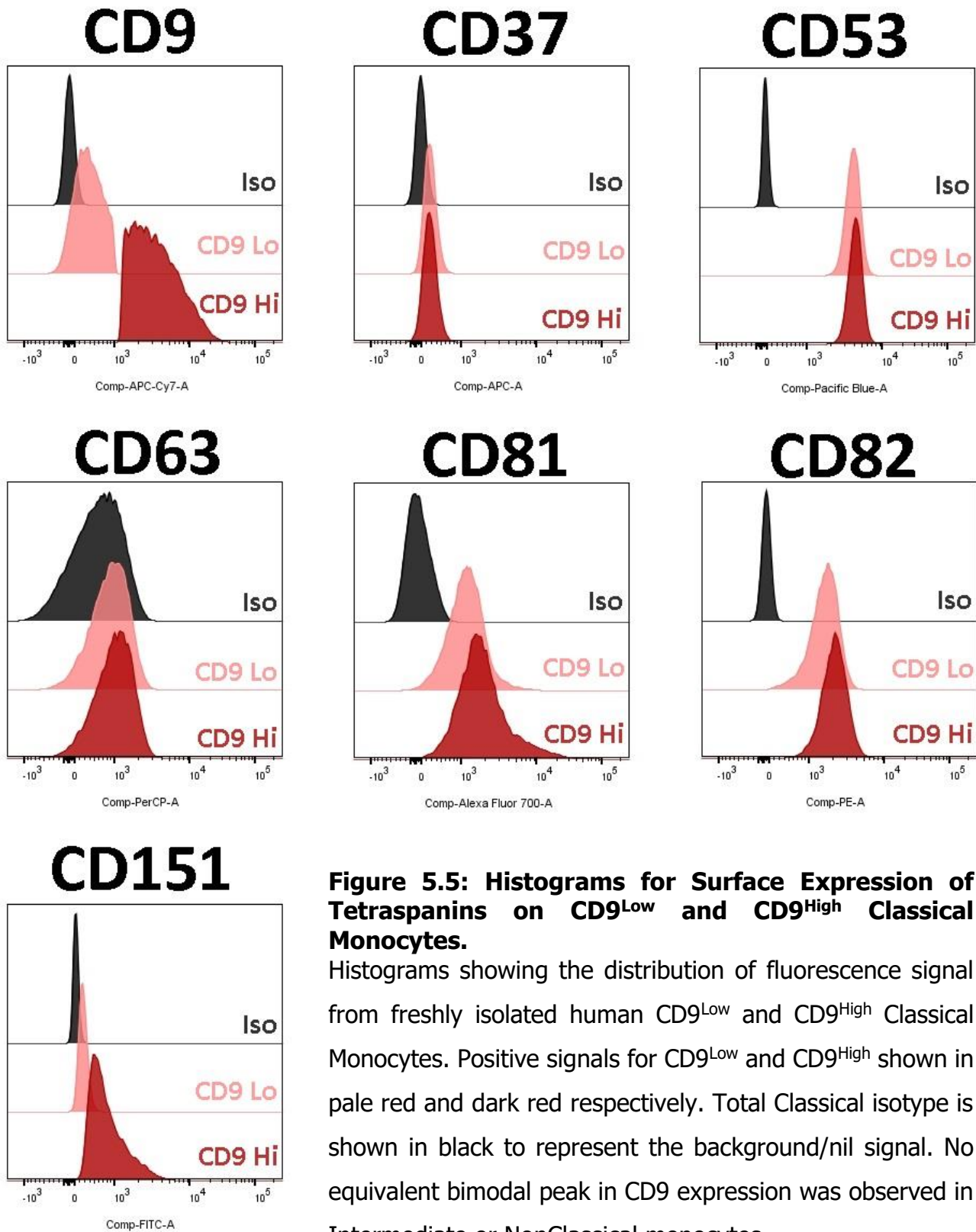


Figure 5.5: Histograms for Surface Expression of Tetraspanins on CD9^{Low} and CD9^{High} Classical Monocytes.

Histograms showing the distribution of fluorescence signal from freshly isolated human CD9^{Low} and CD9^{High} Classical Monocytes. Positive signals for CD9^{Low} and CD9^{High} shown in pale red and dark red respectively. Total Classical isotype is shown in black to represent the background/nil signal. No equivalent bimodal peak in CD9 expression was observed in Intermediate or NonClassical monocytes.

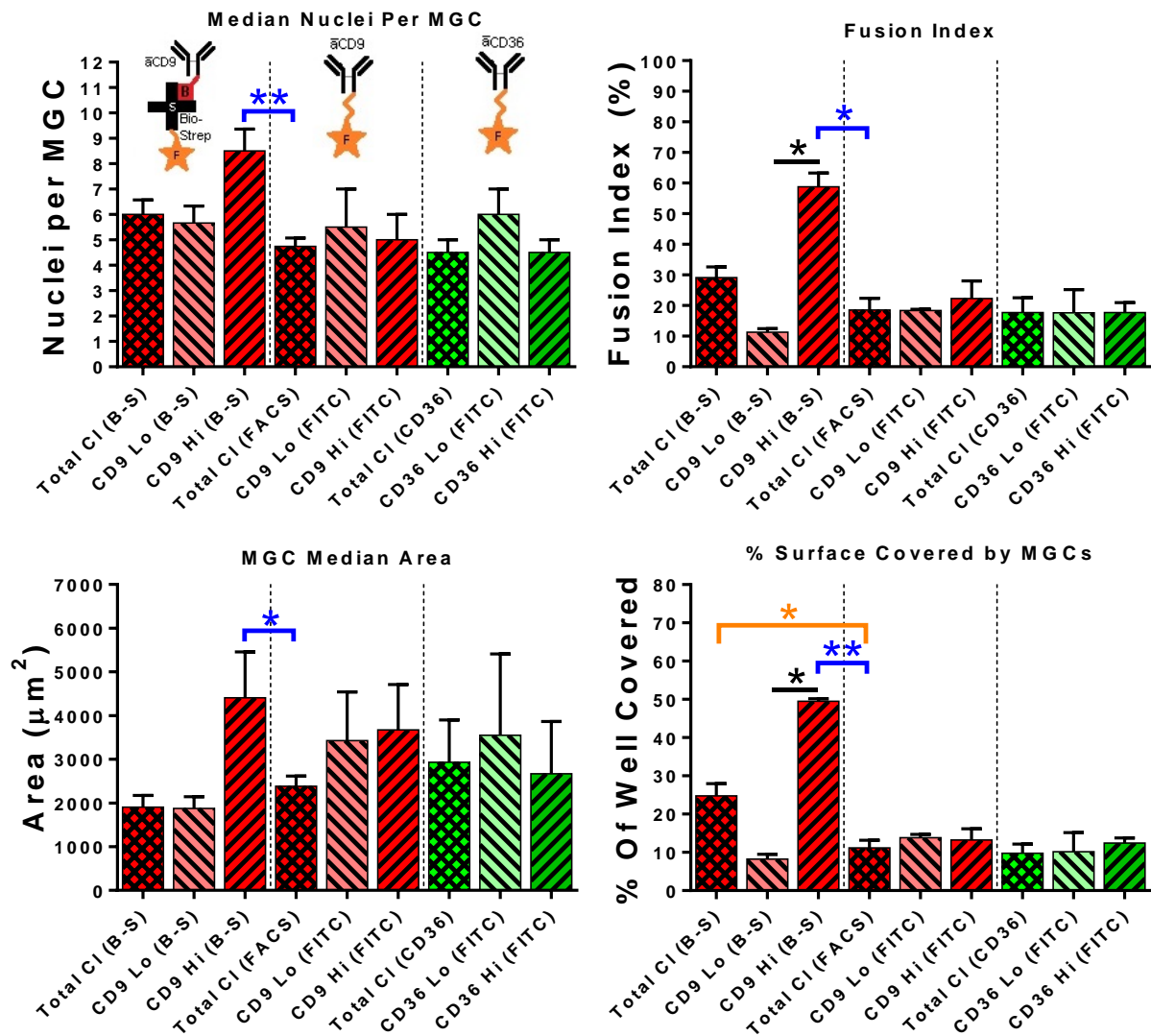


Figure 5.6: Comparison of Fusion Results from Total, CD9^{Low} & CD9^{High} Classical Monocytes from Different FACS Isolation Methods.

The first triad in each graph are Total, CD9^{Low} and CD9^{High} Classical monocytes that had been FACS sorted via an indirect CD9 staining method (Anti-CD9-Biotin+Steptravidin-APC-Cy7). The second triad were sorted using a direct anti-CD9-FITC label. The third triad were sorted into Total, CD36^{Low} and CD36^{High} classical monocytes due to the high CD9/CD36 co-expression in Classical monocytes. This was to see if binding of CD9 in the other methods was affecting fusion. Bars represent the mean \pm SEM. N=25 for Total CI (FACS), N=3 for B-S samples & N=2 for all others. **A)** and **C)**: the means of the B-S triad were tested with a one-way ANOVA with a Tukey multiple comparisons test. For **B)** and **D)**: the B-S triad was tested with a Kruskal-Wallis test with a Dunn's multiple comparisons test. A subsequent test was conducted comparing the B-S CD9^{Low} and CD9^{High} with Total CI (FACS), same statistics models as before; shown in blue. Lastly a T-test (Mann-Whitney; orange) was conducted comparing the means of Total CI (B-S) and Total CI (FACS).

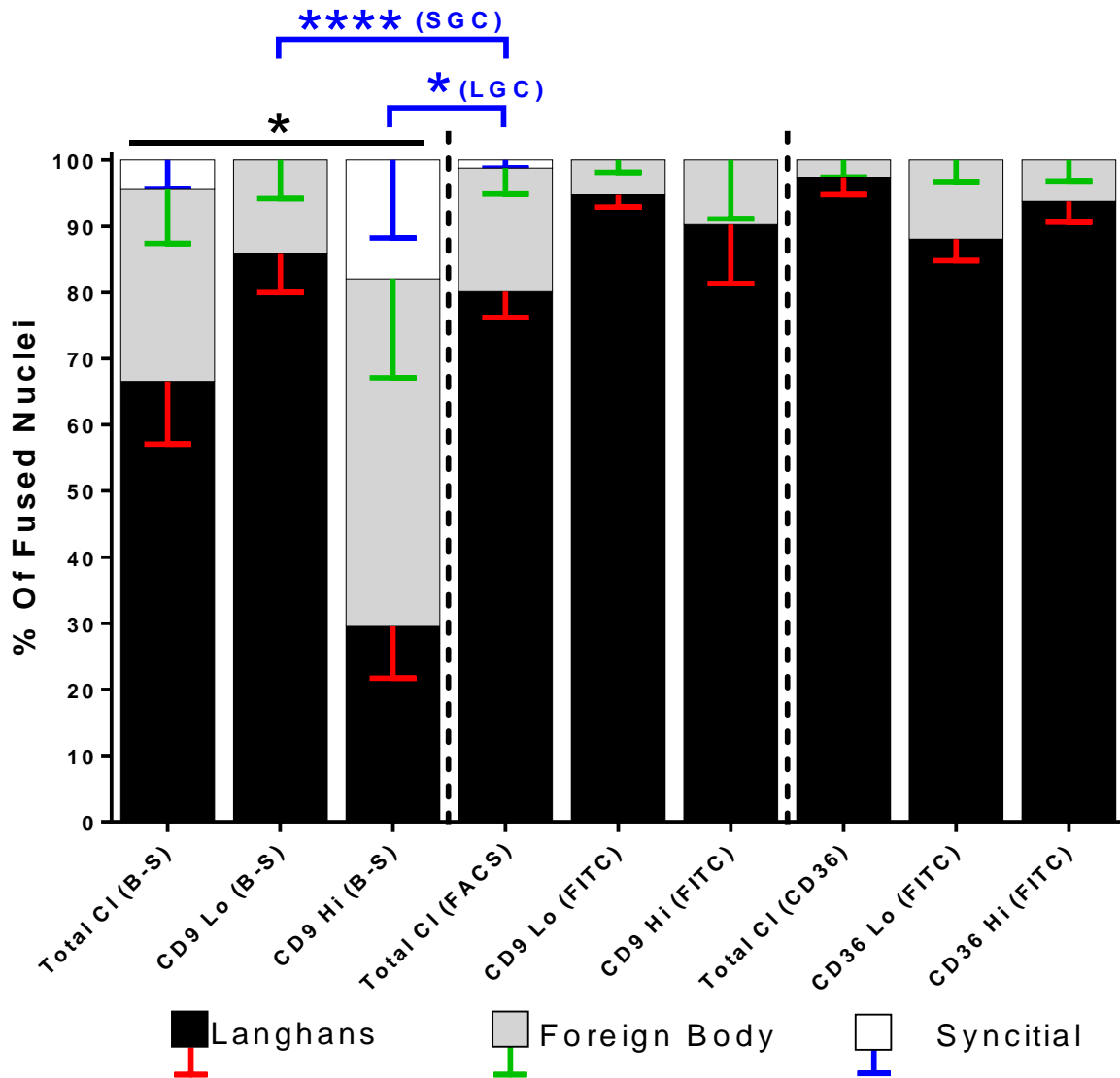


Figure 5.7: MGC Types Formed from CD9^{Low} vs CD9^{High} Classical Monocytes from Different FACS Isolation Methods.

Total, CD9^{Low} and CD9^{High} classical monocytes were FACS purified using an indirect aCD9-biotin-streptavidin-APC-Cy7 reporter (1st triad), a direct aCD9-FITC antibody (2nd triad) and direct CD36-FITC antibody (3rd triad). The bars show the distribution of fused nuclei into different MGC types; LGC, FBGC and SGC. Bars represent the mean ± SEM. N=25 for Total CI (FACS), N=3 for B-S samples & N=2 for all others. A Kruskal-Wallis Test with a post hoc Dunn's multiple comparisons test was used to compare the percentages of fused nuclei in 'like' MGC types in the Biotin-Streptavidin (B-S) triad. A subsequent Kruskal-Wallis & Dunn's test was performed comparing the Total CI (FACS) with the B-S CD9^{Low} and CD9^{High} results (blue).

more of the smaller LGC and fewer of the larger FBGC and SGC (85.79%:14.21%:0%) than the CD9^{High} (B-S) (29.56%:52.48%:17.96%). However, directly labelled CD9^{Low} and CD9^{High} did not produce a large discrepancy in the FBGC and SGC populations nor did they show any differences in the fusion parameters.

To see if the different labels were the cause of this discrepancy the indirectly labelled "Total CI (B-S)" were compared with the direct "Total CI (FACS)". The "Total CI (FACS)" were the values from the FACS purified CI monocytes that have been used in Chapter 4 to characterise the subset fusion (Figure 4.3). There was a significant increase in the % coverage of total CI (B-S) (24.79%) compared to the total CI (FACS) (11.19%; P=0.0405. Figure 5.6D: Orange star). The only difference between "Total CI (B-S)" and "Total CI (FACS)" was that the former was purified with an indirect biotin-streptavidin label and the latter was directly labelled. Thus, it appears as though the indirect B-S purification method was somehow causing cells to fuse at a greater rate (see Figure 5.12 and "5.3. Discussion" section).

As anti-CD9 antibodies have been shown in other studies to influence monocyte fusion behaviour (Parthasarathy *et al.*, 2009; Takeda *et al.*, 2003) we sought to target an alternative marker to separate CD9^{Low} and CD9^{High} CI monocytes. As the scavenger receptor CD36 has been shown to be highly co-expressed with CD9 (Huang *et al.*, 2011); it was selected as an alternative target for FACS sorting (Figure 2.4). The cells were all seeded at 1.5×10^5 cells well⁻¹ in ConA and allowed to fuse for 72hrs. Figure 5.6 and 5.7 show that the CD36^{Low} showed no significant differences in fusion behaviour to CD36^{High}. Furthermore, the CD36 sorted cells were no different to the directly labelled CD9 confirming that the B-S indirect tag was the source of the increased fusion in the B-S labelled cells and not because of the level of CD9 expression.

5.2.3 SURFACE EXPRESSION OF TETRASPANINS ON FACS SORTED MONOCYTE SUBSETS AFTER 4HRS CULTURE IN +/-CONA MEDIA.

To see if tetraspanin expression changed in response to fusion initiation the monocyte subsets were cultured for 4hrs with and without ConA then subjected to flow cytometry. Compared to the freshly isolated monocytes in Figure 5.1 there was a reduction in the overall MFI signal of every tetraspanin (Figure 5.8). After ConA stimulation, only CD53, CD37 and CD82 showed any significant variation with the untreated samples; the MFI values of CD53 and CD82 were both higher in the unstimulated samples. Though the MFIs of CD37 did not show any significant difference in the subsets there was very different reaction to ConA in the % positive cell parameter for CD37. The % positive of CI cells was notably lower in ConA treated CI ($P=0.1095$) and significantly lower in Int ($P=0.0134$) and NCI ($P=0.0013$).

Figure 5.9 shows all the subsets cultured in ConA compared to one another (Figure 5.8 compares ConA treated vs untreated subsets). The percentage of cells expressing CD37 was significantly higher in the Int than the CI ($P=0.0134$) but not to the NCI ($P=0.3193$). CD53 expression was significantly lower in NCI monocytes (MFI: 601) compared to CI (MFI: 1042; $P<0.0001$) and Int (MFI: 941; $P=0.0004$) monocytes. Both the percentage of cells expressing CD82 and the resultant MFIs were significantly higher in the CI cells compared to the Int and NCI cells. The histograms for ConA treated monocytes (Figure 5.10a-c) reveal that the expression of most of the tetraspanins is Gaussian. However, the expression of CD53 is bimodal in CI, negatively skewed in Int and positively skewed for NCI monocytes when treated with ConA (Figure 5.11). CD82 in ConA treated CI also possesses a bimodal distribution but the Int and NCI monocytes show a Gaussian distribution of expression.

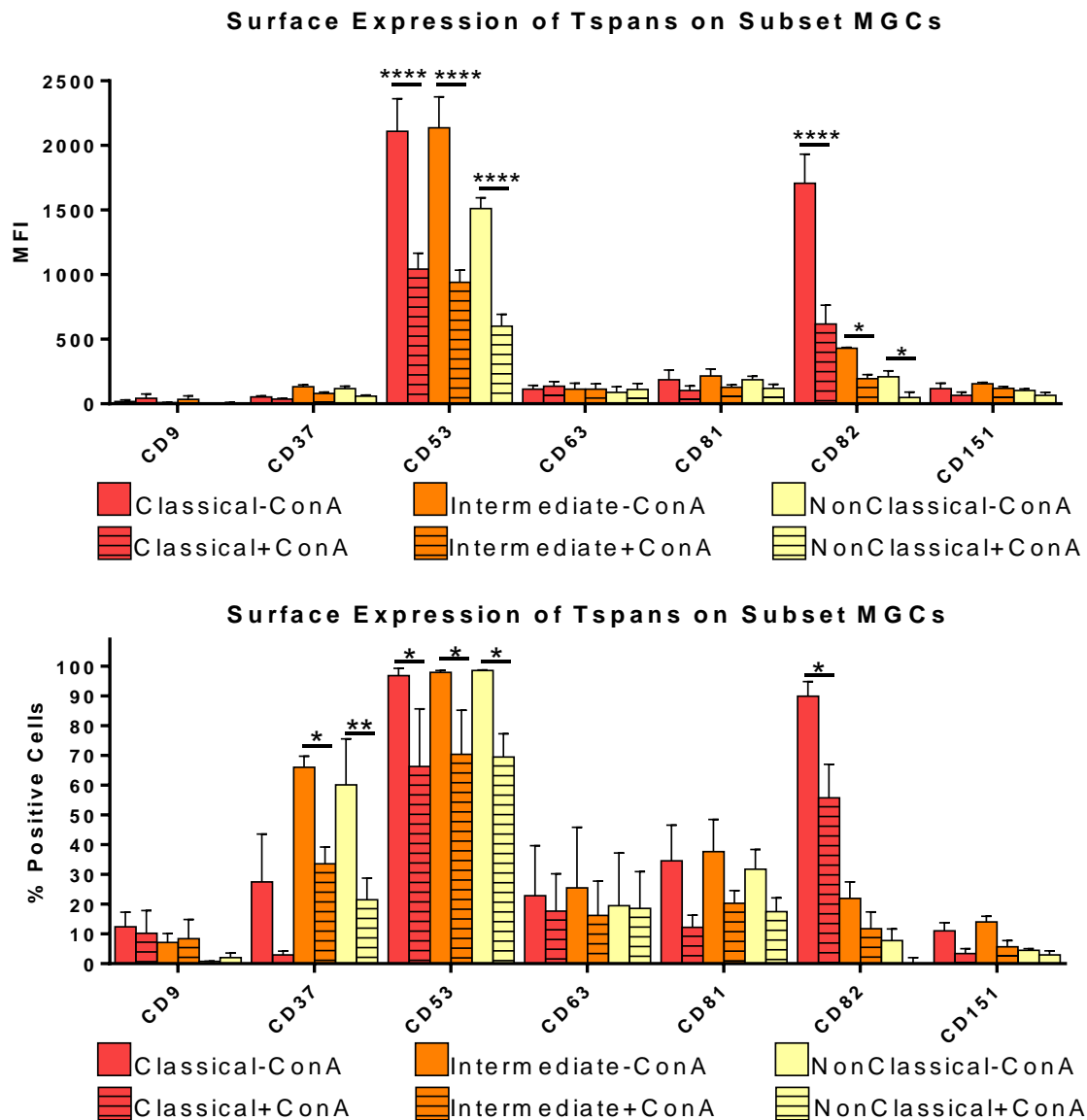


Figure 5.8: Surface Expression of Tetraspanins on FACS Sorted Monocyte Subsets After 4hrs Culture in +/-ConA Media.

Monocytes were first sorted by FACS into subsets, then cultured in normal cIMDM media (empty bars) or ConA media (banded bars) for 4hrs. Cells were then detached, stained and analysed for surface Tspan expression by flow cytometry. MFI and percentage positive graphs are shown above for each tetraspanin detected on the subset derived cells. Bars represent the mean±SEM, N=4. Tested with a two-way ANOVA with an Uncorrected Fisher's LSD post-hoc test to compare column means between cIMDM or cIMDM+ConA cultured subsets.

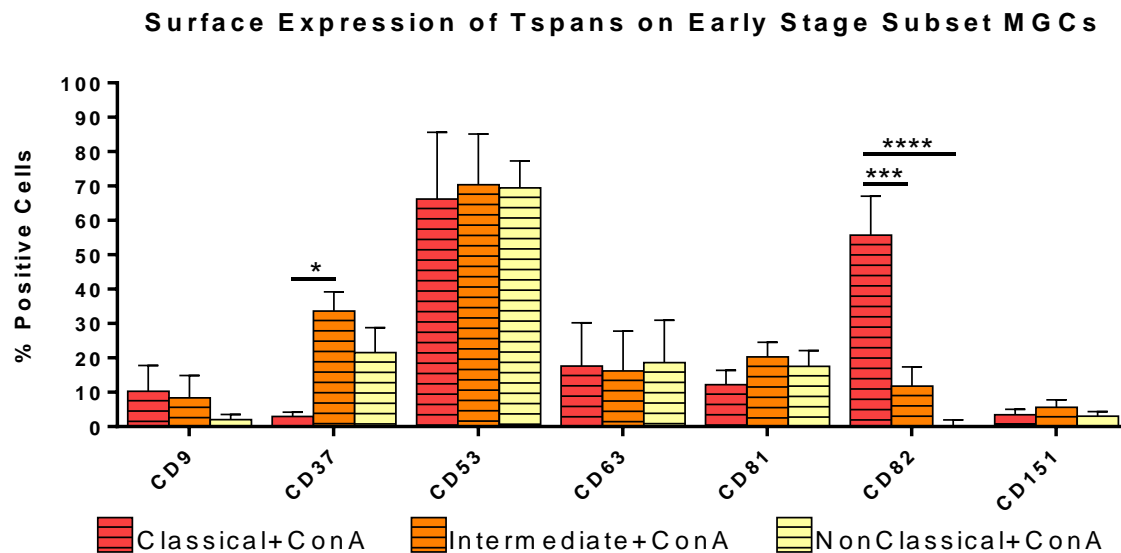
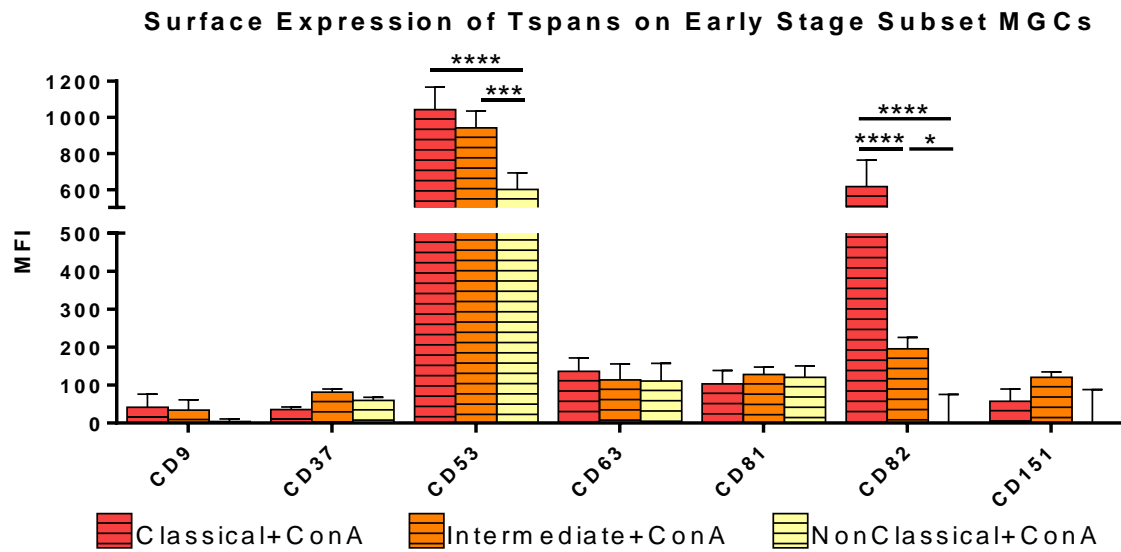


Figure 5.9: Comparison of Surface Tetraspanin Expression on FACS Sorted Monocyte Subsets After 4hrs Culturing in ConA Media.

Only the ConA samples and data from Figure 5.8 are shown above to allow comparison between the fusion-primed cells. MFI and percentage positive graphs are shown above for each tetraspanin detected on the subset derived cells. Bars represent the mean±SEM, N=4. Tested with a two-way ANOVA with an Uncorrected Fisher's LSD post-hoc test to compare column means in MFI or % positive between ConA exposed subset derived cells.

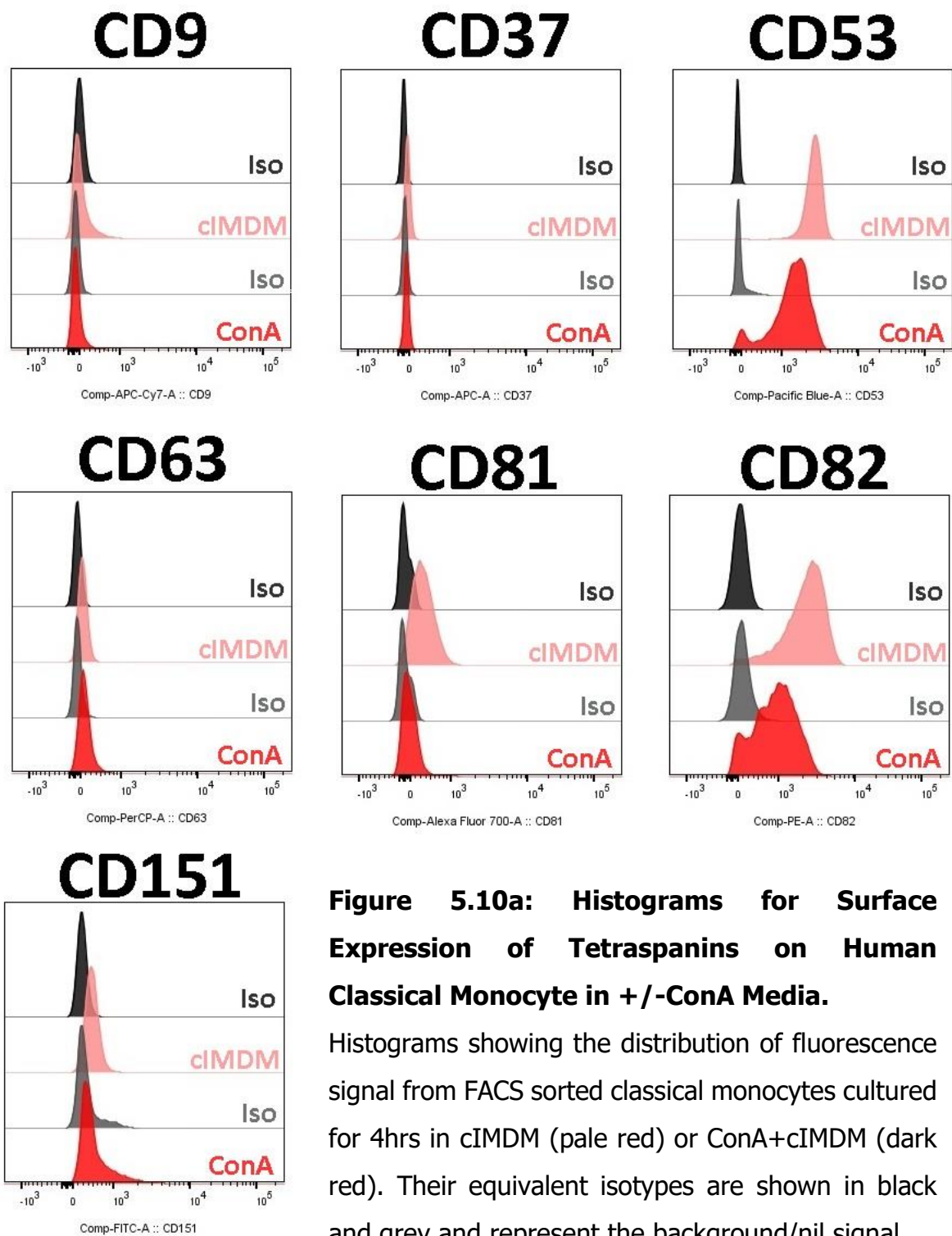


Figure 5.10a: Histograms for Surface Expression of Tetraspanins on Human Classical Monocyte in +/-ConA Media.

Histograms showing the distribution of fluorescence signal from FACS sorted classical monocytes cultured for 4hrs in cIMDM (pale red) or ConA+cIMDM (dark red). Their equivalent isotypes are shown in black and grey and represent the background/nil signal.

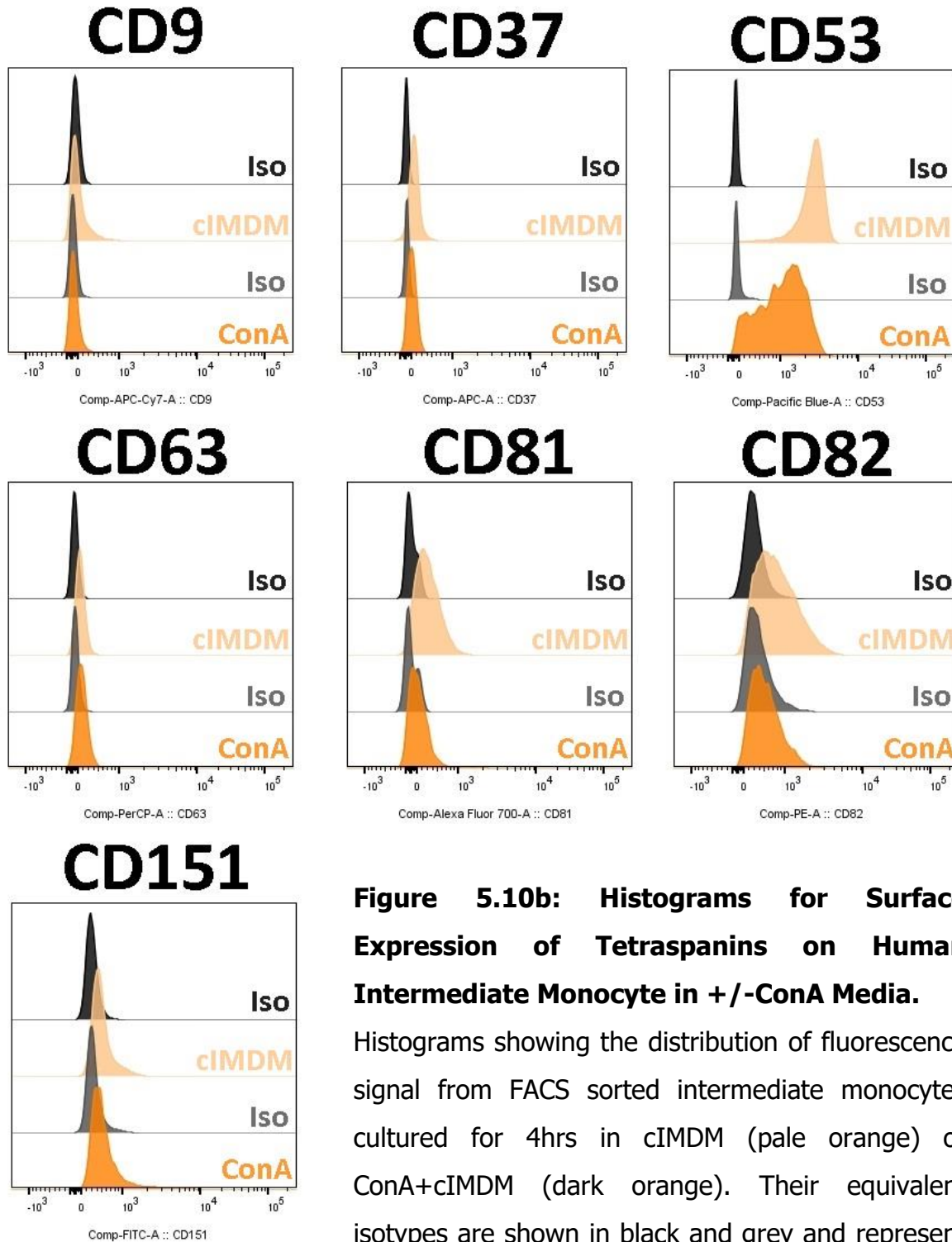


Figure 5.10b: Histograms for Surface Expression of Tetraspanins on Human Intermediate Monocyte in +/- ConA Media.

Histograms showing the distribution of fluorescence signal from FACS sorted intermediate monocytes cultured for 4hrs in cIMDM (pale orange) or ConA+cIMDM (dark orange). Their equivalent isotypes are shown in black and grey and represent the background/nil signal.

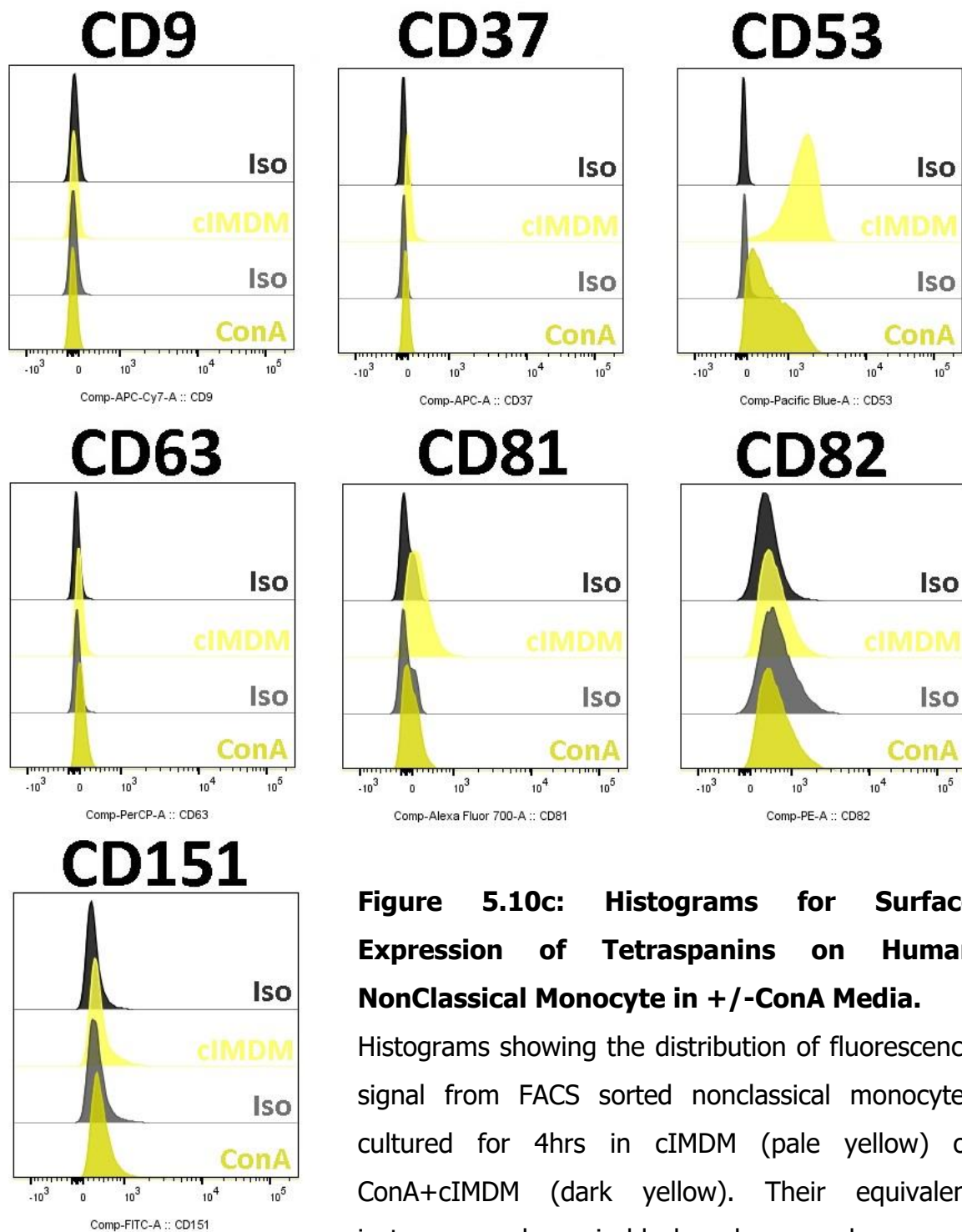
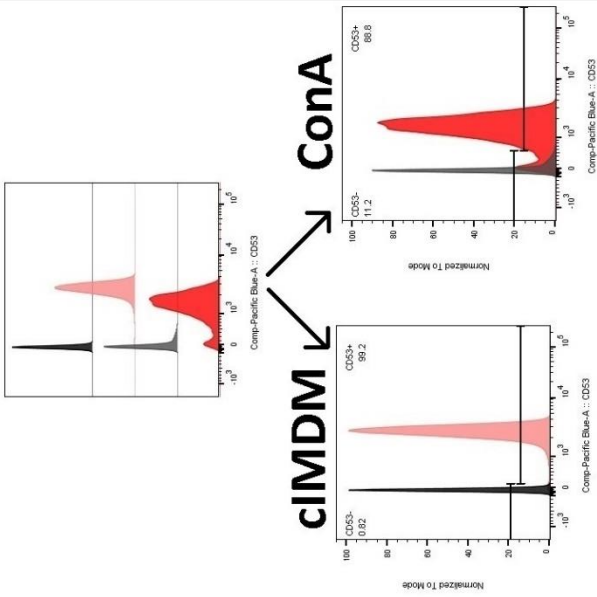


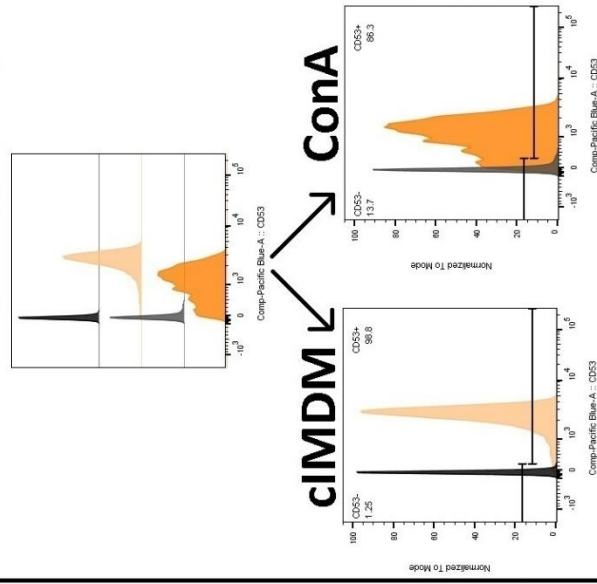
Figure 5.10c: Histograms for Surface Expression of Tetraspanins on Human NonClassical Monocyte in +/-ConA Media.

Histograms showing the distribution of fluorescence signal from FACS sorted nonclassical monocytes cultured for 4hrs in cIMDM (pale yellow) or ConA+cIMDM (dark yellow). Their equivalent isotypes are shown in black and grey and represent the background/nil signal.

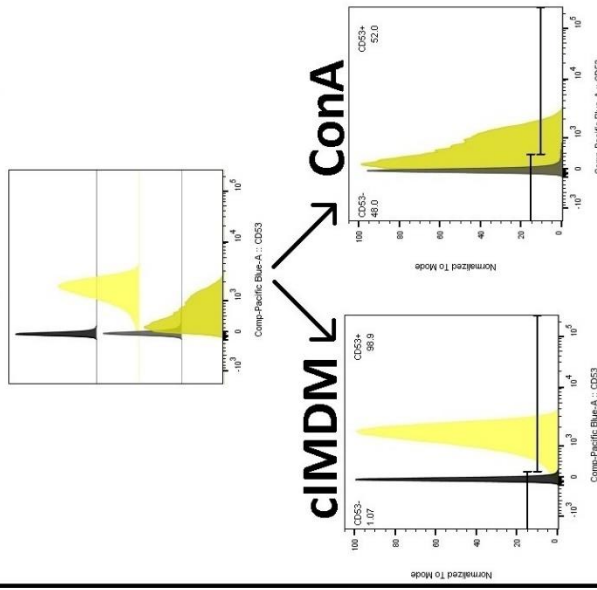
Classical CD53



Intermediate CD53



NonClassical CD53



Classical CD82

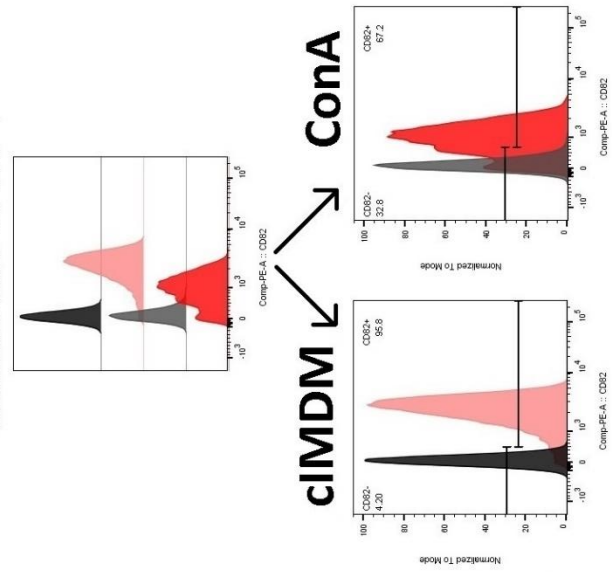


Figure 5.11: Quantification of Bimodal Populations in Fusion Initiated Monocyte Subsets.

The MFI signal repeatedly produced a bimodal peak for CD53 and CD82 for ConA cultured classical monocytes but not when cultured in cIMDM alone. A more negative skew for CD53 was observed in ConA cultured intermediate monocytes while nonclassical monocytes showed a positive skew. The positive signal for cIMDM or ConA+cIMDM is shown for each with limit bars included to show the percentage positive and negative as compared to the black/grey isotypes. CD82 was weakly bimodal in ConA cultured classical subsets but the same phenomenon was not observed in intermediate or nonclassical monocytes so they are not shown.

5.3 DISCUSSION

Intermediate Monocytes Are Tetraspanin Abundant

Depending on the species, cell type and proteome of a cell, a tetraspanin will have a wide range of different binding partners it can associate with and therefore facilitate many possible functions. For this reason it is particularly challenging to deduce the effect that changes in tetraspanin expression might have on cellular functions.

Freshly isolated Int monocytes expressed the highest levels of all tetraspanins except CD82 (highest in the Cl monocytes) and CD63 (equal expression in Cl and Int monocytes). The NCl monocytes had the lowest MFI and percentage of cells positive for CD9 and CD81. CD9 and CD81 have been already been described as fusion regulators (Takeda *et al.*, 2003) with decreased expression in mice resulting in greater degrees of fusion. CD9 forms partnerships with many proteins implicated in fusion: CD47 (Longhurst *et al.*, 1999), CD44 (Schmidt *et al.*, 2004; Yashiro-Ohtani *et al.*, 2000), CD36 (Huang *et al.*, 2011), MMP-9 (Herr *et al.*, 2013) and EWI-2 (Stipp *et al.*, 2001). The higher % of cells positive for CD37 and significantly higher MFI for CD53 in the Int could suggest the Int have a higher baseline of LFA-1 which has been observed in partnership with these tetraspanins (Todros-Dawda *et al.*, 2014; Wee *et al.*, 2015). The higher expression of LFA-1 could confer stronger cell-cell interactions through LFA-1:ICAM-1 binding and enhance fusion. It is unsurprising therefore that when separated and stimulated at equal densities the Int are able to produce larger giant cells at a much faster rate.

The Cl possessed the highest % positive cells and MFI signal for CD82, which has been shown to be important in associating with $\alpha V\beta 3$ (Ruseva *et al.*, 2009) and EWI-2 (Zhang *et al.*, 2003), thus, CD82 has the potential to facilitate surface adhesion and cytoskeletal rearrangements. Though we can only speculate on the binding partners of each tetraspanin in each subset what is clear is that they each have their own tetraspanin fingerprint.

ConA Treatment Induces an Overall Decrease in Tetraspanin Expression

The ConA treated cells showed a general reduction in expression levels and % positive cells (Figure 5.8). ConA induces a significant reduction in both the intensity and % of cells expressing CD53 and a reduction in the % of cells expressing CD37. CD37 and CD53 have both been shown to associate with LFA-1 which mediates cell-cell adhesion and cell crawling by binding and being internalised (Kinashi, 2005). Therefore the decrease in % positive cells for CD37 and CD53 may be a result of the cell becoming polarised upon binding the surface and facilitating increased internalisation of LFA-1 as part of the crawling mechanism. In accordance with this, the decrease in CD81 % positive cells could be a response to internalisation of EWI-2 which facilitates actin polymerisation around LFA-1. It is also possible that ConA enhances the formation of tight tetraspanin clusters (as observed by Zuidsherwoude *et al.* (2015) with MHC class II complexes) which may sterically hinder the binding of antibodies to all of the tightly packed tetraspanins.

CD37 was expressed on a significantly higher % population of ConA treated Int compared to ConA treated CI and NCI (Figure 5.9). This could suggest that the high fusion potential of the Int is largely mediated by its ability to produce more LFA-1 expressing cells compared to the other subsets. In accordance with this, the CI possessed the lowest % positive population of CD37 cells. Multiple studies have reported the effectiveness of anti-LFA-1 antibodies at inhibiting fusion (Gasser and Möst, 1999; Kazazi *et al.*, 1994; Möst *et al.*, 1990), therefore it is possible that co-expression of CD37 and LFA-1 are responsible for the Int high fusion potential.

Due to the increased clumping of ConA treated monocytes we were only able to analyse tetraspanin expression by flow cytometry up to 4hrs without risking blocking the cytometer. However, the significant differences in ConA treated and untreated cells suggests that within 4hrs the monocytes are responding to the ConA and are potentially fusion competent. Flow cytometric analysis into which fusion-related proteins are being trafficked by the tetraspanins is required to make more accurate conclusions. Furthermore, fluorescence microscopy could be used to investigate co-

expression of tetraspanins and fusion-related proteins at the surface at later time-points.

CD9^{High} CI Monocytes Express More CD63, CD81 and CD151

Initially we observed that the CI expression of CD9 was bimodal (Figure 5.2) and that there was a positive correlation between CD9 and CD151 (Figure 5.3). After gating the CI into CD9^{Low} and CD9^{High} we observed that the CD9^{High} cells also had increased (though not significant) expression of CD9, CD63, CD81 and CD151 (9.9-fold, 1.5-fold, 1.4-fold and 6.6-fold increase, respectively) (Figure 5.4). CD9 and CD151 both form associations with MMP-9 which has been shown to enhance migration and EWI-2 which enhances adhesion by linking adhesion proteins to the cytoskeleton. Furthermore, the increased CD63 could result in the CD9^{High} CI having higher expression of E-cadherin. Therefore, the CD9^{High} CI may be able to switch between highly motile or highly adherent behaviours by simply changing their expression of EWI-2 or MMP-9. Alternatively, the CD9^{High} CI could represent a small subset of CI maturing into Int, as Int express higher levels of these tetraspanins.

Suzuki et al (2009) observed that CD9 associates with CD14 to sequester it in a TEM to prevent the formation of the functional CD14:TLR4 LPS receptor. Therefore, it is possible that the CD9^{High} CI represent an LPS-insensitive population of the CI and have no differing fusion potential to CD9^{Low} CI.

Indirect Labelling Caused High Fusion Rates in CD9^{High} CI Monocytes

We hypothesised that these tetraspanin-high CI cells may show different fusion tendencies to the larger CD9^{Low} population. Initially, we sorted the CD9^{Low} and CD9^{High} CI using an anti-CD9-biotin primary antibody with a streptavidin-APC-Cy7 secondary reporter. The initial results indicated that CD9^{High} CI had a significantly higher fusion potential (Figure 5.6), however, when we compared with a directly labelled CD9-FITC or CD36-FITC antibody the increased fusion in CD9^{High} was lost.

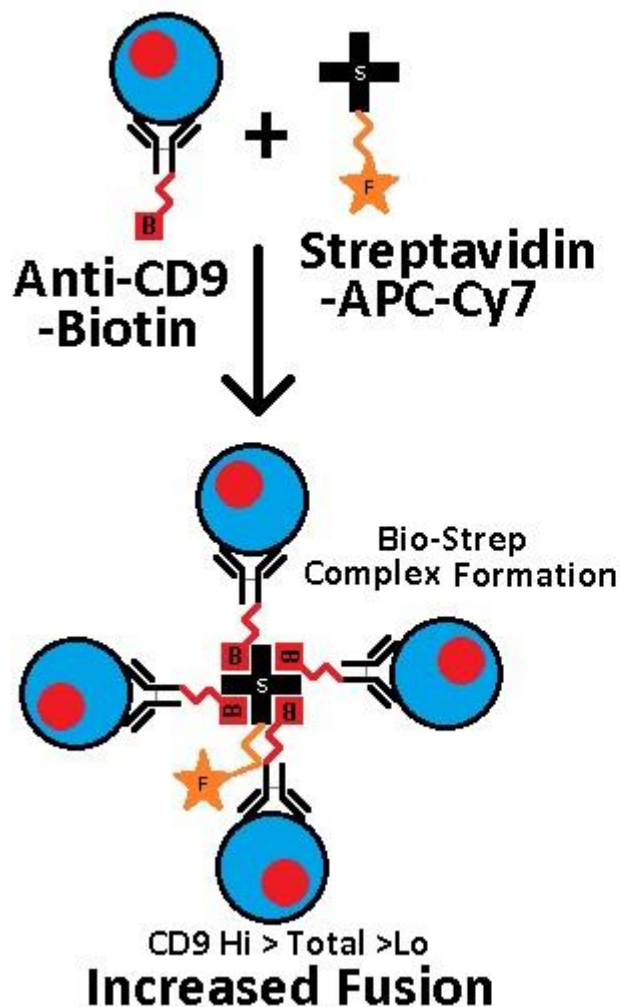
We postulated that because the streptavidin conjugate on the secondary reporter was multivalent (able to bind up to 4 biotin molecules) it was able to tether monocytes

together (Figure 5.12). This would explain why the fusion parameters for the CD9^{High} cells were so much greater than the CD9^{Low} CI. The function of the CD9^{High} CI remains unclear but it does not appear to represent a high-fusing subset of cells. We have also shown that an increase in cell-cell adhesion can significantly enhance the fusion potential of even the relatively low-fusing CI subset. Indeed, perhaps the Int and NCI subsets are able to fuse at a faster rate because they express a higher degree of cell-cell adherence proteins. It would be interesting to see if tethering other tetraspanins in the same way would produce similar increases in fusion or if this effect is specific to CD9 TEMs.

Conclusion:

It seems as though at steady state Int are particularly tetraspanin rich but upon treatment with ConA there is a significant reduction in the expression of tetraspanins involved in adhesion and cytoskeletal polymerisation (CD37, CD53 & CD82); possibly granting them higher motility. ConA also induced the Int to increase the % positive cells expressing CD9 while the opposite was true for CD81. This could indicate that the Int favour the expression of the CD47/CD44 components of the MFR complex as so far only CD9 has been shown to associate with CD47 (Longhurst *et al.*, 1999) and CD44 (Schmidt *et al.*, 2004; Yashiro-Ohtani *et al.*, 2000) and CD81 with MFR (Wang and Pfenninger, 2006). Though a CD9^{High} CI population was identified it did not show any differences in fusion potential compared to CD9^{Low} CI. Furthermore, we found that tethering monocytes by their CD9 molecules enhances fusion indicating that increased cell-cell contacts can enhance the fusibility of monocytes.

Indirect CD9 Labelling



Direct CD9 Labelling

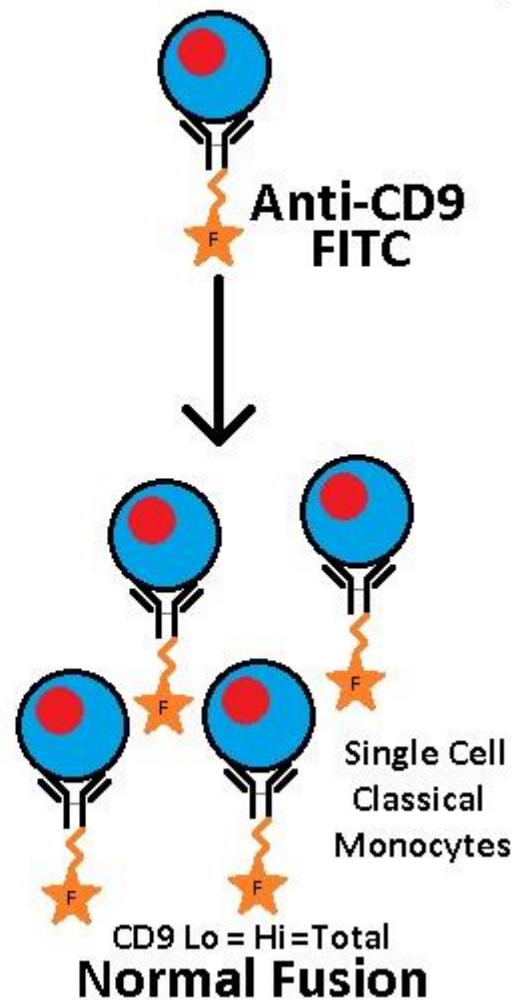


Figure 5.12: Theoretical Explanation for the Increased Fusion in Indirectly labelled CD9^{High} Classical Monocytes.

CD9^{High} Classical monocytes that were FACS purified with an indirect label had fusion parameters far higher than directly labelled equivalents, but the directly labelled cells did not. In the first stage of indirect labelling the monocytes are bound by the anti-CD9-biotin antibody, after washing a streptavidin-APC-Cy7 is added to bind the biotin with high affinity and produce a fluorescence signal. However streptavidin is a multivalent protein; up to four biotins are able to bind every one streptavidin. Once the classical monocytes are seeded after seeding it is possible that the CD9^{High} cells will clump and fuse faster because of the increased number of strong biotin-streptavidin links formed. Directly labelled CD9^{High} or CD36^{High} classical monocytes or did not show similar fusion behaviour.

CHAPTER 6: FINAL DISCUSSION

6.1 INTRODUCTION

Human monocytes are able to migrate from the bloodstream into the tissues and differentiate into M ϕ , moDC and MGC to respond to different pathogens and threats. Monocytes are themselves a heterogeneous population consisting of ~85% CI, ~5% Int and ~10% NCI at steady state and genetic analysis suggests that they mature from CI→Int→NCI (Martinez *et al.*, 2006). Each of the subsets show specialisation towards certain functions, thus they are also been regarded as CI: “phagocytic”, Int: “inflammatory” and NCI: “patrolling”. The blood populations of the Int and NCI have been observed to increase during certain diseases such as tuberculosis (Castaño *et al.*, 2011), Crohn’s disease (Grip *et al.*, 2007), hepatitis B (Zhang *et al.*, 2011a) and rheumatoid arthritis (Rossol *et al.*, 2012).

Monocytes form MGC (osteoclasts) in steady-state at the bone tissues to digest the bone and maintain bone homeostasis (Kotake *et al.*, 1999). However, monocytes also form inflammatory MGC such as Langhans giant cells in response to *Mycobacterium tuberculosis* infections and encase infected M ϕ with LGC to form a granuloma (Byrd, 1998). Alternatively, monocytes can fuse in response to medical implants to form FBGC (Anderson *et al.*, 2008). After fusing the FBGC forms a podosome, secretes acidic H⁺ containing vacuoles and digestive enzymes such as cathepsin K to break down the foreign body (Harkel *et al.*, 2015; Park *et al.*, 2013). The mechanics and mechanism of monocyte fusion is still largely unknown and only a handful of essential proteins have been identified. Furthermore, LGC and FBGC appear to be initiated by different cytokines which could suggest that they coordinate fusion utilising different signal transduction pathways (McNally and Anderson, 1995).

FBGC form in response to IL-4 which results in the activation of the STAT6 and the NF- κ B pathway (Goenka and Kaplan, 2011; Wurster *et al.*, 2000) while LGC form in response to IFN γ and STAT1 promotion (O’Shea *et al.*, 2015). The proteins that are transcribed from these gene upregulations grants the monocytes a fusion-competent

state. Fusion-competent monocytes secrete chemokines to attract more monocytes (CCL2 & CCL3), upregulate cell-cell adhesion proteins (LFA-1, ICAM-1 & E-cadherin) and fusion facilitating proteins such as (MFR, CD47, CD44, DC-STAMP & TREM-2). Once cell-cell contact has been established between two monocytes, they are pulled together and the actin cytoskeleton undergoes rearrangements and a common pathway of fusion mediated by pore-forming P2X7 is performed (Falzoni *et al.*, 1995; Pellegatti *et al.*, 2011).

Such a complex assembly of fusion-mediating proteins at the site of cell-cell contacts requires careful organisation of proteins. Tetraspanins are relatively small proteins that are able to associate homotypically with other tetraspanins and heterotypically with membrane proteins. CD9, CD37, CD53, CD63, CD81, CD82 and CD151 have all been shown to interact with monocyte fusion proteins and anti-tetraspanin antibodies have been shown to inhibit or enhance the formation of MGC (Parthasarathy *et al.*, 2009; Takeda *et al.*, 2003). Recently, CD9, CD53, CD63 and CD81 were shown to be expressed differently on the three monocyte subsets (Tippett *et al.*, 2013) indicating that monocyte subsets may respond differently in fusogenic conditions.

The aims of this study were to assess the effects of anti-tetraspanin antibodies on fusing monocytes, to determine if the monocyte subsets show different propensities to fusion and to determine if the monocyte subsets express different levels of tetraspanins. Further understanding of the contribution of monocyte subsets to fusion and the role tetraspanins play in the fusion process may help develop treatments for granulomatous diseases such as TB and inhibit foreign body reactions during medical implant rejection.

6.2 THESIS SUMMARY

In Chapter 3, we analysed the steps taken to optimise the fusion assay to allow increased sample sizes, higher monocyte purity, more accurate seeding densities and automated nuclei counting. We observed that MACS-purified monocytes fused more aggressively than monocytes purified by adherence. We demonstrated that treatment

of monocytes with anti-tetraspanin antibodies did not affect the adherence of monocytes. Treatment with anti-CD9 antibodies did not produce a significant fusion-enhancement effect as observed previously (Parthasarathy *et al.*, 2009; Takeda *et al.*, 2003). However, certain combinations of anti-tetraspanin antibodies reduced the fusion parameters far more than single antibody treatment. Most notably, combinations containing anti-CD82 and anti-CD151 produced the most significant decreases in fusion.

In Chapter 4, we demonstrated for the first time that monocyte subsets show very different propensities to form MGC in response to ConA stimulation. The Int fused faster and formed more of the larger FBGC and SGC types while the CI fused to form mostly the smaller LGC. We found that ConA induces the secretion of pro-inflammatory and pro-apoptotic cytokines in Int and CI but not NCI. Furthermore, all the subsets secreted chemokines CCL2 and CCL3 but not RANTES in response to ConA. Of the fusion-mediating cytokines, the CI and Int secreted more IL-4, IL-13, IL-17A and GM-CSF while NCI secreted more IL-3 by 48hrs and by the final time-point secreted the most IFN γ . Surprisingly, the monocyte subsets reacted differently to anti-tetraspanin antibodies. Only Int showed significant inhibition to fusion parameters in response to antibodies targeting CD9, CD53, CD63 and CD151.

In Chapter 5, we quantified the surface expression of CD9, CD37, CD53, CD63, CD81, CD82 and CD151 on the surface of the monocyte subsets and found that at steady-state the Int are particularly "tetraspanin rich". We then compared the expression of tetraspanins on ConA treated and untreated monocytes. In ConA the subsets all decrease in % population of CD37 and the intensity of CD53 and CD82 expression decreases. However, the high-fusing Int possess the highest % of cells expressing CD37, which can associate with LFA-1 to establish cell-cell contacts. Therefore the high fusion potential of the Int may be a result of CD37 and LFA-1 co-expression. Finally we identified a small population of CD9^{High} CI that also expressed higher levels of CD63, CD81 and CD151 compared to CD9^{Low}. However, the CD9^{High} CI did not show a greater ability to fuse.

6.3 DIFFERENTIAL EXPRESSION OF TETRASPANINS IN MONOCYTE SUBSETS

At steady-state, CD53 was expressed by 100% of monocytes in all subsets and was by far the most highly expressed tetraspanin observed. Our results for the % of cells expressing CD9, CD53, CD63 and CD81 and their respective expression levels (MFI) do not match those measured by Tippett *et al.* (2013), who observed overall higher % of cells expressing CD9 and CD63 in each subset. Furthermore, they found that the intensity of surface expression of CD9 was ranked Cl>Int>NCl, CD53 was NCL>Int>Cl and CD81 was NCL>Int>Cl whereas in our results all three tetraspanins were highest in Int. However, their CD14/CD16 gating strategy for classifying the subsets was far less restrictive as their subset gates all flowed into one another so there is less clear distinction between the subsets. Furthermore, in their report they do not mention any techniques to remove CD16-positive NK-cells which overlap with NCl in CD14/CD16 plots and could generate erroneous results.

Overall we found the Int to express the highest amounts of all tetraspanins at steady-state with the exception of CD82 which was expressed significantly higher in the Cl. The Cl showed an intriguing bimodal population for CD9 expression (Figure 5.2) and when all the tetraspanins were analysed for co-expression (Figure 5.3) it was clear that there was a positive correlation between CD9 and CD151 expression on Cl. When we gated the Cl into CD9^{Low} and CD9^{High} we observed notable but not significant increases in the surface expression of CD63, CD81 and CD151 but in fusion assays there was no difference in fusion potential. It is possible that these CD9^{High} cells represent an LPS-insensitive population of the Cl monocytes, however, further analysis will be required to confirm this hypothesis.

Though we demonstrated a new flow cytometry panel capable of quantifying seven of the most common tetraspanins in monocytes; there are still other members of the tetraspanin family that were not analysed. Other tetraspanins have been implicated in fusion; such as NET-6 and Tspan-5 which have been shown to decrease and increase in expression respectively in response to RANKL stimulation (Iwai *et al.*, 2007). Tarrant *et al.* (2002) knocked out Tssc6 in mice which produced T-cells that became hyper-stimulated by ConA. The quantification of surface tetraspanins with mass cytometry,

a flow cytometry technique that utilises antibodies tagged with heavy metal isotopes coupled with time-of-flight mass spectrometry allows for over 30 markers to be quantified at once (Bodenmiller *et al.*, 2012; Cheung and Utz, 2011). Using such a technique, it would be possible to measure all the tetraspanins and monocyte surface markers without compensation issues.

6.4 DIFFERENT FUSION POTENTIALS OF MONOCYTE SUBSETS

First it was observed that MACS-purified monocytes had a greater fusion potential than the adherence-purified monocytes. The MACS technique depleted all non-monocyte cells using microscopic magnetic beads coated with antibodies to non-monocytic cells. The adherence method relied on the ability of the monocytes to rapidly adhere to plastic surfaces. However, such a crude technique is vulnerable to contamination by T-cells and NK-cell which could enhance or subdue the cytokine signalling between fusing monocytes. The MACS technique did not rely on a washing step after seeding which also meant that more accurate seeding densities were possible whereas the adherence purified monocytes were seeded assuming ~15% of PBMCs would be monocytes.

We later found from the subset fusion kinetics (Figure 4.8) that not all subsets adhere equally; the Int and NCI were less adherent within the first 24hrs. This could mean that previous fusion studies that used the adherence method purified more of the initially adherent CI and fewer of the high-fusing Int and NCI. Furthermore, the differences in adherence and fusion in Figure 4.8 demonstrates that for subset observations; the fusion index (FI) is not a representative quantification of fusion. This is because FI reports on the ratio of fused to total cells but in the kinetics studies with the subsets it was clear that at some time-points the number of fused cells were the same between Int and NCI but the number of adherent unfused cells was different. This meant that despite initially seeding the same number of cells, the higher number of remaining single cells in the NCI was resulting in a lower FI. The “% of surface covered” measurement was introduced to provide a more accurate quantification of total fusion.

The Int subset was significantly more fusogenic than the other subsets and produced the highest measurements in all fusion parameters (Figure 4.3). For the first time, the MGC type formed from each subset was quantified (Figure 4.4) and showed that the Int and NCI showed a decidedly higher ability to form the larger FBGC and SGC types. Such an observation could have implications for the treatment of medical implant rejection as in our model it is clearly the Int and NCI forming the larger MGC associated with implant rejection. The increased ability of the CI subset to form LGC could mean that they are dedicated to responding to TB infections, as LGC are commonly found in granulomatous infections *in vivo*. Further studies with alternative fusion-inducing molecules needs to be conducted to confirm such a hypothesis. Screening FACS-purified subsets with BCG antigens or IL-4 and analysing their ability to form LGC and FBGC would reveal if the CI are indeed LGC precursors and Int/NCI FBGC precursors.

The subsets show remarkably different cytokine profiles during fusion (Figure 4.10a-c). The Int and CI rapidly secreted pro-apoptotic cytokines (TNF α) within the first 24hrs followed by an increase in pro-inflammatory cytokines (IL-1 α , IL-1 β and IL-6) by 48hrs. IL-1 α and IL-1 β has been shown to be released from cells undergoing apoptosis (Hogquist *et al.*, 1991) and we also observed at these same time-points that a large number of monocytes (57-65%) were dead or detached (Figure 4.8). This could mean that many ConA stimulated monocytes undergo apoptosis, which results in the release of internalised IL-1 and is a necessary step to generate the cytokines to promote fusion. ConA has been shown in human melanoma cell lines (Liu *et al.*, 2009) and mouse M ϕ (Suen *et al.*, 2000) to induce apoptosis by releasing cytochrome c from mitochondria and activating caspase 3 and 9. As the cytokines that we selected were predominantly fusion related molecules it is still too early to draw conclusions. By conducting an assay on the same cryopreserved samples targeting apoptosis markers, it may be possible to confirm if ConA does indeed create fusion-competent monocytes by first inducing some monocytes to commit apoptosis. Apoptosis already appears to be an important process in TB infections as uninfected bystander M ϕ have been observed to undergo apoptosis in close proximity to infected M ϕ (Kelly *et al.*, 2008). However, the NCI were able to achieve fusion rates greater than the CI but did not

release high levels of IL-1 α , IL-1 β or TNF α ; suggesting that they may not undergo apoptosis as a pre-requisite of fusion.

Though Int were observed to be the most fusogenic of the subsets (Figure 4.3 & Figure 4.4), the ConA-stimulated MACS-purified monocytes (Figure 3.6a-b and Figure 3.7) produced even higher fusion parameters and far more FBGC and SGC. This could indicate that even though the Int on their own are high-fusers, their potency is increased with the addition of the other two subsets. Considering that the CI consist of ~85% of blood monocytes at steady state it is possible that Int act as the "fusion initiators" and the CI are the "fusion acceptors". To confirm this the subsets would need to be FACS purified first to ensure absolute purity then recombined with each other at different ratios and seeded at equal densities in ConA. If certain subset combinations produce greater fusion rates than the single subset only equivalents then it would confirm that the subsets have an additive effect on one another.

6.5 ASSESSING THE ROLE OF TETRASPANINS WITH ANTI-TETRASPANIN ANTIBODIES

Anti-tetraspanin antibodies have been used in multiple studies to interfere with tetraspanin functions. In the initial total monocyte studies we observed that only anti-CD151 showed any significant inhibition to fusion in adherence purified monocytes, whereas in MACS purified monocytes, the formation of FBGC and SGC was inhibited by anti-CD63, and anti-CD81 appeared to enhance fusion. Unlike FACS purification, the adherence and MACs purification methods were never sufficient to produce ~100% pure monocyte cultures. Therefore, it is possible that these differences in anti-tetraspanin responses are due to their interaction with contaminating T-cells and NK-cells which are able to secrete cytokines in response to activation and may affect fusion. To ensure absolute purity, freshly isolated monocytes should first be FACS sorted with an anti-CD56 antibody to remove NK cells and seeded as a total population in the presence of ConA and anti-tetraspanin antibodies. This would ensure absolute purity and maintain the monocytes at a steady-state ratio of CI, Int and NCI.

The combination anti-tetraspanin antibody treatment yielded far more significant reductions in fusion parameters than single antibody treatment (Figure 3.8a-d). Combinations containing anti-CD82 or anti-CD151 showed the greatest inhibition to fusion while combinations containing anti-CD9 showed the lowest inhibition. As CD151 and CD82 share a common association with EWI-2 (Charrin *et al.*, 2001; Zhang *et al.*, 2003), we hypothesised that the decreases in fusion potential could be a result of antibody-bound CD82/CD151 interfering with the functions of EWI-2. As the monocytes in these experiments were all purified using adherence purification it is unclear whether the effects seen here are a result of antibody binding monocytes or contaminating lymphocytes. The combination antibody assay requires a large number of cells (at least 3.6 million) so it is not feasible to perform all 24 combinations on subsets in one donor. Therefore, many repeats with multiple donors will be required to account for the donor variability observed in monocyte fusion.

Interestingly, the anti-tetraspanin antibodies had a different effect on the subsets. The Int showed clear significant decreases in fusion parameters and MGC types produced when cultured in anti-CD9, anti-CD53, anti-CD63 and anti-CD151 (Figure 4.12, 4.13 and 4.14) whereas the CI and NCI did not. This suggests that the CI and NCI could be orchestrating fusion differently to the Int and that they possess different partner proteins interacting with these tetraspanins. Alternatively the lower baseline fusion rates of the CI and the NCI could be masking any notable reductions by these antibodies. Using siRNA targeting tetraspanin mRNA could be a potential improvement as it is still not clear whether antibodies binding tetraspanins block the binding of partner proteins or lock them in an active state etc. By knocking down the tetraspanins with siRNA we could ensure that the effects observed would be a direct result of specific tetraspanin downregulation.

Binding of CD9, CD53, CD63 and CD151 with antibodies may interfere with adherence and migration of monocytes resulting in decreased fusion. CD9 and CD151 have both been shown to interact with EWI-2 (Charrin *et al.*, 2001; Stipp *et al.*, 2001) which facilitates actin polymerisation at the sites of adhesion proteins. CD53 associates with LFA-1 (Todros-Dawda *et al.*, 2014) and CD63 knock-downs show arrested motility due

to insufficient β -catenin which facilitates actin polymerisation for E-cadherin (Huber *et al.*, 2014). Therefore, it is possible that the decrease in fusion is a result of arrested mobility and not interference of the fusion mechanics. Further quantification of the subsets' migratory abilities in the presence of anti-tetraspanin antibodies is necessary to determine if these antibodies are inhibiting fusion or migration.

The addition of ConA in the culture media induced significant decreases in the MFI of CD53 and CD82 and a decrease in the % population of cells expressing CD37, CD53 and CD82 (Figure 5.8). It appears as though ConA induces rapid loss of these tetraspanins, though it is still not known if the loss is a result of internalisation, shedding or decreased synthesis. The Int remain significantly high in CD37 expression (Figure 5.9) which could confer the Int a greater ability to form cell-cell interactions via LFA-1. By designing a flow panel targeting fusion proteins commonly associated with tetraspanins we would be able to ascertain what proteins are being internalised with the tetraspanins. Chiu *et al.* (2012) observed that the internalisation of DC-STAMP in RANKL stimulated DC resulted in enhanced fusion and the generation of a fusion leader population. Therefore the internalisation of these tetraspanins and their binding partners may be following a similar mechanism. Rather than forming fusion mediated TEMs the subsets may be playing an essential role as traffickers of other fusion proteins. By running a few repeated analysis on permeabilised cells it would be possible to ascertain if these tetraspanins have indeed been internalised.

6.6 CONCLUSION AND FUTURE DIRECTIONS

In this study we have shown that monocyte subsets possess different propensities to fuse with the smallest blood population, the Int, possessing the greatest ability to fuse and form larger FBGC and SGC. The CI subset though being the most abundant subset in the blood is conversely the least fusogenic of the subsets. The CI and Int secrete high levels of pro-inflammatory cytokines in our fusion assays suggesting they favour a more pro-inflammatory MGC types while the NCI appear to be far less inflammatory. The Int subset also expressed the highest levels of most of the tetraspanins we

observed. Within 4hrs of stimulation with ConA it appears as though all the monocyte subsets rapidly internalise or shed CD53 and CD82.

Further investigation is required on the effect of other cytokine treatments (such as IL-4 and IFN γ) on the subsets, investigating the possibility that the Int are "fusion leaders" and the analysis of tetraspanin associating fusion proteins during fusion. There is still much to be learned about the individual monocyte subset involvement in fusion and indeed the involvement of tetraspanins in this complex process. For every answer we get it seems a hundred new questions appear.

We have shown that monocyte subsets do indeed possess differing propensities to fusion which could have big implications for the future design of treatments against advanced granulomatous diseases and medical implant rejection. With the ever increasing life expectancies of the developed world the demand for medical implants and joint replacements is an ever growing concern. Our research can contribute to the understanding of foreign body rejection and aid in the development of treatments that could target Int monocytes that could be the primary source of FBGC.

BIBLIOGRAPHY

- Abeles, R.D., McPhail, M.J., Sowter, D., Antoniadou, C.G., Vergis, N., Vijay, G.K.M., Xystrakis, E., Khamri, W., Shawcross, D.L., Ma, Y., et al. (2012). CD14, CD16 and HLA-DR reliably identifies human monocytes and their subsets in the context of pathologically reduced HLA-DR expression by CD14(hi) /CD16(neg) monocytes: Expansion of CD14(hi) /CD16(pos) and contraction of CD14(lo) /CD16(pos) monocytes in a. *Cytometry* *81*, 823–834.
- Aeberli, D., Kamgang, R., Balani, D., Hofstetter, W., Villiger, P.M., and Seitz, M. (2016). Regulation of peripheral classical and non-classical monocytes on infliximab treatment in patients with rheumatoid arthritis and ankylosing spondylitis. *Rheum. Musculoskelet. Dis. Open* 3–7.
- Aguilar, P.S., Baylies, M.K., Fleissner, A., Helming, L., Inoue, N., Podbilewicz, B., Wang, H., and Wong, M. (2013). Genetic basis of cell-cell fusion mechanisms. *Trends Genet.* *29*, 427–437.
- Ajami, B., Bennett, J.L., Krieger, C., Tetzlaff, W., and Rossi, F.M. V (2007). Local self-renewal can sustain CNS microglia maintenance and function throughout adult life. *Nat. Neurosci.* *10*, 1538–1543.
- Alarcón, B., Mestre, D., and Martínez-Martín, N. (2011). The immunological synapse: A cause or consequence of T-cell receptor triggering? *Immunology* *133*, 420–425.
- Amano, S.U., Cohen, J.L., Vangala, P., Tencerova, M., Nicoloso, S.M., Yawe, J.C., Shen, Y., Czech, M.P., and Aouadi, M. (2014). Local proliferation of macrophages contributes to obesity-associated adipose tissue inflammation. *Cell Metab.* *19*, 162–171.
- Amir, O., Spivak, I., Lavi, I., and Rahat, M.A. (2012). Changes in the monocytic subsets CD14dimCD16+ and CD14++CD16- in chronic systolic heart failure patients. *Mediators Inflamm.* *2012*.
- Anderson, J.M., Rodriguez, A., and Chang, D.T. (2008). Foreign body reaction to

- biomaterials. *Semin. Immunol.* *20*, 86–100.
- Anderson, L., Dean, A., Falzon, D., Floyd, K., Baena, I.G., Gilpin, C., Glaziou, P., Hamada, Y., Hiatt, T., Char, A.K., et al. (2015). WHO Global Tuberculosis Report 2015 (20th Edition).
- André, M., Le Caer, J.-P., Greco, C., Planchon, S., El Nemer, W., Boucheix, C., Rubinstein, E., Chamot-Rooke, J., and Le Naour, F. (2006). Proteomic analysis of the tetraspanin web using LC-ESI-MS/MS and MALDI-FTICR-MS. *Proteomics* *6*, 1437–1449.
- Andreu, Z., and Yáñez-Mó, M. (2014). Tetraspanins in Extracellular Vesicle Formation and Function. *Front. Immunol.* *5*, 1–12.
- Angus, K.L., and Griffiths, G.M. (2013). Cell polarisation and the immunological synapse. *Curr. Opin. Cell Biol.* *25*, 1–7.
- Antonelli, L.R. V, Leoratti, F.M.S., Costa, P.A.C., Rocha, B.C., Diniz, S.Q., Tada, M.S., Pereira, D.B., Teixeira-Carvalho, A., Golenbock, D.T., Gonçalves, R., et al. (2014). The CD14+CD16+ inflammatory monocyte subset displays increased mitochondrial activity and effector function during acute *Plasmodium vivax* malaria. *PLoS Pathog.* *10*, e1004393.
- Aranday-Cortes, E., Bull, N.C., Villarreal-Ramos, B., Gough, J., Hicks, D., Ortiz-Peláez, J., Vordermeier, H.M., and Salguero, F.J. (2013). Upregulation of IL-17A, CXCL9 and CXCL10 in Early-Stage Granulomas Induced by *Mycobacterium bovis* in Cattle. *Transbound. Emerg. Dis.* *60*, 525–537.
- Arase, H., Mocarski, E.S., Campbell, A.E., Hill, A.B., and Lanier, L.L. (2002). Direct recognition of cytomegalovirus by activating and inhibitory NK cell receptors. *Science* *296*, 1323–1326.
- Athanasou, N.A., and Quinn, J. (1990). Immunophenotypic differences between osteoclasts and macrophage polykaryons: immunohistological distinction and implications for osteoclast ontogeny and function. *J. Clin. Pathol.* *43*, 997–1003.
- Bain, C.C., Bravo-Blas, A., Scott, C.L., Gomez Perdiguero, E., Geissmann, F., Henri, S., Malissen, B., Osborne, L.C., Artis, D., and Mowat, A.M. (2014). Constant

replenishment from circulating monocytes maintains the macrophage pool in the intestine of adult mice. *Nat. Immunol.* *15*, 929–937.

Banerjee, A., Dubnau, E., Quemard, A., Balasubramanian, V., Um, K.S., Wilson, T., Collins, D., de Lisle, G., and Jacobs, W.R. (1994). *inhA*, a gene encoding a target for isoniazid and ethionamide in *Mycobacterium tuberculosis*. *Science* *263*, 227–230.

Barbeck, M., Motta, A., Migliaresi, C., Sader, R., Kirkpatrick, C.J., and Ghanaati, S. (2016). Heterogeneity of biomaterial-induced multinucleated giant cells: Possible importance for the regeneration process? *J. Biomed. Mater. Res. - Part A* *104*, 413–418.

Barros, C., Crosby, J.A., and Moreno, R.D. (1996). Early steps of sperm-egg interactions during mammalian fertilization. *Cell Biol. Int.* *20*, 33–39.

Behar, S., Martin, C., Booty, M., Nishimura, T., Zhao, X., Gan, H., Divangahi, M., and Remold, H. (2010). Apoptosis is an innate defense function of macrophages against *Mycobacterium tuberculosis*. *Mucosal Immunol.* *48*, 1–6.

Berditchevski, F. (2001). Complexes of tetraspanins with integrins: more than meets the eye. *J. Cell Sci.* *114*, 4143–4151.

Berditchevski, F., and Odintsova, E. (1999). Characterization of integrin-tetraspanin adhesion complexes: Role of tetraspanins in integrin signaling. *J. Cell Biol.* *146*, 477–492.

Berditchevski, F., Gilbert, E., Griffiths, M.R., Fitter, S., Ashman, L., and Jenner, S.J. (2001). Analysis of the CD151 α 3 β 1 Integrin and CD151 Tetraspanin Interactions by Mutagenesis. *J. Biol. Chem.* *276*, 41165–41174.

Bianchi, E., Doe, B., Goulding, D., and Wright, G.J. (2014). Juno is the egg Izumo receptor and is essential for mammalian fertilization. *Nature* *508*, 483–487.

Blanchard, J.S. (1996). Molecular Mechanisms of Drug Resistance in Tuberculosis. *Annu. Rev. Biochem.* *65*, 215–239.

Bocchino, M., Galati, D., Sanduzzi, A., Colizzi, V., Brunetti, E., and Mancino, G. (2005). Role of mycobacteria-induced monocyte/macrophage apoptosis in the

- pathogenesis of human tuberculosis. *Int. J. Tuberc. Lung Dis.* *9*, 375–383.
- Bodenmiller, B., Zunder, E.R., Finck, R., Chen, T.J., Savig, E.S., Bruggner, R. V., Simonds, E.F., Bendall, S.C., Sachs, K., Krutzik, P.O., et al. (2012). Multiplexed mass cytometry profiling of cellular states perturbed by small-molecule regulators. *Nat. Biotechnol.* *30*, 858–867.
- Bold, T.D., and Ernst, J.D. (2009). Who Benefits from Granulomas, Mycobacteria or Host? *Cell* *136*, 17–19.
- Bos, S.D., Lakenberg, N., van der Breggen, R., Houwing-Duistermaat, J.J., Kloppenburg, M., de Craen, A.J.M., Beekman, M., Meulenbelt, I., and Slagboom, P.E. (2010). A genome-wide linkage scan reveals CD53 as an important regulator of innate TNF-alpha levels. *Eur. J. Hum. Genet.* *18*, 953–959.
- Van Den Bossche, J., Bogaert, P., Van Hengel, J., Guérin, C.J., Berx, G., Movahedi, K., Van Den Bergh, R., Pereira-Fernandes, A., Geuns, J.M.C., Pircher, H., et al. (2009). Alternatively activated macrophages engage in homotypic and heterotypic interactions through IL-4 and polyamine-induced E-cadherin/catenin complexes. *Blood* *114*, 4664–4674.
- Boucheix, C., and Rubinstein, E. (2001). Tetraspanins. *C. Cell. Mol. Life Sci.* *58*, 1189–1205.
- Brodbeck, W.G., Nakayama, Y., Matsuda, T., Colton, E., Ziats, N.P., and Anderson, J.M. (2002). Biomaterial Surface Chemistry Dictates Adherent Monocyte/Macrophage Cytokine Expression in Vitro. *Cytokine* *18*, 311–319.
- Byrd, T.F. (1998). Multinucleated giant cell formation induced by IFN-gamma/IL-3 is associated with restriction of virulent Mycobacterium tuberculosis cell to cell invasion in human monocyte monolayers. *Cell. Immunol.* *188*, 89–96.
- Cade, C.E., Dlouhy, A.C., Medzihradzky, K.F., Salas-Castillo, S.P., and Ghiladi, R.A. (2010). Isoniazid-resistance conferring mutations in Mycobacterium tuberculosis KatG: Catalase, peroxidase, and INH-NADH adduct formation activities. *Protein Sci.* *19*, 458–474.
- Cao, S., Zhang, X., Edwards, J.P., and Mosser, D.M. (2006). NF-kB1 (p50) homodimers

- differentially regulate pro- and anti-inflammatory cytokines in macrophages. *J. Biol. Chem.* *281*, 26041–26050.
- Castaño, D., García, L.F., and Rojas, M. (2011). Increased frequency and cell death of CD16 + monocytes with *Mycobacterium tuberculosis* infection. *Tuberculosis* *91*, 348–360.
- Chappuis, V., Cavusoglu, Y., Gruber, R., Kuchler, U., Buser, D., and Bosshardt, D.D. (2015). Osseointegration of Zirconia in the Presence of Multinucleated Giant Cells. *Clin. Implant Dent. Relat. Res.* 1–13.
- Charrin, S., Le Naour, F., Oualid, M., Billard, M., Faure, G., Hanash, S.M., Boucheix, C., and Rubinstein, E. (2001). The major CD9 and CD81 molecular partner. Identification and characterization of the complexes. *J. Biol. Chem.* *276*, 14329–14337.
- Charrin, S., Manié, S., Oualid, M., Billard, M., Boucheix, C., and Rubinstein, E. (2002). Differential stability of tetraspanin/tetraspanin interactions: role of palmitoylation. *FEBS Lett.* *516*, 139–144.
- Charrin, S., Manié, S., Billard, M., Ashman, L., Gerlier, D., Boucheix, C., and Rubinstein, E. (2003). Multiple levels of interactions within the tetraspanin web. *Biochem. Biophys. Res. Commun.* *304*, 107–112.
- Charrin, S., Latil, M., Soave, S., Poleskaya, A., Chrétien, F., Boucheix, C., and Rubinstein, E. (2013). Normal muscle regeneration requires tight control of muscle cell fusion by tetraspanins CD9 and CD81. *Nat. Commun.* *4*, 1674.
- Cheung, R.K., and Utz, P.J. (2011). Screening: CyTOF-the next generation of cell detection. *Nat. Rev. Rheumatol.* *7*, 502–503.
- Chiu, Y.H., Mensah, K.A., Schwarz, E.M., Ju, Y., Takahata, M., Feng, C., McMahon, L.A., Hicks, D.G., Panepento, B., Keng, P.C., et al. (2012). Regulation of human osteoclast development by dendritic cell-specific transmembrane protein (DC-STAMP). *J. Bone Miner. Res.* *27*, 79–92.
- Clarkson, S.B., and Ory, P.A. (1988). CD16. Developmentally regulated IgG Fc receptors on cultured human monocytes. *J Exp Med.* *167*, 408–420.

- Cluzel, C., Saltel, F., Lussi, J., Paulhe, F., Imhof, B.A., and Wehrle-Haller, B. (2005). The mechanisms and dynamics of $\alpha\text{v}\beta 3$ integrin clustering in living cells. *J. Cell Biol.* *171*, 383–392.
- Cody, J.J., Rivera, A. a, Liu, J., Liu, J.M., Douglas, J.T., and Feng, X. (2011). A simplified method for the generation of human osteoclasts in vitro. *Int. J. Biochem. Mol. Biol.* *2*, 183–189.
- Cole, L.A. (2010). Biological functions of hCG and hCG-related molecules. *Reprod. Biol. Endocrinol.* *8*, 102.
- Cooper, A.M. (2009). T cells in mycobacterial infection and disease. *Curr. Opin. Immunol.* *21*, 378–384.
- Costa, A.G., Cusano, N.E., Silva, B.C., Cremers, S., and Bilezikian, J.P. (2011). Cathepsin K: its skeletal actions and role as a therapeutic target in osteoporosis. *Nat. Rev. Rheumatol.* *7*, 447–456.
- Coury, F., Annels, N., Rivollier, A., Olsson, S., Santoro, A., Speziani, C., Azocar, O., Flacher, M., Djebali, S., Tebib, J., et al. (2008). Langerhans cell histiocytosis reveals a new IL-17A-dependent pathway of dendritic cell fusion. *Nat. Med.* *14*, 81–87.
- Crawford, A., Angelosanto, J.M., Nadwodny, K.L., Blackburn, S.D., and Wherry, E.J. (2011). A role for the chemokine RANTES in regulating CD8 T cell responses during chronic viral infection. *PLoS Pathog.* *7*.
- Cros, J., Cagnard, N., Woollard, K., Patey, N., Zhang, S.Y., Senechal, B., Puel, A., Biswas, S.K., Moshous, D., Picard, C., et al. (2010). Human CD14^{dim} Monocytes Patrol and Sense Nucleic Acids and Viruses via TLR7 and TLR8 Receptors. *Immunity* *33*, 375–386.
- Daenke, S., McCracken, S.A., and Booth, S. (1999). Human T-cell leukaemia/lymphoma virus type 1 syncytium formation is regulated in a cell-specific manner by ICAM-1, ICAM-3 and VCAM-1 and can be inhibited by antibodies to integrin B2 or B7. *J. Gen. Virol.* *80*, 1429–1436.
- Daniels, K. a, Devora, G., Lai, W.C., O'Donnell, C.L., Bennett, M., and Welsh, R.M.

- (2001). Murine cytomegalovirus is regulated by a discrete subset of natural killer cells reactive with monoclonal antibody to Ly49H. *J. Exp. Med.* *194*, 29–44.
- Davies, L.C., Jenkins, S.J., Allen, J.E., and Taylor, P.R. (2013). Tissue-resident macrophages. *Nat. Immunol.* *14*, 986–995.
- Davis, J.M., and Ramakrishnan, L. (2009). The Role of the Granuloma in Expansion and Dissemination of Early Tuberculous Infection. *Cell* *136*, 37–49.
- DeFife, K.M., Jenney, C.R., McNally, a K., Colton, E., and Anderson, J.M. (1997). Interleukin-13 induces human monocyte/macrophage fusion and macrophage mannose receptor expression. *J. Immunol.* *158*, 3385–3390.
- DeFife, K.M., Jenney, C.R., Colton, E., and Anderson, J.M. (1999). Cytoskeletal and adhesive structural polarizations accompany IL-13-induced human macrophage fusion. *J. Histochem. Cytochem.* *47*, 65–74.
- Deshmane, S.L., Kremlev, S., Amini, S., and Sawaya, B.E. (2009). Monocyte Chemoattractant Protein-1 (MCP-1): An Overview. *J. Interf. Cytokine Res.* *29*, 313–326.
- Epand, R.M. (2003). Fusion peptides and the mechanism of viral fusion. *Biochim. Biophys. Acta - Biomembr.* *1614*, 116–121.
- Epelman, S., Lavine, K.J., Beaudin, A.E., Sojka, D.K., Carrero, J.A., Calderon, B., Brija, T., Gautier, E.L., Ivanov, S., Satpathy, A.T., et al. (2014). Embryonic and adult-derived resident cardiac macrophages are maintained through distinct mechanisms at steady state and during inflammation. *Immunity* *40*, 91–104.
- Fadok, V. a, Warner, M.L., Bratton, D.L., and Henson, P.M. (1998). CD36 is required for phagocytosis of apoptotic cells by human macrophages that use either a phosphatidylserine receptor or the vitronectin receptor (alpha v beta 3). *J. Immunol.* *161*, 6250–6257.
- Falzoni, S., Munerati, M., Ferrari, D., Spisani, S., Moretti, S., and Di Virgilio, F. (1995). The purinergic P2Z receptor of human macrophage cells. Characterization and possible physiological role. *J. Clin. Invest.* *95*, 1207–1216.
- Floyd, D.L., Ragains, J.R., Skehel, J.J., Harrison, S.C., and van Oijen, A.M. (2008).

- Single-particle kinetics of influenza virus membrane fusion. *Proc. Natl. Acad. Sci. U. S. A.* *105*, 15382–15387.
- Flynn, J.L., and Chan, J. (2001). Immunology of Tuberculosis. *Annu. Rev. Immunol* *19*, 93–129.
- Fogg, D., Sibon, C., Miled, C., Jung, S., Aucouturier, P., Littman, D.R., Cumano, A., and Geissmann, F. (2006). A Clonogenic Bone Marrow Progenitor Specific for Macrophages and Dendritic Cells. *Science (80-.)*. *311*, 83–88.
- van Furth, R., Cohn, Z.A., Hirsch, J.G., Humphrey, J.H., Spector, W.G., and Langevoort, H.L. (1972). The mononuclear phagocyte system: a new classification of macrophages, monocytes, and their precursor cells. *Bull. World Health Organ.* *46*, 845–852.
- Ganz, T. (2012). Macrophages and systemic iron homeostasis. *J. Innate Immun.* *4*, 446–453.
- Garner, J.M., Herr, M.J., Hodges, K.B., and Jennings, L.K. (2016). The utility of tetraspanin CD9 as a biomarker for metastatic clear cell renal cell carcinoma. *Biochem. Biophys. Res. Commun.* *471*, 21–25.
- Gasser, a, and Möst, J. (1999). Generation of multinucleated giant cells in vitro by culture of human monocytes with *Mycobacterium bovis* BCG in combination with cytokine-containing supernatants. *Infect. Immun.* *67*, 395–402.
- Geissmann, F., Jung, S., and Littman, D.R. (2003). Blood monocytes consist of two principal subsets with distinct migratory properties. *Immunity* *19*, 71–82.
- Gerbaud, P., and Pidoux, G. (2015). Review: An overview of molecular events occurring in human trophoblast fusion. *Placenta* *36*, S35–S42.
- Gillespie, S. (2002). Evolution of drug resistance in *Mycobacterium tuberculosis*: clinical and molecular perspective. *Antimicrob. Agents Chemother.* *46*, 267–274.
- Goenka, S., and Kaplan, M.H. (2011). Transcriptional regulation by STAT6. *Immunol. Res.* *50*, 87–96.
- Gordon, S., and Taylor, P.R. (2005). Monocyte and macrophage heterogeneity. *Nat.*

Rev. Immunol. *5*, 953–964.

- Gordon, A.H., Hart, P.D., and Young, M.R. (1980). Ammonia inhibits phagosome–lysosome fusion in macrophages. *Nature* *286*, 79–80.
- Goren, M.B., D’Arcy Hart, P., Young, M.R., and Armstrong, J.A. (1976). Prevention of phagosome-lysosome fusion in cultured macrophages by sulfatides of *Mycobacterium tuberculosis*. *Proc. Natl. Acad. Sci. U. S. A.* *73*, 2510–2514.
- Grage-Griebenow, E., Zawatzky, R., Kahlert, H., Brade, L., Flad, H., and Ernst, M. (2001). Identification of a novel dendritic cell-like subset of CD64(+) / CD16(+) blood monocytes. *Eur. J. Immunol.* *31*, 48–56.
- Gratkowski, H., Lear, J.D., and DeGrado, W.F. (2001). Polar side chains drive the association of model transmembrane peptides. *Proc. Natl. Acad. Sci.* *98*, 880–885.
- Greenberg, M.E., Sun, M., Zhang, R., Febbraio, M., Silverstein, R., and Hazen, S.L. (2006). Oxidized phosphatidylserine-CD36 interactions play an essential role in macrophage-dependent phagocytosis of apoptotic cells. *J. Exp. Med.* *203*, 2613–2625.
- Griffith, J.W., Sokol, C.L., and Luster, A.D. (2014). Chemokines and chemokine receptors: positioning cells for host defense and immunity. *Annu. Rev. Immunol.* *32*, 659–702.
- Grip, O., Bredberg, A., Lindgren, S., and Henriksson, G. (2007). Increased subpopulations of CD16+ and CD56+ blood monocytes in patients with active Crohn’s disease. *Inflamm. Bowel Dis.* *13*, 566–572.
- Guilliams, M., and van de Laar, L. (2015). A Hitchhiker’s Guide to Myeloid Cell Subsets: Practical Implementation of a Novel Mononuclear Phagocyte Classification System. *Front. Immunol.* *6*, 406.
- Guilliams, M., Ginhoux, F., Jakubzick, C., Naik, S.H., Onai, N., Schraml, B.U., Segura, E., Tussiwand, R., and Yona, S. (2014). Dendritic cells, monocytes and macrophages: a unified nomenclature based on ontogeny. *Nat. Rev. Immunol.* *14* *VN-r*, 571–578.

- Guirado, E., and Schlesinger, L.S. (2013). Modeling the Mycobacterium tuberculosis Granuloma - the Critical Battlefield in Host Immunity and Disease. *Front. Immunol.* *4*, 98.
- Guleria, I., and Sayegh, M.H. (2007). Maternal acceptance of the fetus: true human tolerance. *J. Immunol.* *178*, 3345–3351.
- Han, X., Sterling, H., Chen, Y., Saginario, C., Brown, E.J., Frazier, W.A., Lindberg, F.P., and Vignery, A. (2000). CD47, a ligand for the macrophage fusion receptor, participates in macrophage multinucleation. *J. Biol. Chem.* *275*, 37984–37992.
- Handsuh, K., Guibourdenche, J., Tsatsaris, V., Guesnon, M., Laurendeau, I., Evain-Brion, D., and Fournier, T. (2007). Human chorionic gonadotropin produced by the invasive trophoblast but not the villous trophoblast promotes cell invasion and is down-regulated by peroxisome proliferator-activated receptor- γ . *Endocrinology* *148*, 5011–5019.
- Hanna, R.N., Cekic, C., Sag, D., Tacke, R., Thomas, G.D., Nowyhed, H., Herrley, E., Rasquinha, N., McArdle, S., Wu, R., et al. (2015). Patrolling monocytes control tumor metastasis to the lung. *Science* *350*, 1–9.
- Harkel, B. Ten, Schoenmaker, T., Picavet, D.I., Davison, N.L., De Vries, T.J., and Everts, V. (2015). The foreign body giant cell cannot resorb bone, but dissolves hydroxyapatite like osteoclasts. *PLoS One* *10*, 1–19.
- Hashimoto, D., Chow, A., Noizat, C., Teo, P., Beasley, M.B., Leboeuf, M., Becker, C.D., See, P., Price, J., Lucas, D., et al. (2013). Tissue-resident macrophages self-maintain locally throughout adult life with minimal contribution from circulating monocytes. *Immunity* *38*, 792–804.
- Hayman, A.R. (2008). Tartrate-resistant acid phosphatase (TRAP) and the osteoclast/immune cell dichotomy. *Autoimmunity* *41*, 218–223.
- Helming, L., Tomasello, E., Kyriakides, T.R., Martinez, F.O., Takai, T., Gordon, S., and Vivier, E. (2008). Essential Role of DAP12 Signaling in Macrophage Programming into a Fusion-Competent State. *Sci Signal* *1*, 1621–1629.
- Helming, L., Winter, J., and Gordon, S. (2009). The scavenger receptor CD36 plays a

- role in cytokine-induced macrophage fusion. *J. Cell Sci.* *122*, 453–459.
- Hemler, M.E. (2001). Specific tetraspanin functions. *J. Cell Biol.* *155*, 1103–1107.
- Hemler, M.E. (2003). Tetraspanin proteins mediate cellular penetration, invasion, and fusion events and define a novel type of membrane microdomain. *Annu. Rev. Cell Dev. Biol.* *19*, 397–422.
- Hemler, M.E. (2005). Tetraspanin functions and associated microdomains. *Nat. Rev. Mol. Cell Biol.* *6*, 801–811.
- Hemler, M.E. (2008). Targeting of tetraspanin proteins--potential benefits and strategies. *Nat. Rev. Drug Discov.* *7*, 747–758.
- Henkle, K.J., Davern, K.M., Wright, M.D., Ramos, A.J., and Mitchell, G.F. (1990). Comparison of the cloned genes of the 26- and 28-kilodalton glutathione S-transferases of *Schistosoma japonicum* and *Schistosoma mansoni*. *Mol. Biochem. Parasitol.* *40*, 23–34.
- Herr, M.J., Kotha, J., Hagedorn, N., Smith, B., and Jennings, L.K. (2013). Tetraspanin CD9 Promotes the Invasive Phenotype of Human Fibrosarcoma Cells via Upregulation of Matrix Metalloproteinase-9. *PLoS One* *8*, e67766.
- Hettinger, J., Richards, D.M., Hansson, J., Barra, M.M., Joschko, A.-C., Krijgsveld, J., and Feuerer, M. (2013). Origin of monocytes and macrophages in a committed progenitor. *Nat. Immunol.* *14*, 821–830.
- Hildreth, J.E. (1998). Syncytium-inhibiting monoclonal antibodies produced against human T-cell lymphotropic virus type 1-infected cells recognize class II major histocompatibility complex molecules and block by protein crowding. *J. Virol.* *72*, 9544–9552.
- Hildreth, J.E., Subramaniam, a, and Hampton, R. a (1997). Human T-cell lymphotropic virus type 1 (HTLV-1)-induced syncytium formation mediated by vascular cell adhesion molecule-1: evidence for involvement of cell adhesion molecules in HTLV-1 biology. *J. Virol.* *71*, 1173–1180.
- Hill, D.J., Crace, C.J., Strain, A.J., and Milner, R.D.G. (1986). Regulation of Amino Acid Uptake and Deoxyribonucleic Acid Synthesis in Isolated Human Fetal Fibroblasts

- and Myoblasts: Effect of Human Placental Lactogen, Somatomedin-C, Multiplication-Stimulating Activity, and Insulin. *J. Clin. Endocrinol. Metab.* *62*, 753–760.
- Hinz, M., Lemke, P., Anagnostopoulos, I., Hacker, C., Krappmann, D., Mathas, S., Dörken, B., Zenke, M., Stein, H., and Scheidereit, C. (2002). Nuclear Factor KappaB Dependent Gene Expression Profiling of Hodgkin's Disease Tumor Cells, Pathogenetic Significance, and Link to Constitutive Signal Transducer and Activator of Transcription 5a Activity. *J. Exp. Med.* *196*, 605–617.
- Hiscott, J., Marois, J., Garoufalos, J., D'Addario, M., Roulston, A., Kwan, I., Pepin, N., Lacoste, J., Nguyen, H., and Bensi, G. (1993). Characterization of a functional NF-kappa B site in the human interleukin 1 beta promoter: evidence for a positive autoregulatory loop. *Mol. Cell. Biol.* *13*, 6231–6240.
- Hogquist, K.A., Nett, M.A., Unanue, E.R., and Chaplin, D.D. (1991). Interleukin 1 is processed and released during apoptosis. *Proc Natl Acad Sci U S A* *88*, 8485–8489.
- Hong, I.K., Jin, Y.J., Byun, H.J., Jeoung, D. Il, Kim, Y.M., and Lee, H. (2006). Homophilic interactions of tetraspanin CD151 up-regulate motility and matrix metalloproteinase-9 expression of human melanoma cells through adhesion-dependent c-Jun activation signaling pathways. *J. Biol. Chem.* *281*, 24279–24292.
- Hsieh, C.L., Koike, M., Spusta, S.C., Niemi, E.C., Yenari, M., Nakamura, M.C., and Seaman, W.E. (2009). A role for TREM2 ligands in the phagocytosis of apoptotic neuronal cells by microglia. *J. Neurochem.* *109*, 1144–1156.
- Huang, W., Febbraio, M., and Silverstein, R.L. (2011). CD9 tetraspanin interacts with CD36 on the surface of macrophages: A possible regulatory influence on uptake of oxidized low density lipoprotein. *PLoS One* *6*.
- Huber, A.M., Mamyrova, G., Lachenbruch, P. a, Lee, J. a, Katz, J.D., Targoff, I.N., Miller, F.W., and Rider, L.G. (2014). Early illness features associated with mortality in the juvenile idiopathic inflammatory myopathies.

- Hulme, R.S., Higginbottom, A., Palmer, J., Partridge, L.J., and Monk, P.N. (2014). Distinct regions of the large extracellular domain of tetraspanin CD9 are involved in the control of human multinucleated giant cell formation. *PLoS One* *9*, e116289.
- Huppertz, B., and Gauster, M. (2011). Trophoblast fusion. *Adv. Exp. Med. Biol.* *713*, 81–95.
- Hynes, R.O. (2002). Integrins: Bidirectional, allosteric signaling machines. *Cell* *110*, 673–687.
- Ikeda, T., Ikeda, K., Sasaki, K., Kawakami, K., Hatake, K., Kaji, Y., Norimatsu, H., Harada, M., and Takahara, J. (1998). IL-13 as well as IL-4 induces monocytes/macrophages and a monoblastic cell line (UG3) to differentiate into multinucleated giant cells in the presence of M-CSF. *Biochem. Biophys. Res. Commun.* *253*, 265–272.
- Imaizumi, Y., Eguchi, K., Imada, H., Hidano, K., Nijima, S., Kawata, H., Fukushima, N., Saito, T., Hiroe, M., and Kario, K. (2016). Electron Microscopy of Contact Between a Monocyte and a Multinucleated Giant Cell in Cardiac Sarcoidosis. *Can. J. Cardiol.* 1–2.
- Ingersoll, M., Spanbroek, R., Lottaz, C., Gautier, E., Frankenberger, M., Hoffmann, R., Lang, R., Haniffa, M., Collin, M., Tacke, F., et al. (2010). Comparison of gene expression profiles between human and mouse monocyte subsets. *Blood* *115*, 10–20.
- Inoue, N., Ikawa, M., Isotani, A., and Okabe, M. (2005). The immunoglobulin superfamily protein Izumo is required for sperm to fuse with eggs. *Nature* *434*, 234–238.
- Iwai, K., Ishii, M., Ohshima, S., Miyatake, K., and Saeki, Y. (2007). Expression and function of transmembrane-4 superfamily (tetraspanin) proteins in osteoclasts: reciprocal roles of Tspan-5 and NET-6 during osteoclastogenesis. *Allergol. Int.* *56*, 457–463.
- Izawa, T., Zou, W., Chappel, J.C., Ashley, J.W., Feng, X., and Teitelbaum, S.L. (2012).

- c-Src links a RANK/ α v β 3 integrin complex to the osteoclast cytoskeleton. *Mol. Cell. Biol.* *32*, 2943–2953.
- Jaguin, M., Houlbert, N., Fardel, O., and Lecreur, V. (2013). Polarization profiles of human M-CSF-generated macrophages and comparison of M1-markers in classically activated macrophages from GM-CSF and M-CSF origin. *Cell. Immunol.* *281*, 51–61.
- Jakubzick, C., Gautier, E.L., Gibbings, S.L., Sojka, D.K., Schlitzer, A., Johnson, T.E., Ivanov, S., Duan, Q., Bala, S., Condon, T., et al. (2013). Minimal differentiation of classical monocytes as they survey steady-state tissues and transport antigen to lymph nodes. *Immunity* *39*, 599–610.
- Jarlier, V., and Nikaido, H. (1994). Mycobacterial cell wall: structure and role in natural resistance to antibiotics. *FEMS Microbiol. Lett.* *123*, 11–18.
- Kaji, K., Oda, S., Shikano, T., Ohnuki, T., Uematsu, Y., Sakagami, J., Tada, N., Miyazaki, S., and Kudo, A. (2000). The gamete fusion process is defective in eggs of CD9-deficient mice. *Nat. Genet.* *24*, 279–282.
- Kanitakis, J., Petruzzo, P., and Dubernard, J.-M. (2004). Turnover of epidermal Langerhans' cells. *N. Engl. J. Med.* *351*, 2661–2662.
- Kashef, J., Diana, T., Oelgeschläger, M., and Nazarenko, I. (2012). Expression of the tetraspanin family members Tspan3, Tspan4, Tspan5 and Tspan7 during *Xenopus laevis* embryonic development. *Gene Expr. Patterns* *13*, 1–11.
- Kasugai, C., Morikawa, A., Naiki, Y., Koide, N., Komatsu, T., Yoshida, T., and Yokochi, T. (2009). Concanavalin A induces formation of osteoclast-like cells in RAW 264.7 mouse macrophage cells. *Immunopharmacol. Immunotoxicol.* *31*, 103–107.
- Kazarov, A.R., Yang, X., Stipp, C.S., Sehgal, B., and Hemler, M.E. (2002). An extracellular site on tetraspanin CD151 determines α 3 and α 6 integrin-dependent cellular morphology. *J. Cell Biol.* *158*, 1299–1309.
- Kazazi, F., Chang, J., Lopez, A., Vadas, M., and Cunningham, A.L. (1994). Interleukin 4 and human immunodeficiency virus stimulate LFA-1-ICAM-1-mediated

- aggregation of monocytes and subsequent giant cell formation. *J. Gen. Virol.* *75*, 2795–2802.
- Kelly, D.M., Ten Bokum, A.M.C., O’Leary, S.M., O’Sullivan, M.P., and Keane, J. (2008). Bystander macrophage apoptosis after *Mycobacterium tuberculosis* H37Ra infection. *Infect. Immun.* *76*, 351–360.
- Khan, U. a., Hashimi, S.M., Bakr, M.M., Forwood, M.R., and Morrison, N. a. (2015). CCL2 and CCR2 are Essential for the Formation of Osteoclasts and Foreign Body Giant Cells. *J. Cell. Biochem.* n/a-n/a.
- Khandwekar, A.P., Patil, D.P., Hardikar, A.A., Shouche, Y.S., and Doble, M. (2010). In vivo modulation of foreign body response on polyurethane by surface entrapment technique. *J. Biomed. Mater. Res. - Part A* *95 A*, 413–423.
- Kierdorf, K., Prinz, M., Geissmann, F., and Gomez Perdiguero, E. (2015). Development and function of tissue resident macrophages in mice. *Semin. Immunol.* *27*, 369–378.
- Kinashi, T. (2005). Intracellular signalling controlling integrin activation in lymphocytes. *Nat Rev Immunol* *5*, 546–559.
- Kingston, W. (2004). Streptomycin, Schatz v. Waksman, and the balance of credit for discovery. *J. Hist. Med. Allied Sci.* *59*, 441–462.
- Kitadokoro, K., Bordo, D., Galli, G., Petracca, R., Falugi, F., Abrignani, S., Grandi, G., and Bolognesi, M. (2001). CD81 extracellular domain 3D structure: insight into the tetraspanin superfamily structural motifs. *EMBO J.* *20*, 12–18.
- Kitazawa, S., Ross, F.P., McHugh, K., and Teitelbaum, S.L. (1995). Interleukin-4 induces expression of the integrin $\alpha v\beta 3$ via transactivation of the $\beta 3$ gene. *J. Biol. Chem.* *270*, 4115–4120.
- Koch, C.A., and Platt, J.L. (2012). T cell recognition and immunity in the fetus and mother. *Cell Immunol* *248*, 12–17.
- Kochi, A., Vareldzis, B.I., and K, S. (1992). Multidrug-resistant tuberculosis and its control. *Res. Microbiol.* *144*, 104–110.

- Komano, Y., Nanki, T., Hayashida, K., Taniguchi, K., and Miyasaka, N. (2006). Identification of a human peripheral blood monocyte subset that differentiates into osteoclasts. *Arthritis Res. Ther.* *8*, R152.
- Kondo, Y., Yasui, K., Yashiro, M., Tsuge, M., Kotani, N., and Morishima, T. (2009). Multi-nucleated giant cell formation from human cord blood monocytes in vitro, in comparison with adult peripheral blood monocytes. *Clin. Exp. Immunol.* *158*, 84–90.
- Kotake, S., Udagawa, N., Takahashi, N., Matsuzaki, K., Itoh, K., Ishiyama, S., Saito, S., Inoue, K., Kamatani, N., Gillespie, M.T., et al. (1999). IL-17 in synovial fluids from patients with rheumatoid arthritis is a potent stimulator of osteoclastogenesis. *J. Clin. Invest.* *103*, 1345–1352.
- Kovalenko, O. V., Yang, X., Kolesnikova, T. V., and Hemler, M.E. (2004). Evidence for specific tetraspanin homodimers: inhibition of palmitoylation makes cysteine residues available for cross-linking. *Biochem. J.* *377*, 407–417.
- Kozlovsky, Y., and Kozlov, M.M. (2002). Stalk model of membrane fusion: solution of energy crisis. *Biophys. J.* *82*, 882–895.
- Krauchunas, A.R., Marcello, M.R., and Singson, A. (2016). The molecular complexity of fertilization: Introducing the concept of a fertilization synapse. *Mol. Reprod. Dev.* *83*, 376–386.
- Kurtz, S., Ong, K., Lau, E., Mowat, F., and Halpern, M. (2007). Projections of primary and revision hip and knee arthroplasty in the United States from 2005 to 2030. *J. Bone Jt. Surg.* *89*, 780–785.
- Kyriakides, T.R., Foster, M.J., Keeney, G.E., Tsai, A., Giachelli, C.M., Clark-Lewis, I., Rollins, B.J., and Bornstein, P. (2004). The CC chemokine ligand, CCL2/MCP1, participates in macrophage fusion and foreign body giant cell formation. *Am. J. Pathol.* *165*, 2157–2166.
- Langhans, T. (1868). Ueber Riesenzellen mit wandstandigen Kernen in Tuberkeln und die fibrose Form des Tuberkels. *Arch. Fur Pathol. Anat. Und Physiol. Und Fur Klin. Med.* *42*, 382–404.

- Lapalombella, R., Yeh, Y.-Y., Wang, L., Ramanunni, A., Rafiq, S., Jha, S., Staubli, J., Lucas, D.M., Mani, R., Herman, S.E.M., et al. (2012). Tetraspanin CD37 directly mediates transduction of survival and apoptotic signals. *Cancer Cell* *21*, 694–708.
- Lastrucci, C., Bénard, A., Balboa, L., Pingris, K., Souriant, S., Poincloux, R., Al Saati, T., Rasolofo, V., González-Montaner, P., Inwentarz, S., et al. (2015). Tuberculosis is associated with expansion of a motile, permissive and immunomodulatory CD16+ monocyte population via the IL-10/STAT3 axis. *Cell Res.* *25*, 1333–1355.
- Lavillette, D., Maurice, M., Roche, C., and Russell, S.J. (1998). A Proline-Rich Motif Downstream of the Receptor Binding Domain Modulates Conformation and Fusogenicity of Murine Retroviral Envelopes. *J. Virol.* *72*, 9955–9965.
- Lavin, Y., Mortha, A., Rahman, A., and Merad, M. (2015). Regulation of macrophage development and function in peripheral tissues. *Nat. Rev. Immunol.* *15*, 731–744.
- Lee, J., Hartman, M., and Kornfeld, H. (2009). Macrophage apoptosis in tuberculosis. *Yonsei Med. J.* *50*, 1–11.
- Lee, J., Breton, G., Oliveira, T.Y.K., Zhou, Y.J., Aljoufi, A., Puhr, S., Cameron, M.J., Sékaly, R.-P., Nussenzweig, M.C., and Liu, K. (2015). Restricted dendritic cell and monocyte progenitors in human cord blood and bone marrow. *J. Exp. Med.* *212*, 385–399.
- Lei, H.-Y., and Chang, C.-P. (2009). Lectin of Concanavalin A as an anti-hepatoma therapeutic agent. *J. Biomed. Sci.* *16*, 10.
- Levaot, N., Ottolenghi, A., Mann, M., Guterman-Ram, G., Kam, Z., and Geiger, B. (2015). Osteoclast fusion is initiated by a small subset of RANKL-stimulated monocyte progenitors, which can fuse to RANKL-unstimulated progenitors. *Bone* *79*, 21–28.
- Lever, E., and Sheer, D. (2010). The role of nuclear organization in cancer. *J. Pathol.* *220*, 114–125.

- Levy, S., and Shoham, T. (2005a). The tetraspanin web modulates immune-signalling complexes. *Nat. Rev. Immunol.* *5*, 136–148.
- Levy, S., and Shoham, T. (2005b). Protein-protein interactions in the tetraspanin web. *Physiology* *20*, 218–224.
- Lewinsohn, D.A., Heinzl, A.S., Gardner, J.M., Zhu, L., Alderson, M.R., and Lewinsohn, D.M. (2003). Mycobacterium tuberculosis-specific CD8+ T Cells Preferentially Recognize Heavily Infected Cells. *Am. J. Respir. Crit. Care Med.* *168*, 1346–1352.
- Li, W. wen, Yu, J. ying, Xu, H. long, and Bao, J. ku (2011). Concanavalin A: A potential anti-neoplastic agent targeting apoptosis, autophagy and anti-angiogenesis for cancer therapeutics. *Biochem. Biophys. Res. Commun.* *414*, 282–286.
- Libermann, T. a, and Baltimore, D. (1990). Activation of interleukin-6 gene expression through the NF-kappa B transcription factor. *Mol. Cell. Biol.* *10*, 2327–2334.
- Lichanska, A.M., and Hume, D.A. (2000). Origins and functions of phagocytes in the embryo. *Exp. Hematol.* *28*, 601–611.
- Liu, B., Min, G.W., and Bao, J.K. (2009). Induction of apoptosis by concanavalin A and its molecular mechanisms in cancer cells. *Autophagy* *5*, 432–433.
- Liu, L., He, B., Liu, W.M., Zhou, D., Cox, J. V., and Zhang, X.A. (2007). Tetraspanin CD151 promotes cell migration by regulating integrin trafficking. *J. Biol. Chem.* *282*, 31631–31642.
- Long, C.L., and Humphrey, M.B. (2012). Osteoimmunology: the expanding role of immunoreceptors in osteoclasts and bone remodeling. *Bonekey Rep.* *1*, 1–7.
- Longhurst, C.M., White, M.M., Wilkinson, D. a, and Jennings, L.K. (1999). A CD9, alphaIIb beta3, integrin-associated protein, and GPIb/V/IX complex on the surface of human platelets is influenced by alphaIIb beta3 conformational states. *Eur. J. Biochem.* *263*, 104–111.
- Lorenz, J., Kubesch, A., Korzinskas, T., Barbeck, M., Landes, C., Sader, R.A., Kirkpatrick, C.J., and Ghanaati, S. (2015). TRAP-Positive Multinucleated Giant Cells Are Foreign Body Giant Cells Rather Than Osteoclasts: Results From a

- Split-Mouth Study in Humans. *J. Oral Implantol.* *41*, e257–e266.
- Van Maarsseveen, T.C.M.T., Vos, W., and Van Diest, P.J. (2009). Giant cell formation in sarcoidosis: Cell fusion or proliferation with non-division? *Clin. Exp. Immunol.* *155*, 476–486.
- MacKenzie, A., Wilson, H.L., Kiss-Toth, E., Dower, S.K., North, R.A., and Surprenant, A. (2001). Rapid secretion of interleukin-1 β by microvesicle shedding. *Immunity* *15*, 825–835.
- MacLauchlan, S., Skokos, E.A., Meznarich, N., Zhu, D.H., Raoof, S., Shipley, J.M., Senior, R.M., Bornstein, P., and Kyriakides, T.R. (2009). Macrophage fusion, giant cell formation, and the foreign body response require matrix metalloproteinase 9. *J. Leukoc. Biol.* *85*, 617–626.
- Maecker, H.T., Todd, S.C., and Levy, S. (1997). The tetraspanin facilitators. *FASEB J.* *11*, 428–442.
- Maltesen, H.R., Nielsen, C.H., Dalbøge, C.S., and Baslund, B. (2010). Methylprednisolone prevents tumour necrosis factor-alpha-dependent multinucleated giant cell formation. *Rheumatology* *49*, 2037–2042.
- Mantovani, A., Sica, A., Sozzani, S., Allavena, P., Vecchi, A., and Locati, M. (2004). The chemokine system in diverse forms of macrophage activation and polarization. *Trends Immunol.* *25*, 677–686.
- Marin, M., Tailor, C.S., Nouri, A.L.I., and Kabat, D. (2000). Sodium-Dependent Neutral Amino Acid Transporter Type 1 Is an Auxiliary Receptor for Baboon Endogenous Retrovirus. *J. Virol.* *74*, 8085–8093.
- Martin, F., Roth, D.M., Jans, D.A., Pouton, C.W., Partridge, L.J., Monk, P.N., and Moseley, G.W. (2005). Tetraspanins in Viral Infections : a Fundamental Role in Viral Biology? *J. Virol.* *79*, 10839–10851.
- Martín-Cófreces, N.B., Baixauli, F., and Sánchez-Madrid, F. (2014). Immune synapse: Conductor of orchestrated organelle movement. *Trends Cell Biol.* *24*, 61–72.
- Martinez, F.O., Gordon, S., Locati, M., and Mantovani, A. (2006). Transcriptional Profiling of the Human Monocyte-to-Macrophage Differentiation and

- Polarization: New Molecules and Patterns of Gene Expression. *J. Immunol.* *177*, 7303–7311.
- Masciopinto, F., Campagnoli, S., Abrignani, S., Uematsu, Y., and Pileri, P. (2001). The small extracellular loop of CD81 is necessary for optimal surface expression of the large loop, a putative HCV receptor. *Virus Res.* *80*, 1–10.
- Maus, U.A., Koay, M.A., Delbeck, T., Mack, M., Ermert, M., Ermert, L., Blackwell, T.S., Christman, J.W., Schlondorff, D., Seeger, W., et al. (2002). Role of resident alveolar macrophages in leukocyte traffic into the alveolar air space of intact mice. *Am J Physiol Lung Cell Mol Physiol* *282*, L1245-52.
- Mazurov, D., Barbashova, L., and Filatov, A. (2013). Tetraspanin protein CD9 interacts with metalloprotease CD10 and enhances its release via exosomes. *FEBS J.* *280*, 1200–1213.
- McHugh, K.P., Hodivala-Dilke, K., Zheng, M.H., Namba, N., Jonathan, L., Novack, D., Feng, X., Ross, F.P., Hynes, R.O., and Teitelbaum, S.L. (2000). Mice lacking B3 integrins are osteosclerotic because of dysfunctional osteoclasts. *J. Clin. Invest.* *105*, 433–440.
- McNally, A.K., and Anderson, J.M. (1995). Interleukin-4 induces foreign body giant cells from human monocytes/macrophages. Differential lymphokine regulation of macrophage fusion leads to morphological variants of multinucleated giant cells. *Am. J. Pathol.* *147*, 1487–1499.
- McNally, A.K., and Anderson, J.M. (2014). Phenotypic expression in human monocyte-derived interleukin-4-induced foreign body giant cells and macrophages in vitro: Dependence on material surface properties. *J. Biomed. Mater. Res. A* 1–11.
- McNally, A.K., MacEwan, S.R., and Anderson, J.M. (2007). alpha subunit partners to beta1 and beta2 integrins during IL-4-induced foreign body giant cell formation. *J. Biomed. Mater. Res. Part A* *82*, 568–574.
- McNally, A.K., Jones, J.A., MacEwan, S.R., Colton, E., and Anderson, J.M. (2008). Vitronectin is a critical protein adhesion substrate for IL-4-induced foreign body giant cell formation. *J. Biomed. Mater. Res. - Part A* *86*, 535–543.

- McNally, K., DeFife, K.M., and Anderson, J.M. (1996). Interleukin-4-induced macrophage fusion is prevented by inhibitors of mannose receptor activity. *Am. J. Pathol.* *149*, 975–985.
- Melcher, K. (2016). Structural biology: When sperm meets egg. *Nature* *534*, 484–485.
- Mensah, K.A., Ritchlin, C.T., and Schwarz, E.M. (2010). RANKL induces heterogeneous DC-STAMP^{lo} and DC-STAMP^{hi} osteoclast precursors of which the DC-STAMP^{lo} precursors are the master fusogens. *J. Cell Physiol.* *223*, 76–83.
- Menten, P., Wuyts, A., and Van Damme, J. (2002). Macrophage inflammatory protein-1. *Cytokine Growth Factor Rev.* *13*, 455–481.
- Mi, S., Lee, X., Li, X., Veldman, G.M., Finnerty, H., Racie, L., LaVallie, E., Tang, X.-Y., Edouard, P., Howes, S., et al. (2000). Syncytin is a captive retroviral envelope protein involved in human placental morphogenesis. *Nature* *403*, 785–789.
- Milde, R., Ritter, J., Tennent, G.A., Loesch, A., Martinez, F.O., Gordon, S., Pepys, M.B., Verschoor, A., and Helming, L. (2015). Multinucleated Giant Cells Are Specialized for Complement-Mediated Phagocytosis and Large Target Destruction. *Cell Rep.* *13*, 1937–1948.
- Mills, C.D., Kincaid, K., Alt, J.M., Heilman, M.J., and Hill, A.M. (2000). M-1/M-2 Macrophages and the Th1/Th2 Paradigm. *J Immunol* *164*, 6166–6173.
- Miyamoto, T., Ohneda, O., Arai, F., Iwamoto, K., Okada, S., Takagi, K., Anderson, D.M., and Suda, T. (2001). Bifurcation of osteoclasts and dendritic cells from common progenitors. *Blood* *98*, 2544–2554.
- Moazed, D., and Noller, H.F. (1987). Interaction of antibiotics with functional sites in 16S ribosomal RNA. *Nature* *327*, 389–394.
- Mollinedo, F., Fontan, G., Barasoain, I., Lazo, P.A., and Fonta, G. (1997). Recurrent infectious diseases in human CD53 deficiency. *Clin Diagn Lab Immunol* *4*, 229–231.
- Moon, H., Cremmel, C.V.M., Kulpa, A., Jaeger, N.A.F., Kappelhoff, R., Overall, C.M., Waterfield, J.D., and Brunette, D.M. (2016). Novel Grooved Substrata Stimulate Macrophage Fusion, CCL2 and MMP-9 Secretion. *J. Biomed. Mater. Res. A*

53079, 1–12.

- Moreno, J.L., Mikhailenko, I., Tondravi, M.M., and Keegan, A.D. (2007). IL-4 promotes the formation of multinucleated giant cells from macrophage precursors by a STAT6-dependent, homotypic mechanism: contribution of E-cadherin. *J. Leukoc. Biol.* *82*, 1542–1553.
- Mori, N., and Prager, D. (1996). Transactivation of the Interleukin-1 α Promoter by Human T-cell Leukemia Virus Type I and Type II Tax Proteins. *Am. Soc. Hematol.* *87*, 3410–3417.
- Morishita, K., Tatsukawa, E., Shibata, Y., Suehiro, F., Kamitakahara, M., Yokoi, T., Ioku, K., Umeda, M., Nishimura, M., and Ikeda, T. (2016). Diversity of multinucleated giant cells by microstructures of hydroxyapatite and plasma components in extraskeletal implantation model. *Acta Biomater.* 1–12.
- Moriuchi, H., Moriuchi, M., and Fauci, A.S. (1997). Nuclear Factor- κ B Potently Up-Regulates the Promoter Activity of RANTES, a Chemokine That Blocks HIV infection. *J. Immunol.* *158*, 3483–3491.
- Möst, J., Neumayer, H.P., and Dierich, M.P. (1990). Cytokine-induced generation of multinucleated giant cells in vitro requires interferon-gamma and expression of LFA-1. *Eur. J. Immunol.* *20*, 1661–1667.
- Möst, J., Spötl, L., Mayr, G., Gasser, a, Sarti, a, and Dierich, M.P. (1997). Formation of multinucleated giant cells in vitro is dependent on the stage of monocyte to macrophage maturation. *Blood* *89*, 662–671.
- Mukherjee, R., Kanti Barman, P., Kumar Thatoi, P., Tripathy, R., Kumar Das, B., and Ravindran, B. (2015). Non-Classical monocytes display inflammatory features: Validation in Sepsis and Systemic Lupus Erythematosus. *Sci. Rep.* *5*, 13886.
- Mustafa, T., Wiker, H.G., Mørkve, O., and Sviland, L. (2008). Differential expression of mycobacterial antigen MPT64, apoptosis and inflammatory markers in multinucleated giant cells and epithelioid cells in granulomas caused by *Mycobacterium tuberculosis*. *Virchows Arch.* *452*, 449–456.
- Naour, F. Le, Rubinstein, E., Jasmin, C., Prenant, M., and Boucheix, C. (2000).

- Severely reduced female fertility in CD9-deficient mice. *Science* (80-.). *287*, 319–321.
- Nathan, B.Y.C.F., Murray, H.W., Wlebe, I.E., and Rubin, B.Y. (1983). Identification of interferon-gamma as the lymphokine that activates human macrophage oxidative metabolism and antimicrobial activity. *J Exp Med* *158*, 670–689.
- Néron, S., Thibault, L., Dussault, N., Côté, G., Ducas, É., Pineault, N., and Roy, A. (2007). Characterization of mononuclear cells remaining in the leukoreduction system chambers of apheresis instruments after routine platelet collection: A new source of viable human blood cells. *Transfusion* *47*, 1042–1049.
- Niehaus, A.J., Mlisana, K., Gandhi, N.R., Mathema, B., and Brust, J.C.M. (2015). High prevalence of inhA promoter mutations among patients with drug-resistant tuberculosis in KwaZulu-Natal, South Africa. *PLoS One* *10*, 1–8.
- Nydegger, S., Khurana, S., Kremmentsov, D.N., Foti, M., and Thali, M. (2006). Mapping of tetraspanin-enriched microdomains that can function as gateways for HIV-1. *J. Cell Biol.* *173*, 795–807.
- O’Shea, J.J., Schwartz, D.M., Villarino, A. V., Gadina, M., McInnes, I.B., and Laurence, A. (2015). The JAK-STAT Pathway: Impact on Human Disease and Therapeutic Intervention. *Annu Rev Med* *66*, 311–328.
- Odegaard, J.I., Ricardo-Gonzalez, R.R., Goforth, M.H., Morel, C.R., Subramanian, V., Mukundan, L., Red Eagle, A., Vats, D., Brombacher, F., Ferrante, A.W., et al. (2007). Macrophage-specific PPAR γ controls alternative activation and improves insulin resistance. *Nature* *447*, 1116–1120.
- Ohradanova-Repic, A., Machacek, C., Fischer, M.B., and Stockinger, H. (2016). Differentiation of human monocytes and derived subsets of macrophages and dendritic cells by the HLDA10 monoclonal antibody panel. *Clin. Transl. Immunol.* *5*, e55.
- Ohto, U., Ishida, H., Krayukhina, E., Uchiyama, S., Inoue, N., and Shimizu, T. (2016). Structure of IZUMO1-JUNO reveals sperm-oocyte recognition during mammalian fertilization. *Nature* *534*, 566–569.

- Okamoto, H., Mizuno, K., and Horio, T. (2003). Langhans-type and foreign-body-type multinucleated giant cells in cutaneous lesions of sarcoidosis. *Acta Derm. Venereol.* *83*, 171–174.
- Orme, I.M., Roberts, A.D., Griffin, J.P., and Abrams, J.S. (1993). Cytokine secretion by CD4 T lymphocytes acquired in response to *Mycobacterium tuberculosis* infection. *J. Immunol.* *151*, 518–525.
- Ovchinnikov, D.A. (2008). Macrophages in the embryo and beyond: Much more than just giant phagocytes. *Genesis* *46*, 447–462.
- Van Overmeire, E., Stijlemans, B., Heymann, F., Keirse, J., Morias, Y., Elkrim, Y., Brys, L., Abels, C., Lahmar, Q., Ergen, C., et al. (2016). M-CSF and GM-CSF receptor signaling differentially regulate monocyte maturation and macrophage polarization in the tumor microenvironment. *Cancer Res.* *76*, 35–42.
- Pandey, K.N. (2009). Functional roles of short sequence motifs in the endocytosis of membrane receptors. *Front. Biosci.* *14*, 5339.
- Paolicelli, R.C., Bolasco, G., Pagani, F., Maggi, L., Scianni, M., Panzanelli, P., Giustetto, M., Ferreira, T.A., Guiducci, E., Dumas, L., et al. (2012). Synaptic Pruning by Microglia Is Necessary for Normal Brain Development. *Science* (80-.). *333*, 1456–1458.
- Paradowska-Gorycka, A., and Jurkowska, M. (2013). Structure, expression pattern and biological activity of molecular complex TREM-2/DAP12. *Hum. Immunol.* *74*, 730–737.
- Park, J., Lee, E., and Song, Y. (2014). Decreased tumour necrosis factor- α production by monocytes of granulomatosis with polyangiitis. *Scand. J. Rheumatol.* *43*, 403–408.
- Park, J.K., Rosen, A., Saffitz, J.E., Asimaki, A., Litovsky, S.H., Mackey-Bojack, S.M., and Halushka, M.K. (2013). Expression of cathepsin K and tartrate-resistant acid phosphatase is not confined to osteoclasts but is a general feature of multinucleated giant cells: Systematic analysis. *Rheumatol. (United Kingdom)* *52*, 1529–1533.

- Parthasarathy, V., Martin, F., Higginbottom, A., Murray, H., Moseley, G.W., Read, R.C., Mal, G., Hulme, R., Monk, P.N., and Partridge, L.J. (2009). Distinct roles for tetraspanins CD9, CD63 and CD81 in the formation of multinucleated giant cells. *Immunology* *127*, 237–248.
- Passlick, B., Flieger, D., and Ziegler-Heitbrock, H.W.L. (1989). Identification and Characterization of a Novel Monocyte Subpopulation in Human Peripheral Blood. *Blood* *74*, 2527–2534.
- Patel, N.R., Zhu, J., Tachado, S.D., Zhang, J., Wan, Z., Saukkonen, J., and Koziel, H. (2007). HIV Impairs TNF- α Mediated Macrophage Apoptotic Response to Mycobacterium tuberculosis. *J. Immunol.* *179*, 6973–6980.
- Pawlaowski, A., Jansson, M., Sköld, M., Rottenberg, M.E., and Källenius, G. (2012). Tuberculosis and HIV co-infection. *PLoS Pathog.* *8*.
- Pegoraro, G., Eaton, B.P., Ulrich, R.L., Lane, D.J., Ojeda, J.F., Bavari, S., DeShazer, D., and Panchal, R.G. (2014). A high-content imaging assay for the quantification of the Burkholderia pseudomallei induced multinucleated giant cell (MNGC) phenotype in murine macrophages. *BMC Microbiol.* *14*, 98.
- Pellegatti, P., Falzoni, S., Donvito, G., Lemaire, I., and Di Virgilio, F. (2011). P2X7 receptor drives osteoclast fusion by increasing the extracellular adenosine concentration. *FASEB J.* *25*, 1264–1274.
- Pelzer, C., and Thome, M. (2011). IKK α takes control of canonical NF- κ B activation. *Nat. Immunol.* *12*, 815–816.
- Peng, H., Jiang, X., Chen, Y., Sojka, D.K., Wei, H., Gao, X., Sun, R., Yokoyama, W.M., and Tian, Z. (2013). Liver-resident NK cells confer adaptive immunity in skin-contact inflammation. *J. Clin. Invest.* *123*, 1444–1456.
- Peng, W.M., Yu, C.F., Kolanus, W., Mazzocca, a, Bieber, T., Kraft, S., and Novak, N. (2011). Tetraspanins CD9 and CD81 are molecular partners of trimeric Fc ϵ RI on human antigen-presenting cells. *Allergy* *66*, 605–611.
- Pfeiffer, I.A., Zinser, E., Strasser, E., Stein, M.F., Dörrie, J., Schaft, N., Steinkasserer, A., and Knippertz, I. (2013). Leukoreduction system chambers are an efficient,

- valid, and economic source of functional monocyte-derived dendritic cells and lymphocytes. *Immunobiology* *218*, 1392–1401.
- Pique, C., Lagaudrière-Gesbert, C., Delamarre, L., Rosenberg, a R., Conjeaud, H., and Dokh lar, M.C. (2000). Interaction of CD82 tetraspanin proteins with HTLV-1 envelope glycoproteins inhibits cell-to-cell fusion and virus transmission. *Virology* *276*, 455–465.
- Podbilewicz, B. (2014). Virus and cell fusion mechanisms. *Annu Rev Cell Dev Biol* *30*, 111–139.
- Qiao, J.H., Mishra, V., Fishbein, M.C., Sinha, S.K., and Rajavashisth, T.B. (2015). Multinucleated giant cells in atherosclerotic plaques of human carotid arteries: Identification of osteoclast-like cells and their specific proteins in artery wall. *Exp. Mol. Pathol.* *99*, 654–662.
- Quinn, M.T., and Schepetkin, I.A. (2009). Role of NADPH oxidase in formation and function of multinucleated giant cells. *J. Innate Immun.* *1*, 509–526.
- Ramana, C. V, Chatterjee-Kishore, M., Nguyen, H., and Stark, G.R. (2000). Complex roles of Stat1 in regulating gene expression. *Oncogene* *19*, 2619–2627.
- Randolph, G.J., Sanchez-Schmitz, G., Liebman, R.M., and Sch kel, K. (2002). The CD16(+) (FcγRIII(+)) subset of human monocytes preferentially becomes migratory dendritic cells in a model tissue setting. *J. Exp. Med.* *196*, 517–527.
- Rassendren, F., Buell, G.N., Virginio, C., Collo, G., North, R.A., and Surprenant, A. (1996). The Permeabilizing ATP Receptor, P2X 7. *J. Biol. Chem.* *272*, 5482–5486.
- Rawat, R., Whitty, A., and Tonge, P.J. (2003). The isoniazid-NAD adduct is a slow, tight-binding inhibitor of InhA, the Mycobacterium tuberculosis enoyl reductase: Adduct affinity and drug resistance. *Proc. Natl. Acad. Sci.* *100*, 13881–13886.
- Rhee, H.J. van der, Hillebrands, W., and Daems, W.T. (1978). Are Langhans giant cells precursors of foreign-body giant cells? *263*, 13–21.
- Rivollier, A., Mazzorana, M., Tebib, J., Piperno, M., Aitsiselmi, T., Jurdic, P., Servet-

- delprat, C., and De, W. (2013). Immature dendritic cell transdifferentiation into osteoclasts: a novel pathway sustained by the rheumatoid arthritis microenvironment Immature dendritic cell transdifferentiation into osteoclasts: a novel pathway sustained by the rheumatoid arthritis mi. *Immunobiology* *104*, 4029–4037.
- Rosas-Tarco, A.G., Arce-Mendoza, A.Y., Caballero-Olin, G., and Salinas-Carmona, M.C. (2006). Mycobacterium tuberculosis Upregulates Coreceptors CCR5 and CXCR4 While HIV Modulates CD14 Favoring Concurrent Infection. *AIDS Res. Hum. Retroviruses* *22*, 45–51.
- Rosol, M., Kraus, S., Pierer, M., Baerwald, C., and Wagner, U. (2012). The CD14^{bright}CD16⁺ monocyte subset is expanded in rheumatoid arthritis and promotes expansion of the Th17 cell population. *Arthritis Rheum.* *64*, 671–677.
- Rubinstein, E., Ziyat, A., Prenant, M., Wrobel, E., Wolf, J.P., Levy, S., Le Naour, F., and Boucheix, C. (2006). Reduced fertility of female mice lacking CD81. *Dev. Biol.* *290*, 351–358.
- Ruseva, Z., Geiger, P.X.C., Hutzler, P., Kotsch, M., Lubber, B., Schmitt, M., Gross, E., and Reuning, U. (2009). Tumor suppressor KAI1 affects integrin $\alpha\beta 3$ -mediated ovarian cancer cell adhesion, motility, and proliferation. *Exp. Cell Res.* *315*, 1759–1771.
- Saginario, C., Qian, H.Y., and Vignery, A. (1995). Identification of an inducible surface molecule specific to fusing macrophages. *Proc Natl Acad Sci U S A* *92*, 12210–4.
- Sakai, H., Okafuji, I., Nishikomori, R., Abe, J., Izawa, K., Kambe, N., Yasumi, T., Nakahata, T., and Heike, T. (2012). The CD40-CD40L axis and IFN- γ play critical roles in Langhans giant cell formation. *Int. Immunol.* *24*, 5–15.
- Sala-Valdés, M., Ursa, Á., Charrin, S., Rubinstein, E., Hemler, M.E., Sánchez-Madrid, F., and Yáñez-Mó, M. (2006). EWI-2 and EWI-F link the tetraspanin web to the actin cytoskeleton through their direct association with ezrin-radixin-moesin proteins. *J. Biol. Chem.* *281*, 19665–19675.

- Sánchez-Torres, C., García-Romo, G.S., Cornejo-Cortés, M. a, Rivas-Carvalho, a, and Sánchez-Schmitz, G. (2001). CD16+ and CD16- human blood monocyte subsets differentiate in vitro to dendritic cells with different abilities to stimulate CD4+ T cells. *Int. Immunol.* *13*, 1571–1581.
- Sarih, M., Souvannavong, V., Brown, S.C., and Adam, A. (1993). Silica induces apoptosis in macrophages and the release of interleukin-1 alpha and interleukin-1beta. *J Leukoc. Biol* *54*, 407–413.
- Schmidt, D.S., Klingbeil, P., Schnölzer, M., and Zöller, M. (2004). CD44 variant isoforms associate with tetraspanins and EpCAM. *Exp. Cell Res.* *297*, 329–347.
- Schottelius, A.J.G., Mayo, M.W., Sartor, R.B., and Badwin, A.S. (1999). Interleukin-10 signaling blocks inhibitor of kappa B kinase activity and nuclear factor kappa B DNA binding. *J. Biol. Chem.* Nov *274*, 31868–31874.
- Schumacher, A., Heinze, K., Witte, J., Poloski, E., Linzke, N., Woidacki, K., and Zenclussen, A.C. (2013). Human chorionic gonadotropin as a central regulator of pregnancy immune tolerance. *J. Immunol.* *190*, 2650–2658.
- Seigneuret, M. (2006). Complete predicted three-dimensional structure of the facilitator transmembrane protein and hepatitis C virus receptor CD81: conserved and variable structural domains in the tetraspanin superfamily. *Biophys. J.* *90*, 212–227.
- Semnani, R.T., Moore, V., Bennuru, S., McDonald-Fleming, R., Ganesan, S., Cotton, R., Anuradha, R., Babu, S., and Nutman, T.B. (2014). Human monocyte subsets at homeostasis and their perturbation in numbers and function in filarial infection. *Infect. Immun.* *82*, 4438–4446.
- Seto, S., Tsujimura, K., and Koide, Y. (2011). Rab GTPases Regulating Phagosome Maturation Are Differentially Recruited to Mycobacterial Phagosomes. *Traffic* *12*, 407–420.
- Shakhov, A.N., Collart, M.A., Vassalli, P., Nedospasov, S.A., and Jongeneel, V.C. (1990). Kappa B-type enhancers are involved in lipopolysaccharide-mediated transcriptional activation of the tumor necrosis factor alpha gene in primary

- macrophages. *J Exp Med.* *171*, 35–47.
- Shen, F., Hu, Z., Goswami, J., and Gaffen, S.L. (2006). Identification of common transcriptional regulatory elements in interleukin-17 target genes. *J. Biol. Chem.* *281*, 24138–24148.
- Sica, A., and Mantovani, A. (2012). Macrophage plasticity and polarization: in vivo veritas. *J. Clin. Invest.* *122*, 787–795.
- Siegel, D.P. (1993). Energetics of intermediates in membrane fusion: comparison of stalk and inverted micellar intermediate mechanisms. *Biophys. J.* *65*, 2124–2140.
- Silverstein, R.L., Baird, M., Lo, S.K., and Yesner, L.M. (1992). Sense and antisense cDNA transfection of CD36 (glycoprotein IV) in melanoma cells: Role of CD36 as a thrombospondin receptor. *J. Biol. Chem.* *267*, 16607–16612.
- Skokos, E.A., Charokopos, A., Khan, K., Wanjala, J., and Kyriakides, T.R. (2011). Lack of TNF- α -induced MMP-9 production and abnormal E-cadherin redistribution associated with compromised fusion in MCP-1-null macrophages. *Am. J. Pathol.* *178*, 2311–2321.
- Sodhi, A., Tarang, S., and Kesherwani, V. (2007). Concanavalin A induced expression of Toll-like receptors in murine peritoneal macrophages in vitro. *Int. Immunopharmacol.* *7*, 454–463.
- Spear, G.T., Kessler, H.A., Rothberg, L., Phair, J., and Landay, A.L. (1990). Decreased Oxidative Burst activity of Monocytes from Asymptomatic HIV-Infected Individuals. *Clin. Immunol. Immunopathol.* *54*, 184–191.
- Stipp, C.S., Kolesnikova, T. V., and Hemler, M.E. (2001). EWI-2 Is a Major CD9 and CD81 Partner and Member of a Novel Ig Protein Subfamily. *J. Biol. Chem.* *276*, 40545–40554.
- Stipp, C.S., Kolesnikova, T. V., and Hemler, M.E. (2003). Functional domains in tetraspanin proteins. *Trends Biochem. Sci.* *28*, 106–112.
- Suen, Y.K., Fung, K.P., Choy, Y.M., Lee, C.Y., Chan, C.W., and Kong, S.K. (2000). Concanavalin A induced apoptosis in murine macrophage PU5-1 . 8 cells through

- clustering of mitochondria and release of cytochrome c. *Apoptosis* 5, 369–377.
- Sun, J.C., Beilke, J.N., and Lanier, L.L. (2009). Adaptive immune features of natural killer cells. *Nature* 457, 557–561.
- Sunderkotter, C., Nikolic, T., Dillon, M.J., van Rooijen, N., Stehling, M., Drevets, D.A., and Leenen, P.J.M. (2004). Subpopulations of Mouse Blood Monocytes Differ in Maturation Stage and Inflammatory Response. *J. Immunol.* 172, 4410–4417.
- Suzuki, M., Tachibana, I., Takeda, Y., Minami, S., Iwasaki, T., Kida, H., Kijima, T., Yoshida, M., Osaki, T., Kawase, I., et al. (2009). Tetraspanin CD9 Negatively Regulates Lipopolysaccharide-Induced Macrophage Activation and Lung Inflammation. *J. Immunol.* 182, 6485–6493.
- Tai, X.-G., Yashiro, Y., Abe, K., Toyooka, K., R.Wood, C., Morris, J., Long, A., Ono, S., Kobayashi, M., Hamaoka, T., et al. (1996). A Role for CD9 Molecules in T Cell Activation. *J. Exp. Med.* 184, 753–758.
- Takashima, T., Ohnishi, K., Tsuyuguchi, I., and Kishimoto, S. (1993). Differential regulation of formation of multinucleated giant cells from concanavalin A-stimulated human blood monocytes by IFN-gamma and IL-4. *J. Immunol.* 150, 3002–3010.
- Takeda, Y., Tachibana, I., Miyado, K., Kobayashi, M., Miyazaki, T., Funakoshi, T., Kimura, H., Yamane, H., Saito, Y., Goto, H., et al. (2003). Tetraspanins CD9 and CD81 function to prevent the fusion of mononuclear phagocytes. *J. Cell Biol.* 161, 945–956.
- Takeda, Y., He, P., Tachibana, I., Zhou, B., Miyado, K., Kaneko, H., Suzuki, M., Minami, S., Iwasaki, T., Goya, S., et al. (2008). Double deficiency of tetraspanins CD9 and CD81 alters cell motility and protease production of macrophages and causes chronic obstructive pulmonary disease-like phenotype in mice. *J. Biol. Chem.* 283, 26089–26097.
- Tarrant, J.M., Groom, J., Metcalf, D., Li, R., Borobokas, B., Wright, M.D., Tarlinton, D., and Robb, L. (2002). The absence of Tssc6, a member of the tetraspanin superfamily, does not affect lymphoid development but enhances in vitro T-cell

- proliferative responses. *Mol. Cell. Biol.* *22*, 5006–5018.
- Tedgui, A., and Mallat, Z. (2006). Cytokines in Atherosclerosis: Pathogenic and Regulatory Pathways. *Physiol. Rev.* *86*, 515–581.
- Telenti, A., Imboden, P., Marchesi, F., Schmidheini, T., and Bodmer, T. (1993). Direct , Automated Detection of Rifampin-Resistant Mycobacterium tuberculosis by Polymerase Chain Reaction and Single-Strand Conformation Polymorphism Analysis. *Antimicrob. Agents Chemother.* *37*, 2054–2058.
- Tippett, E., Cameron, P.U., Marsh, M., and Crowe, S.M. (2013). Characterization of tetraspanins CD9, CD53, CD63, and CD81 in monocytes and macrophages in HIV-1 infection. *J. Leukoc. Biol.* *93*, 1–8.
- Todres, E., Nardi, J.B., and Robertson, H.M. (2000). The tetraspanin superfamily in insects. *Insect Mol. Biol.* *9*, 581–590.
- Todros-Dawda, I., Kveberg, L., Vaage, J.T., and Inngjerdingen, M. (2014). The tetraspanin CD53 modulates responses from activating NK cell receptors, promoting LFA-1 activation and dampening NK cell effector functions. *PLoS One* *9*.
- Tomlinson, M.G., and Wright, M.D. (1996). A New Transmembrane 4 Superfamily Molecule in the the Nematode, *Caenorhabditis elegans*. *J Mol Evol* *43*, 312–314.
- Turnbull, I.R., Gilfillan, S., Cella, M., Aoshi, T., Miller, M., Piccio, L., Hernandez, M., and Colonna, M. (2006). Cutting edge: TREM-2 attenuates macrophage activation. *J. Immunol.* *177*, 3520–3524.
- Ueda, A., Okuda, K., Ohno, S., Shirai, A., Igarashi, T., Matsunaga, K., Fukushima, J., Kawamoto, S., Ishigatsubo, Y., and Okubo, T. (1994). NF-kappa B and Sp1 regulate transcription of the human monocyte chemoattractant protein-1 gene. *J. Immunol. (Baltimore, Md. 1950)* *153*, 2052–2063.
- Verma, S.K., Leikina, E., Melikov, K., and Chernomordik, L. V (2014). Late stages of the synchronized macrophage fusion in osteoclast formation depend on dynamin. *Biochem. J.* *464*, 293–300.
- Via, L.E., Deretic, D., Ulmer, R.J., Hibler, N.S., Huber, L.A., and Deretic, V. (1997).

- Arrest of mycobacterial phagosome maturation is caused by a block in vesicle fusion between stages controlled by rab5 and rab7. *J. Biol. Chem.* *272*, 13326–13331.
- Vignery, A. (2005). Macrophage fusion: are somatic and cancer cells possible partners? *Trends Cell Biol.* *15*, 188–193.
- Wajant, H., Pfizenmaier, K., and Scheurich, P. (2003). Tumor necrosis factor signaling. *Cell Death.Differ.* *10*, 45–65.
- Walter, G.J., Evans, H.G., Menon, B., Gullick, N.J., Kirkham, B.W., Cope, A.P., Geissmann, F., and Taams, L.S. (2013). Interaction with activated monocytes enhances cytokine expression and suppressive activity of human CD4⁺CD45ro⁺CD25⁺CD127^{low} regulatory T cells. *Arthritis Rheum.* *65*, 627–638.
- Wanat, K.A., Rosenbach, M., Ziober, A.F., Zhang, P.J., and Schaffer, A. (2015). E-cadherin is expressed by mono- and multinucleated histiocytes in cutaneous sarcoidal and foreign body granulomas. *Am J Dermatopathol.* *36*, 651–654.
- Wands, J.R., Podolsky, D.K., and Isselbacher, K. j. (1976). Mechanism of human lymphocyte stimulation by concanavalin A: Role of valence and surface binding sites. *Proc. Natl. Acad. Sci. U. S. A.* *73*, 2118–2122.
- Wang, X.X., and Pfenninger, K.H. (2006). Functional analysis of SIRPalpha in the growth cone. *J. Cell Sci.* *119*, 172–183.
- Wang, F., Cassidy, C., and Sacchettini, J.C. (2006). Crystal structure and activity studies of the Mycobacterium tuberculosis β -lactamase reveal its critical role in resistance to β -lactam antibiotics. *Antimicrob. Agents Chemother.* *50*, 2762–2771.
- Wang, H.X., Liu, M., Weng, S.Y., Li, J.J., Xie, C., He, H.L., Guan, W., Yuan, Y.S., and Gao, J. (2012). Immune mechanisms of Concanavalin a model of autoimmune hepatitis. *World J. Gastroenterol.* *18*, 119–125.
- Warner, J.M., and O’Shaughnessy, B. (2012). Evolution of the hemifused intermediate on the pathway to membrane fusion. *Biophys. J.* *103*, 689–701.

- Weber, A., Wasiliew, P., and Kracht, M. (2010). Interleukin-1 (IL-1) pathway. *Sci. Signal.* *3*, cm1.
- Wee, J.L., Schulze, K.E., Jones, E.L., Yeung, L., Cheng, Q., Pereira, C.F., Costin, A., Ramm, G., van Spriel, A.B., Hickey, M.J., et al. (2015). Tetraspanin CD37 Regulates β 2 Integrin-Mediated Adhesion and Migration in Neutrophils. *J. Immunol.* *195*, 5770–5779.
- Whalen, C., Horsburgh, C.R., Hom, D., Lahart, C., Simberkoff, M., and Ellner, J. (1995). Accelerated course of human immunodeficiency virus infection after tuberculosis. *Am. J. Respir. Crit. Care Med.* *151*, 129–135.
- Widmer, U., Manogue, K.R., Cerami, A., and Sherry, B. (1993). Genomic cloning and promoter analysis of macrophage inflammatory protein (MIP)-2, MIP-1 alpha, and MIP-1 beta, members of the chemokine superfamily of proinflammatory cytokines. *J. Immunol.* *150*, 4996–5012.
- Williams, L.M., Ricchetti, G., Sarma, U., Smallie, T., and Foxwell, B.M.J. (2004). Interleukin-10 suppression of myeloid cell activation - A continuing puzzle. *Immunology* *113*, 281–292.
- Wong, K.L., Tai, J.J.-Y., Wong, W.-C., Han, H., Sem, X., Yeap, W.-H., Kourilsky, P., and Wong, S.-C. (2011). Gene expression profiling reveals the defining features of the classical, intermediate, and nonclassical human monocyte subsets. *Blood* *118*, e16-31.
- Wong, K.L., Yeap, W.H., Tai, J.J.Y., Ong, S.M., Dang, T.M., and Wong, S.C. (2012). The three human monocyte subsets: implications for health and disease. *Immunol. Res.* *53*, 41–57.
- Wright, M.D., and Tomlinson, M.G. (1994). The ins and outs of the transmembrane 4 superfamily. *Immunol. Today* *15*, 588–594.
- Wurster, a L., Tanaka, T., and Grusby, M.J. (2000). The biology of Stat4 and Stat6. *Oncogene* *19*, 2577–2584.
- Xia, Z., and Triffitt, J.T. (2006). A review on macrophage responses to biomaterials. *Biomed. Mater.* *1*, R1-9.

- Xu, R., and Wilson, I. a (2011). Structural Characterization of an Early Fusion Intermediate of Influenza Virus Hemagglutinin. *J. Virol.* *85*, 5172–5182.
- Yagi, M., Miyamoto, T., Sawatani, Y., Iwamoto, K., Naobumi Hosogane, N.F., Morita, K., Ninomiya, K., Suzuki, T., Miyamoto, K., Oike, Y., et al. (2005). DC-STAMP is essential for cell-cell fusion in osteoclasts and foreign body giant cells. *J. Exp. Med.* *202*, 345–351.
- Yagi, M., Ninomiya, K., Fujita, N., Suzuki, T., Iwasaki, R., Morita, K., Hosogane, N., Matsuo, K., Toyama, Y., Suda, T., et al. (2007). Induction of DC-STAMP by alternative activation and downstream signaling mechanisms. *J. Bone Miner. Res.* *22*, 992–1001.
- Yáñez-Mó, M., Tejedor, R., Rousselle, P., and Sánchez -Madrid, F. (2001). Tetraspanins in intercellular adhesion of polarized epithelial cells: spatial and functional relationship to integrins and cadherins. *J. Cell Sci.* *114*, 577–587.
- Yang, J., Zhang, L., Yu, C., Yang, X.-F., and Wang, H. (2014a). Monocyte and macrophage differentiation: circulation inflammatory monocyte as biomarker for inflammatory diseases. *Biomark. Res.* *2*, 1.
- Yang, J., Jao, B., Mcnally, A.K., and Anderson, J.M. (2014b). In vivo quantitative and qualitative assessment of foreign body giant cell formation on biomaterials in mice deficient in natural killer lymphocyte subsets, mast cells, or the interleukin-4 receptor?? and in severe combined immunodeficient mice. *J. Biomed. Mater. Res. - Part A* *102*, 2017–2023.
- Yang, X., Claas, C., Kraeft, S.-K., Chen, L.B., Wang†, Z., Kreidberg†, J.A., and Hemler, M.E. (2002). Palmitoylation of Tetraspanin Proteins: Modulation of CD151 Lateral Interactions, Subcellular Distribution, and Integrin-dependent Cell Morphology. *Mol. Biol. Cel* *13*, 767–781.
- Yang, X., Kovalenko, O. V., Tang, W., Claas, C., Stipp, C.S., and Hemler, M.E. (2004). Palmitoylation supports assembly and function of integrin-tetraspanin complexes. *J. Cell Biol.* *167*, 1231–1240.
- Yashiro-Ohtani, Y., Zhou, X.-Y., Toyo-oka, K., Tai, X.-G., Park, C.-S., Hamaoka, T.,

- Abe, R., Miyake, K., and Fujiwara, H. (2000). Non-CD28 Costimulatory Molecules Present in T Cell Rafts Induce T Cell Costimulation by Enhancing the Association of TCR with Rafts. *J. Immunol.* *164*, 1251–1259.
- Yona, S., Kim, K.W., Wolf, Y., Mildner, A., Varol, D., Breker, M., Strauss-Ayali, D., Viukov, S., Guilliams, M., Misharin, A., et al. (2013). Fate Mapping Reveals Origins and Dynamics of Monocytes and Tissue Macrophages under Homeostasis. *Immunity* *38*, 79–91.
- Yu, M., Qi, X., Moreno, J.L., Farber, D.L., and Keegan, A.D. (2011). NF- κ B Signaling Participates in Both RANKL- and IL-4- Induced Macrophage Fusion: Receptor Cross Talk Leads to Alterations in NF- κ B Pathways. *J Immunol* *187*, 1797–1806.
- Zawada, A.M., Rogacev, K.S., Rotter, B., Winter, P., Marell, R.R., Fliser, D., and Heine, G.H. (2011). SuperSAGE evidence for CD14 ++CD16 + monocytes as a third monocyte subset. *Blood* *118*, 50–62.
- Zawada, A.M., Rogacev, K.S., Schirmer, S.H., Sester, M., Böhm, M., Fliser, D., and Heine, G.H. (2012). Monocyte heterogeneity in human cardiovascular disease. *Immunobiology* *217*, 1273–1284.
- Zhang, J.Y., Zou, Z.S., Huang, A., Zhang, Z., Fu, J.L., Xu, X.S., Chen, L.M., Li, B. Sen, and Wang, F.S. (2011a). Hyper-activated pro-inflammatory CD16+ monocytes correlate with the severity of liver injury and fibrosis in patients with chronic hepatitis B. *PLoS One* *6*.
- Zhang, X.A., Lane, W.S., Charrin, S., Rubinstein, E., and Liu, L. (2003). EWI2 / PGRL Associates with the Metastasis Suppressor KAI1 / CD82 and Inhibits the Migration of Prostate Cancer Cells the Migration of Prostate Cancer Cells 1. *Cancer* *63*, 2665–2674.
- Zhang, Y., Ma, C.J., Ni, L., Zhang, C.L., Wu, X.Y., Kumaraguru, U., Li, C.F., Moorman, J.P., and Yao, Z.Q. (2011b). Cross-talk between programmed death-1 and suppressor of cytokine signaling-1 in inhibition of IL-12 production by monocytes/macrophages in hepatitis C virus infection. *J. Immunol.* *186*, 3093–3103.

- Zhao, C., Tan, Y.-C., Wong, W.-C., Sem, X., Zhang, H., Han, H., Ong, S.-M., Wong, K.-L., Yeap, W.-H., Sze, S.-K., et al. (2010). The CD14(+/low)CD16(+) monocyte subset is more susceptible to spontaneous and oxidant-induced apoptosis than the CD14(+)CD16(-) subset. *Cell Death Dis.* *1*, e95.
- Zhao, Q., Topham, N., Anderson, J.M., Hiltner, a, Lodoen, G., and Payet, C.R. (1991). Foreign-body giant cells and polyurethane biostability: in vivo correlation of cell adhesion and surface cracking. *J. Biomed. Mater. Res.* *25*, 177–183.
- Zhou, F.X., Cocco, M.J., Russ, W.P., Brunger, A.T., and Engelman, D.M. (2000). Interhelical hydrogen bonding drives strong interactions in membrane proteins. *Nat. Struct. Biol.* *7*, 154–160.
- Zhou, J., Feng, G., Beeson, J., Hogarth, P.M., Rogerson, S.J., Yan, Y., and Jaworowski, A. (2015). CD14(hi)CD16+ monocytes phagocytose antibody-opsonised Plasmodium falciparum infected erythrocytes more efficiently than other monocyte subsets, and require CD16 and complement to do so. *BMC Med.* *13*, 154.
- Zhou, L., Nazarian, A.A., and Smale, S.T. (2004). Interleukin-10 Inhibits Interleukin-12 p40 Gene Transcription by Targeting a Late Event in the Activation Pathway. *Mol. Cell. Biol.* *24*, 2385–2396.
- Zhu, G.-Z., Miller, B.J., Boucheix, C., Rubinstein, E., Liu, C.C., Hynes, R.O., Myles, D.G., and Primakoff, P. (2002). Residues SFQ (173-175) in the large extracellular loop of CD9 are required for gamete fusion. *Development* *129*, 1995–2002.
- Zhu, X.W., Price, N.M., Gilman, R.H., Recarvarren, S., and Friedland, J.S. (2007). Multinucleate Giant Cells Release Functionally Unopposed Matrix Metalloproteinase-9 In Vitro and In Vivo. *J. Infect. Dis.* *196*, 1076–1079.
- Ziegler-Heitbrock, L., Ancuta, P., Crowe, S., Dalod, M., Grau, V., Hart, D.N., Leenen, P.J.M., Liu, Y.-J., MacPherson, G., Randolph, G.J., et al. (2010). Nomenclature of monocytes and dendritic cells in blood. *Blood* *116*, e74-80.
- Zigmond, E., and Jung, S. (2013). Intestinal macrophages: Well educated exceptions

from the rule. *Trends Immunol.* *34*, 162–168.

Ziyyat, A., Rubinstein, E., Monier-Gavelle, F., Barraud, V., Kulski, O., Prenant, M., Boucheix, C., Bomsel, M., and Wolf, J.-P. (2006). CD9 controls the formation of clusters that contain tetraspanins and the integrin alpha 6 beta 1, which are involved in human and mouse gamete fusion. *J. Cell Sci.* *119*, 416–424.

Zöller, M. (2009). Tetraspanins: push and pull in suppressing and promoting metastasis. *Nat. Rev. Cancer* *9*, 40–55.

Zuidscherwoude, M., Göttfert, F., Dunlock, V.M.E., Figdor, C.G., van den Bogaart, G., and Spriel, A.B. Van (2015). The tetraspanin web revisited by super-resolution microscopy. *Sci. Rep.* *5*, 12201.